REPUBLIC OF BENIN

------000------

MINISTRY OF HIGHER EDUCATION AND SCIENTIFIC RESEARCH

------000------

UNIVERSITY OF ABOMEY - CALAVI

DOCTORAL SCHOOL OF LIFE AND EARTH SCIENCES

------000------

Registered under N°:413

A DISSERTATION

Submitted

In partial fulfillment of the requirements for the degree of

DOCTOR of Philosophy (PhD) of the University of Abomey-Calavi

In the framework of the

Graduate Research Program on Climate Change and Water Resources (GRP-CCWR)

By

Mame Henriette Astou SAMBOU

Public defense on: 04/17/2024

======

CLIMATE CHANGE AND LAND USE LAND COVER CHANGE IMPACTS ON THE HYDROPOWER POTENTIAL IN THE BAFING WATERSHED (SENEGAL RIVER BASIN

======

Supervisors

Expédit Wilfrid Vissin	Full Prof	University of Abomey-Calavi (UAC), Benin
Jean Albergel	PhD, Emerite Research Director	Institut de recherche pour le développement, France
Stefan Liersch	PhD, Senior researcher	Potsdam Institute for Climate Impact Research (PIK), Germany

Reviewers

Luc SINTONDJI	Full Professor	University of Abomey Calavi, (UAC), Benin
Harouna KARAMBIRI	Full Professor	2iE, Burkina Faso
Tidiane SANE	Associate Professor	University Assane Seck of Ziguinchor, Senegal

JURY

Agnidé Emmanuel LAWIN	Full Professor, University of Abomey Calavi (UAC), Benin	President
Luc SINTONDJI	Full Professor, University of Abomey Calavi (UAC), Benin	Reviewer
Harouna KARAMBIRI	Full Professor, 2iE, Burkina Faso	Reviewer
Tidiane SANE	Associate Professor, University Assane Seck of Ziguinchor, Senegal	Reviewer
François Kossi GUEDJE	Associate Professor, University of Abomey Calavi (UAC), Benin	Examiner
Expédit Wilfrid VISSIN	Full Professor, University of Abomey Calavi (UAC), Benin	Supervisor
Jean ALBERGEL	Emerite Research Director, Institut de recherche pour le développement, France	Co-Supervisor
Stefan Liersch	PhD, Senior researcher, Potsdam Institute for Climate Impact Research (PIK), Germany	Co-Supervisor

REPUBLIQUE DU BENIN

------ooo------

MINISTERE DE L'ENSEIGNEMENT SUPERIEUR ET DE LA RECHERCHE SCIENTIFIQUE

------ooo------

ECOLE DOCTORALE SCIENCES DE LA VIE ET DE LA TERRE

------ooo------

Enregistrée sous N°: 413

THESE

Soumise pour obtenir le grade de

DOCTEUR de l'Université d'Abomey-Calavi

Dans la Spécialité :

Changement climatique et Ressources en Eau

Par

Mame Henriette Astou SAMBOU

Soutenue publiquement le : 17/04/2024

======

IMPACTS DU CHANGEMENT CLIMATIQUE ET DU CHANGEMENT DANS L'UTILISATION DES TERRES ET DE LA COUVERTURE TERRESTRE SUR LE POTENTIEL HYDROÉLECTRIQUE DANS LE BASSIN VERSANT DU BAFING (BASSIN DU FLEUVE SÉNÉGAL)

======

Directeurs de thèse

Expédit Wilfrid Vissin	Professeur Titulaire	Université d'Abomey Calavi (UAC), Bénin
Jean Albergel	PhD, Directeur de recherche émérite	Institut de recherche pour le développement, France
Stefan Liersch	PhD, Chercheur principal	Potsdam Institute for Climate Impact Research (PIK), Germany

Rapporteurs

Luc SINTONDJI	Professeur Titulaire	Université d'Abomey Calavi (UAC), Bénin
Harouna KARAMBIRI	Professeur Titulaire	2iE, Burkina Faso
Tidiane SANE	Maître de Conférences	Université Assane Seck of Ziguinchor, Sénégal

JURY

Agnidé Emmanuel LAWIN	Professeur Titulaire, Université d'Abomey Calavi (UAC), Bénin	Président
Luc SINTONDJI	Professeur Titulaire, Université d'Abomey Calavi (UAC), Bénin	Rapporteur
Harouna KARAMBIRI	Professeur Titulaire, 2iE, Burkina Faso	Rapporteur
Tidiane SANE	Maître de Conférences, University Assane Seck of Ziguinchor, Sénégal	Rapporteur
François Kossi GUEDJE	Maître de Conférences, Université d'Abomey Calavi (UAC), Bénin	Examinateur
Expédit Wilfrid VISSIN	Professeur Titulaire, Université d'Abomey Calavi (UAC), Bénin	Superviseur
Jean ALBERGEL	Directeur de recherche émérite, Institut de recherche pour le développement, France	Co-Superviseur
Stefan Liersch	PhD, Chercheur principal, Potsdam Institute for Climate Impact Research (PIK), Germany	Co-Superviseur

WASCAL West African Science Service Centre on Climate Change and Adapted Land Use

Federal Ministry of Education and Research

Dedication

I dedicate this thesis to my parents, Soussou SAMBOU and Fatou CAMARA. Thank you for your unfailing support and encouragement. Your love has given me confidence, motivation, stability and strength. You are the artists of my beautiful life. May Lord provide you with health and long life.

Acknowledgments

My first acknowledgement goes to German Ministry of Education and Research (BMBF). Indeed, This PhD work is realized in the framework of the West African Science Service Center on Climate Change and Adapted Land use (WASCAL) and funded by the German Ministry of Education and Research (BMBF) in collaboration with the Benin Ministry of High Education and Scientific hosted by the University of Abomey Calavi, Benin.

I am also grateful to the Institute of Research and Development (IRD) for their grant support.

I am grateful to my supervisor, Prof. Expédit Wilfrid VISSIN, for his support, guidance, comments, solicitude, and great kindness.

I am deeply grateful to my daily supervisors, Stefan LIERSCH and Hagen KOCH for mentoring me throughout my scientific journey. Thanks for your patience, your supervision, and your constructive comments.

My special thanks to my supervisor, Jean ALBERGEL, for his guidance, endless motivation and support during this journey.

I thank Prof Julien ADOUNKPE and Prof Emmanuel LAWIN, Director and Deputy director respectively of the WASCAL Graduate Research Program Climate Change and Water resource (Benin), for their efforts and encouragement.

I would also like to thank the president of the jury, the reviewers and the examiner of the thesis.

I also thank my brothers, Bafing Cyprien SAMBOU, Ousmane SAMBOU, Michel Abdoulaye SAMBOU and Claude Babacar SAMBOU, for their encouragement.

I also thank my friends for his unwavering support during this journey.

I want to thank my WASCAL colleagues for their support.

Abstract

Located between Mali, Senegal, Mauritania and Guinea, the Senegal River Basin (SRB) is a strategic region for the socio-economic development of these countries. The Senegal River Basin is divided into three main parts: The upper basin, the valley and the delta. The Bafing watershed is the main tributary of the Senegal River and is located in the Upper Senegal River Basin. The management of the Bafing watershed in time and space is possible thanks to the Manantali hydropower dam. The Manantali dam aims to meet the growing water, energy and agriculture need of the member states (Senegal, Mali, Guinea, Mauritania). The organization for the development of the Senegal River (OMVS) plans to build new hydropower dams (Koukoutamba, Boureya) upstream of the Manantali dam to increase hydropower potential in the Bafing watershed.

In the future, water availability and hydropower generation are expected to be profoundly impacted, mainly due to the change in river flow caused by population growth, climate change, and Land use/land cover (LULC) change. In the coming decades, climate change and changes in LULC will further increase the constraints on the already scarce water resources in West Africa. Despite the number of studies and projects carried out on the Bafing watershed, there are not yet studies that have addressed the hydrological and hydropower potential (HPP) responses considering the combined impact of future climate change, LULC change and the future development of planned dams in the Bafing watershed. Therefore, this study aims to fill this gap by investigating the future impacts of climate change, LULC change, and altered water resource management on the water availability and hydropower potential (HPP) in the Bafing watershed.

Firstly, two precipitation products (reanalysis (W-era5) and satellite (CHIRPS)) were compared to the observed precipitation of the Bafing Makana station due to insufficient data caused by numerous gaps in the historical time series. This exercise was done to select the best precipitation product to reproduce the observed precipitation. The results showed that W-era5 represents the observed data more accurately than CHIRPS. After, ten downscaled and bias-adjusted Global Climate Models from ISIMIP 3b were investigated to determine whether the models satisfactorily replicate the reference climate (temperature and precipitation of W-era5) of the Bafing watershed. The results indicated that the 10 GCMs could successfully replicate the reference climate. Hence, the median of the 10 GCMs (MME) was used to analyze the future trend in the near future (P1:2035-2065) and the far future (P2:2065-2095/2066-2095) compared to the reference period (P0:1984-2014) under ssp 126 and ssp 370. The results indicated that, according to the median (MME), a rise in temperature by 1.4°C and 2.0°C under ssp126 and ssp370 is predicted in the near future. In the far future, the difference between both climate scenarios is much larger and spans from 1.6°C to 3.7°C. Projected precipitation is uncertain in the future. Indeed, precipitation is predicted to increase under ssp126 or decrease under ssp 370 in the near future. In the far future, precipitation is expected to decrease under both scenarios.

Secondly, the past and future LULC change was analyzed between 1986 to 2020 and 2020 to 2050. Landsat images and the random forest classification method were used to map LULC of 1986, 2006 and 2020. Future LULC map in 2050 were simulated under business-as-usual assumptions with the Multi-Layer Perceptron and Markov Chain method embedded in the Land Change Modeller software. The LULC change was analyzing using the post classification change detection technique, a pixel-based method. The results showed that between 1986 to 2020, vegetation, settlement, cultivated area and water increased, while the bareground decreased. Between 2020-2050, the results indicated that vegetation, settlement, cultivated area, and water are projected to increase. The Bafing watershed has seen a trend towards "more people, more trees".

Thirdly, an eco-hydrological water management model, the Soil and Water Integrated Model (SWIM), was set up and used to generate river discharge and simulate existing and future dams. SWIM model was driven by ten downscaled and bias adjusted GCMs under ssp 126 and ssp 370 and LULC maps (1986, 2020, 2050). The analysis was carried out using a separation method that includes combining the two components (climate and LULC) and adjusting one factor at a time while holding the other constant. The result indicated that SWIM satisfactorily reproduces the observed flow with statistical performance measures (NSE, KGE) between 0.7 and 0.8. Reservoir module also satisfactory reproduce the inflow, outflow, and water level of the Manantali dam. Under the impact of climate change, the result of the SWIM simulation indicated that the inflow and the HPP of the Manantali dam will decrease except in the near future under ssp 126, following the general trend of the precipitation in the future. Under the impact of LULC change, the inflow and the HPP of the Manantali dam will decrease by -5% and -5.7 respectively due to the conversion of bareground (with high runoff coefficients) to vegetation and cultivated area (low runoff coefficients) during the period 1986-2050. Under the effects of climate change and LULC change, the result of the SWIM simulation pointed out that LULC change has less impact on the inflow and the HPP of the Manantali dam than climate change.

Investment in future dams has advantages, such as increased water storage, greater hydropower potential and improved flood protection. However, future dams will be negatively affected by climate change in the future (except in the near future under ssp 126), and their operation will lead to a loss in the hydropower potential of the Manantali dam. Therefore, the implementation of adaptation techniques to mitigate the impact of climate change and LULC change, as well as the effects of the environmental and social impacts of these dams is essential. Adaptation techniques can be an optimization program or adopting a new common energy policy promoting an energy mix that prioritizes renewable energies, namely solar and wind. The results of this study provide relevant information to the OMVS for the management of the Bafing watershed.

Keyword: Climate change, Land use land cover change, Hydropower generation, water resource management, Bafing watershed, Senegal River Basin

Synthesis

Résumé

Situé entre le Mali, le Sénégal, la Mauritanie et la Guinée, le fleuve Sénégal est une région stratégique pour le développement socio-économique de ces pays. Le bassin du fleuve Sénégal est divisé en trois parties principales : le Haut bassin, la vallée et le delta. Le bassin versant du Bafing est le principal affluent du fleuve Sénégal et est situé dans le haut bassin versant du fleuve Sénégal. La gestion du bassin versant du Bafing est possible dans le temps et dans l'espace grâce au barrage hydroélectrique de Manantali. Le barrage de Manantali vise à répondre aux besoins croissants en eau, en énergie et en agriculture des États membres (Sénégal, Mali, Guinée, Mauritanie). L'organisation pour la mise en valeur du fleuve Sénégal (OMVS) prévoit de construire de nouveaux barrages hydroélectriques (Koukoutamba, Boureya) en amont du barrage de Manantali pour augmenter le potentiel hydroélectrique dans le bassin versant du Bafing.

À l'avenir, la disponibilité de l'eau et le potentiel hydroélectrique devraient être profondément impactées, principalement en raison de la modification du débit des fleuves causée par la croissance démographique, le changement climatique et le changement de l'utilisation des terres et de la couverture terrestre. Malgré la quantité d'étude et de projets sur le bassin versant du Bafing, il n'existe pas encore d'études qui ont abordé la question du potentiel hydrologique et hydroélectrique compte tenu de l'impact combiné du changement futur du climat, de l'utilisation des terres et de la couverture terrestre et du développement des barrages prévus dans le bassin versant du Bafing. Par conséquent, l'objectif de cette étude vise à combler cette lacune en étudiant les impacts du changement climatique, de l'utilisation des terres et de la couverture terrestre et des futurs barrages sur la disponibilité de l'eau et le potentiel hydroélectrique dans le bassin versant du Bafing.

Tout d'abord, les données de deux produits de précipitations (réanalyse (W-era5) et satellite (CHIRPS)) ont été comparées aux précipitations observées en raison de données insuffisantes, causées par de nombreuses lacunes dans les séries chronologiques historiques de la station de Bafing Makana. Cet exercice a été fait pour sélectionner le meilleur produit de précipitation qui reproduit les précipitations observées. Les résultats ont montré que W-era5 représente les données observées avec plus de précision que le CHIRPS. Après cela, dix modèles climatiques globaux (MCG) corrigés de biais et réduits d'échelle de l'ISIMIP 3b ont été analysé pour déterminer si les modèles reproduisent de manière satisfaisante le climat de référence (température et précipitations de W-era 5) durant la période historique (1979-2014). Les résultats ont indiqué que les dix MCG reproduisent avec succès le climat de référence. Par conséquent, la médiane d'ensemble des dix MCG a été utilisée pour analyser la tendance future à l'horizon 2050 (P1 :2035-2065) et à l'horizon 2080 (P2:2065-2095 /2065-2095) par rapport à la période de référence (P0:1984-2014) selon les deux scénarios climatique ssp 126 et ssp 370. Les résultats montrent qu'une augmentation de la température de 1,4 ° C et de 2,0 ° C est prévue à l'horizon 2050 selon les deux scénarios ssp 126 et ssp 370. À l'horizon 2080, la différence entre les deux scénarios climatiques est beaucoup plus grande et s'étend de 1,6 ° C à 3,7 ° C. Les précipitations projetées sont incertaines à l'avenir. En effet, les précipitations devraient soit augmenter selon ssp126 ou soit diminuer selon ssp370 à l'horizon 2050. Les précipitations devraient diminuer selon les deux scénarios à l'horizon 2080.

Ensuite, le changement de l'utilisation des terres et de la couverture terrestre passé et futur a été analysé entre 1986 à 2020 et 2020 à 2050. Les images Landsat et la méthode de classification Random Forest ont été utilisées pour réaliser les cartes de l'utilisation des terres et de la couverture terrestre de 1986, 2006 et 2020. La future carte de l'utilisation des terres et de la couverture terrestre de 2050 a été simulée selon des hypothèses de statu quo avec le modèle Multi-Layer Perceptron et Markov Chain intégrée dans le logiciel Land Change Modeller. Les résultats ont montré qu'entre 1986 et 2020, les zones d'habitat, zones d'eau, végétation, et les zones de culture ont augmenté, tandis que les sols nus ont diminué. Entre 2020 et 2050, les résultats ont indiqué que les zones d'habitat, zones d'eau, végétation, et les zones de culture devraient continuer à augmenter. Une tendance vers "plus de gens, plus d'arbres" est observée dans le bassin versant du Bafing.

Puis, le Soil and Water Integrated Model (SWIM), a été utilisé pour générer le débit et simuler les barrages existants et futurs. Le modèle SWIM a été piloté par les dix MCGs corrigés de biais et réduits d'échelle d'ISIMIP 3b selon les deux scénarios (ssp 126, ssp 370) et les cartes d'utilisation des terres et de couverture terrestre (1986, 2020, 2050). L'analyse a été effectuée à l'aide d'une méthode de séparation qui comprend la combinaison des deux composantes (climat et LULC) et l'ajustement d'un facteur à la fois tout en maintenant l'autre constant. Le résultat indique que modèle SWIM reproduit de manière satisfaisante le débit observé avec des performances statistique (NSE, KGE) comprises entre 0,7 et 0,8. Le module réservoir reproduit

également de manière satisfaisante le débit entrant, le débit sortant et le niveau d'eau du barrage de Manantali.
Sous l'impact du changement climatique, le résultat de la simulation du modèle SWIM a montré que le débit et le potentiel hydroélectrique du barrage de Manantali vont diminuer dans le futur, sauf dans à l'horizon 2050 selon le ssp 126, suivant ainsi la tendance générale des précipitations projetées. Sous l'impact du changement de l'utilisation des terres et de la couverture terrestre, le débit et le potentiel hydroélectrique du barrage de Manantali vont diminuer de -5% et -5,7 respectivement en 2020 et 2050 en raison de la conversion des sols nus (coefficients de ruissellement élevés) en végétation et en zones de culture (faibles coefficients de ruissellement). Sous les effets du changement climatique et du changement l'utilisation des terres et de la couverture terrestre, les résultats de la simulation du modèle SWIM ont mis en évidence le fait que le changement l'utilisation des terres et de la couverture terrestre a un impact plus faible sur le débit et le potentiel hydroélectrique de Manantali que le changement climatique.
L'investissement dans les futurs barrages présente des avantages, tels que l'augmentation du stockage de l'eau, du potentiel hydroélectrique et une meilleure protection contre les inondations dans le bassin versant du Bafing. Cependant, les futurs barrages seront négativement affectés par le changement climatique et l'utilisation des terres et de la couverture terrestre à l'avenir (sauf à l'horizon 2050 selon le ssp 126), et leur exploitation entraînera une perte du potentiel hydroélectrique du barrage de Manantali. Par conséquent, la mise en œuvre de techniques d'adaptation pour atténuer l'impact du changement climatique et de l'utilisation des terres et de la couverture terrestre sont nécessaires. Les techniques d'adaptation peuvent être un programme d'optimisation ou l'adoption d'une nouvelle politique énergétique commune favorisant un mix énergétique qui privilégie les énergies renouvelables, à savoir le solaire et l'éolien. Les résultats de cette étude fournissent des informations pertinentes à l'OMVS pour la planification et la gestion des ressources en eau.

***Mots clés** : Changement climatique, changement de l'utilisation des terres et de la couverture terrestre, production hydroélectrique, gestion des ressources en eau, bassin versant du Bafing, Fleuve Sénégal.*

Introduction

L'eau douce - une ressource fragile - est essentielle à la vie, au développement et à l'environnement (ICWE, 1992). Le premier des quatre principes de Dublin (ICWE, 1992) reflète parfaitement la place de l'eau dans nos sociétés. La ressource en eau est utilisée dans de nombreux secteurs d'activité (agriculture, industrie, tourisme) et en particulier dans le secteur de l'énergie. L'accès à l'énergie est une condition nécessaire à la vie, car elle détermine la satisfaction des besoins sociaux fondamentaux (Keeble, 1988). La transition vers les énergies renouvelables est devenue une nécessité face à l'épuisement prévu des combustibles fossiles et à l'immense défi posé par le changement climatique (Tarroja et al., 2019a; Zakara, 2007). L'exploitation des barrages hydroélectriques est considérée par de nombreux gouvernements et organisations internationales comme une composante essentielle d'une croissance économique durable, en particulier dans les pays en voie de développement (Harrison et al., 1998; IHA, 2019, 2022). En plus de la production d'électricité, les barrages hydroélectriques présentent d'autres avantages tel que l'atténuation des pénuries d'eau douce, la réduction des émissions de gaz à effet de serre (GES) (Kumar et al, 2011; François, 2014 ; Berga, 2016; Fan et al., 2020).

Conscients de tous les bénéfices économiques des barrages hydroélectriques, les états riverains du fleuve Sénégal situés en Afrique de l'Ouest (Sénégal, Mali, Mauritanie, Guinée) se sont regroupés au sein de l'Organisation pour la mise en valeur du fleuve Sénégal (OMVS) dans le but de gérer conjointement les ressources en eau du bassin du fleuve Sénégal. Très tôt un programme d'infrastructure a été défini pour régulariser les débits du fleuve et produire de l'énergie bon marché grâce à la construction de barrages

hydroélectriques (Manantali, Felou, Gouina) (Bader , 2014; Bruckmann, 2016; Anne et al., 2017). L'OMVS gère plusieurs barrages sur le bassin du fleuve Sénégal avec différents usages tels que le barrage de Manantali dans le bassin versant du Bafing. L'OMVS planifie la construction de nouveaux barrages hydroélectriques (Koukoutamba, Boureya) en amont du barrage de Manantali pour augmenter la production hydroélectrique dans le bassin versant du Bafing.

Si les barrages hydroélectriques présentent de nombreux avantages, leurs impacts environnementaux et sociaux, et leur vulnérabilité au changement climatique, posent la question de leur pertinence, notamment en Afrique. La relation entre l'hydroélectricité et le changement climatique est complexe. D'une part, l'hydroélectricité diminue les émissions de gaz à effet de serre (Berga, 2016). D'autre part, le changement climatique devrait modifier le débit des cours d'eau, ce qui affectera la disponibilité et la fiabilité de la production hydroélectrique (Kumar et al, 2011; Schaeffer et al., 2012; Loucks and Beek, 2016; Ranzani et al., 2018). Notre planète est confrontée à la question du changement climatique, qui menace tous les secteurs économiques (IPCC, 2021a). *L'Afrique de l'ouest souffre d'une vulnérabilité importante face à la variabilité et au changement climatique depuis 1970 (Descroix et al. 2013; Cisse et al. 2014; ; Faye 2017; Diallo et al. 2020). Les projections du changement climatique indiquent qu'une modification des cours d'eau est prévue en Afrique (Sylla et al., 2018) et dans le bassin du fleuve Sénégal (Mbaye et al., 2018). Le futur climat mondial est incertain et pourrait avoir de graves répercussions sur l'hydroélectricité à l'avenir (Kim et al., 2022; Sun et al., 2022; Wasti et al., 2022).*

En plus du changement climatique, les changements dans l'utilisation des terres et de la couverture terrestre (LULC), tels que la croissance urbaine et l'augmentation des zones cultivées, peuvent modifier le cycle hydrologique (Chang et al., 2018; Solly et al., 2021). Les LULC peuvent affecter l'écosystème, l'évapotranspiration, la capacité d'infiltration du sol et les régimes d'écoulement de surface et souterrain (Albergel, 1987; Descroix et al., 2013a; Chinwendu, 2019; Roland, 2021). Albergel (1987) a noté une augmentation du débit de la zone sahélienne, malgré la diminution des précipitations. Descroix et al. (2013b) a confirmé cette situation à travers son étude sur l'évolution des pluies extrêmes et la résurgence des inondations au Sahel. Cette situation est décrite comme le « paradoxe sahélien ». Elle est principalement due à la dégradation de la surface terrestre. Par conséquent, les modifications de la surface terrestre sous l'action conjointe de l'homme (déforestation et culture) et du climat ont un impact significatif sur le cycle de l'eau. La question à savoir comment le changement climatique et le LULC auront un impact sur la disponibilité de l'eau et le potentiel hydroélectrique (HPP) des barrages dans le monde en général et en Afrique est cruciale.

Malgré le nombre important d'études et de projets réalisés dans le bassin versant du Bafing (Sambou et al., 2003; Bodian, 2012; Cisse et al., 2014; Bader et al., 2015; Thiam, 2016 ; Faty, 2017; Sane et al., 2017; Ndione et al., 2018; Faye, 2015, 2023), une étude axée sur le potentiel impact du changement climatique et du changement de l'utilisation des terres et de la couverture terrestre sur les ressources en eau et le potentiel hydroélectrique n'a pas encore fait l'objet d'une étude. En effet, il n'existe pas encore d'études qui ont abordé la réponse du HPP compte tenu de l'impact combiné du changement climatique futur, du changement futur LULC et du développement des barrages prévus (Koukoutamba et Boureya) dans le bassin versant du Bafing.

Par conséquent, cette étude vise à combler cette lacune en étudiant les impacts du changement climatique, du LULC et des futurs barrages sur la disponibilité de l'eau et le potentiel hydroélectrique dans le bassin versant du Bafing. Cette étude est divisée en plusieurs objectifs à savoir :

1) *Évaluer la performance de dix modèles climatiques globaux (MCG) corrigés de biais et réduits d'échelle du CMIP 6 de l'ISIMIP 3b pour reproduire le climat observé dans le bassin versant du Bafing et analyser les tendances futures du climat (température et précipitation) dans le bassin versant du Bafing.*
2) *Analyser les changements spatio-temporels passés et futurs de l'utilisation des terres et de la couverture terrestre (LULC) dans le bassin versant du Bafing.*
3) *Évaluer l'impact du changement climatique, des changements de l'utilisation des terres et de la couverture terrestre (LULC) sur la disponibilité en eau et le potentiel hydroélectrique des barrages existants et prévus dans le bassin versant du Bafing.*

Les résultats de cette étude seront d'une grande importance pour les états membres de l'OMVS.

Zone d'étude

La zone d'étude est le bassin versant du Bafing (Figure 1) située dans le Haut bassin versant du fleuve Sénégal. Le Bafing est le principal affluent du fleuve Sénégal et alimente le barrage de Manantali. Il couvre une superficie de 38400 km². Il couvre le nord-ouest de la Guinée Conakry et le sud-est du Mali et s'étend sur les latitudes 10°30′ et 12°30′ N et les longitudes 12°30′. Sa source est le massif du Fouta Djallon en Guinée, qui se trouve à 15 kilomètres de Mamou et dont l'altitude moyenne est de 1200 mètres (Bodian, 2012). La topographie de la zone d'étude est très accidentée dont l'altitude diminue du Sud au Nord (1370 à 100 m). Les formations géologiques du bassin sont dominées par les granitoïdes et ne permettent pas l'existence de nappes importantes. Le climat comprend deux régimes du Sud au Nord (climat guinéen, climat soudanien). La végétation est constituée de forêts denses dégradées au sud et de forêts ouvertes de savane forestière et de savane boisée au nord. Cette densité de la végétation se traduit par une résistance au ruissèlement (Bodian, 2012). Les estimations démographiques ne sont pas très précises. L'agriculture, la pêche, et l'élevage sont les principales activités menées dans ce domaine. Tous ces éléments influencent fortement le comportement hydrologique du bassin versant.

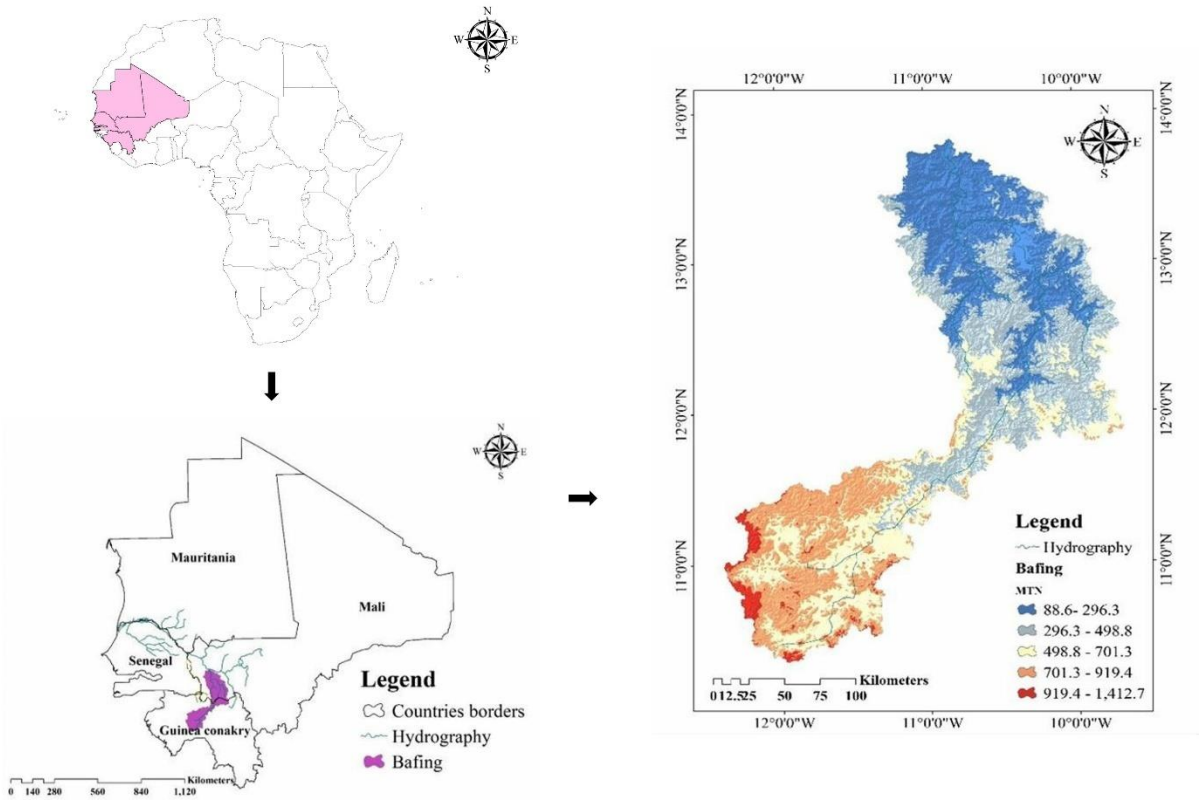

Figure 1: Localisation du bassin versant du Bafing

Données, Matériels et méthodes

1. *Objectif n° 1*

Évaluer la performance de dix modèles climatiques globaux (MCG) du CMIP 6 de l'ISIMIP 3b pour la reproduction du climat observé (température et précipitation) et analyser les tendances futures du climat (température et précipitation) à l'horizon 2050 (P1 : 2035-2065) et à l'horizon 2080 (P2 : 2065-2095) par rapport à la période de référence (P0 : 1984-2014) selon les scénarios ssp 126 et ssp 370.

- *Données*

Les données utilisées pour atteindre l'objectif spécifique sont les données journalières de précipitation de W-era 5 (1979-2016) et de CHIRPS (1981-2022), les données journaliers et mensuelles de précipitation observés (1981-1986 ; 2001-2003) et les données climatiques journaliers de MCG de ISIMIP 3b (CanESM5, CNRM-CM6-1, CNRM-ESM2, EC-Earth3, GFDL-ESM4, IPSL-CM6A-LR, MIROC6, MPI-ESM1-2-HR, MRI-ESM2-0, UKESM1-0-LL).

- *Matériel et méthode*

La série des données observées présente des lacunes et sont insuffisantes à des fins de modélisation dans le bassin versant du Bafing. Ainsi, afin de choisir le meilleur produit de précipitation, les produits de précipitations W-era 5 (donnée réanalyse) et CHIRPS (donnée satellite) ont été comparés aux précipitations observées de la station de Bafing Makana. La performance de ces produits à représenter les tendances observées a été analysée sur la base d'indicateurs statistiques, tels que R^2, RMSE, Pbias, NSE et le

diagramme de Taylor au pas de temps mensuels et annuels. Après, la performance des MCG de l'ISIMIP 3b à reproduire le climat de référence au cours de la période 1979-2014 a été évaluée sur la base d'indicateurs statistiques (R^2, RMSE, Pbias, NSE), le diagramme de Taylor et l'analyse des tendances historiques. Ensuite, l'analyse des tendances futures du climat (précipitation, température) a été effectuée à l'horizon 2050 (P1 : 2035-2065) et à l'horizon 2080 (P2 : 2065-2095) par rapport à la période de référence (P0 : 1984-2014) selon les scénarios ssp 126 et ssp 370.

2. *Objectif spécifique n° 2*

Analyser les changements spatio-temporels passés et futurs de l'utilisation des terres et de la couverture terrestre de 1986 à 2050.

- *Données*

Les images Landsat pour les années d'intérêt 1986, 2006 et 2020 ont été sélectionnées basées sur la disponibilité des données Landsat sur Google Earth Engine, pour réaliser les cartes LULC. Le modèle numérique d'élévation (MNE), la distance par rapport à la route, la distance par rapport au fleuve et la distance par rapport aux zones habitées ont été inclus en tant que données supplémentaires.

- *Matériel et méthodes*

La cartographie de LULC pour les années d'intérêts (1986, 2006 et 2020) a été réaliser en utilisant la méthode de classification Random Forest (RF) dans la plateforme de Google Earth Engine (GEE) (Gorelick et coll., 2017; Shelestov et coll., 2017). Les images Landsat de 1986, 2006 et 2020 ont été utilisées pour construire les cartes de LULC. La cartographie a été réalisée en trois étapes à savoir le prétraitement d'image Landsat, la classification supervisée avec la méthode de classification de Random Forest et l'évaluation de la précision de la classification. Cinq classes de LULC à savoir les zones d'habitat, zones d'eau, végétation, zones de culture, et les sols nus ont été utilisées dans la classification. Une matrice de confusion a été générée dans GEE et la précision globale (O), la précision de l'utilisateur (U), la précision du producteur (P) et l'indice kappa (K) ont ensuite été utilisés pour évaluer la fiabilité de la classification. La prédiction du changement de LULC pour l'année d'intérêt 2050 a été effectuée à l'aide du modèle hybride le Multilayer Perceptron neural network (MLP) and Markov chain (MLP_MC) intégré dans le logiciel Land Change Modeller (LCM). La prédiction de changement de LULC à l'horizon 2050 s'est faite en cinq étapes : l'analyse des changements, l'identification des variables explicatives, la création de cartes de potentiel de transition, la prévision du changement et la validation du modèle. Pour la validation du modèle, les cartes de LULC des années 1986 et 2006 ont été utilisées pour l'analyse de changement, la création des cartes du potentiel de transition et la prédiction de la carte LULC de 2020. Les indicateurs de performance tels que le caractéristique opérationnelle relative (ROC) et les statistiques de validation d'indices Kappa (Kno, Klocation, KIA) entre la carte classifiée et la carte prédite de 2020 ont été utilisés pour évaluer la précision de la prédiction (Ponce et Batchu, 2003). Après avoir démontré la capacité de notre modèle à prédire la carte LULC de 2020, la même technique de simulation a été utilisé pour prédire les cartes LULC de 2050 en utilisant les cartes de la couverture terrestre de 1986 et 2020 sur la base du scénario Business As Usual (BAU) (Mas et al., 2014).

3. *Objectif n° 3*

Évaluer l'impact du changement climatique, du changement de l'utilisation des terres et de la couverture terrestre sur la disponibilité de l'eau et le potentiel hydroélectrique des barrages existants et prévus à l'horizon 2050 (P1: 2035-2065) et à l'horizon 2080 (P2: 2065-2095) par rapport à la période de référence (P0: 1984-2014) selon les scénarios ssp 126 et ssp 370 et sur la base des changements de l'utilisation des terres et de la couverture terrestre de 1986 à 2050.

- *Données*

Les données utilisées pour atteindre l'objectif spécifique n° 3 sont les données climatiques de ISIMIP 3b (1984-2095), de W-era 5 (1984-2014), de débit de la station de Bafing Makana et de Dakka Saidou (1979-2014), topographiques (DEM MERIT), les cartes de l'utilisation des terres et de couverture terrestre de 1986, 2006, 2020 et 2050 et les caractéristiques physiques des barrages (Manantali, Koukoutamba et Boureya).

- *Matériel et méthodes*

Le modèle hydrologique Soil and Water Intergrated Model (SWIM) a été choisi pour simuler les processus hydrologiques dans le bassin versant du Bafing en vue de la prise en compte des changements de LULC, du changement climatique et des barrages (existants et futures). Le calage du modèle a été fait durant la période 1979-1986 et la validation sur la période 1987- 1993 avec l'intégration des barrages (Manantali, Koukoutamba et Boureya). Les scénarios de développement (SD) ont été établi de manière que les futurs barrages soient pris en compte dans la simulation. Dans le contexte de cette étude, l'intérêt principal est d'évaluer l'effet du changement climatique et du changement de LULC sur l'hydrologie et le potentiel hydroélectrique (HPP) dans le bassin versant de Bafing en considérant d'abord le barrage de Manantali seul (SD1), puis le barrage de Manantali et de Koukoutamba (SD2), ensuite le barrage de Manantali, de Koukoutamba et de Boureya (SD3). L'hypothèse selon laquelle le changement climatique et le changement de LULC sont indépendants a été faite afin de séparer les contributions respectives de ces deux facteurs. Leurs effets ont été calculés à l'aide d'une méthode de séparation qui consiste à modifier un facteur à la fois (soit le climat, soit le LULC en maintenant l'autre constant) et la combinaison des deux facteurs (Fenta Mekonnen et al., 2018). Un ensemble d'indicateurs de performance pertinents tel que la fiabilité, le volume déversé et les probabilités de dépassement (P99, P90, P95) a été utilisé pour comparer les changements futurs avec la période de référence.

Résultats et discussion

Les résultats de la comparaison des données de la précipitation de W-era5 et de CHIRPS avec les données observées indiquent que les données de W-era 5 représentent les précipitations observées avec une plus grande précision que les données de CHIRPS. Ainsi, les données de W-era 5 ont été utilisées comme données de référence pour évaluer la performance de dix MCG de l'ISIMIP 3b et pour la calibration et la validation du modèle hydrologique. Ce choix est également justifié par le fait que la correction du biais et la réduction d'échelle des dix MCG de ISIMIP 3b ont été fait avec les données de W-era5. Les résultats ont montré que les dix MCG sont capables de reproduire la structure unimodale des précipitations, la structure bimodale de la température, ainsi que la tendance historique des précipitations et températures de W-era 5. La médiane d'ensemble (MME) a été utilisée pour analyser et décrire les tendances futures du climat à l'horizon 2050 (P1) et à l'horizon 2080 (P2) par rapport à la période de référence (P0). Selon la médiane d'ensemble

(MME), une augmentation de la température est projetée à l'horizon 2050 (P1) et à l'horizon 2080 (P2) selon les deux scénarios (ssp 126 et ssp 370). Pour la projection de la précipitation, il y a beaucoup d'incertitudes. En fait, les précipitations devraient soit augmenter selon le ssp126, soit diminuer selon le ssp 370 à l'horizon 2050 (P1). À l'horizon 2080 (P2), les précipitations devraient diminuer selon les deux scénarios (ssp126 et ssp 370).

Les résultats des cartes de LULC indiquent que le Random Forest (RF) a fourni une classification très satisfaisante. Les résultats de la détection des changements post-classification de 1986 à 2020 ont montré que les surfaces occupées par les zones d'habitat, zones d'eau, végétation, et les zones de culture ont augmenté, tandis que les sols nus ont diminué de manière significative entre 1986 et 2020. Dans un contexte de croissance socio-économique, démographique, ainsi que de déforestation, l'augmentation de la végétation entre 1986 et 2020 est un résultat intéressant. En effet, la surface occupée par la végétation est passée de 36% à 44%, devenant la classe d'occupation la plus dominante en 2020. L'augmentation de la végétation, des zones d'habitat, et des zones de culture suggèrent que lorsque la croissance démographique s'accompagne de l'adoption de pratiques de gestion durable des terres, elle peut conduire à une meilleure conservation des terres et de l'eau. En effet, dans le sud du bassin versant du Bafing en Guinée (Fouta Djallon), l'intensification écologique des activités rurales établie depuis longtemps ne menace pas la végétation (Descroix et al., 2020). Au nord du bassin versant du Bafing au Mali, plusieurs projets, tels que la réserve de faune du Bafing (Mali), le statut de réserve de biosphère (Mali), ont été adoptés pour lutter contre les pertes de biodiversité après la construction du barrage de Manantali (Faty, 2017). Les résultats de la modélisation de LULC indiquent que le modèle MLP-MC dans LCM a raisonnablement simulé la carte de l'utilisation des terres et de la couverture terrestre de 2020 et peut-être utilisé pour projeter la carte LULC de 2050 du bassin versant du Bafing. En 2050, les résultats de la prédiction montrent que la végétation couvrira 49% de la zone d'étude, soit une augmentation de 3% par rapport à 2020. Il s'ensuit des zones d'habitat avec une augmentation de 1% par rapport à 2020. Les sols nus seront la troisième classe avec 22%, ce qui représente une perte de 6% par rapport à 2020. Les zones d'eau et les zones de culture augmenteront pour atteindre 4,8% de la superficie totale. L'analyse de la dynamique de l'état de surface a révélé que la croissance démographique et l'évolution des activités anthropiques (socio-économiques) étaient les principaux moteurs des changements de LULC.

Le modèle hydrologique SWIM a été utilisé pour simuler les processus hydrologiques et la gestion des barrages dans le bassin versant du Bafing. Les résultats des simulations effectuées par le modèle SWIM suite au paramétrage, au calage et à la validation ont montré que le modèle SWIM reproduit les débits observés de manière satisfaisant avec des valeurs de Nash et de KGE supérieur à 0,8 et 0.7 respectivement pour la période de calibration (1979-1986) et de validation (1987-1993). Le module barrage de SWIM reproduit également de manière satisfaisant la dynamique des apports, des débits sortants et du niveau d'eau du barrage de Manantali.

Dans un premier temps, l'impact du changement climatique sur le débit et le potentiel hydroélectrique (HPP) du barrage de Manantali a été analysé à l'horizon 2050 (P1) et à l'horizon 2080 (P2) par rapport à la période de référence (P0) selon les scénarios ssp 126 et ssp 370. Les résultats de la simulation du modèle

SWIM ont montré que le débit et le potentiel hydroélectrique (HPP) du barrage de Manantali suivent la tendance générale des précipitations projetées. À l'horizon 2050 (P1), une augmentation du débit entrant de 6% entraînera une augmentation de la HPP de 3% selon la ssp 126 ou une réduction du débit entrant de -1% entraînera une perte de -1% de HPP selon le ssp 370 du barrage de Manantali. À l'horizon 2080 (P2), une diminution du débit entrant de -4% et -8% entraînera une diminution de HPP de -8% et -14% respectivement selon le ssp 126 et le ssp 370.

Ensuite, l'impact du changement de LULC sur le débit et le potentiel hydroélectrique (HPP) du barrage de Manantali a été examiné de 1986 à 2050. Les résultats ont indiqué que le changement de LULC a un impact négatif sur le débit entrant et le HPP du barrage de Manantali. En effet, le changement de LULC entraînera une diminution de -5% du débit et de -5,7% du HPP respectivement entre 1986-2050. Ces résultats peuvent s'expliquer par la conversion des sols nus (avec des coefficients de ruissellement élevés) à la végétation et aux zones de culture (coefficients de ruissellement faible) au cours de la période d'étude (1986,2020,2050). Le bassin versant de Bafing a connu une tendance « plus de gens, plus d'arbres ».

Par la suite, l'analyse de l'impact combiné du changement climatique et de l'utilisation des terres et de la couverture terrestre sur le débit et le potentiel hydroélectrique (HPP) du barrage de Manantali a montré que bien que le changement de LULC ait un effet significatif sur le débit et le potentiel hydroélectrique (HPP) du barrage de Manantali, il est moindre face à celui du changement climatique. En effet, même si le changement de LULC réduit le HPP du barrage de Manantali de -5% en P1 selon le ssp126, les simulations combinées du changement climatique et de LULC prévoient toujours une augmentation de 3,2% du HPP du barrage Manantali. Ces résultats confirment l'hypothèse de Albergel (1987) et Bernadette Nnomo (2016) selon laquelle pour un bassin versant soudanien comme celui du Bafing, la diminution du débit est un effet de la détérioration du climat plutôt que celui du changement de LULC.

Ensuite, l'effet de développement des futurs barrages (DS2, DS3) sur le potentiel hydroélectrique (HPP) du bassin versant du Bafing a été examiné. Les résultats de la simulation ont montré que l'exploitation conjointe des trois barrages (DS3) augmente le potentiel hydroélectrique (HPP) moyenne annuelle de 820 GWh/a (Manantali) à 2207 GWh/a (Manantali, Koukoutamba et Boureya) sur la période de référence (P0). De plus, les futurs barrages (Koukoutamba et Boureya) réduiront le risque que le niveau d'eau du barrage de Manantali atteigne le seuil inférieur de turbine, ce qui améliorera sa fiabilité. Les futurs barrages contribueront également à la réduction des volumes déversés en régulant le débit de pointe en amont du barrage de Manantali, réduisant ainsi le risque d'inondation dans la vallée du fleuve Sénégal. Bien que les futurs barrages vont augmenter le HPP dans le Bafing, ils seront négativement affectés par le changement climatique et le changement de LULC sauf à l'horizon 2050 (P1) selon le ssp 126. Il est donc essentiel de trouver des stratégies d'adaptation (programme d'optimisation ou mix énergétique) pour ajuster le fonctionnement de ces trois barrages et pour faire face aux effets des changements futurs.

Conclusion

Le présent travail décrit l'impact du changement climatique, du changement de LULC ainsi que des futurs aménagements hydrauliques (Koukoutamba, Boureya) sur la disponibilité de l'eau et le potentiel hydroélectrique dans le bassin versant de Bafing.

- *Sous l'effet du changement climatique, le débit et le potentiel hydroélectrique du barrage de Manantali vont diminuer sauf à l'horizon 2050 (P1) selon le ssp 126. Ces résultats peuvent être attribués à la projection du changement climatique sur le bassin versant du Bafing.*
- *Sous l'effet du changement de l'utilisation des terres et de la couverture terrestre, le débit et le potentiel hydroélectrique (HPP) du barrage de Manantali vont diminuer à cause de la conversion des sols nus (avec des coefficients de ruissellement élevés) à la végétation et les zones de culture (coefficients de ruissellement faible) au cours de la période d'étude (1986,2020,2050). Le bassin versant de Bafing connait une tendance « plus de gens, plus d'arbres ».*
- *Sous l'effet du changement climatique et de l'utilisation des terres et de la couverture terrestre, la variation du débit et du potentiel hydroélectrique est causée par la modification du climat plutôt que celui du changement de l'utilisation des terres et de couverture terrestre.*
- *L'investissement dans les futurs barrages présente des avantages, tels que l'augmentation de stockage de l'eau, l'augmentation du potentiel hydroélectrique et l'amélioration de la protection contre les inondations. Cependant, les barrages seront affectés négativement par le changement climatique à l'avenir (sauf à l'horizon 2050 (P1) selon le ssp 126), et leur exploitation entraînera des pertes du potentiel hydroélectrique du barrage de Manantali. La mise en place d'une stratégie d'adaptation pour ajuster le fonctionnement de ces trois barrages et pour faire face aux effets du changement climatique et de l'utilisation des terres et de la couverture terrestre est primordiale. Un programme d'optimisation ou un mix énergétique combinant l'hydroélectricité, l'énergie solaire et l'énergie éolienne sont des solutions d'adaptation pertinente.*

Bien qu'il existe des incertitudes liées à la modélisation (hydrologique avec SWIM, l'utilisation des terres et de couverture terrestre avec LCM), le présent travail a contribué à améliorer la planification et la gestion des ressources en eau dans le bassin versant du Bafing dans le cadre du changement climatique et du changement de LULC. En effet, les résultats obtenus fournissent des informations pertinentes à l'OMVS pour la planification et la gestion des ressources en eau.

Cependant, il serait important d'étudier davantage les conséquences du changement climatique, de l'utilisation des terres et de la couverture terrestre sur le potentiel hydroélectrique, l'agriculture, l'irrigation, et la navigation dans le bassin versant du Bafing. En effet, des informations additionnelles sur les pertes du potentiel hydroélectrique en faveur d'autres utilisations telles que l'irrigation, le soutien aux crues pour l'agriculture de décrue et les services écosystémiques connexes seront d'une importance capitale pour permettre une stratégie de gestion intégrée des aménagements hydrauliques conformément aux objectifs de développement durable (ODD), en particulier la faim zéro (2), l'eau propre et l'assainissement (6), l'énergie propre et abordable (7), la vie aquatique (14).

Table of content

List of Acronyms and Abbreviations

Acronyms	Significations
BAU	- Business as Usual
CA-MC	- cellular automata-Markov chain
CHIRPS	- Climate Hazards Group Infrared Precipitation with Stations
CMIP	- Coupled Model Intercomparison Project
CORDEX	- Coordinated Regional Climate Downscaling Experiment
DEM	- Digital elevation modele
DS	- Development scenario
EROS	- Earth Resources Observation and Science
ESA	- European Space Agency
GCM	- Global Climate Model
GEE	- Google Earth Engine
GHGs	- Greenhouse Gas emissions
GWh/y	- Gigawattheure by year
HBV	- Hydrologiska Byråns Vattenbalansavdelning
HPP	- Hydropower generation
HRU	- hydrological response unit
IPCC	- Intergovernmental Panel on Climate Change
ISIMIP	- Inter-sectoral Impact Model Inter-comparison Project
KGE	- Kling-Gupta Efficiency
KIA	- Kappa for agreement index (KIA)
Klo	- Kappa for location (denoted Klocation)
km²	- square kilometer
Kno	- Kappa for no information (Kno),
LCM	- Land Change Modeller
LDCs	- least developed countries
NDVI	- Normalized Difference Vegetation Index
NDWI	- Normalized Water Difference Index
NDBI	- Normalized Difference Accumulation Index
m	- meter
MLP_MC	- Multilayer Perceptron neural network and Markov chain
Mm	- millimeter
MME	- median of the 10 Global climate model from ISIMIP 3b
MODIS	- Moderate-Resolution Imaging Spectroradiometer
MW	- Megawatt
NSE	- Nash-Sutcliffe efficiency
O	- overall occuracy
OMVS	- Organisation pour la Mise en Valeur du fleuve Sénégal
P (90, 95, 99)	- probabilities of exceedance (90,95,99)
P	- Producer accuracy
Pbias	- Percentage of Bias
PIDA	- Program for Infrastructure Development in Africa

R2	-	Pearson correlation
RCM	-	Regional climate model
RF	-	Random Forest
RMSE	-	Root Mean Square Error
ROC	-	relative operational characteristic
RPCs	-	Representative Concentration Pathways
SDG	-	Sustainable development goal
SOGED	-	Société de Gestion et d'exploitation de Diama
SPOT	-	Système Probatoire d'Observation de la Terre
SRB	-	Senegal River Basin
SRES	-	Special Report on Emissions Scenarios
SSPs	-	Shared Socio-Economic Pathways
ST-MC	-	Stochastic Markov chain
SWAT	-	Soil and Water Assessment Tool
SWIM	-	Soil and Water Integrated Model
U	-	user accuracy
WASCAL	-	West African Science Service Centre on Climate Change and Adapted Land Use
WCRP	-	World Climate Research Program
W-era 5	-	Watch Forcing Data methodology applied to ERA5 reanalysis data.

List of Figures

List of Tables

Chapter 1 : General Introduction

Chapter 1 presents an overview of the research, the context and problem statement, literature reviews and the identified gaps in knowledge. We have also dealt with the research questions, the main and specific objectives, hypothesis and novelty, as well as the scope of the thesis with expected results and benefits. The outline of the thesis concludes this chapter.

1.1 Context and problem statement

Freshwater - a fragile resource - is essential for life, development, and the environment (ICWE, 1992). The first of the four Dublin principles (ICWE, 1992) reflects perfectly the place of water in our societies. The water resource is used to supply drinking water for the populations and in many sectors of activity (agriculture, industry, tourism), particularly in the energy sector. Water and energy are inseparable. Indeed, Water is involved in most energy conversion methods (power plant cooling, hydropower generation, and extraction of conventional and non-conventional fossil resources) (Olsson and Lund, 2017). Access to energy is a necessary condition for growth as it determines the satisfaction of basic social needs (Keeble, 1988). The African continent is relatively lagging regarding access to energy, both in rural and urban areas. In 2014, half of the continent's population of 1.2 billion people did not have access to electricity (Cantoni and Musso, 2018). According to Berga (2016), there are 1.2 billion people without access to energy in the world, mostly in Africa and Asia (where 80% of the people live in rural regions). To ensure sustainable development in Africa, the issue of access to energy for all is at the forefront. The transition to renewable energies has become necessary with regard to the projected depletion of fossil fuels and the immense challenge posed by climate change (Tarroja et al., 2019a; Zakara, 2007). Many countries in the world promote the development of green energy in an environmentally friendly manner. The deployment of renewable energy has been re-motivated by the severe environmental and economic effects of fossil fuel-based energy sources (Tarroja et al., 2019b). Many governments and international organizations view the exploitation of the hydropower potential of dams as an essential component of sustainable economic growth, particularly in the Least Developed Countries (LDCs) (Harrison et al., 1998). In addition to power generation, hydropower dams have other advantages. The storage capacity of hydropower dams can alleviate freshwater scarcity by providing security during periods of low flow and drought for drinking water supply, irrigation, and navigation services (François, 2013; Kumar et al., 2011). In periods of high flow, these dams can also help in flood control (François, 2013; Kumar et al., 2011). Hydropower considerably reduces emissions of

greenhouse gases (GHGs) and participates in the mitigation of global warming (Berga, 2016; J. L. Fan et al., 2020). Notwithstanding their positive aspects, dams can have significant environmental and ecological issues, including habitat destruction, displacement of people and wildlife, water quality degradation, social and cultural impacts (Chirag, 2022; Wang, 2012). Indeed, the construction of large dams can result in flooding vast areas, leading to the destruction of habitats and displacement of wildlife. This can result in the loss of biodiversity and ecosystem services. Dams can also cause water quality degradation due to the accumulation of nutrients, sediments, and pollutants. This can lead to the eutrophication of water, affecting negatively aquatic ecosystems. Another side effect is the displacement of local communities and the loss of cultural heritage sites, (which can have significant social and cultural impacts) (Chirag, 2022; Wang, 2012).Thus, hydropower dams developed and operated in an economically viable, environmentally sound and socially responsible represent the best concept of sustainable development (Brundtland, 1987).

The construction of large dams in Africa is one of the responses of governments to address the significant challenges of water management, and to meet national electricity needs (Skinner et al., 2009). In Africa, 15.5% of the electricity supply is based on hydropower (Obahoundje and Diedhiou, 2022). Hydropower dams are a crucial source of electricity generation, especially in Eastern and Southern Africa (Conway et al., 2017). According to Conway et al. (2017), 90% of national electricity generation in Ethiopia, Malawi, Mozambique, Namibia and Zambia comes from hydropower dams (Conway et al., 2017). West Africa has invested relatively little in large-scale hydropower infrastructure, and the Senegal and Niger basins allow more than 90% of the runoff to pass through, even though it could be used for agriculture, irrigation and hydropower generation (Anne et al., 2017). More than 50% of hydropower potential (HPP) in West Africa is yet untapped, but some large hydropower dams have been built and other projects are underway (Kabo-Bah, 2018). The share of hydropower in the energy mix is expected to continue to increase and to promote clean and renewable energy driven by national and regional energy plans such as the Program for Infrastructure Development in Africa (PIDA) (Conway et al., 2017). Scientific interest in hydropower in Africa is growing, due to the significance of hydropower in African countries and for compliance with the Paris Agreement (Obahoundje and Diedhiou, 2022).

Aware of all the economic benefits of hydropower dams, the States bordering the Senegal River (Senegal, Mali, Mauritania, Guinea) have come together within the "L’Organisation pour la

Mise en Valeur (OMVS) du fleuve Sénégal". "L'Organisation pour la Mise en Valeur du fleuve Sénégal" is a French acronym that translates to "Organization for the development of the Senegal River (OMVS)". The OMVS is an intergovernmental organization established in 1972 by the governments of Senegal, Mauritania, Mali, and Guinea with the goal of jointly managing and developing the water resources of the Senegal River Basin. The primary objectives of the OMVS are to develop the hydropower potential of the river, to improve irrigation for agriculture, to facilitate navigation, and to promote integrated water resources management in the basin. The OMVS oversees the management of water resources and infrastructure projects in the basin and is responsible for ensuring that the benefits of these projects are equally shared among the countries. The organization has played a key role in the development of the Senegal River Basin, including the construction of the Manantali multipurpose dam in the Bafing watershed, the Diama Dam in the valley, and the Felou and Gouina hydropower dam in Senegal watershed. These projects have contributed to the economic development of the basin by providing electricity, improving irrigation, and facilitating navigation. OMVS continues to work on various water management and infrastructure projects in the basin to improve the livelihoods of the people living in the region. Energy is a strategic choice for the OMVS (Anne et al., 2017; Bader , 2014; Bruckmann, 2016). In the whole area (Senegal, Mali, Mauritania, Guinea), weak access to electricity is a real obstacle to development. These countries face severe shortages and growing energy demands. The current requirement of the basin's riparian States is estimated at 4400 GWh/year. If the increase rate is maintained, the energy needs will be of the order of 15000 GWh in 2040 (Thiam, 2016). OMVS manages several dams on the Senegal River Basin with different uses (Diama, Manantali dam, Guinea and Felou). Simultaneously with the construction of dams, the OMVS is carrying out an integrated management strategy for shared facilities in line with Sustainable Development Goals (SDGs), specially:

- The Zero Hunger (2),
- Clean Water and Sanitation (6),
- Clean and Affordable Energy (7),
- Aquatic Life (7).

The OMVS is also planning the construction of new hydropower dams at Koukoutamba and Boureya in the Bafing watershed with the objective of boosting hydropower generation in the watershed.

While hydropower dams have many advantages, their environmental and social impacts and vulnerability to climate change raise the question of their relevance with the current form, particularly in Africa. The relationship between hydropower and climate change is complex. On the one hand, hydropower significantly avoids greenhouse gas emissions and mitigates global warming (Berga, 2016). On the other hand, climate change is expected to alter river flows, which will affect the availability and reliability of hydropower generation (Berga, 2016). According to Teotónio et al. (2017), the energy system is one of the economic sectors most impacted by climate change. Indeed, changes in river flows (runoff volume, variability and seasonality of discharges) and extreme weather phenomena (floods and droughts) associated with climate change can have an impact on water availability and hydropower generation (Kumar et al, 2011; Schaeffer et al., 2012; Loucks and Beek, 2016; Ranzani et al., 2018). Several studies have shown that rainfall variations have strongly influenced the evolution of flows in West Africa over the last decades (Faye, 2015; Sadio et al., 2020). Climate change projections indicate that river regimes are expected to change in Africa (Sylla et al., 2018). The future global climate is uncertain and could have severe implications for hydropower in the future (Harrison et al., 1998; Kumar et al, 2011; Ranzani et al., 2018; Tarroja et al., 2019; Vicuña et al., 2011). The demand for a reliable supply of clean water to meet energy, food and industrial needs of a growing population and to maintain viable natural ecosystems continues to grow (Loucks and Beek, 2016). As climate change becomes more evident, there is increasing interest in identifying possible impacts on different sectors of the economy (Vicuña et al., 2011).

In addition to climate change, changes in land use/land cover (LULC), such as increases in cultivated area or settlement, can alter the hydrological cycle. Changes in LULC can affect the ecosystem, evapotranspiration, soil infiltration capacity, and surface and subsurface flow regimes (Albergel, 1987). Albergel (1987) has noted the increase in the runoff of the Sahelian zone, despite the decrease in rainfall. Descroix et al. (2013b) have confirmed this situation by studying the evolution of extreme rains and the resurgence of floods in the Sahel. This situation is described as the "Sahelian paradox", mainly due to land surface change. Changes in LULC under the joint actions of man (deforestation and cultivation) and climate significantly impact the water cycle. Knowledge of LULC change is one of the essential, necessary information for an integrated water management system (Richaud et al., 2019).

The question of how climate and land use/land cover change (LULC) will impact the water availability and the hydropower potential (HPP) in the world in general, and specially in Africa is crucial. The potential impacts of climate change on hydropower dams were carried out by numerous works to assess the consequences on water availability and hydropower potential (Schaefli et al., 2007;Hamududu and Killingtveit, 2012; Schaeffer et al., 2012; François, 2013; Sun et al., 2022; Wasti et al., 2022; Kim et al., 2022). In West Africa, few studies have been devoted to the impact of climate change and LULC change on water availability and hydropower generation, particularly in the Senegal River Basin. The West African Regional Centre on Renewable Energy and Energy Efficiency (ECREEE, 2017) states that although the consequences of climate change on West Africa's water resources are well established, research on how they may affect hydropower generation is lacking. Because of the importance and urgency of this issue, studies to assess the impacts of climate change and LULC change on the water availability and the hydropower potential of the Senegal River Basin are of great importance to the member states of the OMVS.

1.2 **Literature review**

This section provides an overview of climate change, the main issues raised by the effects of climate change and LULC change on water and hydropower generation reported in the literature. Additionally, it presents the state of the art of hydrological modelling and previous studies in the Bafing watershed.

1.2.1 Climate change

The climate system is a complex, interactive system composed of the atmosphere, land surface, snow and ice, oceans and others water bodies (Treut et al., 2007). The climate system varies over time under the influence of its internal dynamics and due to changes caused by external factors (called ‘forcings’) (Treut et al., 2007). External factors seem to be linked to human activity, which contributes to the release of greenhouse gases (carbon dioxide, methane) into the atmosphere (Biasutti, 2019). The warming of the climate system is strongly linked to the atmosphere-land-ocean system (Ashenafi, 2014). Climate models are essential tools for evaluating changes in climate due to external forcing and internal variability (Hausfather et al., 2020). A climate model is a computer simulation based on mathematical equations (Ashenafi, 2014). Climate models are the main instrument used to describe the behavior and interactions between the different components of the climate system (atmosphere, oceans, rivers, soil and ice) (Kattsov et al. 2013; Ashenafi 2014). They help reproduce past conditions and anticipate

how the climate system is likely to be modified on a global and regional scale (Kattsov et al. 2013; Ashenafi 2014). Climate models offer the opportunity to project future climate for various scenarios using external forcings such as anthropogenic Greenhouse Gas emissions (GHGs) and population growth and activities (Ly et al., 2019). The Coupled Model Intercomparison Project (CMIP) outputs are among the climate outputs used in the climate impact assessment. The Coupled Model Intercomparison (CMIP) is set up to conduct coordinated climate simulations among diverse research groups. This initiative, led by the World Climate Research Program (WCRP), enables a better understanding of the differences between climate models and the uncertainties brought on by model inaccuracy. There are two types of climate models: the Global Climate Model (GCM) and the Regional Climate Model (RCM). Global climate models (GCMs) can cover and simulate realistically large-scale characteristics of atmospheric circulation over the globe. They have a coarse horizontal resolution (100-200 km), with a poor representation of relief, topographic gradient, and land use (Ambrizzi et al., 2019). These are essential forcings of mesoscale circulations for global impact studies (Ambrizzi et al., 2019). Therefore, local climate replication by GCMs is challenging.

To address the situation, "dynamic or statistical" downscaling techniques have been developed to achieve much finer spatial resolutions of the order of 10 to 50 km. Two international projects, the Inter-sectoral Impact Model Inter-comparison Project (ISIMIP; https://www.ISIMIP.org) and Coordinated Regional Climate Downscaling Experiment (CORDEX; http://www.cordex.org), have been established to define harmonized climate projections for the impact and adaptation of climate change studies at the regional scale and to deepen our understanding of regional climate (Giorgi et al., 2009; ISIMIP, 2018). The ISIMIP provides a bias adjustment and statistical downscaling to 0.5 degrees using GCM from CMIP6 (Coupled Model Intercomparison Project phase 6) (Liersch et al., 2023). Future projections are available for 10 GCMs from CMIP6 (Liersch et al., 2023). The CORDEX provides a dynamic downscaling using RCMs from different models and spatial resolution for the regional domains from CMIP5 (e.g. 0.11 degrees in Europe, 0.44 degrees in Africa) (Nikulin et al., 2012). The difference between these two experiments lies in the selection of models from the GCMs. For ISIMIP, models are selected from a subset of globally consistent models (Ito et al., 2020). In contrast to ISIMIP, the CORDEX project is a region-specific model subset for each region of interest (Ito et al., 2020).

To assess the future impact of the evolution of the GHGs emitted into the atmosphere, a

multitude of projections of population growth and its activities have been developed. Climate projections are typically presented for various scenarios using external forcings such as solar radiation, aerosols, natural, anthropogenic GHGs emissions, and population growth (Ly et al., 2019). Scenarios are plausible representations of an uncertain future climate and help to explore climate change (IPCC, 2021a). The scenarios cover a wide range of the main drivers of GHGs including demographic, economic and technological aspects. In its Sixth Assessment Report, the Intergovernmental Panel on Climate Change (IPCC) recommended the Shared Socio-Economic Pathways (SSPs), a group of emission scenarios utilized in CMIP6 to define the development of GHGs by 2100 (Masson-Delmotte et al., 2021). The Shared Socio-Economic Pathways (SSPs) scenarios are the most complex created to date and span a range from very ambitious mitigation to ongoing growth in emissions. The SSPs represent alternative storylines about how the world might develop over the coming century based on different climate policy assumptions. The SSPs combine elements from the previous two iterations of scenarios, the Special Report on Emissions Scenarios (SRES) and Representative Concentration Pathways (RPCs). The SSPs were designed to work with an updated version of the RCPs. Five SSPs (Figure 2, Table 1) were created, with varying assumptions about human development, including population, education, urbanization, gross domestic product, economic growth, rate of technological development, GHGs, aerosol emissions, energy supply and demand, LULC changes, etc. A core set of five illustrative scenarios based on the Shared Socio-Economic Pathways (SSPs) are consistently used: ssp 119, ssp 126, ssp 245, ssp 370, and ssp 585. These scenarios cover a broader range of greenhouse gas and air pollutant futures, including high-CO2 emissions pathways without climate change mitigation and new low-CO2 emissions pathways (Figure 2) (IPCC, 2021b). These ssp 126 and ssp 370 were chosen to comply with the Paris Agreement by pursuing efforts to limit temperature increase to 1.5°C above pre-industrial levels within the framework of ssp 126 (which is the sustainable development scenario) and ssp 370 (the regional rivalry or medium-high scenario). Moreover, they have never been used in the study area. Table 1 briefly overviews each of the five scenario narratives (Riahi et al., 2017).

Table 1:Climate scenario definition (Riahi et al., 2017).

Shared Socio-Economic (SSPs)	Definition
SSP1-1.9	Very ambitious scenario to represent the 1.5°C target of the Paris Agreement
SSP1-2.6	Sustainable Development Scenario or moderate scenario
SSP2-4.5	Intermediate scenario
SSP 370	Scenario of regional rivalries or medium–high scenario
SSP5-8.5	Development based on fossil fuels

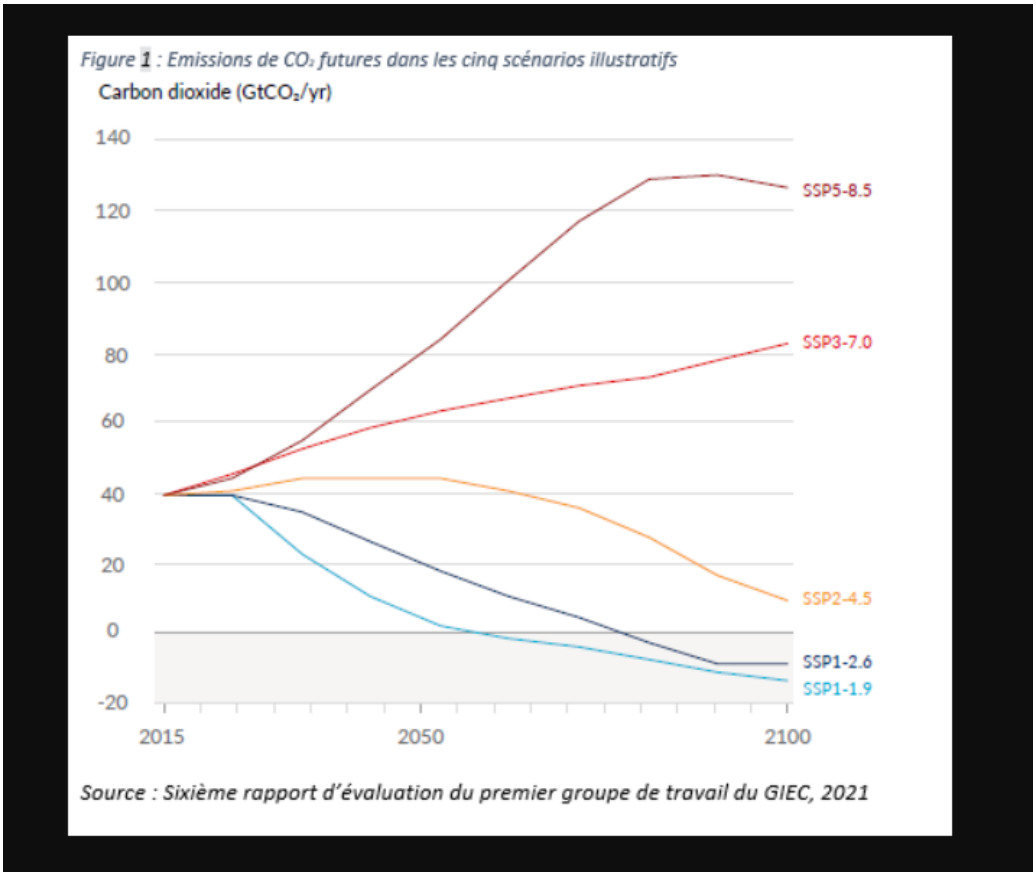

Figure 2:Climate scenario from IPCC (https://www.i4ce.org/dou-viennent-les-cinq-nouveaux-scenarios-du-giec-climat/)

1.2.2 Climate change and water resources

Like many other regions in the world, water resources in West Africa are facing changes in climate. Several studies have shown that climate change has strongly influenced the evolution of flows in West Africa since 1970 (Cisse et al., 2014; Descroix et al., 2013b; Diallo et al., 2020; Faye, 2017). Oyebande and Odunuga (2013) analyzed climate change impact on water resources at the transboundary basin in West Africa: the cases of Senegal, Niger, and Volta River Basins. Their findings showed a decrease in river flows, groundwater levels and accelerating desertification. Mahe et al. (2011) carried out a study to provide a global overview of hydrological changes in the Niger River in its various sub-catchments. Their results revealed that there has been substantial inter-annual variability in flows at Koulikoro and in the upstream basins since 1907 and a sharp decrease since 1970. Soro et al. (2011) analyzed climate variability and its impact on water resources in the Bandama watershed in Côte d'Ivoire. Their findings showed a decrease between 13% to 28% in rainfall and 58% in flow between 1966 and 1981. Sadio et al. (2020) studied the hydroclimatic variability and change in the watershed of the Casamance River in Senegal. The results obtained by Sadio and his co-researchers showed high potential evapotranspiration (1993–2013) and considerable rainfall deficits (1970s and 1980s). The study of hydro-climatic variability over the period 1955-1992 by Vissin (2007) showed that the rainfall deficits of the 1970s and 1980s were greatly amplified in the flows of all the rivers (Mékrou, Alibori, Sota) of the Beninese basin of the Niger River. In recent years, a recovery of rainfall is noted in WA after the drought period of 1960-1970. Several authors mention a recovery in rainfall in West Africa (Lebel et al., 2009; Diop et al., 2016; Bodian et al., 2020; Nouaceur and Murarescu, 2020). Bodian et al. (2020) studied the hydroclimatic variability and change between 1940 and 2013 in the Senegal River Basin (SRB). These findings indicate a rise in yearly rainfall in the SRB, which raises surface water availability. Climate change projection is uncertain in West Africa. Projections show that river flow are expected to change in many West African basins (Bates, 2008). Ouémé River is projected to decrease about 6.58 m^3/s under Representative Concentration Pathways (RCP 4.5) while an insignificant increasing trend is found under RCP 8.5 (Lawin et al., 2019). The Senegal River, for example, is expected to experience a decrease in water availability (Mbaye et al., 2018). According to the results obtained by Ardoin-Bardin (2004), the variations in flows in the future follow those in precipitation: for example, a decrease for the Senegal River and an increase for the Chari basin in Tchad.

1.2.3 Land use/land cover change and water resource

Changes in land use and land cover (LULC) are a global challenge and a major area of study for global change research (Verburg et al., 2011; Chang et al., 2018). Land use (habitat, agricultural) and land cover (forests, wetlands, grasslands and water) have different meanings and are often used interchangeably (Tadese et al., 2021). LULC changes are the result of changes in the Earth's land surface, such as the transformation of natural land cover (forests, grasslands and deserts) into human-dominated ecosystems (cities, agricultural and industrial areas) (Liping et al., 2018; Winkler et al., 2019). These changes significantly affect critical elements of our natural capital, such as vegetation, water resources and biodiversity (Chang et al., 2018; Solly et al., 2021). Globally, the findings of LULC change research by Winkler et al. (2019) showed that various LULC change occurred over around one-third of the planet between 1960 and 2019. Several areas of the Earth's surface have recorded these changes (Roy et al., 2015; Solly et al., 2021). However, due to several influencing factors, the dynamics of LULC change vary globally from one region to another (Berihun et al., 2019). Although anthropogenic influences have been identified as the primary agents of change, other elements such as slope, appearance, and altitude can also have an impact on these changes (Subedi et al., 2013; Kleemann et al., 2017; Anwar et al., 2022).

In West Africa, where agriculture is the backbone of the economy (ECOWAS, 2015), gross LULC changes have also been observed (Cabral and Lagos, 2017; Andrieu, 2018; Diallo and Zhengyu, 2018; Traore, 2018; Barnieh et al., 2020; Traore et al., 2022). These authors shown that WA has undergone significant changes over the years, and the causes are generally attributed to rapid population growth and increased agricultural areas. In fact, the study conducted in West Africa by Barnieh et al. (2020) revealed a 1.6% decrease in natural vegetation cover, enormous net gains in agriculture land (107.8%), the increase of artificial water bodies, and rapid population growth. The question regarding LULC changes and their impacts on hydrological flows are of primary interest for water and land management (Blöschl et al., 2019). Several studies have been conducted in West Africa to improve information on the influences of LULC change on water resources (Albergel, 1987; Chinwendu, 2019; Descroix et al., 2013a; Roland, 2021). These works have shown that these changes influence, modify, and affect the hydrological processes of the watersheds, with great variability due to topography and the local climate.

1.2.4 Climate change, Land use/land cover change and hydropower generation

The largest and most popular renewable energy source in the world is hydropower. Hydropower generation is predicted to undergo significant changes in the twenty-first century, primarily because of the altered river flow brought on by climate change and LULC change. Existing studies have indicated that climate change may negatively affect hydropower in the future. Indeed, Vicuña et al. (2011) analyzed the effects of climate change on two high-altitude hydropower systems in California. They reported a decrease in runoff associated with precipitation decreased and temperature increased; thus reducing hydropower generation and associated revenues. Fan et al. (2020) further examined the impact of climate change on the hydropower system of China. The results showed that hydropower is sensitive and vulnerable to climate change, which leads to many uncertainties about its future development. Kim et al. (2022) also analyzed the climate change impact on water availability and hydropower generation in Northern Manitoba in Canada. Their findings indicated that hydropower generation is expected to increase in spring and summer but decrease in winter and fall. Spalding-Fecher et al. (2017) explored the impact of climate change on hydropower in the Zambezi basin. The results projected a 10-20% decrease in hydropower generation in a dry climate and a marginal increase in a humid climate. Bahati et al. (2021) examined how climate change and LULC change will affect the hydrology and hydropower generation in Ugandan rivers. Their findings indicated that there will be a large increase in annual hydropower capacity for the combined future influence of climate and LULC changes. Obahoundje et al. (2021) evaluated the impacts of (i) LULC change, (ii) climate change (CC), and (iii) development conditions on water resources and the hydropower potential in the Mono Basin (West Africa) using CORDEX data and WEAP Model. Their results showed that under both RCPs in the near (2020-2050) and far (2070-2090) futures, the temperature is expected to rise significantly, but the precipitation change is unknown. These changes in climate variables consequently affected simulated water availability and the hydropower generation the near and far futures.

1.2.5 Hydrological modelling

Water resources are variable in time and space; so their estimation at the watershed scale requires the use of hydrological models (Poncelet, 2016). Modelling the hydrological behavior of the watersheds is essential for managing water resources and land use planning (Gnouma, 2006). Hydrological modelling aims to study the water cycle and understand the interactions between precipitation, evapotranspiration, runoff, and infiltration at the spatial and temporal scales of the watershed (Leye, 2023). The hydrological model converts the climate time series

representing a watershed into a series of flows (Oñate-Valdivieso et al., 2016). A hydrological model is only a simplification of the hydrological system of a watershed (Ahbari, 2013). It involves using mathematical expressions to define quantitative relationships between inputs and outputs (Ashenafi, 2014). With the introduction of GIS, satellite remote sensing images, high-resolution digital elevation models, distributed hydrologic models, and real-time flood predictions, hydrological modelling has significantly advanced in recent years (Chinwendu, 2019). Nowadays, different models exist to simulate the hydrology cycle of watersheds under LULC and climate change. There are numerous hydrological models in the literature, ranging from global models to distributed models, and they differ mainly on their physical foundations, level of complexity, and data requirements (Singh, 1995) (Table 2).

Hydrological models can be classified according to three criteria: the way processes are described, the spatial scale, and the temporal scale (Victora et al., 2008). Considering the description of flow processes, a distinction is made between empirical, conceptual, and physics-based models. Empirical models are built around mathematical relationships that establish connections between input and output variables without considering the internal laws and processes of the watershed (Leye, 2023). Unlike empirical models, physical-based models depend on the laws of physics and physical knowledge of the system to describe the mechanisms of flows within the watershed (Sadar Shahraki et al., 2016). These patterns determine the physical processes as they occur in nature. Conceptual models rely on a particular conceptualization of how the system works while involving empirical relationships based on mathematical functions to describe it (Leye, 2023). These models treat input parameters as global ones over the entire watershed (Karambiri et al., 2003).

Depending on the spatial scale, a distinction is made between global, distributed and semi-distributed models. The global model carries out a simple hydrological balance using parameters weighted on the surface of the watershed. These models do not consider spatial variations of the input variables. Distributed models are rainfall-runoff models, considering the spatial distribution of input variables, boundary conditions and watershed characteristics (Leye, 2023). The production and transfer functions are not homogeneous throughout the watershed. The semi-distributed models were developed to combine the advantages of global and distributed models. These models are broken down into homogeneous spatial units (hydrological response units) (Krysanova et al., 2015a). Based on the temporal scale, a distinction is made between "event-based" and "continuous" models, depending on how the

model operates over time. Continuous models make it possible to continuously simulate the hydrological process and follow the evolution of state variables and outputs over a given period (Roland, 2021). In contrast, event-based models simulate hydrological processes for events such as flood episodes (Karambiri et al., 2003).

Table 2: A non-exhaustive list of some hydrological models (This Table is inspired from Soussou Sambou et al. (2003); Valentina Krysanova, Hattermann, and Wechsung (2005); Bodian (2012); Faty (2017); Didier Maria Ndione et al. (2020); Moussé Landing Sane et al. (2020))

Models	**Definition**	**Type**
MIKE SHE	Mike Système Hydrologique Européen	Physical, Distributed
HBV	Hydrologiska Byrans Vattenavdelning model	Conceptual, continuous, Semi-distributed
TOPMODEL	TOPopgraphy based hydrological MODEL	Physical, Distributed
GR (GR4J)	Génie Rural	Conceptual, global, continuous, empirical
SWAT	Soil Water Assessment Tool	Semi-distributed, continuous with physical based
HEC-HMS	Hydrologic Modelling System	Events, continuous, physically-based, distributed
SWIM	Soil and Water Integrated Model)	Semi-distributed, continuous or event-based, physically based
TOPMODEL	TOPography based hydrological model	Distributed, continuous
VIC	Variable Infiltration Capacity	Semi-distributed, conceptual, continuous

1.2.6 The Bafing watershed

The Senegal River Basin (SRB), located in West Africa, is a transboundary basin bordered by four countries: Guinea, Mali, Mauritania, and Senegal. It cumulates several sub-watersheds, including the Bafing watershed. The Bafing watershed is the main tributary of the Senegal River and feeds the large Manantali multi-purpose dam. A dense scientific bibliography exists on the Bafing watershed. Most of the works has been carried on the impact of climate change or variability on water availability. Other studies on the effects of the Manantali dam on the downstream flow have been carried out. Cisse et al, (2014) studied the evolution of the hydrological regime to understand the effect of climate variability and dam on flows. Faye (2015) assessed the impacts of climate change and the hydraulic development on the water resources. Faty (2017) further studied the issue of climate change impact on water resources in the context of hydro-climatic variability and LULC change (2007-2014). He carried out modelling based on geospatial data and established the relationships between climate variability, LULC change and flows between 2007 and 2014. Sambou et al. (2019) investigated the influence of the Manantali dam on the water levels in Bakel for the month of September. Numerous other works relate to the management and planning of the water resources. Bodian et al. (2012) for instance, analyzed the water resources management issue in the Bafing watershed. Integrated water resource management appears to be a necessity at all levels (local, regional, national, and international) due to the often-dramatic consequences of water scarcity on the human, economic and political levels. Bader (2001) and Bader et al. (2016) have made several studies concerning Manantali dam management to satisfy the water needs of all users (Program for Optimization of Dam Management (POGR)), especially the artificial flooding for flood recession cultivation (Bader and Albergel, 2015). Thiam (2016) assessed the impacts of future dams on the long-term availability of water resources with the WEAP model. Furthermore, studies on the future effects of climate change on water resources have also been carried out. Ardoin-Bardin (2004) attempted to provide elements of knowledge on the relation between climate variability and water resources. Ardoin-Bardin (2004) assessed the impact of climate change on the flow of large rivers in West and Central Africa (Senegal, Gambia, Sassandra, Logone-Chari) based on the outputs of GCMs. Mbaye et al. (2015) assessed the future impact of climate change on water resources using bias-corrected data from REMO (regional climate model developed by the Max Planck Institute for Meteorology in Hamburg, Germany) for two scenarios particularly the representative concentration pathways RCP4.5 and RCP8.5). Sane et al. (2019) analyzed the trends and flow shifts using the SWAT model and

three GCMs from 2006-2090 at the Bafing Makana station. Ndione et al, (2020) implemented an ensemble forecasting system to provide helpful inflow forecasts of the Manantali dam.

Despite the amount of documentation and numerous projects in the Bafing watershed, a study on the potential impact of climate change and land use/land cover change on water resources and the hydropower potential has not been yet carried out. Indeed, there are no studies, up-to-now, that have addressed the hydrological and hydropower potential (HPP) response considering the combined impact of future climate change, land use/land cover change (LULC change) and the development of planned dams in the Bafing watershed.
Based on the problem statement, the following research questions are raised.

1.3 Research Questions

- What will be the effects of climate change and land use/land cover change on water availability in the Bafing watershed?

- What will be the impact of climate change and land use/land cover change on the hydropower generation of the Manantali dam in the Bafing watershed?

- What will be the positive or negative impacts of the future planned hydropower dam on water availability and hydropower generation considering climate and LULC changes in the Bafing watershed?

1.4 Objectives

1.4.1 Main objective

The main objective of the research is to assess the impacts of climate and land use/land cover change on water availability and the hydropower potential in the Bafing watershed located in the Senegal River Basin. Emphasis will be placed on current and future hydropower dams in the Bafing watershed. The proposed approach is based on the "Water-Energy " Nexus.

1.4.2 Specific objectives

The following specific objectives will be adopted to achieve the main objective of the research.

- **Specific objective 1**: To analyze the performance of Global Climate Model (GCM) of CMIP 6 from ISIMIP 3b in reproducing the observed climate (temperature and precipitation) (1979-2014) and the future (temperature and precipitation) trends for the near future (P1: 2035-2065) and the far future (P2: 2065-2095) compared to the reference period (P0: 1984-2014) under ssp 126 and ssp 370.

- **Specific objective 2:** To analyze the land use and land cover changes (LULC) based on the historical period between 1986, 2006 and 2020 and projection of the LULC change of the year 2050.
- **Specific objective 3**: To evaluate the impact of climate change, land use/ land cover changes on the water availability and hydropower potential of the existing and planned dams in the near future (P1: 2035-2065) and the far future (P2: 2065-2095) compared to the reference period (P0: 1984-2014) under ssp 126 and ssp 370 and based on LULC change from 1986 to 2050.

1.5 Hypothesis

The hypothesis of this study is as follows:

- Combined changes in climate and land use/land cover will have a negative impact on the water availability in the Bafing watershed.
- Combined changes in climate and land use/land cover will have a negative impact on the hydropower potential in the Bafing watershed.
- The exploitation of the future dams will have a positive impact on the water resource management and hydropower generation in the Bafing watershed.

1.6 Novelty

The main novelty of the thesis is the combined analyses of the climate change, land use/land cover change, and planned dams on the water management and hydropower generation in Bafing watershed.

1.7 Scope of the thesis

The OMVS works on many infrastructure and water management projects to enhance the standard of living for residents. For shared facilities, the regional organization is implementing an integrated management strategy in line with sustainable development goals, in particular, Zero Hunger (2), Clean Water and Sanitation (6), Clean and Affordable Energy (7), Aquatic Life (14). The framework of the thesis is based on quantifying the combined impacts of climate change and land use/land cover change on water and hydropower generation as well as modelling the existing and future dams in the Bafing watershed.

The thesis focuses also on the SDGs (7) (clean and Affordable Energy) under climate change and land use land/cover change in the Bafing watershed. Thus, future work should look at the synergies and trade-offs in water resources management in the Senegal River Basin considering

the SDGs (7) (clean and Affordable Energy) and the SDGs (2) (Zero Hunger) under climate change and land use/land cover change.

1.8 Expected results and benefits.

The main expected benefit of the study is that information on the future impact of climate change, land use/land cover change, and planned dams will be provided to the regional decision-makers. Such information will probably help to improve knowledge of the nexus "Water, Energy" in the Bafing watershed. It is a starting point for developing better adaptation strategies to manage water resources. Elsewhere, we hope that this research will be of interest and a great contribution on the research fields of the West African Science Service Centre on Climate Change and Adapted Land Use (WASCAL). WASCAL is an essential player in the region whose mission is to provide information and knowledge at the local, national and regional levels. One of the main goals is to create a critical mass of the next generation of scientists and specialists on various issues related to climate change through its Capacity Building Department.

1.9 Outline of the thesis

This thesis report includes a general introduction, six chapters and a general conclusion and recommendations. The outline is as follows:

Chapter 1 presents the overview of the thesis research, the state of the art, and the knowledge gaps. Moreover, research questions, main and specific objectives, hypothesis and novelty, as well as thesis scope with expected results and benefits, are described.

Chapter 2 introduces the study area. It describes the localization, relief, vegetation, climate, hydrography, soil, land use and demography, social and economic activities of the study area.

Chapter 3 deals with the overall data, materials and method used.

Chapter 4 presents the first objective, which is to evaluate the performance of GCMs of CMIP 6 from ISIMIP 3b in reproducing the observed climate (temperature and precipitation) and to analyze future (temperature and precipitation) trends for the near future (P1: 2035-2065) and the far future (P2: 2065-2095) compared to the reference period (P0: 1984-2014) under ssp 126 and ssp 370.

Chapter 5 deals with the second objective, which is to analyze the land use and land cover changes (LULC) based on the historical period between 1986, 2006 and 2020, and the projection of the LULC changes to 2050.

Chapter 6 addresses the third objective by analyzing the impact of LULC change, climate change, and the exploitation of future dams on water availability in the near future (P1: 2035-2065) and the far future (P2: 2065-2095) compared to the reference period (P0: 1984-2014) under ssp 126 and ssp 370 and based on LULC change from 1986 to 2050.

Chapter 7 addresses the third objective by analyzing the impact of LULC change, climate change and the exploitation of future dams on hydropower generation in the near future (P1: 2035-2065) and the far future (P2: 2065-2095) compared to the reference period (P0: 1984-2014) under ssp 126 and ssp 370 and based on LULC change from 1986 to 2050.

Chapter 8 summarizes the main conclusion and recommendations. It concludes the thesis by showing the main findings, providing research limitations, and giving orientation for future research.

Chapter 2: Study area

Chapter 2 presents the study area of this study. It focuses on the characteristics of the area (location, relief, vegetation, climate, hydrography, soil, land use and demographics), as well as social and economic activities. This chapter also describes existing and planned hydropower projects.

2.1 Localization

The Senegal River, located in West Africa, is the third largest transboundary basin in West Africa. The Senegal River Basin covers four countries: Guinea, Mali, Mauritania and Senegal (Figure 3). It is 1700 km long and drains a basin of approximately 300,000 km². The Senegal River Basin (SRB) is divided into three main parts: The upper basin, the valley and the delta. The study area concerns only the upper SRB, the Bafing watershed (Figure 3). The Bafing watershed is the main tributary of the Senegal River. The Bafing watershed covers an area of around 38400 km² and spreads from northwestern Guinea Conakry to southeastern Mali and extends over latitudes 10°30' and 12°30' N and longitudes 12°30'. It has its source in the Fouta Djallon's mountains. The Fouta Djalon is a natural and cultural mountainous region of middle guinea in the northern part of the country and extends to the borders of Senegal and Mali (Orange, 1990). The Fouta Djalon is unanimously recognized as "the water tower of West Africa" in reference to the many international rivers (Niger, Senegal, Gambia, Tominé and Konkouré) that have their source there (Descroix et al., 2020).

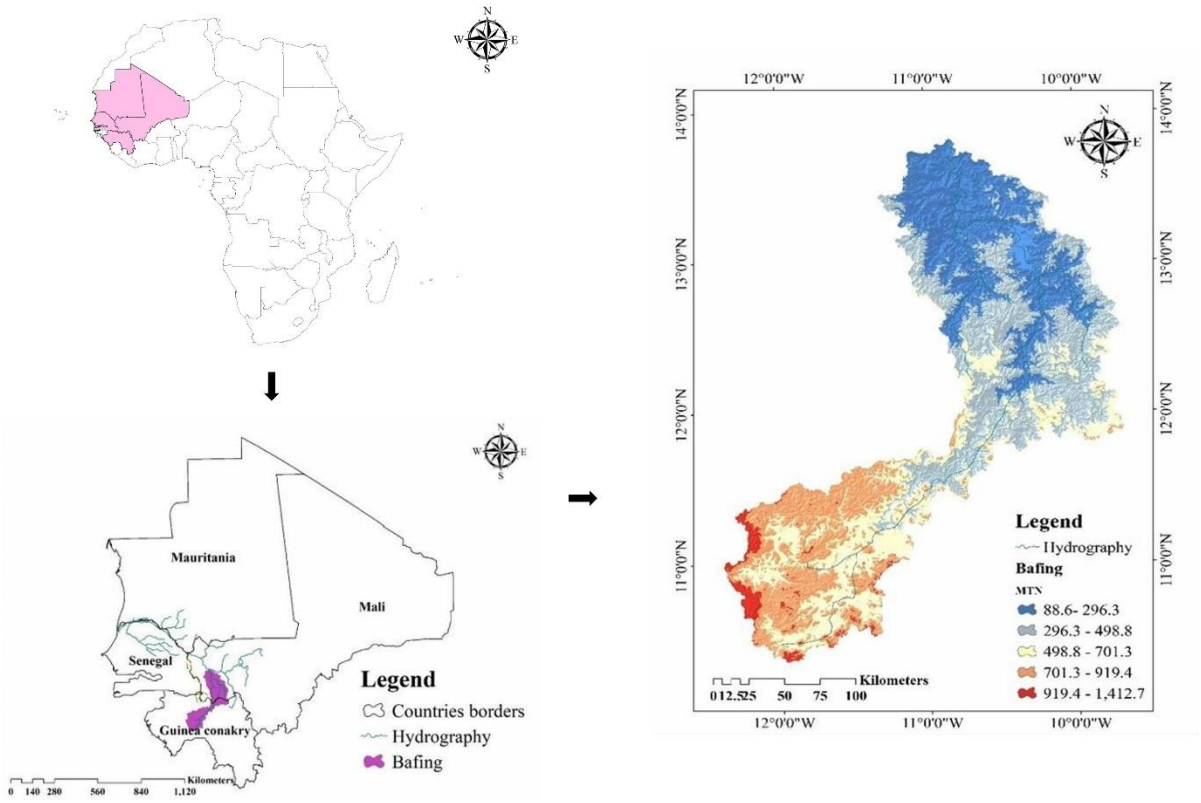

Figure 3:Location of the Bafing watershed. The background in color gradient indicates the elevations of the relief on the basin.

2.2 Relief

Relief is essential for understanding the hydrological behavior of a watershed. It establishes the soil's suitability for runoff, infiltration and evaporation (Bodian, 2012). Relief data have been established from a digital elevation model (Merit DEM). Figure 4 shows the distribution of altitudes on the basin, which vary between 89 m to 1370 m with an estimated average altitude of 338 m. The analysis of Figure 3 shows that the southern part of the Bafing watershed is the most mountainous, with altitudes between 730 and 1370 m. The altitude decreases towards the North where these plateaus reach only 100 to 400 m. The study area presents a succession of sub-tabular reliefs, consisting of dolerite and granitic formations, covered discontinuous lateritic formations (Bodian, 2012).

Figure 4:Digital Elevation Model of the Bafing watershed

Hypsometric curves and slope indices also make it possible to appreciate the relief. The hypsometric curve represents the distribution of the watershed's surface area (cumulative percentage of area) as a function of its altitude (Asfaw and Workineh, 2019). The hypsometric curve of the Bafing River appears in Figure 5. Slope indices are determined from knowledge of the hypsometric distribution over the watershed (Choudhari et al., 2018). The overall index (I_g) is obtained by the following equation:

$$I_g = \frac{\mathrm{D}}{\mathrm{L}} \quad (6)$$

Where Ig is the slope, L is the length, D is the difference of altitude,

$D = H5 - H95$ where H5 (altitude corresponding to 5% of the watershed on the hypsometric curve) and H95 (altitude corresponding to 95% of the watershed on the hypsometric curve)

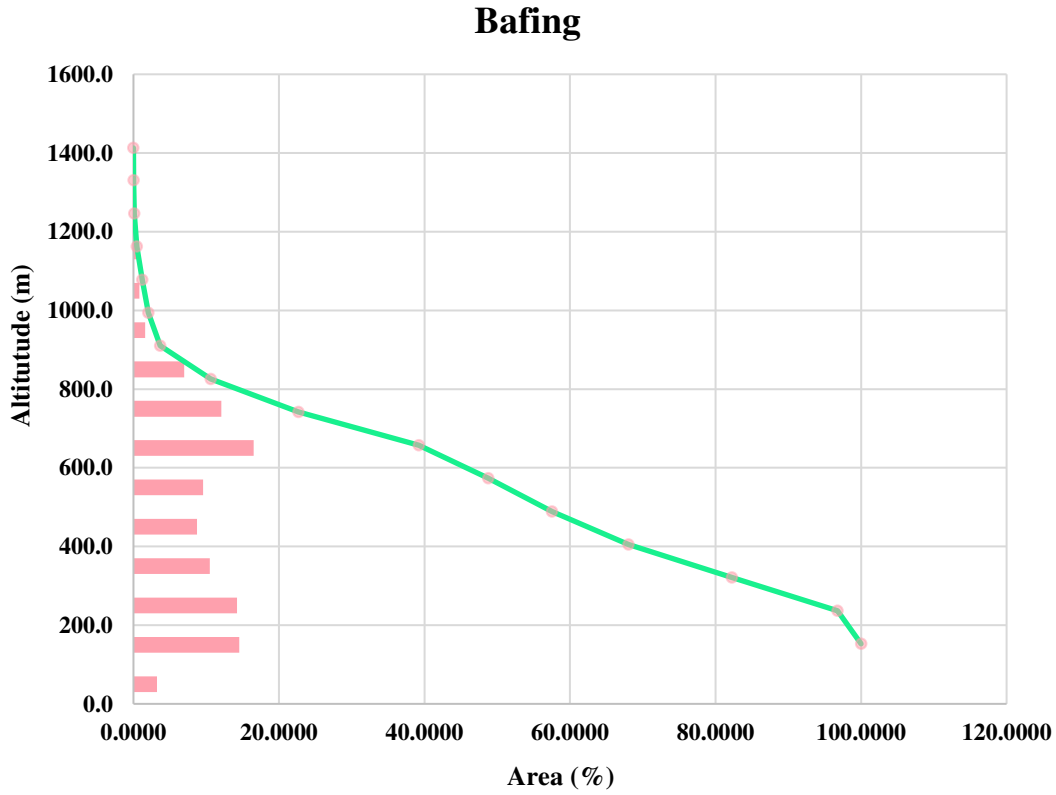

Figure 5:Hypsometric curve of the Bafing watershed

A watershed is a collector device meant to collect rainwater by channeling it to the outlet. How the volume of water is distributed over time will depend on the shape of the watershed, its relief, and the drainage network. Watershed delineation of the Bafing is based on Digital Elevation Model (DEM) data. GRASS Geographic Information System (GIS) software, a free and open-source GIS software package that is generally used for geospatial data management, analysis, and visualization, is used to determine watershed surfaces and perimeters. To characterize the shape of a watershed, the compactness index of Gravelius is used. The watershed area (S_b) (1) (km^2), the watershed perimeter (P_b) (2) (km) and the compactness index (K_g) (3) are calculated by applying the following formulas:

$$S_b = \text{Lb} \times \text{lb} \quad (1)$$

$$P_b = 2(\text{Lb} + \text{lb}) \quad (2)$$

$$K_b = 0.28 \times \frac{\text{Pb}}{\sqrt{\text{Sb}}} \quad (3)$$

With L_b (4) the equivalent rectangle length, l_b (5) the equivalent rectangle width, L_b et l_b have been calculated using by the following equations:

$$L_b = \frac{Kg\sqrt{Sb}}{1.12}\left[1 + \sqrt{1 - (\frac{1.12}{Kg})^2}\right] \quad (4)$$

$$l_b = \frac{Kg\sqrt{Sb}}{1.12}\left[1 - \sqrt{1 - (\frac{1.12}{Kg})^2}\right] \quad (5)$$

The physical characteristics of watersheds are presented in Table 3.

Table 3: The physical characteristics of the Bafing watershed (catchment and sub catchment) based on the digital elevation model (Merit DEM) and GRASS Gis*;* min=*minimun*, max=*maximun*, L= Stream length*, Ig= slope*

Catchment		Area (Km²)	Perimeter (Km)	Ig	Longueur (Km)	Largeur (Km)	Min (m) elevation	Max (m) elevation	L (km)
Catchment	Bafing	28142	1744	3	839	34	153	1415	57
Sub-Catchment	Manantali dam	6010	516	2	232	26	153	671	11
Sub-Catchment	Bafing makana	6389	597	2	275	23	223	882	12
Sub-Catchment	Dakka Saidou	921	179	2	78	12	307	904	4
Sub-Catchment	Boureya	4149	496	2	230	18	329	986	15
Sub-Catchment	Koukoutamba	10674	695	2	314	34	463	1413	14

2.3 Climate

The Bafing watershed has a Sudano-Guinean climate. The Sudano-Guinean climate which predominates in Guinea, is in transition between a very humid climate observable in the south and a drier climate of the "Sudanese" type in the north. It is explained by the movements of the Inter-tropical Boreal Front, which separates the harmattan (cool and dry wind, blowing in the North-South direction) and the Monsoon (hot and humid wind blowing in a south-north direction). These two fluxes differ from their humidity; therefore dividing the year into two distinct seasons: dry and wet. Thus, there are two weather conditions the dry season from December to March and the rainy season from May to October. The rainfall regime is unimodal, with annual rainfall varying roughly between 600 mm and 1600 mm at the Bafing Makana station, considering the periods 1979-1984 and 2001-2003. Figure 6 shows the average monthly

rainfall profile in the Bafing Makana station. It clearly pinpoints that July, August, and September are the rainiest months.

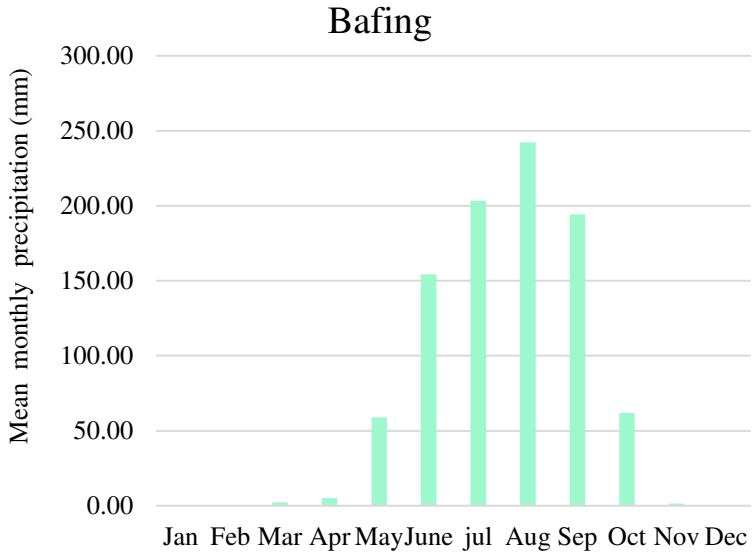

Figure 6: Average monthly rainfall at Bafing Makana over the period 1979-1984 (Observed data)

Annual temperatures vary between 23.3°C (mean minimum) and 37.7°C (average maximum) (Bodian et al., 2012). The Potential Evapotranspiration (PET) calculated by Bodian et al. (2012) with the Penman-Monteith method at the Labe station is an average of 134 mm (monthly cumulation).

2.4 Vegetation

The vegetation in the Bafing watershed is divided into two domains associated with decreasing rainfall from south to north (Bader J-C., 2014). Those domains are:

1) The Guinean domain covered by dense forest.

2) The Sudanese domain characterized in the south by open forest, savannah and parklands, whose density decreases towards the north to make way for a wooded savannah. The gallery forest is also observable. Regarding biodiversity, there are also several classified reserves (Faty, 2017):

1. The Baoulé Loop Biosphere Reserve (Mali).
2. The Bafing Wildlife Reserve (Mali).

3. The chimpanzee sanctuary (Mali) - the Bafing – Faleme transboundary protected area (Mali – Guinea), in the process of being classified as a biosphere reserve.
4. The Ramsar Bafing – Source and Bafing – Faleme (Guinea) sites.

Nowadays, the area is threatened by the extension of human settlement sites, the increase in livestock and livestock stocking in the surrounding areas, the practice of slash-and-burn agriculture, the advance of the cotton front, hunting, industrial and artisanal exploitation of gold, gold panning, deforestation, and poaching (Faty, 2017).

2.5 Hydrography

The Bafing River has its source in the Fouta-Djallon massif, about 800 meters above sea level, a source located nearly at fifteen miles northwest of Mamou, in the Guinean territory. The Bafing network (Figure 7) includes several rivers that flow between the granite and dolerite massifs forcing it to take very diverse directions (Bodian, 2012). The profiles along the Bafing River are very rugged and cut off many rapids (Figure 8). The Bafing River is 1006 km long for a total vertical drop of 789 meters, and an average slope of 0.78 %. Water drained from the Bafing watershed flows into the Manantali dam.

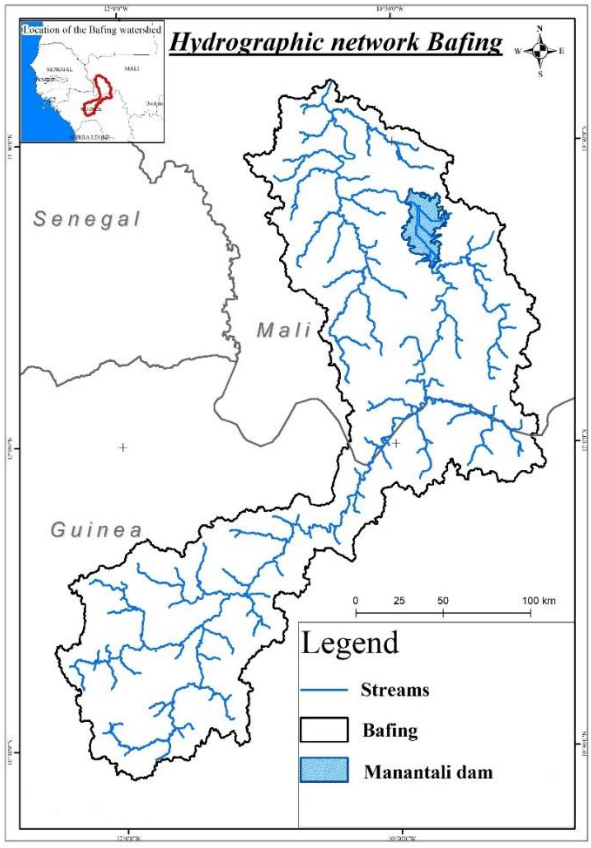

Figure 7:Spatial representation of the hydrographic network (Merit Dem and GRASS Gis)

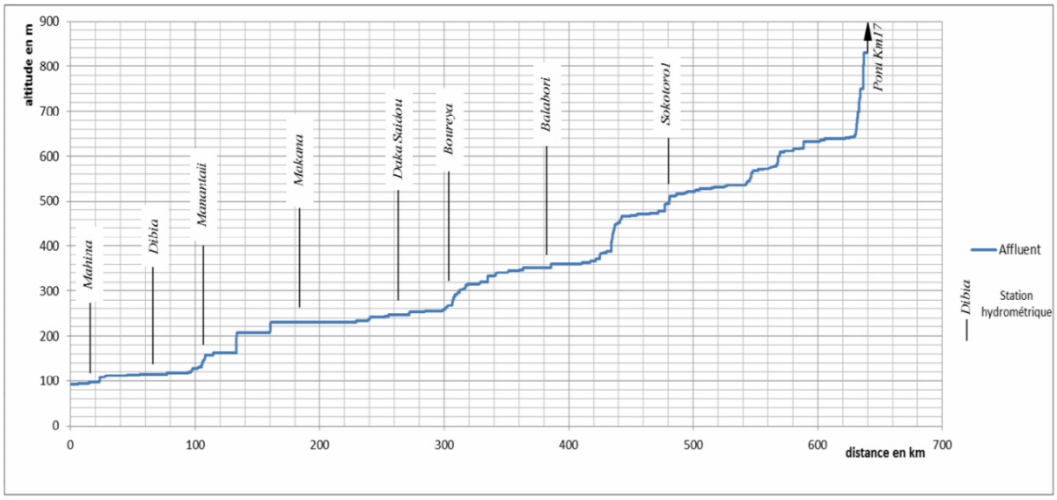

Figure 8:Hydrographic network (Bader, 2014)

2.6 Soil

The texture of different soil types, such as vertisols and para vertisols, tropical eutrophic brown soils, allomorphs, and soils rich with tropical and hydromorphic ferruginous exists in the study area. The geological formations of Fouta Djalon have undergone a long evolution during which tectonic movements, climatic changes, and variations in sea level have shaped the main landscapes through flattening surfaces. According to the report entitled "Monographie du fleuve Sénégal" by Bader in 2014, there are three types of geological formation: Precambrian bedrock, Paleozoic bedrock and Tertiary bedrock. The Precambrian bedrock is composed of schists or mica schists, quartzites and ancient rocks transformed into green stones. Granites cover these different rocks. The Paleozoic consists of sandstone, quartzites, and limestones. The tertiary is formed by clay sands of varied colours in which clay or sandstone levels are interspersed.

2.7 Demography and environmental, social, and economic activities

The population of the Bafing watershed is not accurately assessed. Agriculture (rainfed agriculture and irrigation) is the main activity in the watershed. The main crops are millet, fonio, rice, maize, potato, cassava and groundnuts. Livestock farming is the second activity. The river's mineral resources are highly exploited, especially by the development of gold panning in Mali. The current water needs of the mining sector are estimated at 13 billion m^3.

2.8 Hydropower projects

To meet the development challenge, the OMVS has made its contribution by evolving hydropower dams. The management of water resources in the SRB has been achieved through various hydraulic structures that perform multiple and sometimes contradictory functions through RUD (Resource User Decision) processes (Bader, 2014). The main hydraulic developments carried out to date on the Senegal River are the four functional dams with different vocations: the Diama (1986), the Manantali dam (1988) and Felou (July 2013) and the Gouina (Bader, 2014).

Only the Manantali dam is located in the Bafing watershed and has operated since 1987 (Bader, 2014). It has a height of 68 m and a length of 1476.35 m (Figure 9). It covers an area of 477 km² and ensures a strong regulation of the river flow. It is a multi-purpose hydropower dam designed and operated to provide various services. Such services include generating electricity (approximately 876 GWh/y of per year), mitigation of floods, low-flow support for navigation and irrigated agriculture in the valley, the supply of drinking water, flood support ensuring sufficient annual flooding in the valley for traditional agriculture practices and ecosystem maintenance (Bader and Albergel, 2015).

The management principles are defined in the Dam Optimization and Management Program (Bader et al., 2015) and aim to optimize the use of water resources in a context of competition between users. The proposed management of the Manantali dam consists of applying a series of instructions assigned by priority and management constraints. The Institut de Recherche pour le Développement (IRD) has developed the Simulsen software, which models the management of a dam in detail at daily time steps. It manages flow propagation times and allows an optimal calculation of the limit limnigrams to be respected in the Manantali dam (Bader and Rolland, 2005).

The construction of new hydropower dams is on the future agenda of the Bafing watershed. These dam projects include the Koukoutamba and the Boureya upstream of Manantali dam (Figure 9). The development of these future dams aims at improving water resource management. They will therefore play an essential role in sustainable and integrated management that reconciles economic objectives, social well-being and environmental concerns. They are considered assets for the restoration and sustainable management of the river ecosystem in general (Bader, 2014; Faty, 2017).

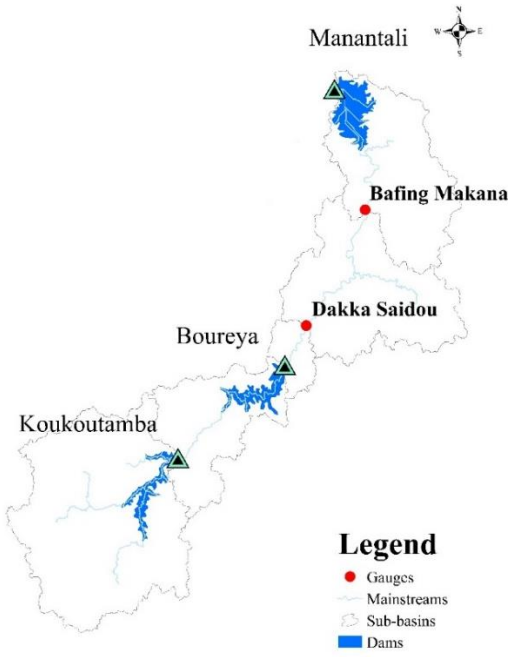

Figure 9:Existing and planned hydropower dams (OMVS, 2012a)

2.9 Conclusion

The study of the features of a watershed (topography, geology, hydrogeology, climate, vegetation) is necessary for understanding hydrological behavior and hydrological modelling. Indeed, these parameters, according to their influence, determine the modalities of the flow. The topography of the study area is characterized by a sub-tabular dolerite or granitic relief whose altitude decreases from South to North (1370 to 100 m). The Precambrian, Paleozoic and Tertiary basements are the main geological formations recorded in the area. The climate includes two regimes from South to North (Guinean climate, Sudanian climate). The distribution and density of vegetation directly influence river flow as well as climatic factors. The vegetation in the Bafing watershed is densely degraded forests in the south and open savannah forests in the north. This density of vegetation translates into resistance to river flow. Indeed, from the beginning of the rains, the soil behaves like a vegetated zone soil, absorbing most of the rainwater through litter, even dry and residual, then highly developed root systems. Runoff only appears once the soil is saturated. This is known as saturation runoff or "Cappusian" behaviour (Descroix, 2020). Population estimates are not very precise. Agriculture, fishing, and livestock are the main activities. All these physiographic elements strongly influence the hydrological behaviour of a watershed.

Chapter 3: Data, materials, and methods

Chapter 3 presents data, materials and methods based on each objective.

3.1 Data

3.1.1 Climate data

- **Observed data**

Hydrological modelling requires long, complete and accurate time series (precipitation, temperature, relative humidity, solar radiation) (Cucchi et al., 2020). Data selection criteria are generally based on four fundamental factors: large sample size, proximity to the study area i.e. geographical position, data quality (small gaps in the observed series) and the geopolitical context of the country (Faty, 2017). At the level of the Bafing watershed, the monitoring and collection of climate data are the responsibility of the National Directorates of Meteorology of Guinea and Mali.

The Bafing Makana station in the Bafing watershed has many gaps in the historical time series and only includes precipitation data (Table 4). The transboundary nature of the basin and the inadequacies of the monitoring network in recent years have led to difficulties in accessing available data. Regions of West Africa are generally marked by the challenge of insufficient data, due to the scarcity of the ground-based observation network and many gaps in historical time series (Chinwendu, 2019; Sambou et al., 2018). Therefore, other data sources must be taken into account (Ma et al., 2019). Several studies were conducted in data-scarced or ungauged catchments using satellite-based and reanalysis datasets to simulate streamflow with hydrological models (Gao et al. 2018).

- **Reanalyzed and satellite data**

In recent decades, satellite data and reanalysis data have been among the most attractive methods for generating continuous and regionally dispersed climate datasets with high spatial and temporal resolutions to replace observed data due to their low cost and high spatial coverage (Moges et al., 2022). Satellites have greater spatio-temporal coverage, but their precipitation estimates are sensitive to low-intensity precipitation, systematic bias and poor performance over snow-covered areas (Ougahi and Mahmood, 2022). Reanalysis products better describe large-scale weather systems. Due to their low spatio-temporal resolution, they are unable to differentiate spatial variability (Ougahi and Mahmood, 2022).

Among the estimates based on reanalysis, the ERA-Interim global reanalysis has been widely used as a reference by the climate community (Cucchi et al., 2020). ERA5 is a state-of-the-art global atmospheric reanalysis dataset produced by the European Centre for Medium-Range Weather Forecasts (ECMWF). The Watch Forcing Data methodology applied to ERA5 reanalysis data (W-era5) is a new meteorological forcing dataset for land surface and hydrological models based on the ERA5 reanalysis. It provides a long-term record of a wide range of atmospheric variables at high spatial and temporal resolutions, such as temperature pressure, wind, and precipitation (Cucchi et al., 2020). The W-era5 dataset covers the period from 1979 to 2016, with data available for the entire period. It has a spatial resolution of 0.5 degrees (approximately 31 km). It includes data at various vertical levels of the atmosphere and has a high temporal resolution of 3 hours per day (Cucchi et al., 2020). The dataset can be downloaded free of charge at https://doi.org/10.24381/cds.20d54e34.

Several satellite data are available (Bamweyana et al., 2021). The Climate Hazards Group Infrared Precipitation with Stations (CHIRPS) is widely used worldwide (Chinwendu, 2019; López-Bermeo et al., 2022). The CHIRPS data is an estimate of precipitation from rain gauges and satellite observations. It was set up in collaboration with scientists at the Earth Resources Observation and Science (EROS) Center to provide comprehensive, reliable and up-to-date datasets for several early warning purposes, such as trend analysis and seasonal drought monitoring (Bamweyana et al., 2021). It also features gauge-based bias correction that differentiates it significantly from unsampled satellite products. In addition, the CHIRPS dataset has a long recording period, from 1981 up-to-day, and high spatial resolution (0.05°) compared to other products such as the Merged Analysis of Precipitation (spatial resolution of 2.5° * 2.5°), and the Tropical Rainfall Measuring Mission (spatial resolution of 0.25° * 0.25°). The data can be downloaded free of charge at https://data.chc.ucsb.edu/products/CHIRPSS-2.0/.

Satellite and reanalysis precipitation estimates have a significant bias, which must be examined before using it in hydrological applications (Sahlu et al., 2017). Their relevance as reference dataset due to the limited amount of observed data will be determined by comparing them to observed precipitation. Details of observed, reanalysis, and satellite data used in this study are presented in Table 4.

Table 4: Climate data used in the study are from the observed station, satellite-based and reanalyzed precipitation products.

Data	Starting year	Ending year	Time scale
Observed	1981	1986	monthly
	2001	2003	daily
W-era5	1979	2016	daily
CHIRPS	1981	2022	daily

- **Global Climate model data (GCM)**

The Inter-Sectoral Impact Model Intercomparison Project (ISIMIP3b) offers simulations of ten GCMs used in the CMIP6 project (Eyring et al., 2016). It presents a bias adjustment and statistical downscaling based on W-era5 climate data that differentiates it considerably from other GCM of the CMIP6 project. The method used for bias adjustment and statistical downscaling in ISIMIP3b was developed by Lange (2020). The projections of these 10 GCMs were adjusted and statistically reduced to a horizontal resolution of 0.5 degrees with ISIMIP3BASD v2.5.0 as part of Phase 3b of ISIMIP 3b project by Lange (2020). The training period used for bias adjustment and statistical downscaling was from 1979 to 2014. The ISIMIP provides climate forcing on CMIP6 global climate model simulation sets under three scenarios ssp126 (ssp1-RCP2.6), ssp370 (ssp3-RCP7.0) and ssp 585 (ssp5-RCP8.5) over the historical period between 1979 and 2014 and climate projections covering the period from 2015 and 2100. Model results are available at spatial resolutions of 0.5° x 0.5°. The two climate scenarios, ssp 126 (moderate scenario) and ssp 370 (medium–high scenario), were chosen because they represent a wide range of uncertainties in potential future trajectories. According to Meinshausen et al. (2020), the ssp 370 scenario is a medium-high reference scenario in the socio-economic family “regional rivalry”, while the ssp 126 scenario corresponds approximately to the previous generation of the RCP 2.6 scenario. It describes a "best-case" future from a sustainability perspective. Indeed, the ssp1 scenario marks a low mitigation adaptation challenge and describes a world marked by strong international cooperation, prioritizing sustainable development with a radiative forcing of 2.6 W/m2 in the year 2100. The ssp3 scenario (High Adaptation Challenge, High Mitigation Challenge) depicts a fragmented world affected by competition between countries, slow economic growth, security-oriented and environmentally unconscious policies and industrial production with a radiative forcing of 7.0

W/m2 in the year 2100 (Mondon and Imbard, 2013). Climate models from ISIMIP 3b are frequently used for climate impact assessments worldwide (Ito et al., 2020; Adigun et al., 2022; Golub et al., 2022). They have never been used in the study area, unlike the climate data from CORDEX Africa, which has been used and bias-corrected by Mbaye et al. (2018). Therefore, a set of ten GCMs from ISIMIP 3b (Table 5) were used under two climate scenarios ssp126 (moderate scenario) and ssp370 (medium–high scenario) in this study. The dataset can be downloaded free of charge at https://data.isimip.org/.

Table 5: Global climate Model from ISIMIP 3b

GCM Model	Characteristics GCM (forcing)
CanESM5	Canadian Center for Climate Modelling and Analysis – Canada
CNRM-CM6-1	Centre National de Recherches Météorologiques (CNRM)and Cerfacs –
CNRM-ESM2	Centre National de Recherches Météorologiques (CNRM)and Cerfacs – France
EC-Earth3	Royal Netherlands Meteorological Institute (KNMI) – Pays-Bas
GFDL-ESM4	The GFDL Earth System Model
IPSL-CM6A-LR	Institut Pierre-Simon Laplace (IPSL)
MIROC6	The Model for Interdisciplinary Research on Climate (MIROC) by The University of Tokyo Center for Climate System Research – Japon
MPI-ESM1-2-HR	The Max Planck Institute for Meteorology,
MRI-ESM2-0	The Meteorological Research Institute Earth System Model Version 2.0
UKESM1-0-LL	U.K. Earth System Model

3.1.2 Hydrological data

The Organization for the Development of the Senegal River (OMVS) provided daily-observed flow data from 1979 to 2017 at Bafing Makana and Dakka Saidou stations. These data were used for model calibration and validation. To simulate the management of dams, the dam module of SWIM requires information about the characteristics of the hydropower plants and the dam. These data were obtained from published reports (Bader, 2001; OMVS, 2011, 2012b). The main characteristics of the implemented dams are in Table 6. The efficiency factors for hydropower plants are calculated using the maximum head and capacity values of the hydropower plant.

Table 6:Characteristics of existing and future dams

Main characteristics of dams	Manantali	Boureya	Koukoutamba
Maximum dam capacity, including dead storage (Mm^3)	12966	5500	3600
Dead storage (Mm^3)	3387	2650	678
Maximum height of hydropower power station [m]	54.16	54	83.7
Turbined capacity [m3/s]	455	370	448
Installed capacity (MW)	205	160.7	294
Firm yield (MW)	100	52	81.1
State	Existing	Planned	Planned

3.1.3 DEM

Topography in Figure 10 is identified using the MERIT Digital elevation model (Multi-Error-Removed Improved-Terrain DEM) (Yamazaki et al., 2017). MERIT DEM is a high-accuracy global DEM at 3″ resolution (~90 m at the equator). The DEM was used to delineate the watershed, derive sub-catchments, and their stream networks. It has also been used to obtain some terrain-specific measurements, such as topological and morphometric properties of the land surface terrain and for the LULC mapping.

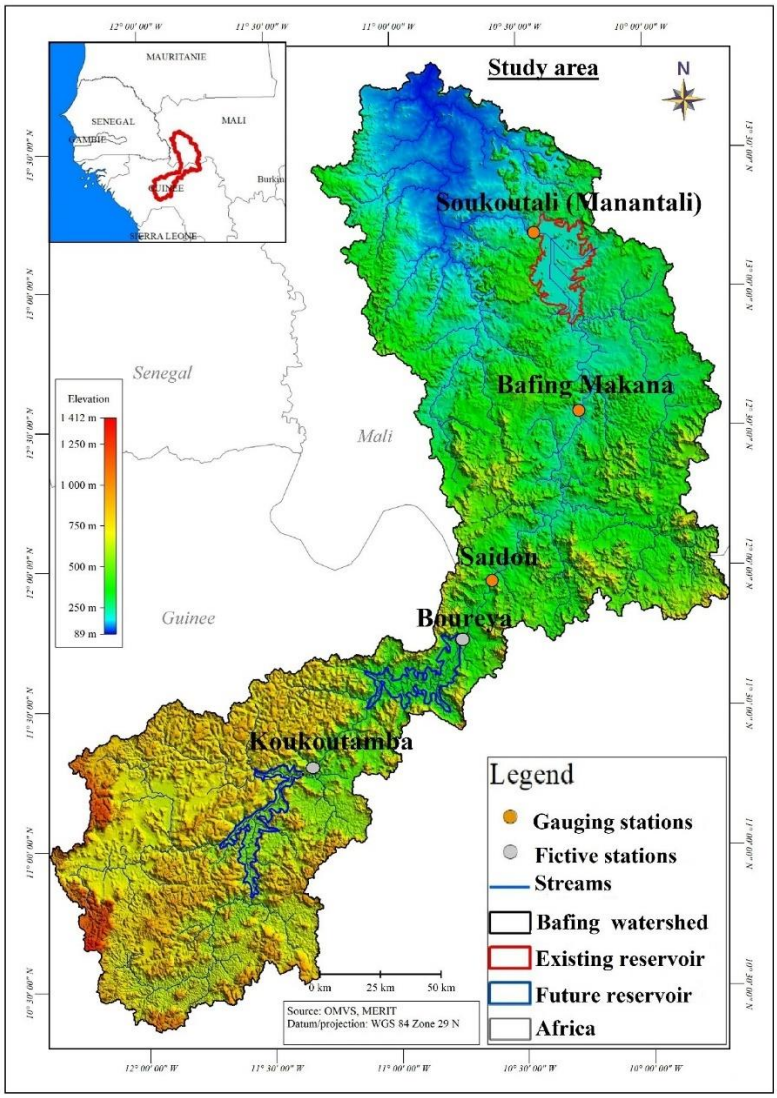

Figure 10:Topographic map of the Bafing watershed

3.1.5 Soil data

Soil types and textures in the Bafing watershed, based on the World Harmonized Soil Database (HWSD) (http://www.fao.org/geonetwork/srv/en/main.home#soils) are presented in Figure 11. The majority of soil types of the Bafing watershed are lithosol and regosol. There are also small percentages of cambisol and ferric acrisol.

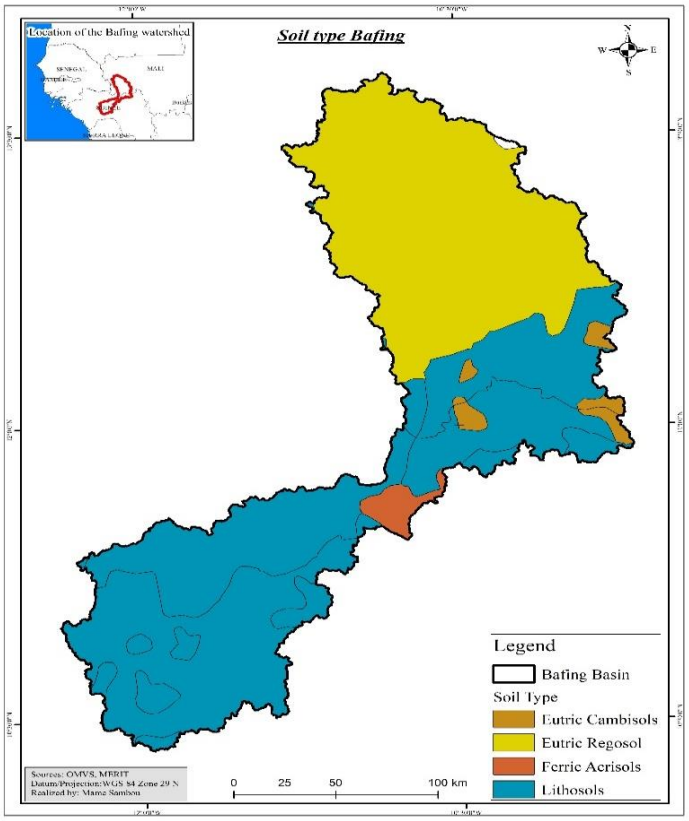

Figure 11: Spatial distribution of soil types (HWSD) (http://www.fao.org/geonetwork/srv/en/main.home#soils

3.1.6 Land use/land cover data

Acquiring satellite images is the first step to carry out land use/land cover mapping. Satellite images are digital observational images of the earth's surface assembled from the capture by special sensors mounted on satellites. A satellite image depends on the resolution of the sensor and the altitude (i.e. its orbit around the Earth) of the remote sensing satellites (Jensen, 2006). Several remote sensing satellites have already been deployed in orbit. The sensors on board in these satellites have undergone enormous technological advances, moving from spectral to hyperspectral. Spectral and spatial resolutions have also increased gradually. The passage frequency on the same observation sites has been reduced from months to date. In addition, more and more remote sensing data are being made freely and completely open. Table 7 lists the characteristics of satellite images that are frequently used in the LULC mapping.

Table 7: Synthesis of sensors used in remote sensing adopted from (Zhu et al., 2018)

Satellite	Launch years	Sensors	Spatial resolution (m
Landsat	1972, 1975, 1978, 1982, 1984,1993, 1999,2013, 2020	Panchromatic and Multispectral	15, 30, 60, 100, 120
Sentinel 1-6 (ESA)	2014, 2015, 2016, 2017, 2021	Radar, Superspectral	5--60
SPOT	1986, 1990, 1993, 1998, 2002, 2012	Spectro-radiometry	2,5, 5, 10, 20
MODIS	1999, 2002	Spectro-radiometry	250-1000
QuickBir	2000, 2001	Spectro-radiometry	0,61--2,62
IKONOS	1999	Spectro-radiometry	0,8--3,2

* SPOT (Système Probatoire d'Observation de la Terre) - MODIS (Moderate-Resolution Imaging Spectroradiometer). ESA: European Space Agency.

In this study, Landsat satellite images were chosen. It is the oldest of the earth observation programs since 1972. It have an extensive archive of images over a long period; approximately more than 30 years (Woodcock et al., 2008). The data are freely available and have an appreciable spatial resolution for a wide range of surfaces (snow, soil, water, vegetation). Actually, it offers a sufficient level of detail to identify the characteristics of the land cover, such as mapping and analysis of water bodies, vegetation phenology, agriculture, forest monitoring, surface temperature, evapotranspiration, hydrology (Wulder et al., 2019). Table 8 shows the generations of Landsat characteristics and specifications.

Table 8 : Description of Landsat sensors adapted from (Wulder et al., 2019)

Landsat sensor	**Wavelenght**	**Launch years**	**Frequency of passage**	**Resolution**
Landsat 1-3	Multispectral Scanner (MSS)	1972-1983 (1-3) 1975-2013 (4-5)	18 days	60m
Landsat 4-5	Multispectral Scanner (MSS)	1975-2013	18 days	60m
Landsat 4 et 5	Thematic Mapper ™	1975-2013	16 days	30m, 120m (TIR)
Landsat 7	Enhanced Thematic Mapper Plus (ETM+)	since 1999	16 days	15m (P), 60m (TIR)
Landsat 8	Enhanced Thematic Mapper Plus (OLI/TIRS)	since 2003	17 days	30m, 15m (P), 30m (C), 100m (TIR1, TIR2)

Google Earth Engine (GEE) provides surface reflectance images that are atmospherically corrected and improve the detection of changes (Wahap and Shafri, 2020). The choice of satellite images is based on four criteria:

- spatial resolution,
- spatial coverage,
- available years,
- cloudiness (minimum) (Horning, 2004; Martignac, 2005).

The images selected according to these criteria are presented in Table 9.

Table 9:Characteristics of Landsat images selected for the LULC mapping.

Dataset	*Satellite*	*Sensor*	*Spatial resolution*	*Date of acquisition*	*Band*
Image 1	USGS Landsat 5 (Surface Reflectance Tier 1)	MSS/TM	30 m	1986	Multispectral
Image 2	USGS Landsat 5 (Surface Reflectance Tier 1)	MSS/TM (Surface Reflectance Tier 1)	30 m	2006	Multispectral
Image 3	USGS Landsat 8 (Surface Reflectance Tier 1)	OLI/TIRS (Surface Reflectance Tier 1)	30 m	2020	Multispectral

The global human settlement data have been downloaded from the European Commission (https://ghsl.jrc.ec.europa.eu) to identify settlement zones for the sampling. Ground truth samples were collected using Google Earth. The Digital Elevation Model, slope, distance from the road, and distance from the river (Figure 12) were included as supplementary input data for the LULC modelling.

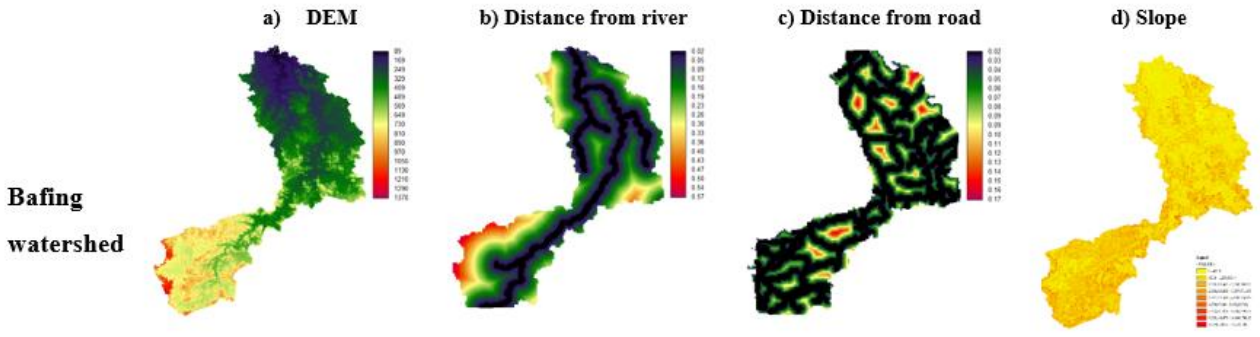

Figure 12:Explanatory variables used for the calibration in the land use/land cover change modelling.

3.2 Materials

3.2.1 Hydrological modelling

3.2.1.1 Hydrological model selection criteria

With the increasing number of hydrological models, the choice of a model depends on well-defined research objectives. In the case of analyzing the impact of climate change and LULC change on water and hydropower generation, the following criteria should be considered:

- A model that incorporates the hydrological space-time variability of input data,
- A model that can simulate the hydrological response continuously over a long period to consider the projection of climate change,
- A model that can consider the hydrological characteristics of surface state to represent the physical processes of flows over the watershed (LULC change),
- A model that has not yet been applied or partially applied to the study area.
- A model that integrates dam management,
- An accessible and trainable model.

In addition, the degree of complexity and the large quantity of input data is also essential to consider.

In the context of the Bafing watershed, several models and approaches have been tested for flow simulation. Faty (2017) used the Mike SHE model to study hydrological phenomena and changes in surface states in the Bafing watershed. The GR4J model has been calibrated and validated on the Bafing watershed (Sambou et al., 2003; Bodian, 2012). The SWAT model was used to assess the impact of climate change on water resources and the management of the Manantali dam (Sane et al., 2020). HBV-Light was used to have the hydrological forecasts in the Bafing watershed (Ndione et al., 2020). In the framework of this study, the SWIM model (Soil and Water Integrated Model), developed by Krysanova et al. (2005), has been selected because it corresponds to the predefined criteria and has not yet been applied to the Bafing watershed.

Over the past decade, SWIM has been tested on intermediate and large basins for hydrological processes. Krysanova et al. (2015) synthesized the various research results on hydrological processes with SWIM in their studies. They highlighted the broad scope of the SWIM model (water quality, groundwater, flood, irrigation, wetlands, soil moisture, erosion, crop yield, forest

dynamic, climate change impact on floods, climate change impact on crop yields, climate change impact on water, land-use change impact on water). For example, the SWIM model has been applied to the Grand Ethiopian Renaissance Dam to assess the management scenarios and their impacts under current and future climates. Furthermore, Liersch et al. (2017) investigated the impacts of projected climate change on the hydrology of the Upper Blue Nile catchment using the SWIM model. Koch et al. (2020) simulate the effects of climate change on hydrological processes and water resources management with SWIM model in Semi-arid regions. The authors laid the emphasis on describing problems and generating solutions when calibrating and validating the eco-hydrological model SWIM for semi-arid areas in the example of the Pajeú watershed in northeastern Brazil. Wortmann et al. (2014) investigate the glacier-lake outburst floods at the Tarim River in northwest China. They experimented the SWIM model on water resources and highlighted the influences on the downstream water balance. Lobanova et al. (2016) address the effects of projected climate change on the water availability in the Tagus River basin and the potential changes on hydropower generation of three important dams. The SWIM model allowed them to simulate the flow and dam management.

3.2.1.2 Presentation of the SWIM model

The Soil and Water Integrated Model (SWIM) is a semi-distributed, continuous eco-hydrological model based on physical equations and empirical methods (Krysanova et al., 2005, 2015). It is built on the SWAT and MATSALU tools, two previously invented models. The SWIM offers a complete GIS tool for linked modelling of hydrological processes, vegetation and water quality, as well as for analyzing the effects of climate change and land use change on these systems at the regional level. SWIM simulates hydrological processes, vegetation growth, erosion, and nutrient dynamics at the river-basin scale. It incorporates relevant natural elements, such as climate, hydrology, vegetation, nutrient transport, land use/land cover management and water management (Figure 13). It is composed of several modules such as reservoir and crop rotation. The modelling procedure is based on a three-step process. At first, water, vegetation growth and nitrogen dynamics are determined for every hydrological response unit (HRU). Then, the outputs from the HRU, especially the lateral water and nutrient flows are averaged to calculate the sub-basin output. Finally, the routing procedure is applied to the sub-basin outputs, considering transmission losses.

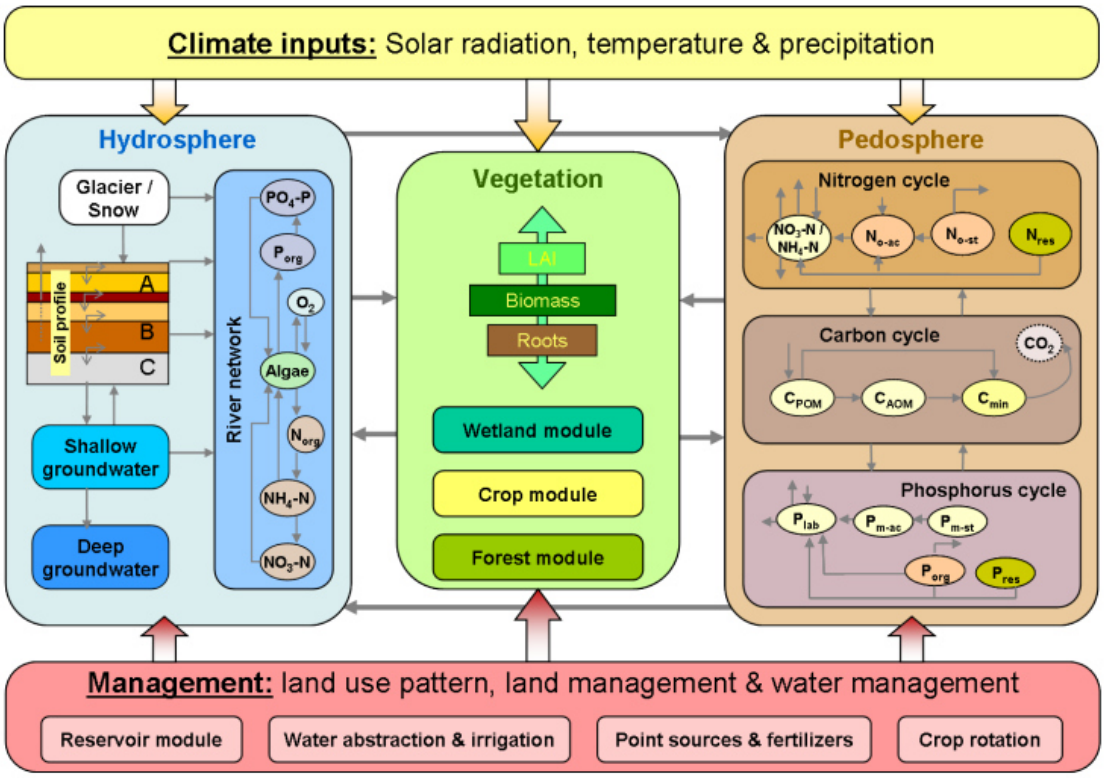

Figure 13: Flow chart of the SWIM model component

3.2.1.3 Spatial disaggregation of the SWIM model

The SWIM model uses a three-level disaggregation scheme composed of basin, sub-basins, and HRUs inside sub-basins (Figure 14). The model considers the watershed as an area that is further divided into sub-basins and HRUs (Krysanova et al., 2021). Watershed boundaries are delineated by a DEM that represents the terrain's topography. Due to spatial connections between sub-basins, water flows from upstream to downstream to the outlet in a sub-basin. The river system has branches present in each sub-basin to ensure drainage. SWIM links each branch to create the river network extending over the entire watershed. Next, the sub-basins are divided into HRUs. Overlaying elevation, slope, LULC, sub-basins, and soil files create these HRUs. HRHs are the main calculation elements for the simulation of hydrological processes. With regard to biophysical processes, HRUs are considered as units with the same features. There is no interaction between HRUs. Indeed, an HRU is typically a group of disjointed sub-basin units with a distinct land use and soil type. It is reasonable to assume that an HRU will behave hydrologically in the same way throughout the sub-basin. The water balance is calculated once the watershed is spatially organized in SWIM (Krysanova et al., 2021).

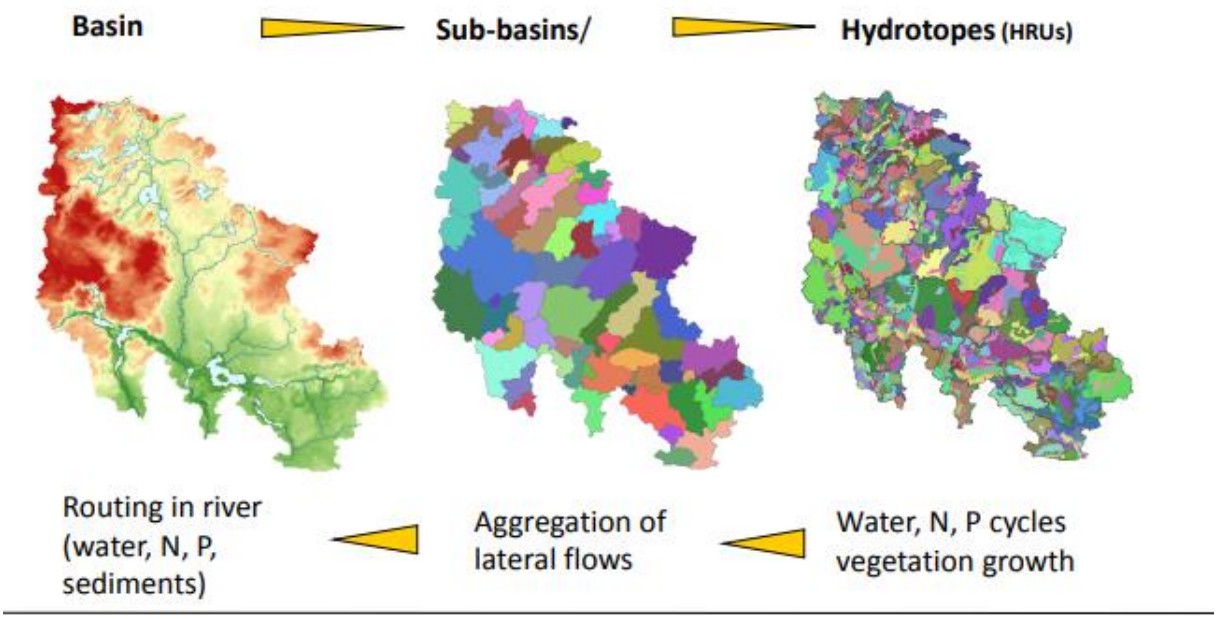

Figure 14:Spatial disaggregation in SWIM (Krysanova et al., 2005, 2015)

3.2.1.4 Hydrological processes

Hydrological processes involved in SWIM model are based on the water balance equation (7), taking into account precipitation, evapotranspiration, percolation, surface runoff and groundwater runoff for the soil column subdivided into several layers (Figure 15).

$$SW\,(t+1) = SW(t)\ + PRECIP - Q\ - ET\ - PERC - SSF \quad (7)$$

Where SW (t) is the soil water content in the day t, PRECIP – precipitation, Q – surface runoff, ET -evapotranspiration, PERC – percolation, and SSF subsurface flow.

Precipitation is an input data, with the assumption that it can vary between sub basins. Still, it is equally distributed within each sub basin. The surface runoff, evapotranspiration, percolation, and subsurface flow appear as in the figure below:

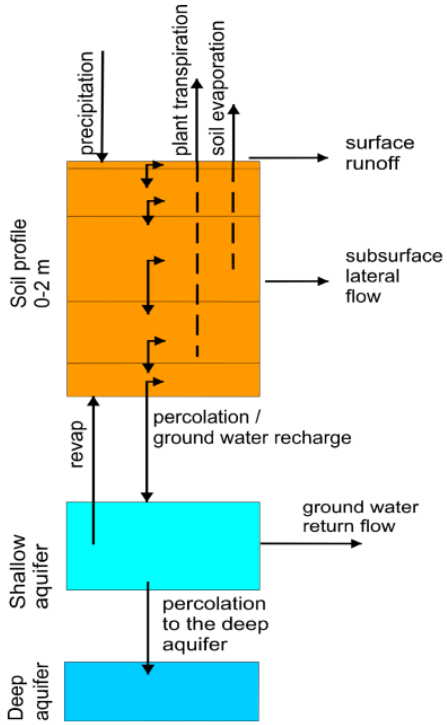

Figure 15: Flow chart of hydrological processes in soil implemented in SWIM (Krysanova et al., 2021)

- Surface runoff (Q)

Surface runoff is defined as the flow occurring along the slope surface and begins when the soil is already saturated with water (Leye, 2023). The model simulates the surface runoff volumes and peak runoff rates using the daily precipitation as input. The method used to calculate the runoff volume is a modification of the Soil conservation service (SCS) curve number method (Leye, 2023). It is defined by the following equation:

$$Q = \frac{(PRECIP - 0.2 \times SMX)^2}{(PRECIP + 0.8 \times SMX} \text{ if } PRECIP\ 0.2\ \times SMX \quad (8)$$

$$Q = 0, \text{ if } PRECIP \leq 0.2 \times SMX$$

Where Q is the daily runoff in mm, PRECIP is the daily precipitation in mm, and SMX is a retention coefficient. The retention coefficient SMX and curve number (CN) are connected with the following equation:

$$SMX = 254 * (\frac{100}{CN} - 1) \quad (9)$$

The CN is a dimensionless parameter. The values of CN are related to land use types, hydrologic soil groups and management practices. Peak Runoff Rate is calculated by using the modified Rational formula (Krysanova et al., 2021).

- Percolation (PERC)

Percolation is defined as the entry of water into the soil layer (Leye, 2023). In SWIM, a storage routing technique is used to simulate percolation through each soil layer. It is defined by the equation (10) (Krysanova et al., 2021)

$$PERCi = SWi * (1 - \exp\left(\frac{\Delta t}{TTi}\right)) \quad (10)$$

where PERC is the percolation rate in mm d^{-1}, SWi are the soil water contents at the beginning and end of the day in mm, Δt is the time interval (24 h), and TTi is the travel time through layer i in hour, d is the day.

- Potential Evapotranspiration (PET)

Potential Evapotranspiration (PET) is a collective term encompassing all the processes by which water on the Earth's surface is converted into water vapour (Leye, 2023). This includes canopy evaporation, transpiration, sublimation and soil evaporation. The PET is the rate at which evapotranspiration occurs from a large area completely and evenly covered with growing vegetation that has access to an unlimited soil water supply. Evapotranspiration is calculated in SWIM with the Priestley-Taylor method, requiring only solar radiation, air temperature, and elevation as inputs (Krysanova et al., 2021). The Priestley-Taylor method calculates potential evapotranspiration (Eta) as a function of net radiation as follows:

$$PET = 1.28 * \left(\frac{RAD}{HV}\right) * \left(\frac{\delta}{\delta+\gamma}\right) \quad (11)$$

where is PET is the potential evaporation in mm, RAD is the net radiation in MJ m^{-2}, HV is the latent heat of vaporization in MJ kg^{-1} , δ is the slope of the saturation vapour pressure curve in kPa C^{-1}, and γ is a psychrometer constant in kPa C^{-1}.

- Lateral sub-surface flow (SSF)

Lateral subsurface flow is determined simultaneously with percolation. The SWIM estimates the subsurface flow with the kinematic storage model (Krysanova et al., 2021).

- Groundwater flow

The percolation from the soil profile is supposed to recharge the shallow aquifer. The surface runoff, the lateral subsurface flow from the soil profile, and the return flow from the shallow aquifer supply the stream flow.

The Medema and Rycroft method (Krysanova et al., 2021) is used to determine groundwater contribution to streamflow:

$$GWQ = 8 \times \frac{KD \times GWH}{DS^2} \quad (12)$$

where GWQ is the return flow or groundwater contribution to streamflow, KD is the hydraulic conductivity of groundwater in mm d^{-1}, DS is the drain spacing in m, and GWH is the water table height in m.

- River Routing

Once SWIM has determined the flows of water, sediment and nutrients to the main channel, the flows are routed through the network of streams in the watershed using the Muskingum flow routing method (Krysanova et al., 2021).

3.2.1.5 Presentation of the dam module

The SWIM reservoir module, a conceptual representation of dam management processes developed by Koch et al. (2013), was created to consider existing or future dams in water management (Figure 16). The dam module provides advanced functions to evaluate hydropower potential, analyze storage effects, provide water resources for various users, and simulate flood protection. Operation rules control the reservoir release. These rules are separately defined for the filling period and regular operation. Actual evapotranspiration from the reservoir area is calculated using the weighted sums of evaporation from the open water surface of the lake and actual evapotranspiration from the land area. The daily seepage rate is calculated as a user-defined fraction of the current total storage volume. The lakes of the reservoirs are considered as a sub-basin in SWIM. The model incorporates watershed dams as distinct, individual "sub-basins" into the sub-basin map. The reservoir model is called in the SWIM model during the routing procedure. If the routing routine reaches a reservoir-sub-basin, the reservoir routine is called instead of the “normal” sub-basin routine and the simulation is carried out according to the management options set. SWIM has provided three management options to simulate dam management rules:

(i) Variable daily minimum discharge to meet environmental targets downstream under consideration of maximum and minimum water levels in the reservoir,

ii) Daily release based on firm energy yield by a hydropower plant at the reservoir (the release to produce the required energy is calculated depending on the water level

iii) Daily release depending on water level (rising/falling release with increased/falling water level), depending on the objective of reservoir management.

The reservoir release for option (ii) is used to simulate hydropower generation (Koch et al., 2013). The hydropower generated per day is calculated with the equation (13):

$$P = Q \times \rho \times g \times H \times \eta \quad (KWh) \qquad (13)$$

where P is the electricity produced (kW), Q is the flow rate through the turbine (m^3/s), H is the water head (m), ρ is the density (kg/m3) (Water = 1000), g is the acceleration of gravity (=9.81) (m/s^2) , η = global efficiency ratio (usually between 0.7 and 0.9).

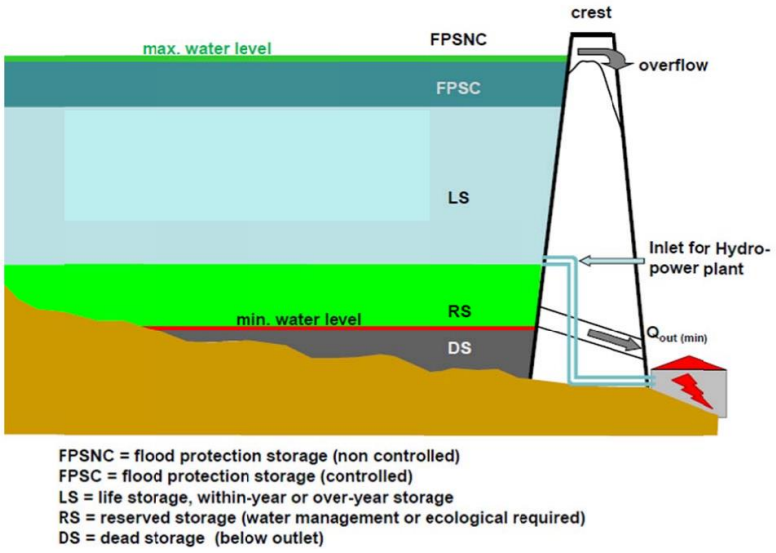

Figure 16: Overview of the separation of reservoirs in different compartments in SWIM (Krysanova et al., 2021)

3.2.1.6 Dam integration into SWIM model

To integrate dam management as a module into SWIM, the outlet of the dam must be located at the same position as one outlet of a SWIM sub-basin. This must be safeguarded in the pre-processing. To avoid multiplying the calculation of precipitation and evaporation over the dam surface, these hydrological response units are turned off. During the routing process, the SWIM model calls the dam module. The dam routine is called and the simulation is run in accordance with the management settings set if the routing routine reaches a dam-sub-basin outlet. The outflow is sent through the following downstream sub-basin after the dam has been simulated. Integrating new dams to account for potential changes in the water infrastructure is possible. In this instance, the dam is empty when the simulation first begins. A prerequisite for implementing and using the dam module is the model with (very) good results for calibration and validation periods. A more detailed description of SWIM is available in its manual with a user guide (Koch and Liersch, 2021).

3.2.2 Google earth engine (GEE) platform

The Google Earth Engine (GEE) is an open-source, cloud-based geospatial processing platform that provides access and seamless processing of large-scale data analyses from freely available satellite imagery (Gorelick et al., 2017; Shelestov et al., 2017). GEE is the most popular big geo data processing platform, which provides a set of state-of-the-art classifiers for pixel-based classification used for LULC mapping (Yang et al., 2022). The main advantage of GEE is the close link between the data and the algorithms, both accessible via an Application Programming Interface (Gorelick et al., 2017; Shelestov et al., 2017). Due to its accessible and user-friendly design, it has grown in popularity recently (Jampani et al., 2020; Dubertret et al., 2022; Nasiri et al., 2022; Ougahi and Mahmood, 2022).

3.2.3 Land change modeller

The Land Change Modeller (LCM), developed by Clark Labs at the University of Worcester (Eastman and Toledano, 2018), is an innovative land use planning and decision support system fully integrated with TerrSet software. The LCM is a collection of tools for the rapid assessment of change, evaluation of gains and losses, net change, persistence and recognition of transitions between LULC classes in statistical and graphical representations (Eastman and Toledano, 2018). It uses historical LULC changes to model empirically the relationship between land cover transitions and explanatory variables to map future changes. The basic principle of this module is to assess the changing trend from one land use category to another. It uses the

influencing factors such as roads, slope, aspect, and soil type, to predict future land use scenarios based on the previous change trend (https://clarklabs.org/terrset/land-change-modeller). Compared to alternative modelling approaches, it have the advantage of being able to simultaneously learn and replicate many surface state transitions while integrating a variety of different parameters into a single operation (Dang and Kawasaki, 2016). This model predicts LULC change from thematic raster images with the same number of classes in the same sequential order. LCM was used to simulate and predict future changes in LULC.

3.3 Methodology

The overall methodology includes precipitation products (W-rea5, CHIRPS) validation, GCM performance assessment, climate change projection, LULC change monitoring and prediction, hydrological modelling, and analysis of the hydrology and hydropower potential response to climate change and LULC changes.

3.3.1 Assessment of Satellite-Based and Reanalysis Precipitation products to reproduce the observed precipitation in the Bafing watershed.

Due to the limited number of observed quality data in the Bafing watershed, the satellite based (CHIRPS) and reanalysis (W-era5) precipitation datasets were first compared to the observed data. This exercise was conducted to determine the most appropriate product to use as a reference data set. The comparison was first made using statistical measures, namely Pearson Correlation Coefficient (R^2), Percentage bias (Pbias), Root Mean Square Error (RMSE) and Nash-Sutcliffe coefficient efficiency (NSE) (Table 10) on a monthly and annual scale. According to Sambou et al. (2018), they are very useful for evaluating estimates.

- Nash-Sutcliffe coefficient efficiency (NSE) (14): NSE is a standardized statistic, that indicates the degree of correspondence between observed and simulated data (Nash and Sutcliffe, 1970).
- The Pearson correlation ($R^{2)}$ (15): R^2 evaluates the statistical association between two continuous variables. It is considered the best method for determining the relationship between the variables of interest because it is based on the covariance method. The values of the coefficients range from +1 to -1, where +1 indicates a perfect positive relationship, -1 indicates a perfect negative relationship, and 0 suggests that no relationship exists (Kanda et al., 2020).
- Percentage bias (16): Pbias measures the average tendency of simulated data to be larger or smaller than their observed counterparts (Lamontagne et al., 2020). The optimal value

of Pbias is 0, with low magnitude values indicating an accurate simulation of the model. Positive values indicate model underestimation bias and negative values indicate model overestimation bias (Lamontagne et al., 2020).

- Root Mean Square Error (RMSE) (17): RMSE is considered one of the best indicators to summarize model performance. Its value also varies between 0 and $+\infty$. Again, models estimates with RMSE values closer to 0 are considered better (Ali and Abustan, 2014)
- The Taylor diagram (Taylor, 2001) was used to get a visual representation of the comparison in correlation, root mean square error and standard deviations.

Then, analyses of the seasonal cycle were carried out on a monthly scale for the historical period 1979-2014.

Table 10: Statistical metrics used in this study. Pobs stands for the observed rain-gauge, Pp stands for the precipitation products (W-era5, CHIRPS), n refers to the sample size.

Statistical metric	**Formula**	**Value range**	**Performance classification**	
NSE	$1-\frac{\sum(P_{obs}-P_p)^2}{\sum(P_{obs}-\overline{P}_{obs})^2}$	$0.75 \leq NSE < 1$ $0.65 \leq NSE < 0.75$ $0.50 \leq NSE < 0.65$ $0.40 \leq NSE < 0.50$ $NSE \leq 0.4$	Very well Good Satisfactory Acceptable Not satisfactory	(14)
Pearson correlation (R^2)	$\frac{\sum((P_{obs}-\overline{P}_{obs})(P_p-\overline{P}_p))^2}{\sum(P_{obs}-\overline{P}_{obs})^2 * \sum(P_p-\overline{P}_p)^2}$	$R^2 > 0.5$	R^2 values >0.5 acceptable for simulation	(15)
Percentage bias (Pbias)	$\frac{\sum(P_{obs}-P_p)*100}{\sum(P_{obs})}$	PBIAS $< \pm 10$ $\pm 10 \leq$ PBIAS $< \pm 25$ $\pm 10 \leq$ PBIAS $< \pm 25$ $\pm 25 \leq$ PBIAS $< \pm 40$ PBIAS $\geq \pm 10$	Very well Good Satisfactory Acceptable Not satisfactory	(16)
Root Mean square error (RMSE)	$\sqrt{\frac{\sum(P_{obs}-P_p)^2}{n}}$	$0 \leq$ to $< \infty$	0 indicates perfect fit	(17)

3.3.2 Assessment of the performance of 10 GCMs from ISIMIP 3b

The evaluation of the performance of climate models consists of analyzing their ability to reproduce the reference climate. Assessment is complex because climate simulations are not intended to reproduce or predict weather conditions for a given day, month or year (Liersch et

al., 2018). Therefore, only statistical variables averaged over approximately 30 years can be used for comparison (Liersch et al., 2018). In the first stage of the assessment, the precipitation and temperature of the 10 GCMs from ISIMIP were compared to the reference data using statistical measures (NSE, R^2 , Pbias, RMSE), the Taylor diagram (Taylor, 2001), and the seasonal cycle. The assessment was carried out on a monthly scale for the historical period 1979-2014. The Mann-Kendall statistical test has been used as an additional criterion to see if GCMs from ISIMIP3b can reproduce the observed trend in annual precipitation and temperature. The nonparametric Mann-Kendall test is used to determine whether an identifiable trend in a time series is statistically significant (Faye et al., 2015). Student's t-tests and the Mann Kendall (MK) test were performed at 95% confidence intervals to determine the statistical significance of climate change signals period 1979-2014 for temperature and precipitation.

The test statistic is given by the equation 18 :

$$Z = \sum_{i=1}^{n-1} \sum_{j=i+1}^{n} \mathrm{sgn}(xj - xi) \quad (18)$$

With

$$\mathrm{sgn}(xj - xi) = \begin{cases} 1 \text{ if } (xj - xi) > 0 \\ 0 \text{ if } (xj - xi) = 0 \\ -1 \text{ if } (xj - xi) < 0 \end{cases} \quad (19)$$

It is accepted that:

$$E(S) = 0 \quad (20)$$

$$\mathrm{Var}(S) = \frac{n(n-1)(2n+5)}{18} \quad (21)$$

$$C_q = \sum_{q=1}^{n} tq \frac{q(q-1)(2q+5)}{18} \quad (22)$$

The statistical variable Z is given by:

$$\begin{cases} Z = \frac{S-1}{\sqrt{\mathrm{var}(S)}} & \text{if } S > 0 \\ Z = 0 & \text{if } S = 0 \\ Z = \frac{s+1}{\sqrt{\mathrm{var}(S)}} & \text{if } S < 0 \end{cases} \quad (23)$$

The regression line estimator, called Sen's slope, is used to determine the magnitude of the trend when the null hypothesis "H0: no trend" of the Mann Kendall test is rejected (Abdulkareem and Sulaiman, 2016). A positive value S denotes an increase trend, and a negative value indicates a downward trend (Mishra et al., 2014). The slope can be estimated using a simple

nonparametric procedure. It consists of calculating the slopes of all the data in the series according to equation 24.

$$Q_j = \frac{x_j - x_i}{j - i} \quad (24)$$

where $x_{j\ et\ i}$ with $j > i$.

The median slope is obtained by one of equations 25 or 26.

$$\beta = Q_{\frac{(N+1)}{2}} \quad (25)$$

$$\beta = \frac{1}{2}\left(Q_{\frac{N}{2}} + Q_{\frac{(N+2)}{2}}\right) \quad (26)$$

Under the normality assumption of the median slope series, the ranks and ascending order of the median slopes corresponding to the limits of the confidence interval at the significance level are calculated by equations 27 and 28.

$$M_1 = \frac{N - C_\alpha}{2} \quad (27)$$

$$M_2 = \frac{N + C_\alpha}{2} \quad (28)$$

Where C_α is obtained by equation 29

$$C_\alpha = Z_{1-\frac{\alpha}{2}}\sqrt{Var(S)} \quad (29)$$

3.3.3 Mapping and Projection of Land use/land cover change

Our methodological approach is presented in three steps. The first step is to establish the LULC maps of 1986, 2006 and 2020. The second approach is to setup the model and the third step is to predict the land use/land cover map for the year 2050.

3.3.3.1 Land use and land cover mapping

The methodological approach for LULC mapping was divided into three significant steps: Landsat image processing, supervised classification, and classification accuracy. This study used the GEE editor (Gorelick et al., 2017; Shelestov et al., 2017) to build the LULC map with individual scripts for each year. The custom scripts combine several components from official Google resources and other references. Figure 17 describes the general procedures used for the LULC mapping. Details will be provided in the following sections. After the LULC mapping, the change detection analysis was performed to observe the changes between two-time scales.

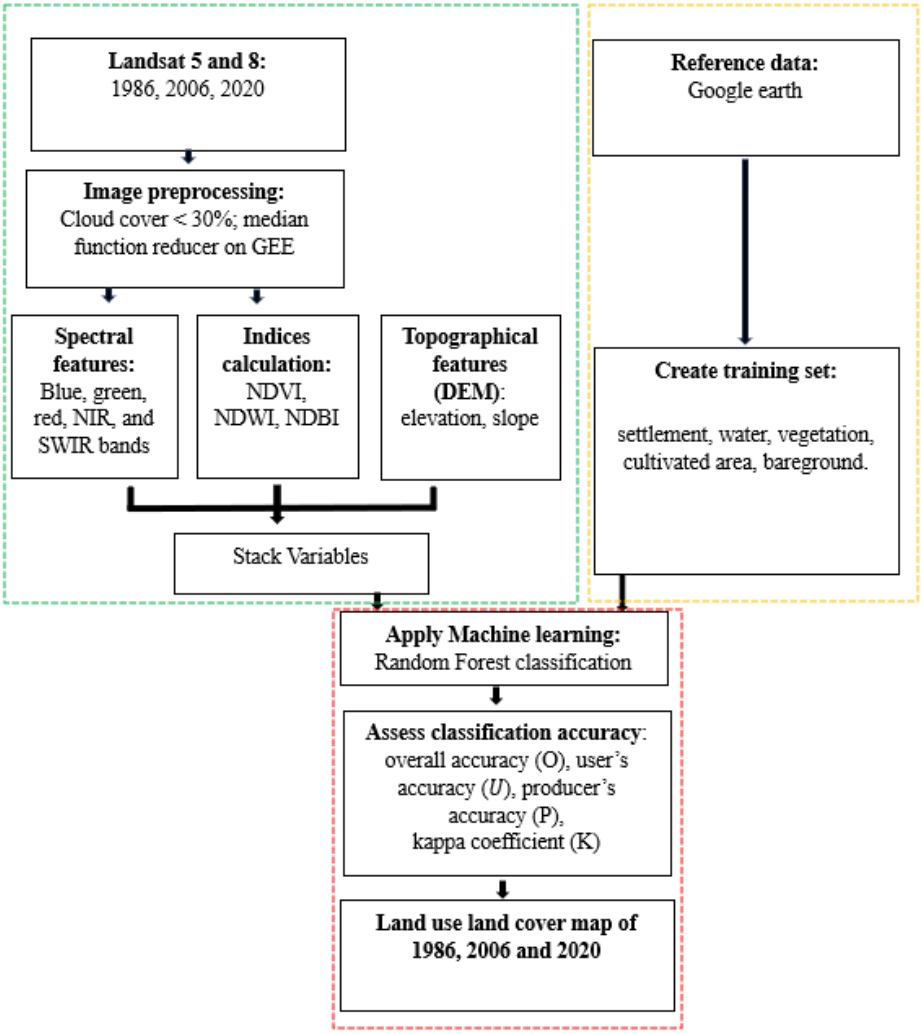

Figure 17: The procedures used for the LULC mapping.

3.3.3.1.1 Image preprocessing

Pre-processing is essential to remove innate noise that could affect classification before using satellite data to produce a LULC map (Thiam et al.,2022). Atmospheric corrected Landsat Surface Reflectance Tier 1 images available for Landsat OLI/TIRS and TM sensors were gathered in GEE for the years of interest (1986, 2006 and 2020). The collection of annual Landsat images with a cloud cover of less than 30% was chosen using cloud cover function in GEE. To "reduce" the collection of Landsat images to a single output image that represents the median of the images, the median ee.Reducer function on GEE was used (Noi Phan et al., 2020; Dubertret et al., 2022).

3.3.3.1.2 Construction of features

The spectral and topographic feature sets were used as input features for LULC classification algorithm (Table 11). Blue, green, red, NIR, and SWIR spectral image bands were selected as spectral features because they can distinguish comparable spatiotemporal phenomena, enhancing the separability of LULC classes (Thiam et al., 2022). Additionally, numerous studies have demonstrated that using spectral features from indices as input features for classification will significantly increase the accuracy of LULC. Examples of these indices include the Normalized Difference Vegetation Index (NDVI), Normalized Water Difference Index (NDWI), and Normalized Difference Accumulation Index (NDBI) (Kulkarni & Vijaya, 2021; Tsai et al., 2018). The NDVI allows determining the vegetation's features. Information on the properties of water bodies is available from the NDWI. The artificial characteristics of the earth's surface can be obtained from the NDBI. Additionally, topographical features such as altitudes and slopes improve the precision of land cover classification (Yang et al., 2021). Hence, the elevation and slope data were extracted from the DEM as features for LULC classification.

Table 11:The spectral and topographic features

Type of feature	**Feature Name**
Spectral Bands	Blue, green, red, NIR, SWIR
Indices	NDVI, NDBI, NDWI
Terrain	Elevation, slope

NIR=near infrared (NIR), SWIR (shortwave infrared)

$$\text{NDVI} = \frac{\text{NIR} - \text{Red}}{\text{NIR} + \text{Red}} \tag{30}$$

$$\text{NDWI} = \frac{\text{Green} - \text{SWIR}}{\text{Green} + \text{SWIR}} \tag{31}$$

$$\text{NDBI} = \frac{\text{SWIR} - \text{NIR}}{\text{SWIR} + \text{NIR}} \tag{32}$$

3.3.3.1.3 Classification

Image classification aims to categorize or label a satellite image. The satellite image can include pixels, pixel density, distributions, features, histograms, color distribution, etc. LULC classification consists of classifying LULC into different classes (crops, forests, roads, residential or industrial areas) using the feature of the spatial-spectral band of the image (Wang

et al., 2022). The success of any image classification depends on a number of factors, including selecting an appropriate classification algorithm (Lu and Weng, 2007). LULC classification algorithms can be classified into different groups of classifiers based on various criteria. Depending on the knowledge of the analyst in the area, one can distinguish between supervised classification algorithms and non-supervised classification algorithms. In unsupervised classification, an algorithm is used to identify spectral classes, and the analyst assigns the identified spectral classes to a LULC class (Richards, 2006). With supervised classification, the analyst guides the classification procedure by selecting areas in the image called drive zones to represent the typical spectral classes representing the surface state (Richards, 2006).

Classification algorithms can also be classified into parametric and non-parametric. Parametric classification is based on the assumption that input data for each class are normally distributed, while nonparametric classification is not constrained by any statistical distribution (Wang et al., 2022).

Classification algorithms can also be classified into pixel-based and object-based algorithms (Pandey et al., 2021). Although pixel-based methods focus primarily on pixel independence in classification, they have some limitations for classifying mixed entities. In contrast, object-based methods classification is done based on objects instead of a single pixel (Pandey et al., 2021). Thus, this approach may not be practical for detailed LULC classification. Consequently, pixel-based classification is more famous for LULC classification (Wang et al., 2022).

Advanced classification algorithms such as Regression Trees (CART), Random Forest (RF), kNearest Neighbor (k-NN), Support Vector Machine (SVM), Artificial Neural Network (ANN), Multinomial Logistic Regression (MLR), Maximum Likelihood Classification (MLC), and Bayesian classifiers have received a lot of attention in the classification of LULC mapping recently (Ma et al., 2019; Macarringue et al., 2022). To find the best and most accurate classification algorithm for LULC mapping, researchers such as Kulkarni and Lowe (2016) and Talukdar et al. (2020) have done comparative studies between several algorithms. According to their findings, Random Forest is the best for the LULC classification compared to other classifiers. RF is a pixel-based non-parametric classifier method that enables supervised classification. RF is widely used in LULC classification for the ensuing reasons (Amini et al., 2022; Noi Phan et al., 2020):

(1) effective management of outliers and noisy datasets;

(2) satisfactory results with multi-source and high-dimensional datasets;
(3) superior accuracy to other widely used classifiers, like SVM or MLC in many applications;
(4) speeding up processing by concentrating on essential factors.
Moreover, the Random forest is suitable for classifying hyper-spectral data, where the curse of dimensionality and highly correlated data pose significant issues to other available classification methods (Biau and Scornet, 2016; Fawagreh et al., 2014). Hence, this study used RF to produce LULC maps for 1986, 2006, and 2020. This method combines the sampling approach and random feature selection to build a collection of decision trees with a controlled variation. RF is a method using decision trees classifiers {h(x,Hk), k = 1,...,} where the "Hk" stands for independent identically distributed random vectors and "x" stands for an input pattern (Breiman, 2001). In training, RF creates multiple CART-like trees, each trained on a bootstrapped sample of the original training data. It establishes a split by examining a randomly selected subset of the input variables (Gislason et al., 2006). In the classification process, each tree gives a unit vote for the most popular class at input x, and the classification of each tree is referred to as a "vote" for that class (Kulkarni and Lowe, 2016). A complete mathematical description of RF is presented by Breiman (2001). Two important parameters must be optimized to get more accurate results: the number of trees (*Ntree*) generated, and the number of features randomly chosen to divide each node (*Mtry*). Using the results of the data pretests, the number of trees was set to 100, and Mtry was set to the default value (square root of the total number of features).

Five LULC classes were used in the classification, namely (1) settlement, (2) water, (3) vegetation, (4) cultivated area, (5) bareground. The choice of these five classes was based on information from key stakeholders in the watershed and in line with previous regional studies, which used comparable classes (Faty, 2017; Thiam et al., 2022). The details are specified in Table 12.

Table 12: Description of the five classes used in the study.

Class	Name	Description
1	Settlement	The human (urban and rural) settlement, housing, roads, transport, mining, and industry.
2	Water	Rivers, streams, ponds, lakes, dams, estuaries, and wetlands.
3	Vegetation	Forest, savannah and riparian vegetation, Herbaceous Rangeland, Shrub and Brush Rangeland.
4	Cultivated area	Agriculture area (irrigated crops, rainfed crops), orchards and Pasture.
5	Bareground	Deserts, sand fields, exposed bareground rock, sand and temporary bareground ground, transitional.

The training sample selection was done manually by following the probability sampling method based on available references and aiming for overall precision as an estimation goal (Olofsson et al., 2014). The probabilistic sampling method can be performed in two steps: sampling design and response design (Szantoi et al., 2021). In practice, the number of samples has been increased due to the breadth and complexity of the environment. Some classes, such as water, and cultivated area, cover a small area in the region. Therefore, fewer samples were taken. The spatial distribution of samples was determined using a combination of random sampling and expert knowledge. The number of good samples was studied experimentally by running the script repeatedly to obtain acceptable visual and statistical results. These samples were used as regions of interest (ROI) to train the RF. Each ROI was given a certain LULC class designation. 70% of the sample was used for training, while 30% was used for internal validation.

3.3.3.1.4 Classification accuracy

In the remote sensing application, evaluating the accuracy of the classification results is crucial. There are many methods used to carry out this verification. Many researchers recommend using a confusion matrix (Table 13) to represent accuracy (Congalton, 1991; Olofsson et al., 2014; Szantoi et al., 2021). The confusion matrix reveals information on the overall accuracy O, user's accuracy U, producer's accuracy (Szantoi et al., 2021; Foody Giles 2022). The overall accuracy

is the sum of perfectly classified pixels divided by the total sample size of pixels. The producer's accuracy informs the analyst (producer) of the percentage of correctly classified LULC compared to the real world. The user's accuracy measures errors of commission, which shows the probability of a classified pixel matching LULC type's user of its corresponding real-world location (Foody, 2020; Rwanga and Ndambuki, 2017). Therefore, the overall accuracy (O), user's accuracy (U), producer's accuracy (P) were used to assess the reliability of the classification. In addition, the agreement's kappa coefficient (K) was used to control only those pixels that may have been correctly classified by chance (Szantoi et al., 2021; Foody, 2022). The values of these indices range from 0 (indicating disagreement) to 1 (indicating perfect agreement)). A value above 0.80 for the K is considered satisfactory (Stehman, 2014).

Table 13: Typical confusion matrix for classification validation (This Table has been adapted from (Roland, 2021))

Classes	1	2	…	k	…	q	Total
1	N_{11}	N_{12}	…	N_{1k}	…	N_{1q}	N_{1+}
2	N_{21}	N_{22}	…	N_{2k}	…	N_{2q}	N_{1+}
…	…	…	…	…	…	…	…
K	N_{k1}	N_{k2}	…	N_{kk}	…	N_{kq}	N_{k+}
…	…	…	…	…	…	…	…
q	N_{q1}	N_{q1}	…	N_{qk}	…	N_{qq}	N_{q+}
Total	N_{+1}	N_{+2}	…	N_{+k}	…	N_{+q}	N

$$Oi = \sum_{j=1}^{q} Pjj \tag{33}$$

$$Ui = \frac{Pii}{Pi} \tag{34}$$

$$pj = \frac{Pjj}{Pj} \tag{35}$$

$$k = K_i = \frac{N \sum_{i=1}^{q} Pii - \sum_{i=1}^{q} (Pi+ * P+i)}{N^2 - \sum_{i=1}^{q} (Ni+ N+i)} \tag{36}$$

P = nombre de pixel

3.3.3.1.5 Change detection analysis

After the classification accuracy, the change detection analysis was done between the LULC maps obtained. Various change detection techniques have been developed throughout the years, namely layer arithmetic, direct classification, change vector analysis, transformation, and hybrid change detection (Tewkesbury et al., 2015). Post-classification change detection is one of the most established and widely used change detection methods applicable to Landsat class imagery (Tewkesbury et al., 2015). The fundamental advantage of this technique is that the basic classification and change transitions are explicitly known (Lu et al., 2004). LULC maps of the different dates were used to calculate the area of each LULC class and observe the changes that occurred (Zurqani et al., 2018). In addition, indicators such as spatial trend and the annual rate of LULC were then used for change detection and spatio-temporal quantification. From these pixel-based classification result images, the area of each LULC class and the rate of change were calculated using formulas (37), (38) and (39).

$$S_i\ (\%) = \frac{\mathrm{Si}}{\mathrm{St}} * 100\% \quad (37)$$

$$S_i = \mathrm{Si\,t1} - \mathrm{Sit2} \quad (38)$$

$$S_{ir} = \left(\frac{\mathrm{Sit1}}{\mathrm{Sit2}} - 1\right) * 100\% \quad (39)$$

where S_i denotes the area of LULC type i, St denotes the total study area, and S_i (%) represents the percentage of each LULC type area. S_{it1} and S_{it2} refer to the whole site of LULC type i in specific years 1 and 2, respectively. S_{ir} refers to the rate of change between the specified years.

3.3.3.2 Land use change modelling and future scenarios

Predicting and evaluating potential LULC is important for community leaders scientists, and natural resource managers to support land use planning and policy (Pocewicz et al., 2008). It is crucial to understand LULC change and how it may change in the future. A literature review showed that remote sensing and Geospatial Information System (GIS) techniques and the driver variables are the most widely used method for detecting and predicting LULC change (Singh et al., 2015; Liping et al., 2018; Wang et al., 2021). Over the last two decades, many LULC models have been developed to understand, evaluate, and project the future LULC change at spatial and temporal scales (Lambin et al., 2001).

Models can be static or dynamic (Agarwal et al., 2002; Lantman et al., 2011). Models can also be classified into non-hybrid and hybrid methods. The non-hybrid approaches, such as Markov Chain (MC), Artificial Neural Network (ANN), Cellular Automata (CA), have been widely used to identify the transitions in LULC classes and have been accurate in predicting LULC changes (Silva et al., 2020; Singh et al., 2022). The Non-hybrid methods have limitations in predicting LULC changes, no single model takes all characteristics of LULC into consideration. (Noszczyk, 2019).

To overcome the shortcomings of individual models, hybrid models have been introduced by combining several modelling approaches to address the complexity of real-world systems (Gaur et al., 2020). The hybrid models can capture LULC changes with greater accuracy (Gaur et al., 2020; Sankarrao et al., 2021). In the hybrid models, transition potentials of each LULC class are identified using regression models, and spatial characteristics are captured with transition sets and neighborhood effects. Compared to the individual models (individual CA and MC), hybrid models could more accurately capture LULC change at the basin level (Mishra et al., 2018). Clark Labs developed a LULC model based on GIS and remote sensing, known as the Land Change Modeller (LCM), to explore future changes in LULC using a Multilayer Perceptron neural network (MLP) and Markov chain (MC) (MLP-MC) (Mishra et al., 2014).

The MLP-MC model subsequently used a non-stationary relationship between selected explanatory variables and LULC maps to predict the future LULC. Mishra et al. (2018) endeavors to evaluate and compare three hybrid models: Stochastic Markov chain (ST-MC), cellular automata-Markov chain (CA-MC), and multi-layer perceptron-Markov chain (MLP-MC) to predict future land use/land cover (LULC) scenario in Varanasi district. The findings of this study are that the MLP-MC model yielded reliable and best results. The results demonstrate the potentiality of MLP-MC hybrid model for better understanding of spatio-temporal dynamics and predicting future landscape scenario in Varanasi district of Uttar Pradesh, India. Gaur et al. (2020) used hybrid and non-hybrid models to capture LULC scenarios for the Subarnarekha River and found that the MLP_MC model was the best-suited model. Therefore, the Multi-Layer Perceptron Markov Chain model (MLP-MC) embedded in LCM will be used in this study. The integration of MLP and MC takes advantage of both models (Leta et al., 2021; Sankarrao et al., 2021). While MLP is used to construct the transition potential maps (TPMs) for each transition, MC is used to perform time analysis. MLP is composed of a neural network based on feed-forward algorithm with three layers: the input,

hidden and output layers (Mas and Flores, 2008). One of the main advantages of MLP is its ability to model several or even all transitions at once. It adjust the weights of the input and output layers using the backpropagation process. MLP-MC uses explanatory variables and land-use change as inputs to forecast LULC changes (Sankarrao et al., 2021). Examples of applications can be found in (Fathizad et al., 2015; Mishra et al., 2018; Leta et al., 2021; Sankarrao et al., 2021).

Predicting future LULC was done in five steps: change analysis, identification of explanatory variables, creation of transition potential maps, change prediction, and validation. LULC maps of the years 1986 and 2006 were employed to analyze the trend of change, to calculate transition potential maps and to predict the LULC map of 2020. For model validation, the LULC classified map for 2020 was compared with the predicted LULC map of 2020. After demonstrating our model's ability to predict the LULC map of 2020, the same simulation technique was used to predict the LULC maps of 2050 using the LULC maps of 1986 and 2020 based on the business as usual (BAU) scenario (Mas et al., 2014). The BAU scenario is a scenario in which future LULC distributions follow the observed trends in the past and are formulated based on the transition probabilities and driving factors as predicted by the model. The assumption that the climate will not be disturbed by human activities has been adopted. The general scheme of the study is presented in Figure 18.

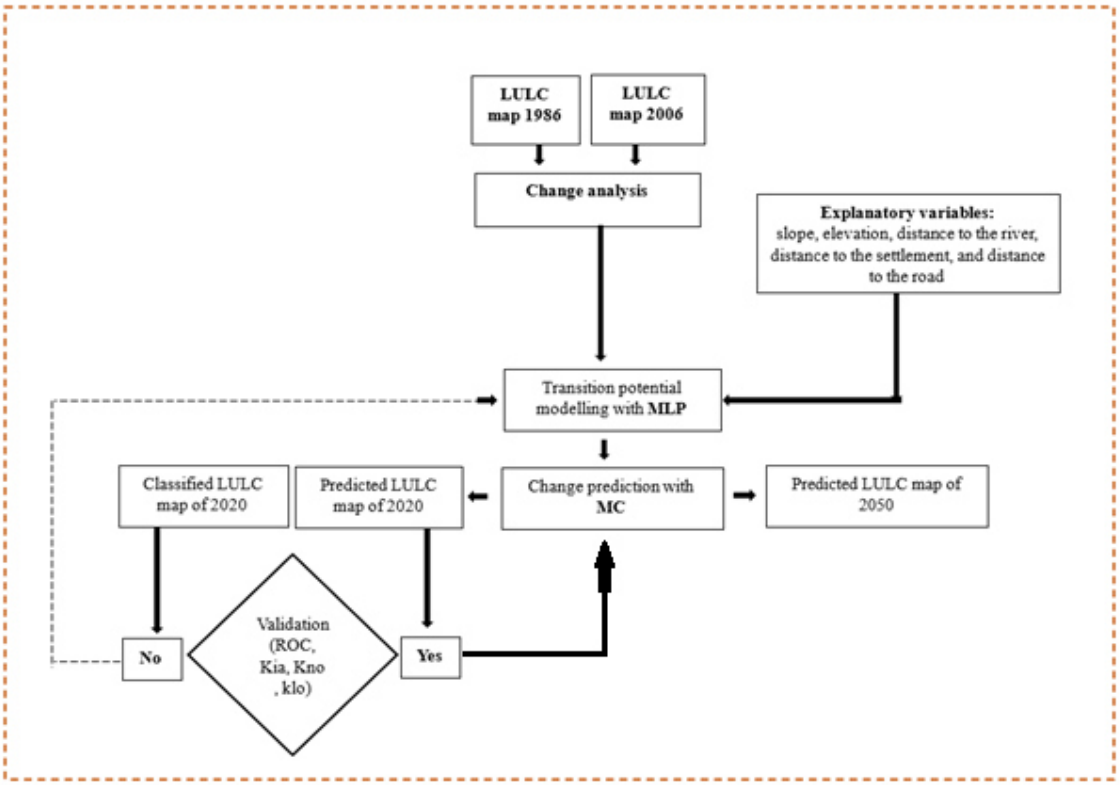

Figure 18:The procedures used to set up the Land change modeller and to simulate the future LULC map of 2050.

3.3.3.2.1 Changes analysis

The first step was the change analysis to define the transition classes. Changes are described as transitions from one class of LULC to another (Azari et al., 2022). The change analysis was performed by using the two earlier LULC maps with the module change analysis in LCM. The module change analysis estimates the gains and losses of each class between the two earlier LULC maps. Changes in terms of loss (Lij) and gain (Gij) are calculated using equations (40) and (41) (Thiam et al., 2021).

$$Lij = (Pi - Pii)\left(\frac{Pj}{\sum j=1 Pj}\right), \quad \text{where } i \neq j \tag{40}$$

$$Gij = (Pj - Pjj)\left(\frac{Pi}{\sum i=1 Pi}\right), \quad \text{where } i \neq j \tag{41}$$

where Lij is the proportion of loss from category i to j under random processes of loss, Pii is the proportion of category i that showed persistence between the two times, Gij is the proportion of gain from category i to j, Pj is the proportion of the landscape in category j at the end of time, Pjj is the observed persistent proportion of category j, and Pi is the entire area of category i at the starting point.

3.3.3.2.2 Identification of the explanatory variables

The second step was the identification of the explanatory variables that have driven past LULC changes. The simulation of LULC change depends on explanatory variables. Explanatory variables that have driven past LULC changes are influential in future changes and are selected based on available data and their explanatory capabilities (Murgante et al., 2014; Chinwendu, 2019). Based on the literature, slope, elevation, distance to the river, distance to the settlement, and distance to the road were selected as the main variables influencing the change in LULC over time (Murgante et al., 2014; Chinwendu, 2019). Slope and distance to the river were selected to represent the accessibility of a neighborhood. Distance to road and distance to settlement were used to highlight the proximity of urbanization.

3.3.3.2.3 Transition potential modelling

The third step was the determination of transition potential maps with the multilayer perceptron (MLP) model in LCM. MLP adjust the weights of the input and output layers using the backpropagation process. It only incorporates conductive factors with strong predictive capacity into the computation procedure, resulting in different transition potential maps for each sub-model. These maps show the ability to change from one LULC class to another (Mishra et al., 2014). The MLP model was established and tested using the explanatory variables and the change analysis obtained between the two earlier images as input. The MLP first created a random sample of cells that transitioned among LULC classes during the required time and started the automatic training process. The sample is divided into two equal parts, 50% of the sample for training and the remaining 50% for testing the performance. Transition potential maps were generated after the successful execution of MLP training for each class.

3.3.3.2.4 Change prediction

The fourth step was using Markov Chain (MC) in LCM to predict the LULC map for a specified future date. The historical rate change determined during the change analysis phase and transition potential maps are used as input in the MC model to predict the future LULC. The MC model is a stochastic process that shows the probability that one state will change into another. The MC model uses this information as the basis to predict future changes. The MC model creates a transition probability matrix of changes by examining past changes (Mishra et al., 2018). Based on a projection of the transition potentials into the future, the technique estimates LULC expected to transition from the later date to the forecasted date and provides a transition probability file (Mishra et al., 2014). The following equation represents the Markov chain analysis:

$$S(t, t+1) = Pij \times S(t) \quad (42)$$

Where,

S(t) is the state of the system at time t,

S(t+1) is the state of the system at time t+1 ;

Pij is the state transition probability matrix, which is calculated according to the following formula:

$$Pij = \begin{bmatrix} P1,1 & P1,2 & P1,N \\ \dots & \dots & \dots \\ PN,1 & PN,2 & PN,N \end{bmatrix}, (0 \leq Pij \leq 1) \quad (43)$$

Where P is the transition probability; Pij represents the probability of changing from the current state i to another state j at the next time; PN is the probability of the state at any time. The high transition has possibilities close to (1), and the low change will have a probability close to (0) (Wang et al., 2021).

3.3.3.2.5 Model validation

Model validation is a crucial component of the modelling process. It aims to verify the accuracy rate of the simulated map compared to a reference map. Two approaches have been used for model validation. The first approach is to use the metric performance indicators between the classified map and the predicted 2020 map to assess the accuracy of the prediction (Pontius and Batchu, 2003). These are the relative operational characteristic (ROC/AUC) and the validation

statistics of various Kappa indices, namely Kappa for no information (Kno), Kappa for location (denoted Klocation), KIA for h Kstandard. The relative operational characteristics (ROC/AUC) quantify the certainty of predicting the location of the change (Pontius and Batchu, 2003). Kappa for no information (Kno) gives the overall success of the simulation (Pontius, 2000). Kappa for location (denoted as Klocation) shows the agreement on location (Nadoushan et al., 2012). Kappa for agreement index (KIA) confounds disagreement on quantity with disagreement on location (Nadoushan et al., 2012). These Kappa indices reflect a perfect simulation when equal to 1, satisfactory when greater than 0.70, respectively, and excellent when greater than 0.8, respectively (Tiné et al., 2019). LULC model is valid if the Kstandard is greater than 70%, according to Zadbagher et al. (2018). The second approach is to compare the predicted and actual area of each LULC class.

3.3.4 Methodology for hydrological modelling of the Bafing watershed

The steps involved data preparation, model simulation, sensitive analysis, calibration, validation, and performance evaluation. The general approach adopted for the hydrological modelling is presented in Figure 19.

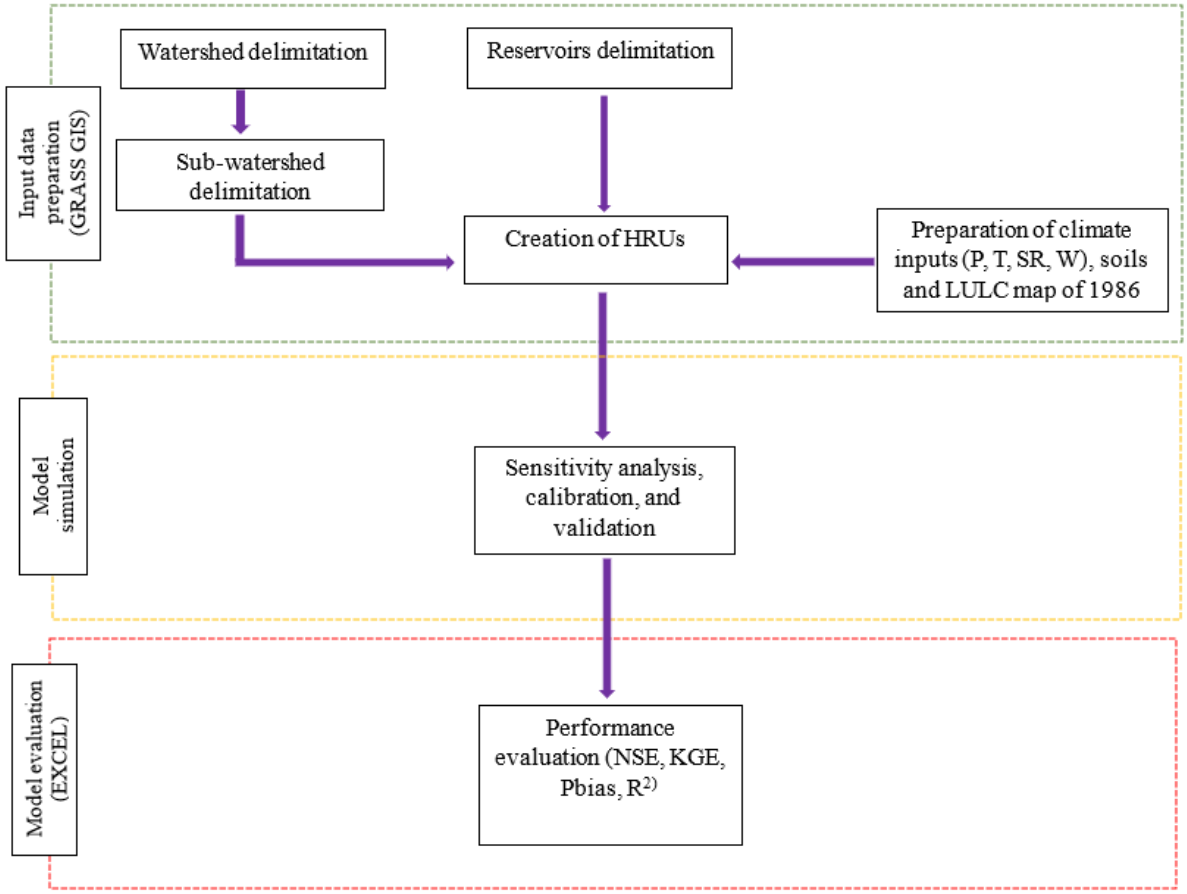

Figure 19: General Modelling approach adopted for this study.

P= precipitation, T=temperature, SR=solar radiation, W=wind.

3.3.4.1 Input data preparation

The first step was the preparation of input data in GRASS GIS (Figure 20). First, The MERIT DEM was used to delineate the watershed and analyze drainage patterns. After, with the function m.Swim: subbasins in GRASS GIS, the watershed was separated into several sub-basins. The function m.Swim: subbasins used the elevation from MERIT DEM and gauges station as input data. After the HRUs file was created using the GRASS GIS function m.Swim: hydrological response units. The function m.Swim: hydrological response units used the

subbasins file, soil map and LULC map as input data. LULC map was obtained with Landsat images and RF classification method. The HRUs have soil, slope, and land use characteristics that increase the accuracy of calculations. Then, the routing and file.cio was created by using the functions m.Swim:routing, m.Swim: substats with subbasins, accumulation and mainstreams files as input data. For the reservoirs, data such as the relationships between the dam surface area, water level, and water volume were computed for the two planned dams using the function r.lake in GRASS GIS at different inundation levels. The DEM and the location of the dams served as input data to the function r.lake in GRASS GIS. All these created files were used as input data to the SWIM model for the setup and simulation of the SWIM model.

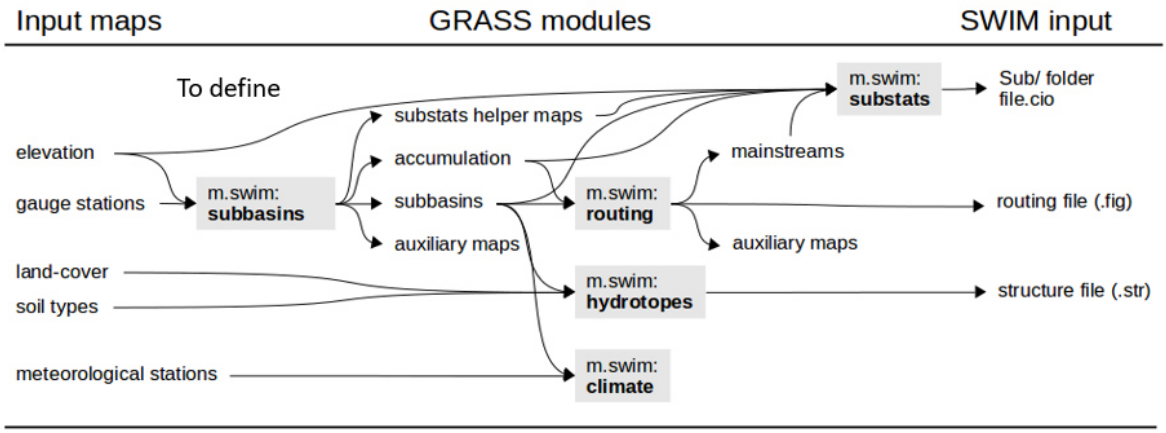

Figure 20: Approach adopted for input data preparation (Didovets, 2021)

3.3.4.2 Sensitivity analysis, calibration, and validation

For optimizing the model performance, sensitivity analysis, calibration and validation were performed.

3.3.4.2.1 Sensitive analysis

The sensitivity analysis was performed after the setup and simulation of the SWIM model. The sensitivity analysis aims to identify parameters and input variables that strongly or weakly influence the outputs of the model (Sane et al., 2020). Sensitivity analysis allows reducing the number of parameters to be use for the calibration (Sane et al., 2020). As part of this work, the sensitivity analysis was conducted manually. The procedure consists of changing only one parameter at a time on a predefined range of values while keeping the other constants and repeating the operation for the remaining parameters (Sane et al., 2020). However, it does not

quantify the interaction effects between parameters (Griensven, 2009). The 24 parameters to calibrate in the SWIM model are presented in the Table 14.

Table 14: Description of parameters in SWIM

Parameter	Description	Range
Evapotranspiration, routing, curve number, conductivity, precipitation		
ecal	Potential evapotranspiration	0.7 – 1.3
thc	Potential evapotranspiration on sky emissivity	0 – 1 (0 = without sky emissivity)
roc2 roc4	River routing coefficients for quick and slow components	1-50 (1 = quick routing; 50 = slow routing
cncor	Curve number	0.75 – 1.25
sccor	Soil hydraulic conductivity	1 – 50 the higher the value the higher conductivity
prcor	Precipitation	0.8 – 1.2
Groundwater		
bff	Base flow factor used to calculate return flow travel time	0.1 – 3
abf	Alpha factor for groundwater. This parameter characterizes the ground water recession	0.0005 – 0.95
delay	Groundwater delay (days). The time it takes for water leaving the bottom of the root zone until it reaches the shallow aquifer where it can become groundwater flow	1 – 200?
revapc	Fraction of recharge that "re-evaporates" directly from the shallow groundwater aquifer	0 – 0.3
rchrgc	Deep aquifer percolation coefficient. The amount of water that is allowed to percolate from shallow into the deep aquifer	0 – 1
revapmn	Revap storage (mm). Shallow aquifer storage must exceed REVAPMN before groundwater flow can begin	
Transmission losses		
tlrch	Transmission losses riverbed	0 – 3 (0 = no losses)
evrch	Evaporation from river surface	0 – 3 (0 = no losses)
tlgw	Destination of transmission losses	0 = to shallow gw; 1 = to deep gw; 2 = to both in equal terms
Elevation-based precipitation & temperature correction		
xgrad1	Precipitation factor	(-)3 – (+)3
tgrad1	Temperature factor	?
ulmax0	holding capacity	?
rnew	fresh snow density	
Snow		
tsnf	Snow fall temperature	(-)3 – (+)3
tmelt	Snow melt temperature	(-)3 – (+)3
smrte	Snow melt rate	?
gmrte	Glacier melt rate	?

3.3.4.2.2 Calibration and validation of SWIM model

After the sensitive analysis of the model, the calibration and validation of the model was realized based on the parameters obtained. Calibration is a phase that involves adjusting model parameters so that the simulated flows correspond to the observed flows (Sane et al., 2020). The objective is to determine the values of the parameters of the model that allow it to obtain the best performance of a given criterion. The calibration of the hydrological model is explained as follows: first, all parameters inherit a default value from the attributes or parameterization of the input data of the model (soil type, land cover, etc.). The SWIM model was calibrated and validated with the observed flow data on a daily time step at the Bafing Makana and Dakka Saidou gauges. Thus, the Nash-Sutcliffe efficiency (NSE), the Kling-Gupta efficiency (KGE), Percent Bias (Pbias) and the coefficient of determination R^2 were used to evaluate the model performance.

Firstly, the calibration was carried out without the integration of the reservoir module for the period from 1979 to 1986 at the gauge of Dakka Saidou and Bafing Makana. Calibration was performed manually with sensitive parameters obtained after sensitivity analysis.

Secondly, the Manantali dam was included in the model through the reservoir module (Figure 21). The values of parameters obtained during the first step of the calibration were used as a starting set to calibrate the daily inflow in the Manantali dam. The simulated inflow, outflow and water stored in the Manantali dam were compared with the observed inflow, outflow and water level during the period 2003 to 2009 based on pre-established management rules. The calibration was based on the allocation of the minimum target downstream flow (hydropower generation requirement) and the adjustment of the special annual cycle coefficient, which regulates the percentage of volume that can be discharged each month.

Thirdly, the future Boureya and Koukoutamba dams were included in the model (Figure 21). To calibrate the inflow in koukoutamba and boureya dams, the set of parameters obtained during the second step of calibration was used as a starting set to calibrate the sub-basins upstream of the Bafing Makana and Dakka Saidou stations. The calibration was also based on the assignment of the minimum target downstream flow (hydropower generation requirement) and the adjustment of the special annual cycle coefficient, which regulates the percentage of the water volume that can be released in a given month.

During the fourth stage, the entire watershed (excluding the sub-basins of the upstream Koukoutamba and Boureya dams) was recalibrated manually, taking the flow of the Bafing Makana station and Dakka Saidou as objective functions. Once the model is calibrated, it must be passed to a validation step which consists in verifying by a comparison of the data simulated and observed through a quality criterion (Sane et al., 2020). Its principle is to test the model on a series of data other than the data used in the calibration phase. The model was validated during the period of 1987-1994 using the latest parameters obtained during the recalibration of the entire watershed.

3.3.4.2.3 Performance evaluation of the model

To determine how closely the model's simulated values matched the actual values, the model's performance was examined. Various objective functions are offered to evaluate the effectiveness of the model. Thus, the performance of the model was evaluated using the NSE, KGE, Pbias and R^2. The NSE is the most used tool for evaluating the correctness of model simulation results. The R^2 provides a measure of how well observed outcomes are replicated by the model. The Pbias is used for quantifying the volume errors. The ideal value for Pbias is zero and lower values indicates accurate model simulation while positive and negative values indicate model underestimation and overestimation biases respectively. The KGE simultaneously optimizes three aspects of the model's predictive capability: correlation, bias and variability (Pulighe et al., 2020). In addition, the value of KGE corresponds to the minimum of the values taken by its three components, making it an easy index to interpret. The dimensionless structure of these criteria allows the performance evaluation across several catchments, making them particularly helpful in model evaluation (Sane et al., 2020). According to Moriasi et al. (2007) and Kling et al. (2012), a simulation model can be considered satisfactory based on the thresholds defined in Table 15.

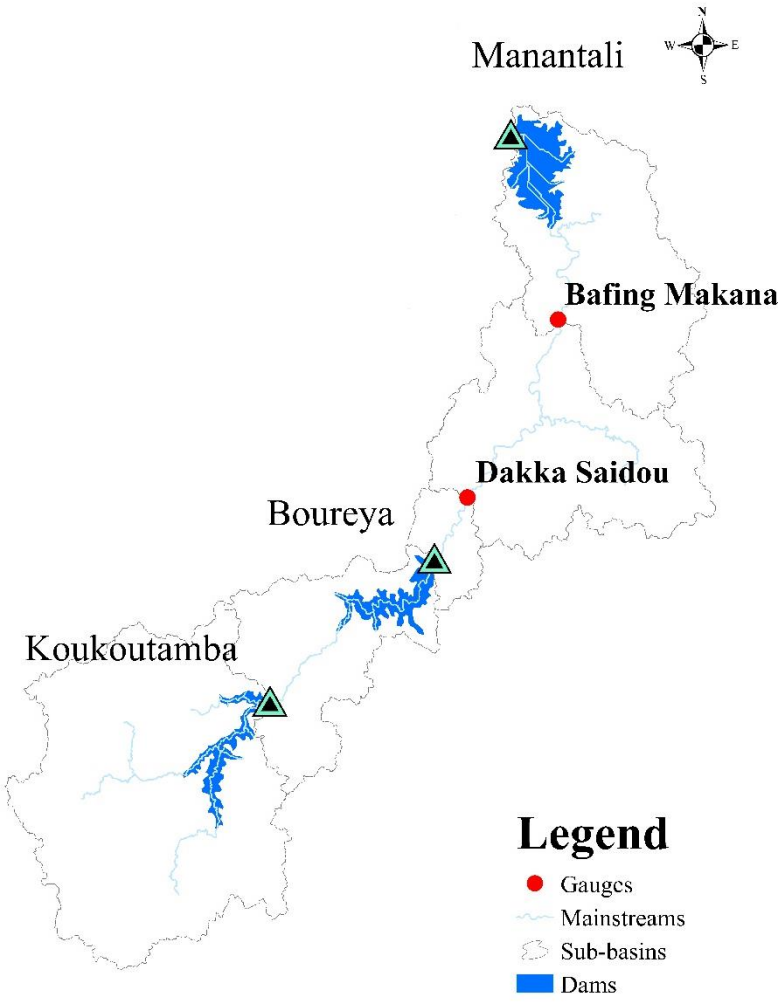

Figure 21: Localization of the existing (Manantali) and future dams (Koukoutamba and Boureya) in the Bafing watershed.

Table 15: Interpretation for the performance evaluation on the SWIM model.

Performance evaluation of the hydrological model	**Formula**	**Value range**	**Classification des Performances**	
NSE	$1-\frac{\sum(Q_{obs}-Q_{sim})^2}{\sum(Q_{obs}-\overline{Q}_{obs})^2}$	0.75 < NSE ≤ 1.00 0.65 < NSE ≤ 0.75 0.50 < NSE ≤ 0.65 0.4 < NSE ≤ 0.50 NSE ≤ 0.4	Very well Good Satisfactory Acceptable Not satisfactory	(44)
R^2	$\frac{\sum((Q_{obs}-\overline{Q}_{obs})(Q_{sim}-$ $\sum(Q_{obs}-\overline{Q}_{obs})^2 * \sum(Q_{sim}$	R^2>0.5	R^2 values >0.5 acceptable pour la simulation	(45)
Percentage bias (PBIAS)	$\frac{\sum(Q_{obs}-Q_{sim})*100}{\sum(Q_{obs})}$	PBIAS $<\pm10$ $\pm10 \leq$ PBIAS $<\pm25$ $\pm10 \leq$ PBIAS $<\pm25$ $\pm25 \leq$ PBIAS $<\pm40$ PBIAS $\geq\pm10$	Excellent Good Satisfactory Acceptable Not satisfactory	(46)
KGE	KGE $= 1$ $-\sqrt{(r-1)^2+(\beta-1)^2+}$	KGE ≥0.90 0.90 ≥ KGE ≥ 0.75 0.75≥ KGE ≥ 0.5 0.5≥ KGE ≥ 0	Excellent Good Satisfactory not satisfactory	(47)

Where r is the Pearson correlation coefficient, $\beta = \mu s/\mu 0$ the ratio of simulated (μs) and observed ($\mu 0$) flow means and $\gamma = CVs//CV0$ the ratio of simulated (CVs) and observed flow ($CV0$) coefficients of variation (Roland, 2021); Q obs= observed flow, Q sim= simulated flow.

3.3.4.3 Water management scenarios

The development scenarios (DS) are designed so that future dams are considered in the simulation (Table 16).

Table 16: Dam development scenarios

Development scenario 1 (DS1)	Manantali dam only
Development scenario 2 (DS2)	Manantali and Koukoutamba dams
Development scenario 3 (DS3)	Manantali, Koukoutamba and Boureya dams

3.3.4.4 Simulation periods

The reference period (P0) around the year 2000 represents the period 1984–2014. The near future around 2050 (P1) is the period 2035–2065, the far future around 2080 (P2) correspond to the period 2065–2095.

3.3.4.5 Impact assessment

In the context of this study, the main objective is to evaluate the impact of climate change and LULC change on hydrology and the hydropower potential (HPP) of the system by first considering the Manantali dam alone (DS1), then the Manantali dam, Koukoutamba system (DS2) and Manantali dam, Koukoutamba Boureya system (DS3). Climate change and LULC change are assumed to be independent in order to differentiate the respective contributions of these two factors. Their impacts are estimated by a separation method consisting of changing one factor at a time (either climate or LULC) by keeping the other constant (Mekonnen et al. 2018) and combining the two factors (climate and LULC). A set of relevant performance indicators is used to compare future scenarios with the reference period. These indicators are spill, and probabilities of exceedance. In this case, the spill is considered as a failure associated with the maximum capacities, which could negatively affect the hydropower generation. For future dams, management objectives have not yet been established. Thus, the criterion reliability is applicable only to the Manantali dam. Table 17 provides a detailed explanation of each indicator used and the accompanying measurement technique.

Table 17: List of performance indicators names, definitions, and measurement methods

Indicator name	Definition	Measurement method
Production (GWh/y)	Mean annual electricity production	Mean of produced electricity during the simulated periods compared to the reference
Spill (Mm^3/a?)	Spilled volume	Sum of the volumes spilt during the simulated periods compared to the reference
Probability of exceedance	The exceedance probabilities correspond to the annual electricity production level that is reached with a defined probability.	Probability of exceedance (EP99, EP90 and PP95) during the simulated periods compared to the reference

3.4 Conclusion

Observational data are insufficient for modelling purposes (1979-1986 and 2001-2003) in the Bafing watershed. Thus, in order to choose the best precipitation product, the precipitation products W-era5 (reanalysis data) and CHIRPS (satellite data) were compared to the observed precipitation for the Bafing Makana station. The performance of these products in representing observed trends was analyzed based on statistical indicators, such as R^2, RMSE, Pbias, NSE, the Taylor diagram at monthly and annual time steps and seasonal analysis. Next, the performance of 10 GCMs from ISIMIP 3b in reproducing the reference climate over the period 1979-2014 was assessed based on statistical indicators (such as R^2, RMSE, Pbias, NSE), the Taylor diagram, seasonal analysis and the analysis of historical trends with the Man Kendal test. Then, the analysis of future climate trends (precipitation, temperature) was carried out in the near future (P1: 2035-2065) and the far future (P2: 2065-2095) compared to the reference period (P0: 1984-2014) under ssp 126 and ssp 370.

The land use and land cover mapping (1986, 2006 and 2020) was carried out using the Random Forest (RF) classification method in the Google Earth Engine (GEE) platform. Landsat imagery from 1986, 2006 and 2020 was used for the LULC mapping. The mapping was carried out in

three steps namely Landsat image preprocessing, supervised classification with the Random Forest classification method and evaluation of classification accuracy. Five classes of LULC namely settlement, water, vegetation, cultivated areas, and bareground were used in the classification. A confusion matrix was generated in GEE and the overall accuracy (O), user accuracy (U) and producer accuracy (P) and kappa index (K) were then used to assess the reliability of the classification.

The prediction of LULC change for 2050 was performed using the Multilayer Perceptron neural network (MLP) and Markov chain (MLP_MC) model in Land change Modeller (LCM). The prediction of LULC map of 2050 was done in five steps: analysis of changes, identification of explanatory variables, creation of transition potential maps, prediction and validation of the model. The maps of LULC of the years 1986 and 2006 were used for the change analysis, the creation of transition potential maps and the prediction of LULC map of 2020. For model validation, performance indicators such as relative operational characteristic (ROC) and Kappa index validation statistics (Kno, Klocation, KIA) between the classified map and the predicted map of 2020 were used to assess the accuracy of the prediction. After the validation of the model, the same simulation technique was used to predict the LULC map of 2050 using the LULC map of 1986 and 2020 based on the BAU scenario.

The Soil and Water Integrated Model (SWIM) was chosen to simulate hydrological processes in the Bafing watershed considering the LULC change, climate change and the management of existing and future dams. The SWIM model was simulated with the outputs of the ten GCMs and the LULC maps of 1986, 2006 and 2020. The calibration of the model was done during the period 1979-1986 and the validation over the period 1987-1993 with the integration of dams (Manantali, Koukoutamba and Boureya). Model performance was evaluated using NSE, KGE, Pbias, R^2. Development scenarios (DS) were established so that future dams were considered in the simulation process. The hypothesis that climate change and LULC change are independent was done to separate the respective contributions of these two factors. Their effects were calculated using a separation method that involves changing one factor at a time (either climate or land cover while holding the other constant) and combining the two factors. A set of relevant performance indicators was used to compare future changes with the reference period. These indicators include volume spilled and probabilities of exceedance (P99, P90, P95).

Chapter 4: Global Climate Model performance and future trend analysis in the Bafing watershed

This chapter provides results on the ability of two precipitation products (satellite-based data (CHIRPS) and reanalysis data (W-era5)) to reproduce the observed precipitation in the Bafing watershed (Bafing Makana rainfall station) during the period 1981-1986 and 2001-2003. After, the historical simulations of ten GCM data from ISIMIP 3b were compared with the reference data for the period 1979-2014 (of which both data are available). Further, the projection of temperature and precipitation were used to study the projected change in climate in the near future (P1:2035-2065) and the far future (P2: 2065-2095) compared to the reference period (P0: 1984-2014) under the ssp 126 and the ssp 370.

4.1 Assessment of the ability of two precipitation products (satellite-based data (CHIRPS) and reanalysis data (W-era5)) to reproduce the observed precipitations data

- **Statistical results (monthly and annual scale)**

On a monthly scale, the values of the correlation coefficients obtained are positive and comprise between 0.9 and 1, indicating a strong association between the observed data and the two precipitation products (CHIRPS, W-era5) (Table 18). However, the correlation is more assertive with the W-era5 data with a value of 0.94 (Table 18). Similarly, the Pbias values obtained are acceptable because they range between -20 to 20. The Pbias value obtained with W-era5 is close to 0, indicating that the W-era5 are almost identical to the observed data (Liu et al., 2019). Ideally, the RMSE value should be 0 (Ali and Abustan, 2014), but the values obtained with W-era5 are lower than that obtained with CHIRPS (Table 18). The NSE values obtained are greater than 0.80 (CHIRPS) and 0.9 (W-era5), showing that the two products reproduce satisfactorily the observed precipitation. The results of the RMSE and correlation of the Taylor diagram (RMSE, correlation) coincide with the statistical results found (Figure 22). The results of the standard deviation of the Taylor diagram show that the difference between the observed and CHIRPS data is between 100 and 150, while between the observed and the W-era5 data is between 50 and 100. The results show that the W-era5 data better represents the observed data than the CHIRPS data on a monthly scale.

On an annual scale, there is an acceptable degree of correlation (0.7) and a poor NSE (0.3) between CHIRPS and the observed data (Table 18). On the other hand, the correlation between W-era5 and the observed data is very high, with a value of 0.9 and an acceptable NSE (0.6).

The values obtained from RMSE are very high for both products (Table 16). However, the value obtained with W-era5 is lower (226%) than that obtained with CHIRPS.

In summary, these results highlight that the W-era5 data represents better the observed data than the CHIRPS data on a monthly and annual scale based on the statistical results.

Table 18: Pearson correlation, Pbias, RMSE and NSE calculated between observed and estimated rainfall products (W-era5, CHIRPS) at monthly and annual scales.

Station	**Period**	**RMSE**	**Pbias (%)**	**NSE**	**Pearson Cor**
Monthly scale					
Bafing	W-era5	35	1.5	0.91	0.94
	CHIRPS	45.1	11.9	0.82	0.91
Annual scale					
Bafing	W-era5	168	1.5	0.641	0.904
	CHIRPS	228	11.9	0.337	0.741

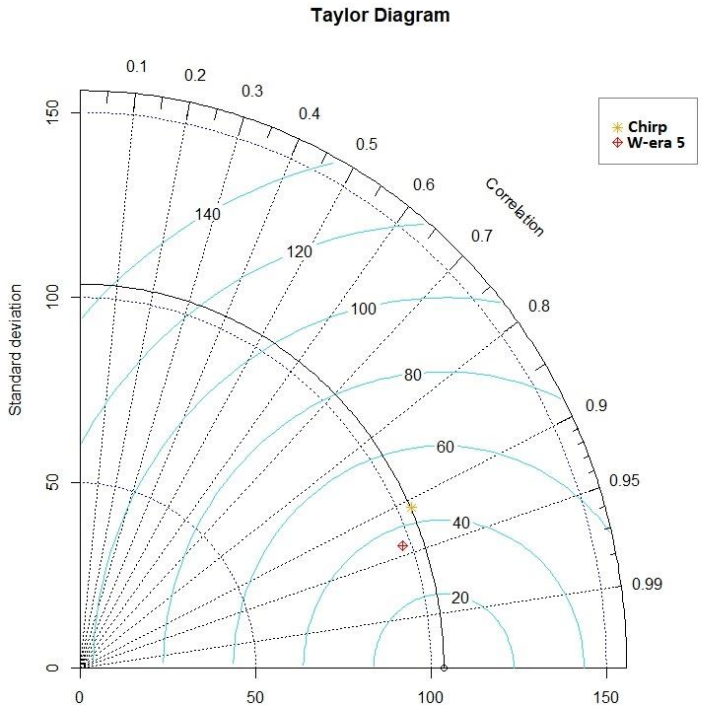

Figure 22: Spatial representation by Taylor diagram (Pbias, RMSE and standard deviation) between observed and estimated rainfall products at monthly scale

➢ **Seasonal analysis**

At the seasonal scale, the unimodal profile of observed precipitation was reproduced by both products (W-era5 and CHIRPS) (Figure 23). The beginning (April), the end (November) and the rainiest month (August) of the rainy season for both products are also consistent with the observed data (Figure 23). However, there is an overestimation of 15% of precipitation by CHIRPS and 4% by W-era5 for the rainy season (especially in August). In conclusion, the observed seasonality is better represented by W-era5 than CHIRPS.

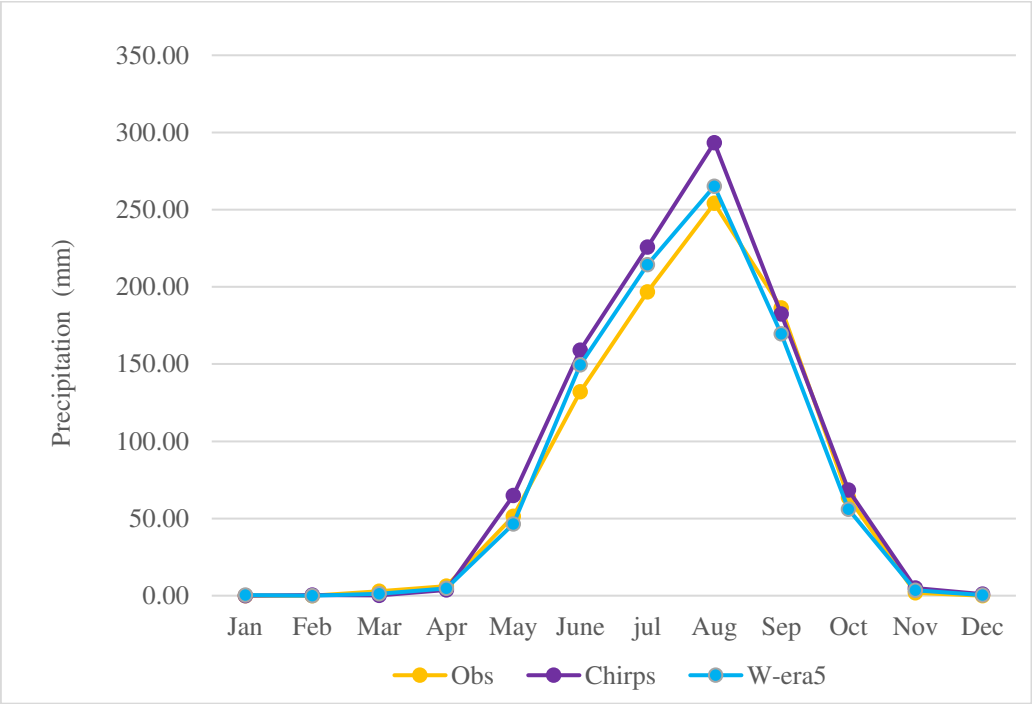

Figure 23: Comparison of monthly reanalysis (W-era5) and satellite precipitation (CHIRPS) with observed precipitation during the period 1981-1986 and 2001-2003.

➢ **Interannual variability**

The analysis of interannual variability shows substantial year-to-year variations, although the intervals are too short to accurately describe interannual rainfall variability in the Bafing watershed. Figure 24 shows that, although both products overestimate annual precipitation, the overestimation obtained by CHIRPS is higher than those of W-era5, except in 2003.

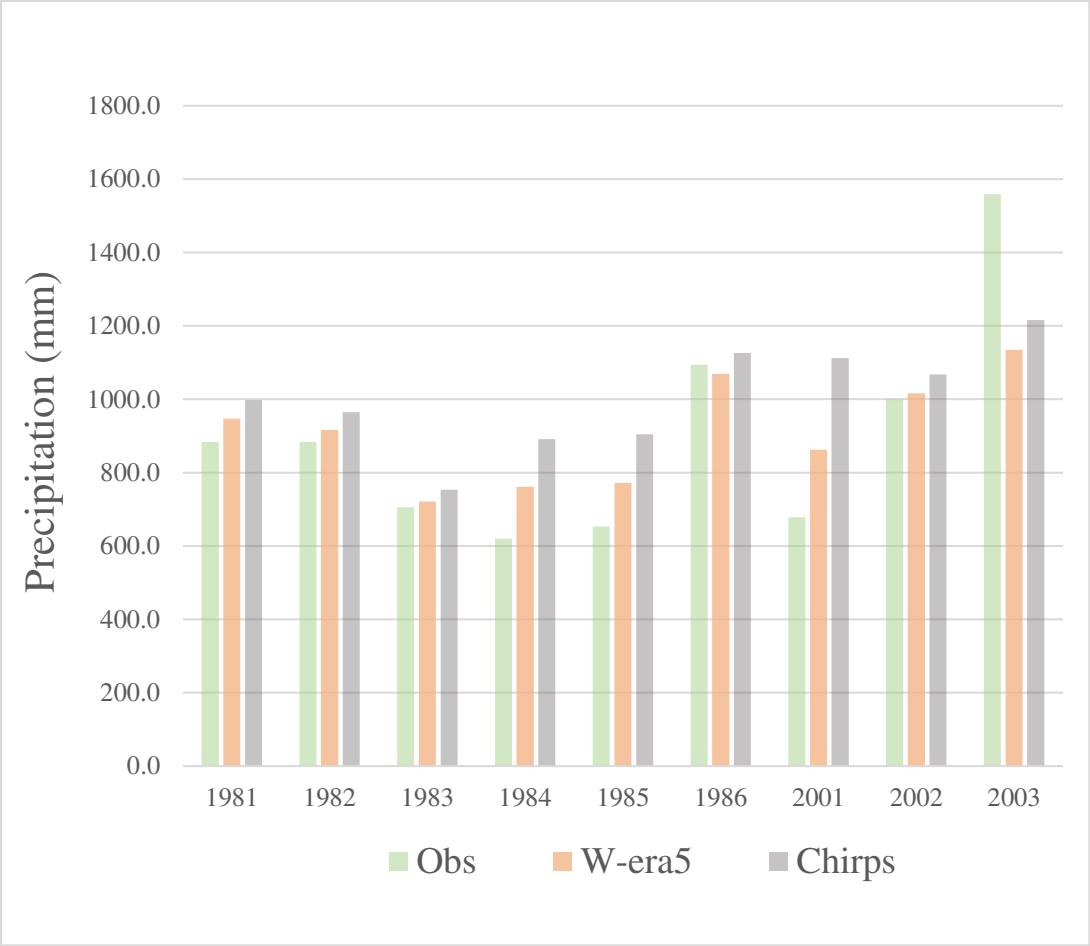

Figure 24: Analysis of interannual variability between W-era, CHIRPS and observed precipitation during the period 1981-1986 and 2001-2003

In this section, two precipitation products: reanalysis data (W-era5) and satellite data (CHIRPS), were compared with observed precipitation of the Bafing Makana station on an annual, monthly and seasonal basis. Different characteristics were observed between the reanalysis data and the satellite data. Both products tend to overestimate observed precipitation, but it is more pronounced with CHIRPS than W-era5. In addition, W-era5 showed the highest accuracy with a good monthly and annual correlation and low bias values based on statistical measures. Thus, the reanalysis data (W-era5) will be used to evaluate the performance of climate model data to reproduce the observed climate.

4.2 Evaluation of the performance of GCM from ISIMIP 3b to reproduce temperature and precipitation of the reference climate data (W-era5)

This performance assessment was based on the comparison of W-era5 and 10 GCMs from ISIMIP 3b data over the period 1979-2014.

4.2.1 Statistical Analysis (monthly scale)

The statistical analysis (R^2, RMSE, Pbias, NSE) results performed on a monthly scale to evaluate the ability of 10 GCMs from ISIMIP 3b models to reproduce the W-era5 reference data are presented in Table 17 and Figure 21.

- **Precipitation**

The values of the correlation coefficients obtained are positive and greater than 0.8 on the monthly scale, demonstrating a significant correlation between the reference (W-era) and the ten GCMs (Table 19). The bias values obtained are acceptable because they are close to 0 or equal to 0 (Liu et al., 2019). The RMSE values are between 49.8 and 68. Ideally, the RMSE value should be 0, but the values obtained are still acceptable (Ali and Abustan, 2014). The NSE values obtained are between 0.6 and 0.8, indicating that the ten models satisfactorily reproduce the reference data (W-era5). Considering the median and mean of the 10 GCMs from ISIMIP3b (stand for the multi model ensemble of the 10 GCMs from ISIMIP (MME)), they have both a positive correlation and an acceptable NSE higher than those obtained with the individual models. The RMSE values are lower than those obtained with the individual models. It is also noted that the median of MME is 6% lower than the mean (MME). The values of the Pbias for both (median and mean of MME) are high exceeding the range of -20 and 20. They are also superior to those obtained with individual models. Another aspect to highlight is that the median of MME is 26% lower than the mean (MME). The results of the RMSE and correlation of the Taylor diagram (RMSE, correlation) are consistent with the statistical results found (Table 19, Figure 25).

Table 19: Statistical analysis (Pearson correlation, Pbias, RMSE and NSE) between reference data (W-era5) and GCM of ISIMIP 3b precipitation at monthly scale.

Climate models	Year	Rmse	Pbias	NSE	R^2
CanESM5	1979-2014	60.2	-0.8	0.69	0.85
CNRM-CM6-1	1979-2014	59.4	-1.1	0.69	0.85
CNRM-ESM2-1	1979-2014	68	-2.8	0.60	0.82
EC-Earth3	1979-2014	62.3	-1.4	0.66	0.85
GFDL-ESM4	1979-2014	59.5	-4.8	0.69	0.85
IPSL-CM6A-LR	1979-2014	52.8	-0.3	0.76	0.88
MIROC6	1979-2014	59.2	-0.9	0.70	0.85
MPI-ESM1-2-HR	1979-2014	61	-1.4	0.68	0.85
MRI-ESM2-0	1979-2014	59.4	1.7	0.69	0.86
UKESM1-0-LL	1979-2014	49.8	0.0	0.79	0.89
Mean	1979-2014	41.2	26.1	0.80	0.93
Median	1979-2014	38.6	19.1	0.82	0.93

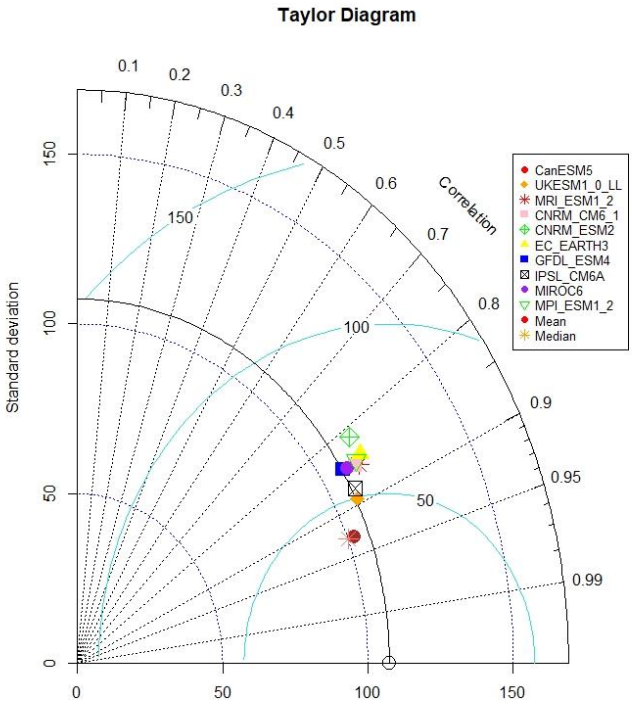

Figure 25: Spatial representation by Taylor diagram (Pbias, RMSE and standard deviation) between W-era5 and 10 GCMs of ISIMIP 3b precipitation at monthly scale

- **Temperature**

On a monthly scale, the temperature simulated by the ten GCMs from ISIMIP 3b satisfactorily reproduces the reference data (W-era5) with correlations greater than 0.9, NSE greater than 0.8 and RMSE values and bias close to 0 (Table 20). The median and mean of MME have a better performance than the individual models. The results obtained with the Taylor diagram (RMSE, correlation) agree with the statistical results found (Figure 26, Table 20). In addition, according to the Taylor diagram, the gap between the reference data (w-era5) and the data from the ten single GCM is more significant than the mean/median (MME).

Table 20: Statistical analysis (R^2, Pbias, RMSE and NSE) between reference data (W-era5) and GCM of ISIMIP 3b temperature at monthly scale.

Temperature					
Climate models	Year	**Rmse**	**Pbias**	**NSE**	**Pearson Cor**
CanESM5	1979-2014	1.06	0.20	0.83	0.92
CNRM-CM6-1	1979-2014	1.01	0.10	0.85	0.93
CNRM-ESM2-1	1979-2014	0.96	0.10	0.86	0.93
EC-Earth3	1979-2014	1.05	-0.10	0.84	0.92
GFDL-ESM4	1979-2014	0.96	0.00	0.86	0.93
IPSL-CM6A-LR	1979-2014	0.98	0.10	0.86	0.93
MIROC6	1979-2014	1.11	-0.50	0.82	0.91
MPI-ESM1-2-HR	1979-2014	1.00	-0.20	0.85	0.93
MRI-ESM2-0	1979-2014	1.07	0.00	0.83	0.92
UKESM1-0-LL	1979-2014	0.90	0.10	0.88	0.94
Mean	1979-2014	0.69	-0.10	0.93	0.96
Median	1979-2014	0.70	-0.10	0.93	0.96

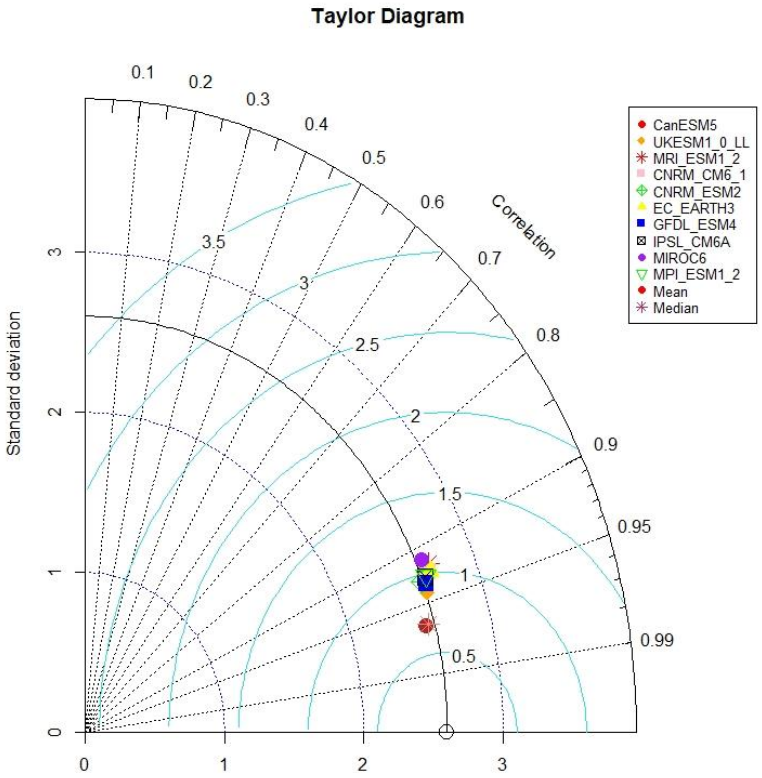

Figure 26: Spatial representation by Taylor diagram (Pbias, RMSE and standard deviation) between W-era5 and the ten singles GCM, the mean of MME and the median of MME of temperature at monthly scale

4.2.2 Seasonal analysis

- **For precipitation**

All climate models capture the unimodal profile and the peaks of August. However, some models such as CNRM-CM6-1, GFDL-ESM4, MIROC6, MRI-ESM2-0, CNRM-ESM2-1 overestimate the peak of August, while other models such as CanESM5, EC-Earth3, MPI-ESM1-2, UKESM1-0-LL underestimate it (Figure 27). Considering the MME, the Median and Mean are both in agreement with the W-era5 precipitation (Figure 27).

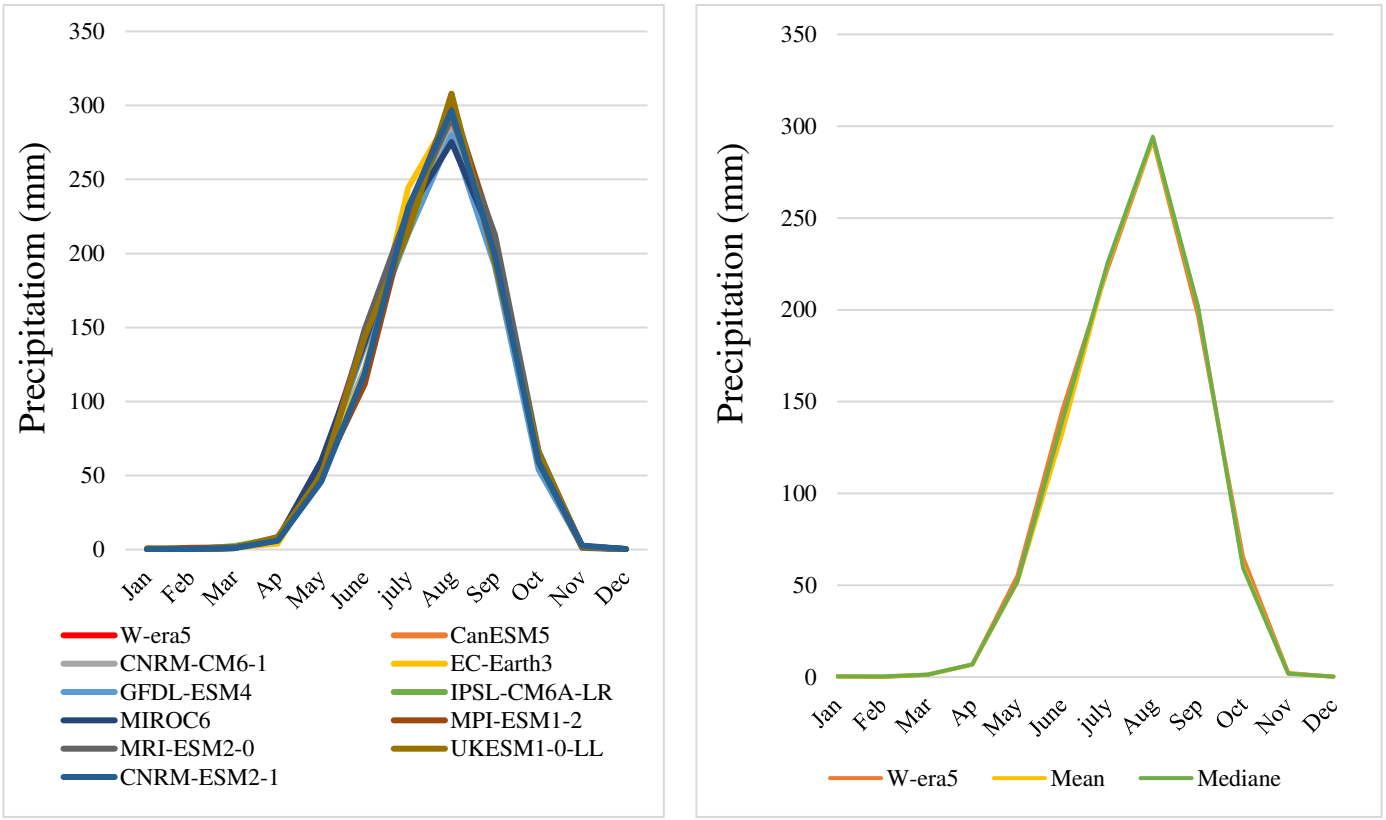

Figure 27: Comparison of the W-era5 and the 10 GCM from ISIMIP 3b models, the mean and the median (MME) of precipitation (mm) over the period 1979-2014

➢ **For temperature**

All climate models have captured the bimodal temperature profile provided by W-era5, with a first peak in March (around 30 °C) and the second peak in October (around 27 °C). The result implies that the models were able to reproduce the warmest and coldest months in the study area. The median and mean are in perfect agreement with the W-era5 data (Figure 28).

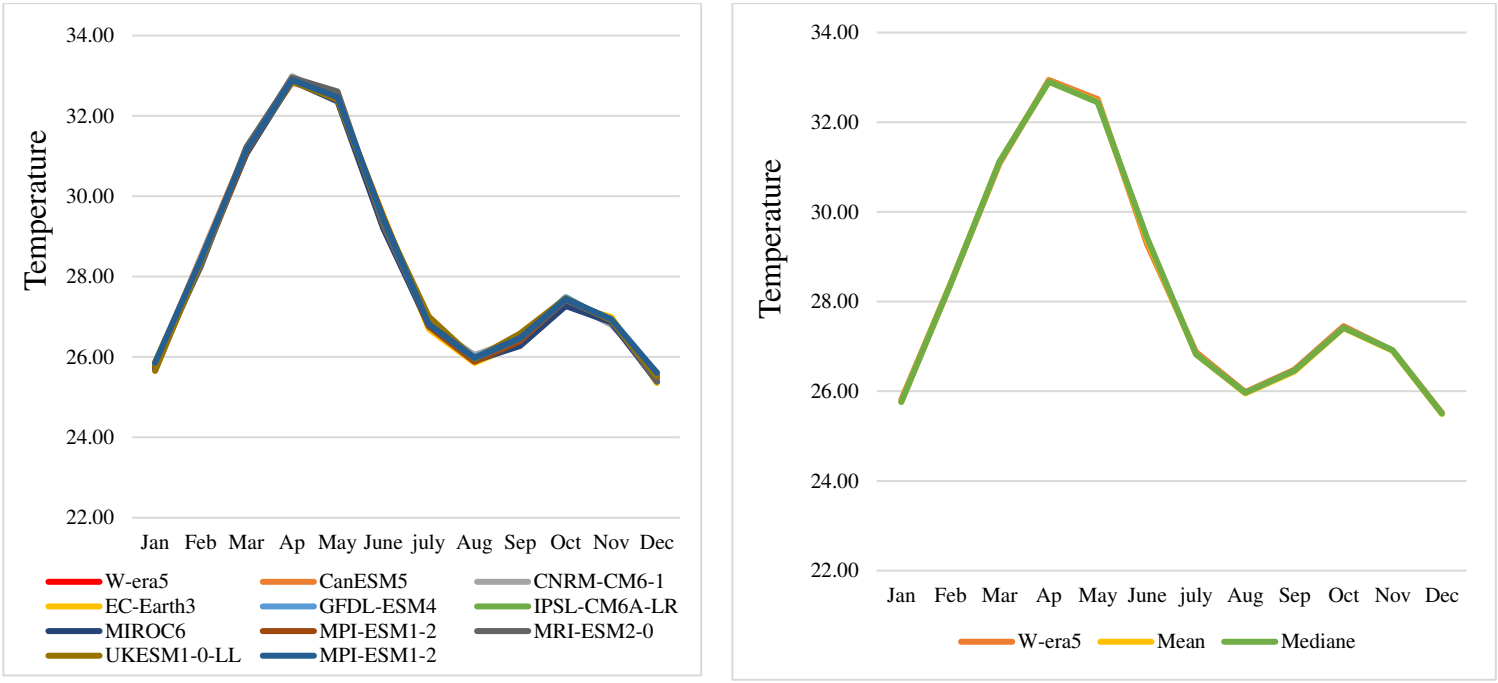

Figure 28:Comparison of the W-era5 and the 10 single GCM, the mean and the median of MME of temperature over the period 1979-2014

4.2.3 Past trend analysis (annual scale)

The results of the Mann-Kendall trend tests and the Sen-slope are presented in Table 21. In these tests, the null hypothesis (H0) indicates no trend in the series, while the alternative hypothesis (H1) indicates that there are downward or upward trends. The level of statistical significance of trends for the p-value is 0.05. The trend is non-significant (N.S.) for p-values ≥ α=5%. It is up for a n positive Sen slope and a p-value < α. For precipitation, the W-era5 reference data does not show a significant trend. All models show no significant trend as W-era5 trend except CNRM-CM6-1 and MRI-ESM2-0. For temperature, the results show that there is a significant upward trend of W-era5. The results also indicate that all models could reproduce this upward temperature trend over the Bafing watershed.

Table 21: Mann-Kendall and Sen test for precipitation and temperature by W-era5, GCMs, median and mean of MME during 1979-2014

Models	Annual precipitation (1979-2014)			Annual temperature (1979-2014)		
	Z	p-value	Sen's slope	Z	P-value	Sen's slope
W-era5	1.21	0.23	0.1379	3.72	0.00019000000	0.42
CanESM5	1.96	0.05	0.22	5.17	0.00000022300	0.59
CNRM-CM6-1	-0.477	0.6328	-0.06	4.023	0.00005746000	0.46
EC-Earth3	2.6	0.0089	0.30	3.72	0.00019820000	0.42
GFDL-ESM4	1.2572	0.2087	0.14	4.2744	0.00001910000	0.49
IPSL-CM6A-LR	0.125	0.9	1.56	4.4	0.00001080000	0.50
MPI-ESM1-2-HR	0.35	0.724	0.04	2.489	0.01200000000	0.28
MRI-ESM2-0	-0.35	0.724	-0.04	3.847	0.00011960000	0.44
UKESM1-0-LL	1.15	0.24	0.13	4.75	0.00000201000	0.54
CNRM-ESM2-1	0.804	0.421	0.09	4.3	0.00001700000	0.49
MIROC6	2.5898	0.0096	0.29	0.35	0.72430000000	0.04
Mean	3.5201	0.00043	0.40	6.38	0.00000000017	0.72
Median	3.23	0.001233	0.37	6.48	0.00000000009	0.74

These results showed that GCM from ISIMIP 3b can reproduce the precipitation and temperature of W-era5 and provide reliable projections. For the multi-model ensemble of the 10 GCMs from ISIMIP 3b (MME), the median of MME can be considered more representative of W-era5 compared to the mean of MME. The results of statistical measurements show that the median of MME is more efficient than mean of MME to reproduce the reference data (W-era5). In addition, the median of MME can handle outliers that would carry too much weight if the mean were used. Thus, it will be used for the analysis of future trends for the near future (P1: 2035-2065) and the far future (P2: 2065-2095) compared to the reference period (P0: 1984-2014).

4.3 ISIMIP3b climate projections over the Bafing watershed

Precipitation and temperature trends were analyzed by comparing the near future (P1: 2035-2065) and the far future 2080 (P2: 2065-2095) with the reference period (P0: 1984-2014).

- **Precipitation**

On an annual scale, according to the median of MME and compared to the reference period, precipitation is not projected to change substantially in the near future (P1). The median of MME ranges between an increase of average annual precipitation of 1% in ssp126 and a decrease of 1% in ssp370 (Figure 29). In the far future (P2), the climate scenario plays a larger role in precipitation projections. In both scenarios, a decrease in average annual precipitation by - 4% and - 8% in ssp126 and ssp370, respectively, is projected. A significant difference between the scenarios is that under ssp126, the median of MME is within the range of P0 but drops under the range in ssp370 (Figures 29 and 30). Figure 30 also shows that the two models CanESM5 and EC-Earth3 project much higher values than the other eight models of the ensemble.

a) ssp 126

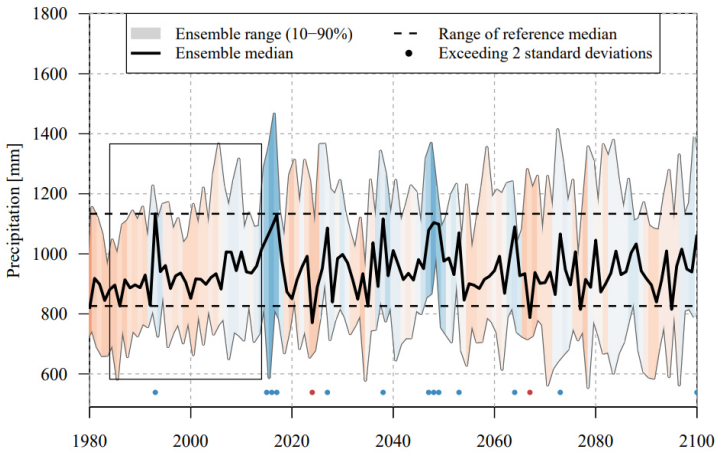

b) ssp 370

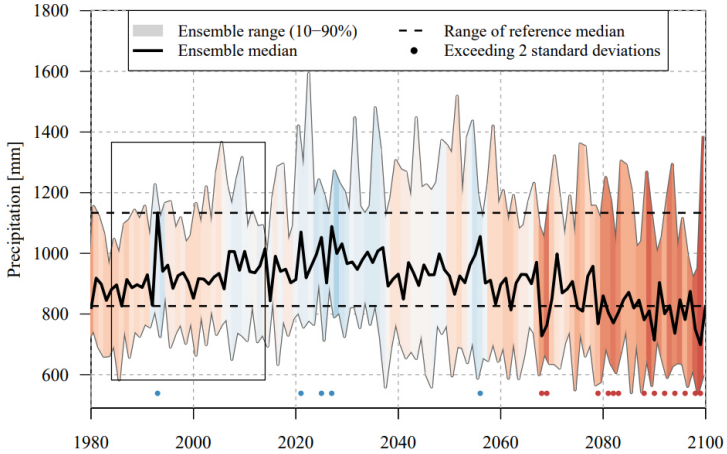

Figure 29: Annual precipitation (mm) projection under a) ssp 126 and b) ssp 370 for future (2016-2100) compared to the reference period (1984-2014)

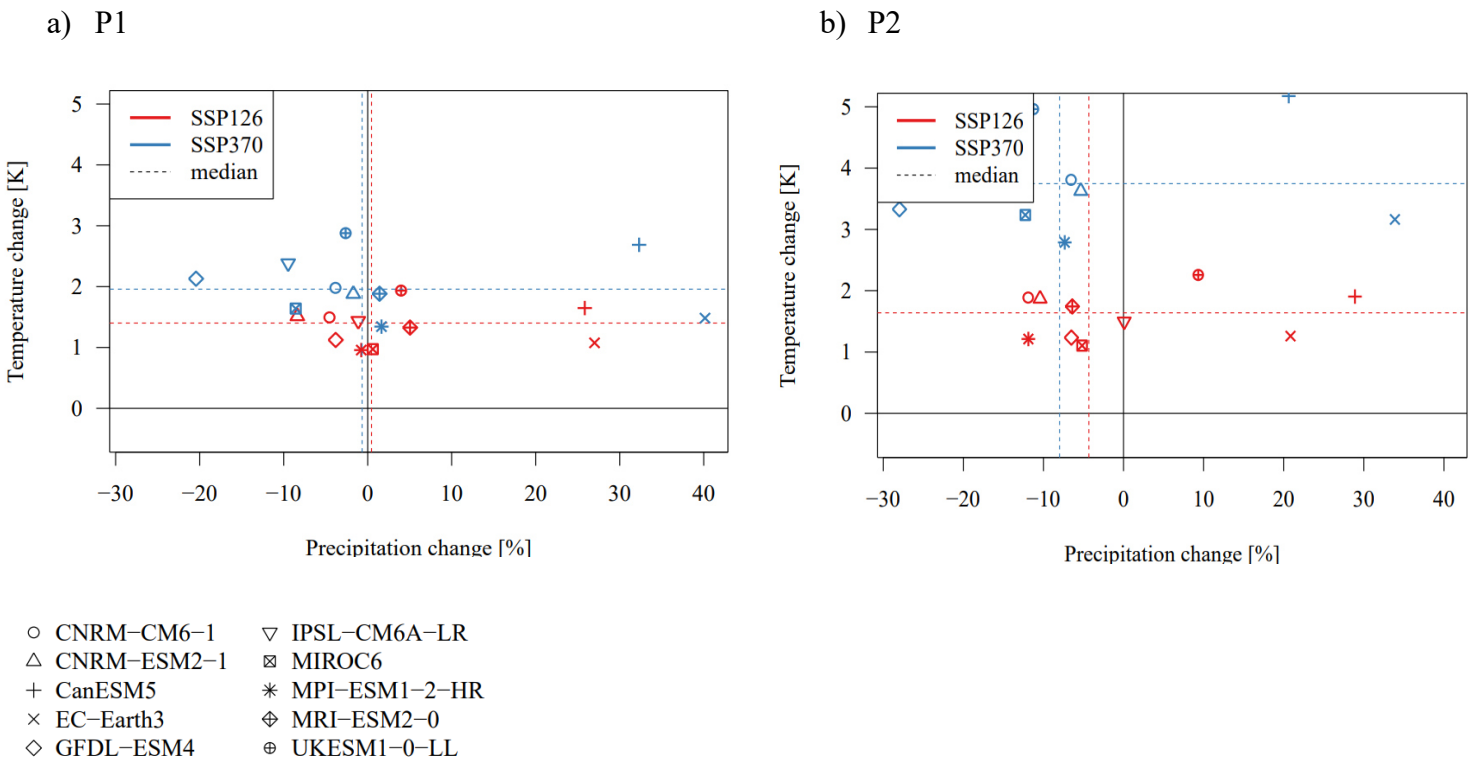

Figure 30: Precipitation and temperature projections from 10 single GCM and the median of MME from ISIMIP 3b for a) the near future and b) the far future compared to the reference period under ssp 126 and ssp 370

At the seasonal scale, in the near future, the median of MME projects an increase in precipitation during the rainy season except in June under ssp 126 and a decrease in precipitation during the rainy season except May, June and July under ssp 370 (Figure 31). In the far future, the median MME projects a reduction in the mean monthly precipitation during the rainy season except September under both scenarios.

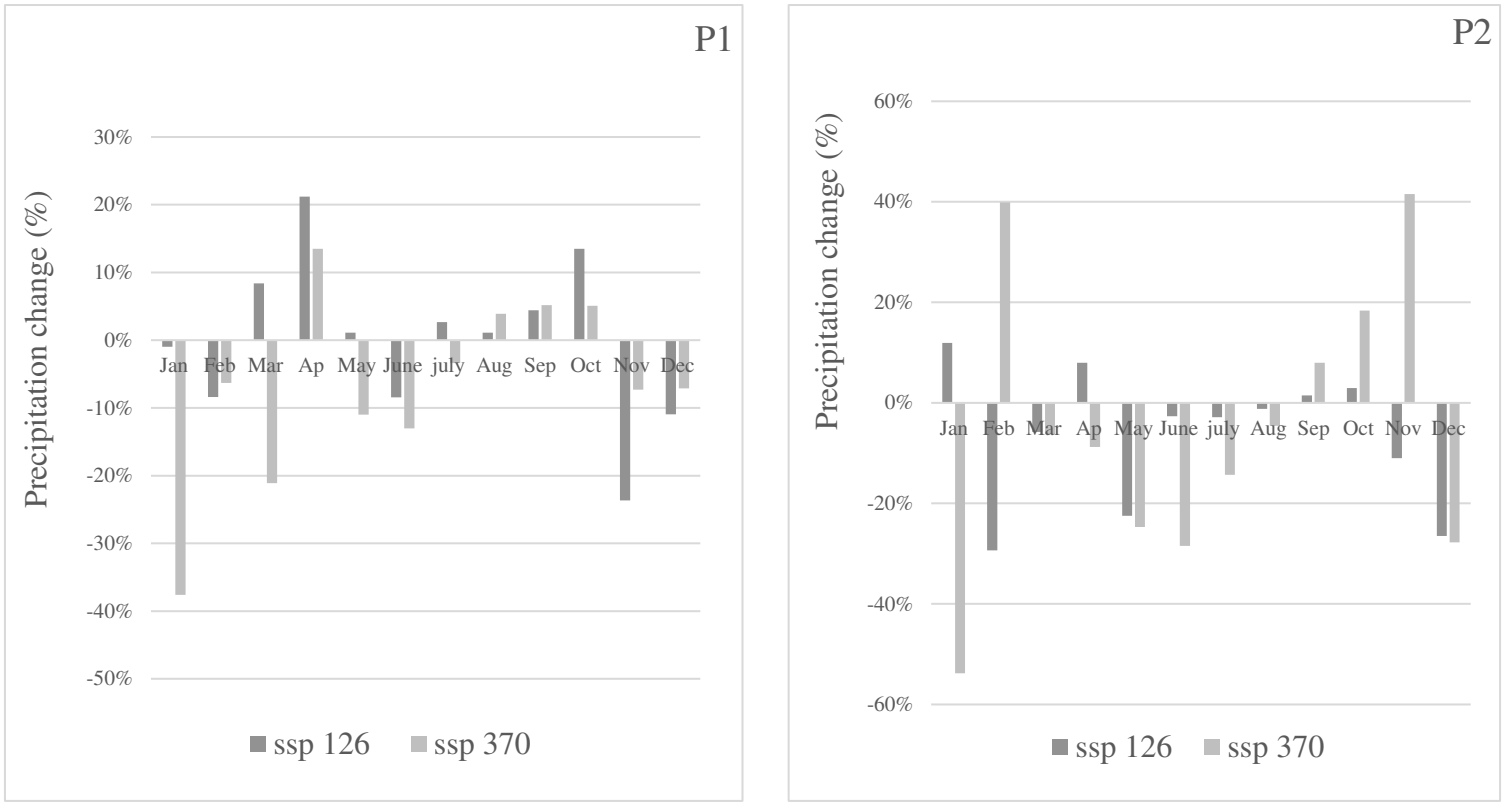

Figure 31: Relative changes (%) in mean monthly precipitation of the median of MME of ISIMIP 3b for the near future (P1:2035-2065) and the far future (P2: 2065-2095) compared to the reference period (P0: 1984-2014) under ssp 126 and ssp 370.

➢ **Temperature**

On an annual scale, according to the median of MME, mean air temperature is projected to increase between 1.4°C and 2.0°C in the near future under ssp126 and ssp370, respectively. In the far future, the difference between both climate scenarios is more significant and ranges from 1.6°C to 3.7°C (Figure 32).

a) ssp 126 b) ssp 370

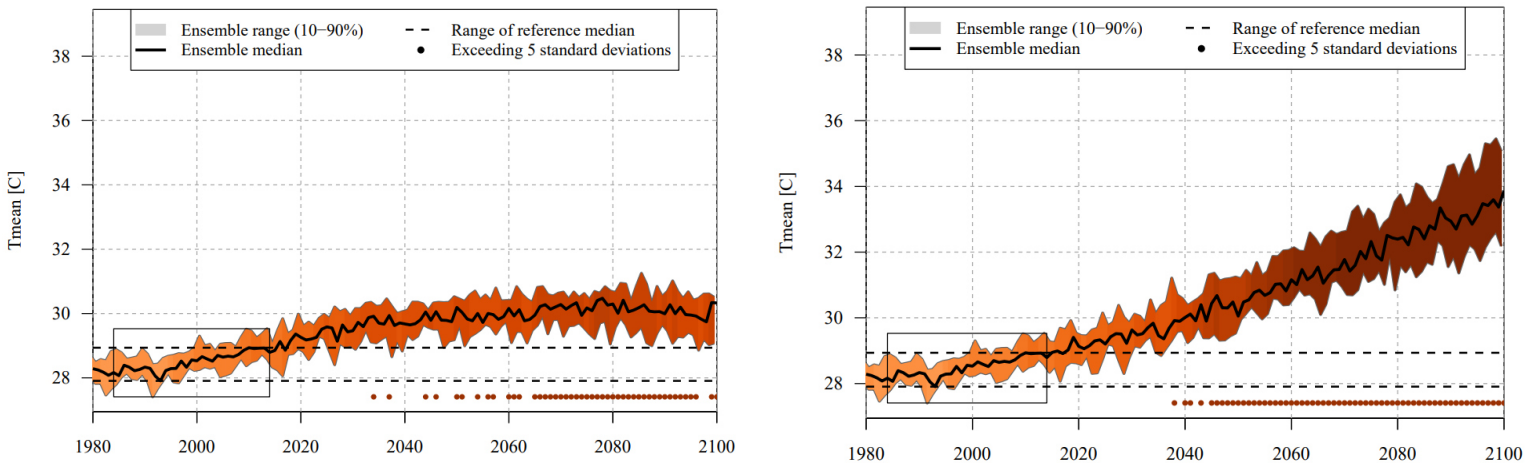

Figure 32: Annual temperature projection based on the ISIMIP 3b models for future (2015-2100) relative to the reference period P0 (1984-2014) under a) ssp 126 and b) ssp 370

At the seasonal scale, every month shows an increase in temperature according to the median (MME) in the future for both scenarios. April, May, and June will be among the warmest for both scenarios in the near and the far future (Figure 33). However, a higher increase in temperature is predicted under ssp 370 than under ssp 126.

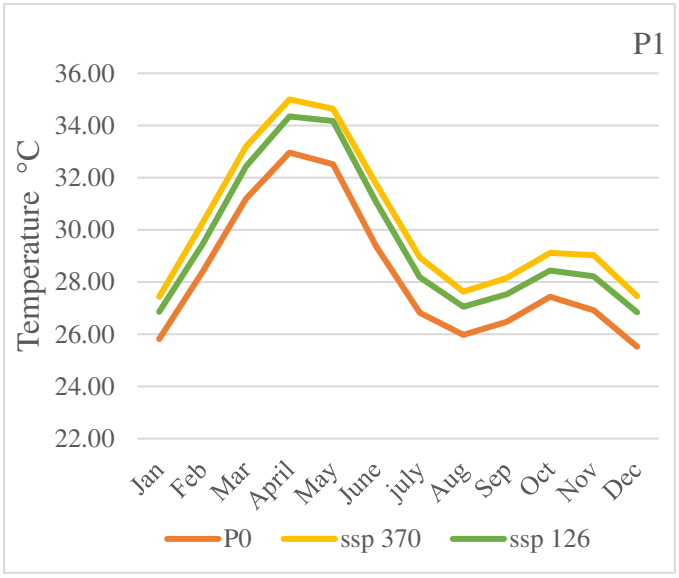

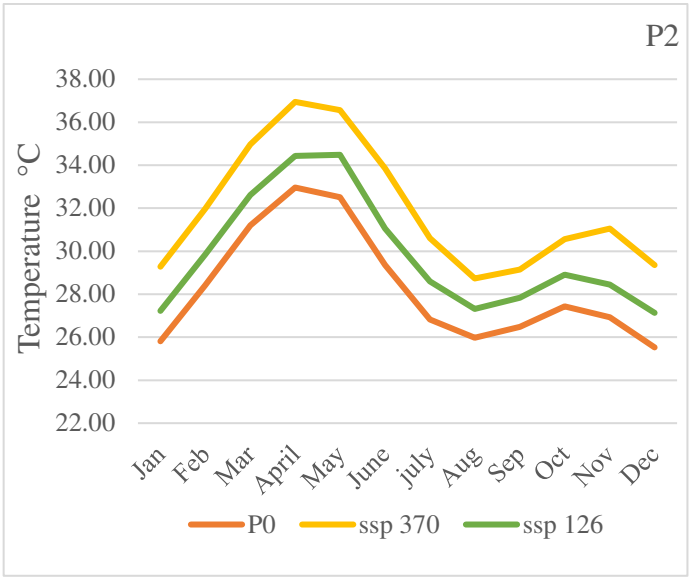

Figure 33:Monthly mean temperature changes based on the median of MME of the ISIMIP 3b for near future (P1:2035-2065) and far future (P2:2065-2095) compared to the reference period P0 (1984-2014) under a) ssp 126 and b) ssp 370

4.4 Conclusion

In this chapter, the ability of two precipitation products (the satellite product (CHIRPS) and the reanalysis (W-era5)) to reproduce the observed precipitation was compared and evaluated during the periods 1979 to 1986 and 2001 to 2003. The comparison shows that W-era5 reproduces observed precipitation better than CHIRPS. All statistics measures show the observed and the W-era5 data are almost equivalent in terms of Pbias, R^2, NSE and RMSE on an annual and monthly scale. In addition, seasonal and interannual analysis indicates that W-era5 better represents observed precipitation than CHIRPS. These results are coherent with those of Ougahi and Mahmood (2022), who evaluate the suitability of five precipitation products (ERA5, CFSR, MERRA2, PERSIANN-CDR And CHIRPS) to serve as a reference for the selection of precipitation data as input, to the SWAT model. According to their findings, reanalysis data outperforms satellite data, and ERA5 data outperforms CHIRPS data. Thus, W-era5 dataset were used as reference data to evaluate the performance of ten GCMs from ISIMIP 3b and for the calibration and validation of the hydrological model.

The ten models from ISIMIP 3b were downscaled and bias adjusted using the W-era5 dataset (Lange, 2019). The evaluation was carried out using statistical measures (R^2, RMSE, NSE, Pbias), the Taylor diagram, and the Mann Kendall test. The assessment was performed at monthly timescales. The statistical results showed that the models can reproduce the precipitation and temperature of W-era5. The results obtained with the Taylor diagram (RMSE, correlation) agree with the statistical results found. The result indicated also that the models can fairly reproduce the unimodal structure (rather simulated bimodal) of the W-era precipitation (temperature). Furthermore, the median of MME outperformed the mean of MME because the results of statistical measurements show that median of MME is more efficient than mean of MME to reproduce the reference data (W-era5). The median of MME can provide reliable projections at the monthly scale. Therefore, the median of MME was used to analyze the future trend of the near future (P1:2035-2065) and the far future (P2:2065-205) compared to the reference period (P0:1984-2014).

According to the median (MME), the average temperature is expected to increase in the near and the far future under ssp 126 and ssp 370 compared to the reference period. On the other hand, uncertainties about the precipitation projection are high. Indeed, precipitation is likely to increase under ssp 126 or decrease under ssp 370 in near future (P1). In the far future (P2), both scenarios agree on a decrease in precipitation. These results are consistent with Diakhaté et al.

(2022) who analysis the Projected Changes in the Rainfall Annual Cycle over the Senegal River Basin Using CMIP5 bias-Corrected Simulations. These uncertainties in the projections of precipitation by Climate Models have been reported by Rowell et al. (2016) Diedhiou et al. (2018), (Nikulin et al., 2018), Almazroui et al. (2020) and Dosio et al. (2020, 2019) when investigating future climate changes over West Africa. Their results showed that West Africa is one of the regions where the majority of models project a significant change in mean precipitation, but they do not agree on its sign.

According to previous studies (e.g. Nikulin et al., 2012; Akinsanola and Ogunjobi, 2017; Akinsanola and Zhou, 2019) the large uncertainties associated with climate projections of precipitation over Africa are partly due the fact that climate models show significant limitations in simulating complex systems like the West African Mousson. Indeed, the annual cycle of precipitation over the region is linked to the passage of the West African Monsoon (WAM), which is driven by the interaction of atmosphere, ocean, and land-surface, and strongly related to mid-tropospheric circulation (Dosio et al., 2020). The large uncertainties associated with global climate projections of precipitation over Africa can also be partially attributed due to the strong interannual variability of precipitation and to strong disagreements across GCMs (Bichet et al., 2020). This has important implications for decision makers formulating long terms strategies development plans.

Chapter 5: Analysis of land use and land cover changes

This chapter examines the LULC changes between 1986 and 2020. It predicts LULC change of 2050 utilizing LULC's past trend and land change modeller (LCM) to contribute to the establishment of appropriate development policies and land management strategies.

5.1 Land use/land cover maps accuracy

This section presents the results of LULC classification (Table 22). The overall accuracy O (28), user's accuracy U (29), producer's accuracy P (30) were used to assess the reliability of the classification (Foody Giles M, 2022; Szantoi et al., 2021). The overall accuracy is the sum of perfectly classified pixels divided by the total sample size of pixels. The producer's accuracy informs the analyst (producer) of the percentage of correctly classified LULC compared to the real world. The user's accuracy measures errors of commission, which shows the probability of a classified pixel matching LULC type's user of its corresponding real-world location. The overall accuracy obtained is equal to 96%, 95% and 95% for 1986, 2006 and 2020, respectively. The values of overall accuracy O (28), user's accuracy U (29), producer's accuracy P are comprised between 0.75 and 0.98 (indicating perfect agreement). The Kappa coefficient (K) obtained for both maps is above the threshold of 0.8, which is considered satisfactory (Congalton, 1991; Olofsson et al., 2014; Szantoi et al., 2021). Therefore, the classification could be identified as accurate.

Table 22: Classification accuracies: user's accuracy (U), producer's accuracy (P), overall accuracy (O) and the Kappa coefficient (K)

Land cover/land use classes	**1986**		**2006**		**2020**	
	P	**U**	**P**	**U**	**P**	**U**
Settlement	0.84	0.96	0.94	0.93	0.97	0.95
Water	0.99	0.99	0.98	0.99	0.93	0.96
Vegetation	0.99	0.99	0.98	0.96	0.96	0.95
Cultivated area	0.75	0.87	0.90	0.97	0.85	0.93
Bareground	0.98	0.95	0.97	0.94	0.96	0.95
Overall accuracy (O)	0.96		0.95		0.95	
Kappa index (K)	0.95		0.94		0.94	

5.2 Land use land cove change detection

Figures 34 and 35 show the results of the independently classified map for 1986, 2006 and 2020. In 1986, the area covered by bareground was the most dominant LULC class, covering 60% of the watershed. Over the 34 years, this area has gradually decreased to almost half, from 60% to 30%. The vegetation area represents the second most dominant LULC class, covering 36% of the watershed. This class has continuously increased from 36% in 1986 to 44% in 2020. Settlement was the third most dominant LULC class and covered 2.8% in 1986. However, settlement significantly increased to 16% in 2006 and 18% in 2020. The cultivated area was the fourth LULC class, covering 0.8% of 1986 in the watershed. The extent of cultivated area increased from 0.8% in 1986 to 4% in 2020. The area covered by water was the lowest but increased continuously over the study period from 0.6% to 3.3%.

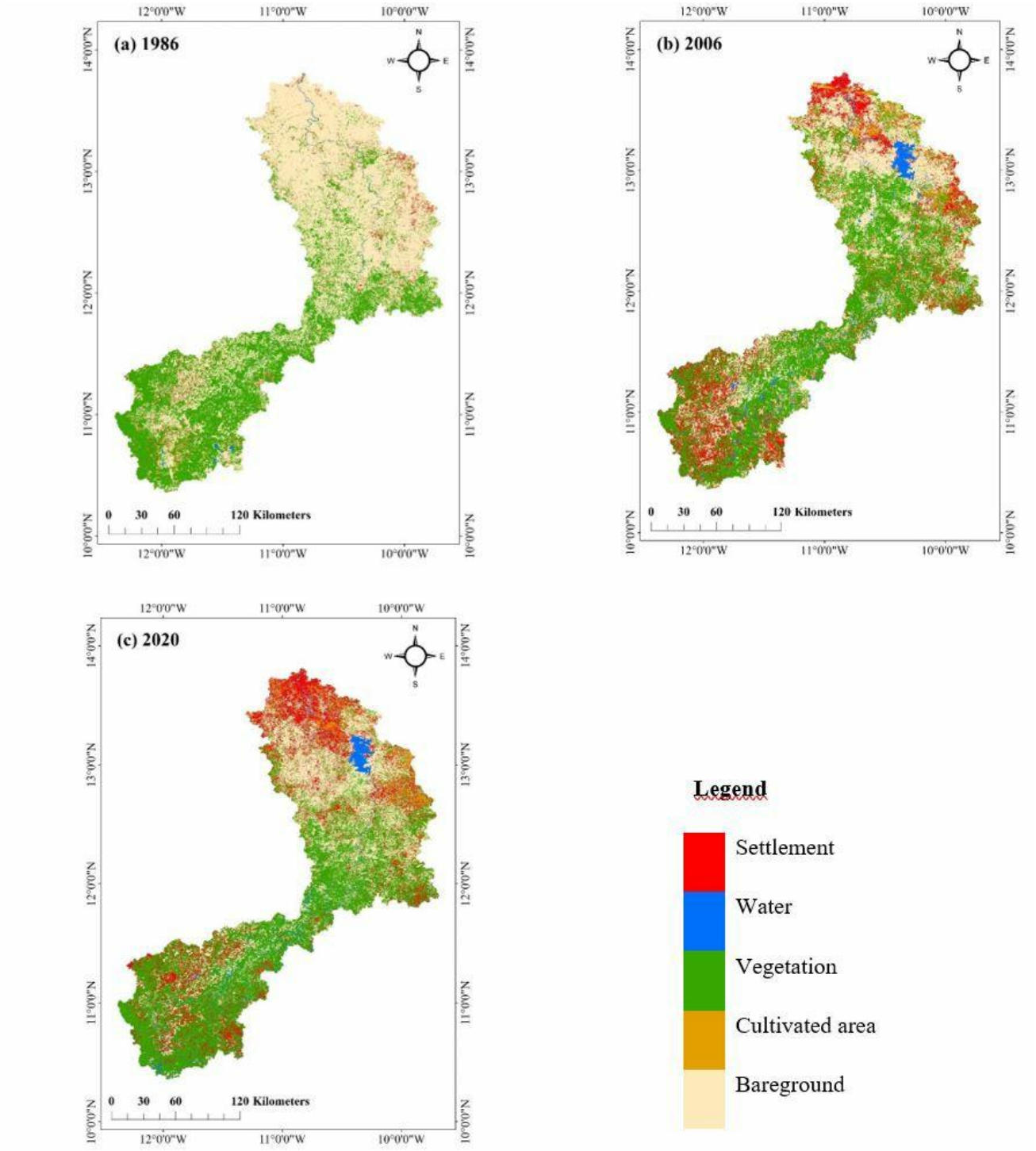

Figure 34: LULC maps of the Bafing watershed for a) 1986, b) 2006, and c) 2020

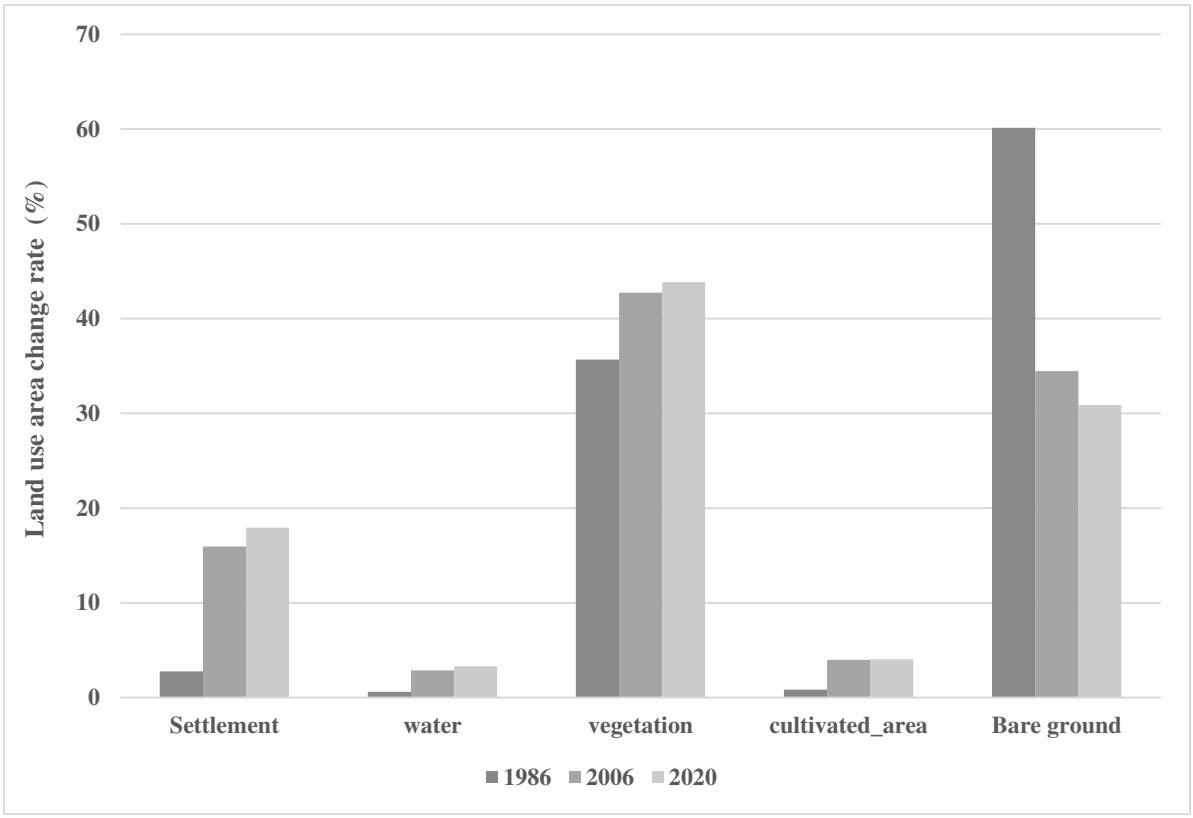

Figure 35: Percentage of area per LULC category for 1986, 2006, and 2020

5.3 Land use/land cover change prediction

5.3.1 Transition potential

The result of transition potential (Figure 36) shows that, for example, the contribution to net change of the settlement class is the bareground and vegetation. This reflects that bareground and vegetation classes have been converted into the settlement class. From 1986 to 2006 and from 2006 to 2020, conversions from bareground to vegetation, settlement, cultivated area, and water were the most significant for Bafing (Figure 36). The most significant conversion was analyzed between 1986, 2006 and 2020 to select the main conversion in the modelling procedure.

Figure 36: Contribution to net change in each LULC type

5.3.2 Model validation

LULC changes prediction involves two different aspects. The first is the amount of change, and the second is the spatial distribution of change. The Multilayer Perceptron neural network and Markov chain (MLP-MC) model embedded in LCM reproduce very satisfactorily the amount of change (Figure 37). Indeed, on the simulated LULC map of 2020, the areas occupied by settlement, vegetation, bareground, water and cultivated area are 18.75%, 44.76%, 28.50%, 3.91%, and 4.08%, respectively, against 17.93%, 43.85%, 30.87%, 3.30%, and 4.04%, respectively, on the reference map of 2020. Regarding the spatial distribution of change (Figure 38), the visual comparison of the simulated 2020 map with the reference map reveals some differences.

Indeed, the model predicts an increase in settlement mainly in Guinea, whereas in reality, the most significant increase in settlement has been observed in the northern part of Mali. These results can be explained by the limitation of the model to represent spatial distribution or the choice of explanatory variables. Nevertheless, the validation indicators provide values of ROC= 81.6%, κia (kstandard) = 78.34%, Klo = 79.86% and kno= 86.83% (reflecting the overall accuracy of the simulated map), which are considered satisfactory (Okafor et al., 2019; Roland, 2021; Tiné et al., 2019). Based on all these results, the MLP-MC model reasonably simulate the LULC map of 2020 and can be used to project future LULC change in the Bafing watershed.

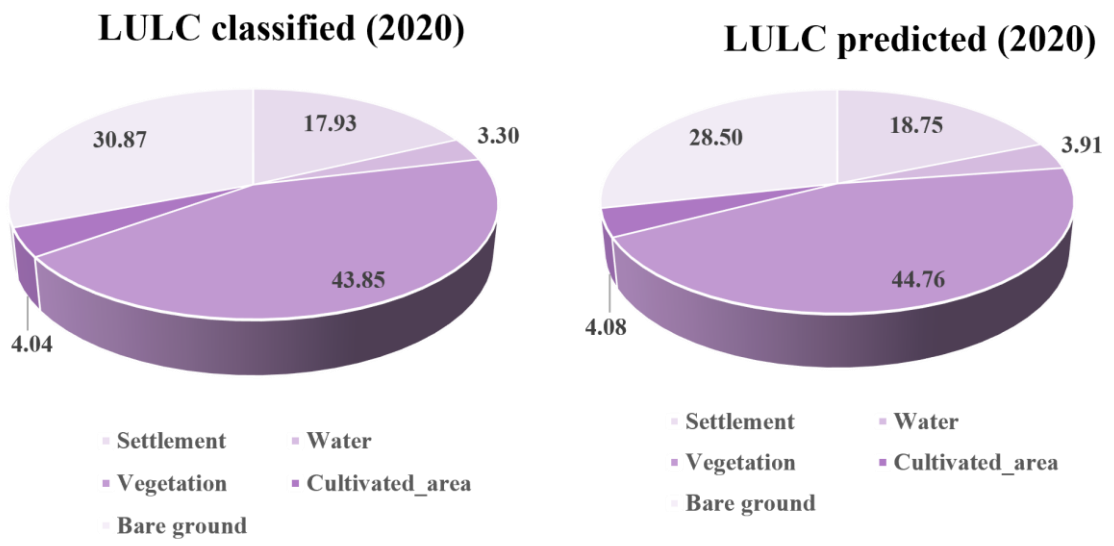

Figure 37: Relative change (%) between the classified and the predicted LULC map of 2020

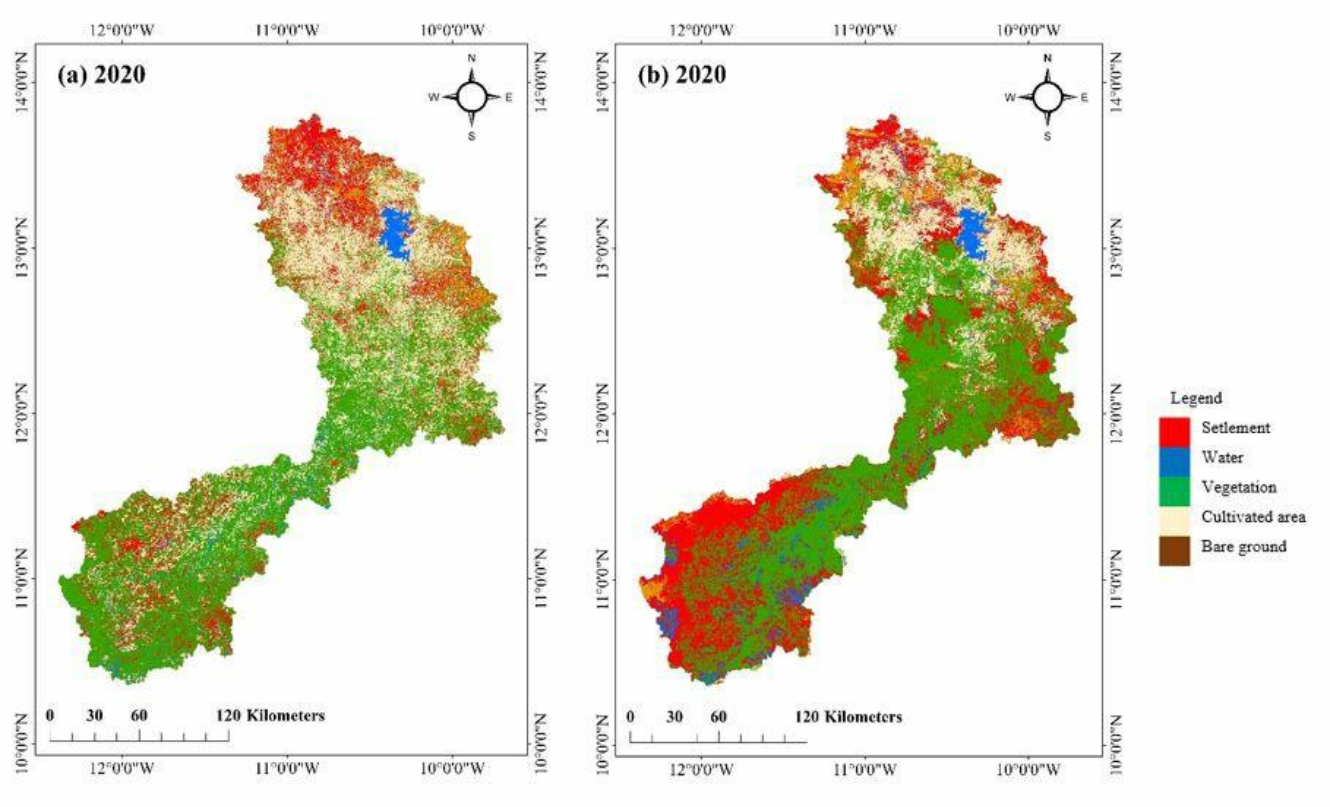

Figure 38: Comparison of a) reference LULC maps and b) simulated LULC maps of 2020 in the Bafing watershed.

5.3.3 Projected LULC maps

Changes in LULC between 1986 and 2020 were first analyzed, leading to transition potential maps and a probability matrix illustrating the significant LULC change. The transition

probability matrix for the classified maps between 1986 and 2020 is presented in Table 23. The results show that between 1986 and 2020, the settlement, cultivated area, and bareground classes were the most dynamic. Indeed, the settlement and cultivated area classes indicate a 45% and 18% probability of not changing to another LULC class, respectively. At the same time, the area of cultivated area and bareground has a probability of 24% and 21% converting into settlement. Similarly, the vegetation class also shows stability with a chance of 80.7%. Bareground have a high possibility of converting into vegetation (22%).

Table 23**:** Transition probability matrix (%) of the LULC map for the period from 1986 to 2006 of the Bafing watershed.

LULC classes	**Settlement**	**Water**	**Vegetation**	**Cultivated area**	**Bareground**
Settlement	**0.4515**	0.0158	0.2527	0.1149	0.165
Water	0.0491	**0.06236**	0.2236	0.0014	0.1024
Vegetation	0.0796	0.0358	**0.8065**	0.0139	0.13
Cultivated area	0.2364	0.0544	0.4893	**0.1813**	0.3122
Bareground	0.2089	0.0216	0.2157	0.0471	**0.6836**

Finally, the LULC projection scenarios in 2050 were simulated based on the probability matrix obtained using the 1986 and 2020 maps. Figure 39 shows the predicted LULC maps for 2050. The results of this simulation indicate that vegetation will cover the largest area with 49% in 2050, followed by settlement with an area of 19.4%. Bareground will be the third most dominant LULC class and will cover 22% in 2050. Water and cultivated area will each cover 4.8%.

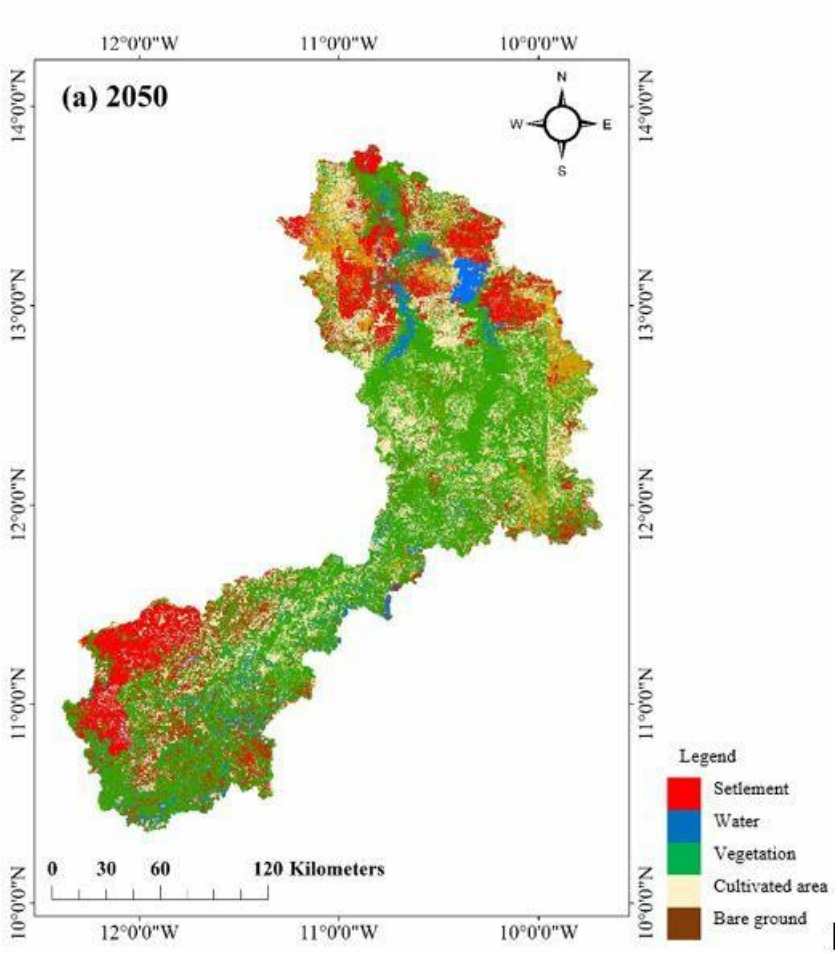

Figure 39:Predicted LULC map of 2050

5.4 Conclusion

In this chapter, LULC changes over 34 years in the Bafing watershed were analyzed, and the predicted LULC changes in 2050 were simulated with the status quo (BAU) assumption. This study used Landsat images from 1986, 2006 and 2020 and the RF classification algorithm. RF classification results are very satisfactory with good accuracy. This confirms the findings obtained by Zurqani et al. (2018), who suggest that the RF algorithm performs better in regions where LULC types are dominated by vegetation. The analysis of the post-classification change detection has reported significant changes in LULC during the study period. The analysis and detection of post classification change revealed the expansion of settlement and cultivated area during the study period. From 1986 to 2020, settlement and cultivated area increased steadily from 2.8% to 18% and 0.8% to 4%, respectively. This expansion can be attributed to the acceleration of population growth. The average growth rates are 2.5% and 2.7%, respectively,

for the countries covering the study areas, namely, Guinea, Mali and Senegal. Tabutin and Schoumaker (2020) observed a high population rate and the resulting socioeconomic impacts (increase in cultivated area). The study by Lambin et al. (2003) indicates that the cultivated area in WA increased due to population growth. This is confirmed by Herrmann et al. (2020), whose results prove that the intensity of LULC change within a 10 km radius of new settlement sites was up to three times higher than the regional average, confirming the crucial role of population pressure as a driver of change in WA. These results also mirror those of Berihun et al. (2019), who also found that population increase was consistent and positively correlated with the expansion of cultivated area between 1982 and 2006 in Ethiopia. An interesting result is the vegetation growth between 1986 and 2020. The area occupied by vegetation increased from 36% to 44%, becoming the most dominant LULC class in 2020. This result is consistent with the results of UCAD (2019) and Descroix et al. (2020), who found a regreening in the Fouta Djallon Plateau of the Bafing watershed in Guinea. The increase in vegetation that coincides with population growth suggests that population growth does not always lead to deforestation. Indeed, Descroix et al. (2020) pointed out that the densely populated areas of the Fouta Djallon Plateau of the Bafing watershed in Guinea are those where the vegetation cover is not threatened and where the ecological intensification of rural activities has long been established. Therefore, the claim "more people, more trees" proposed in Tanzania by Kabanza et al. (2013) seems valid in the Fouta Djallon Plateau of the Bafing watershed in Guinea. In addition, several projects have been adopted in the Bafing watershed in Mali to fight biodiversity losses after the construction of the Manantali Dam. These projects include the Bafing Faunal Reserve (Mali), the status of biosphere reserve (Mali), the Natural Resources Management Project (PGRN/World Bank) in the 1990s and 2000s, the Project for the Extension and Strengthening of Protected Area Systems, the Bafing transboundary area protected area project during the period 2010-2015 (Faty, 2017). Another significant result obtained is the increase in water from 0.6% to 3.3% between 1986 and 2020. The observed increase in water can be explained by the recovery of rainfall in this region in the 1990s, after the drought period of 1960-1970. Many authors (Diop et al., 2016; Bodian et al., 2020; Nouaceur and Murarescu, 2020) noted a recovery in rainfall in WA. Bodian et al. (2020) studied the recent evolution of hydroclimatic variables in the SRB from 1940 to 2013. These results show a recovery in the SRB's annual rainfall, improving surface water availability. Recovery of annual flow was reported after the 1990s in the Bafing watershed (at Bafing Makana station) (Sane et al., 2017). The observed increase in water can also be attributed to the construction of the Manantali dam in the Bafing watershed.

The Manantali Dam, built in 1988, has an area of approximately 477 km2 and a capacity of 11791.8 million m^3 (Bader, 2001). It aims to make surface water available and sustainable throughout the year and to satisfy energy production and flow regulation, especially in the context of climate change and variability (Bader et Rolland, 2005). The predicted LULC map of 2050 was realized using the MLP-MC model embedded in LCM with the BAU scenario. LULC change prediction is based on the amount of change and the spatial distribution of change. LCM provides the amount of change and the spatial distribution of change by comparing initial (1986) and second (2006) LULC maps and then predicting future land cover (2020) using the MC transition probability matrix for the future. Model validation is performed by comparing the simulated LULC map (2020) with the classifier LULC map (2020)'. The results revealed that while the percentages of LULC between the reference map (2020) and the simulated map (2020)' have a very high degree of concordance; the spatial distribution appears to be quite different. These results can be explained by the fact that Markov chain (MC) model ignores the spatial distribution of changes. Indeed, according to Mishra et al. (2018), the main limitation of the MC model is that it just considers the temporal trends without considering spatial aspects. However, the validation indicators (ROC, kia, Klo and kno) and the good agreement in the amount of change indicate that the Multilayer Perceptron neural network and Markov chain (MLP-MC) model reasonably reproduce the LULC map of 2020 and can be used to project future LULC change in the Bafing watershed. During the period 2020-2050, the prediction results (based on the past trend (1986-2020) revealed that vegetation would be the dominant LULC, but an increase in cultivated area, water, and settlement will also be observed in 2050. A trend toward "more people more tree" is seen in the Bafing watershed. This combination of results suggests that population increase, and anthropogenic activities are the primary drivers of LULC changes. The results showed that when population growth is accompanied by adopting sustainable land management practices (appropriate policies and regulations), it can lead to better land and water conservation. The presence of a large dam in the Bafing watershed has led to the implementation of virtuous policies favourable to the environment.

Chapter 6: Assessment of the potential impacts on the hydrology in the Bafing watershed

This chapter presents the results of hydrological modelling and the dam module of the SWIM model in the Bafing watershed. After the setup and the simulation of SWIM model, the impacts of climate change, land use/land cover change (LULC change), and the exploitation of future dams (koukoutamba and boureya) on the hydrology of the Manantali dam were estimated for the near future (P1:2035-2065) and far future (P2:2065-2095) under a) ssp 126 and b) ssp 370 compared to the reference period (P0: 1984-2014) and the LULC change from 1986 to 2050. Ten GCMs of ISIMIP 3b data under a) ssp 126 and b) ssp 370 and the LULC maps of 1986, 2020, and 2050 were used as input data in the SWIM model to simulate the hydrological processes.

6.1 Sensitivity analysis, calibration and validation of the SWIM model

6.1.1 Sensitive analysis

Sensitivity analysis allowed to reduce the number of parameters used to calibrate the model. Sensitivity analysis for the Bafing watershed carried out over the calibration period (1979-1986) showed that 11 of the 24 parameters were sensitive. The parameters are presented in decreasing order from the most sensitive to the least sensitive in Table 24. According to the Table 24, the most sensitive parameters are related to runoff (scoor, roc2, roc4, bff, cncor,prcor), groundwater flow (abf, revapc, rchrgc, delay, revapmn) and transmission losses (tlrch). The interaction between groundwater and surface runoff can explain these findings.

Table 24: Parameter classified in decreasing order after sensitivity analysis.

Parameter	Description	Range
sccor	Soil hydraulic conductivity	1 – 50 the higher the value the higher conductivity
roc2 roc4	River routing coefficients for quick and slow components	1-50 (1 = quick routing; 50 = slow routing
cncor	Curve number	0.75 – 1.25
prcor	Precipitation	0.8 – 1.2
abf	Alpha factor for groundwater. This parameter characterizes the ground water recession	0.0005 – 0.95
revapc	Fraction of recharge that "re-evaporates" directly from the shallow groundwater aquifer	0 – 0.3
rchrgc	Deep aquifer percolation coefficient. The amount of water that is allowed to percolate from shallow into the deep aquifer	0 – 1
bff	Base flow factor used to calculate return flow travel time	0.1 – 3
tlrch	Transmission losses riverbed	0 – 3 (0 = no losses)
delay	Groundwater delay (days). The time it takes for water leaving the bottom of the root zone until it reaches the shallow aquifer where it can become groundwater flow	1 – 200
revapmn	Revap storage (mm). Shallow aquifer storage must exceed REVAPMN before groundwater flow can begin	

6.1.2 Calibration and validation of the SWIM model

The calibration process involved finding model parameter values to obtain simulated flows as close as possible to observed flows. In this study, the parameters were calibrated for the whole watershed, not by HRU, at a daily time scale with the LULC map 1986. The values of the parameters used for each sub-basin during the calibration process is presented in Table 25.

Table 25: Parameter values calibrated in SWIM for each subbasin.

Parameters					Subbasins				
Name	Definition	Parameter default	Parameter Min	Parameter Max	Koukoutamba	Boureya	Dakka Saidou	Bafing makana	Manantali
roc2	River routing coefficients for quick and slow components	3	1	50	6	6	6	6	6
roc4	River routing coefficients for quick and slow components	3	1	50	7	7	7	7	7
sccor	Soil hydraulic conductivity (the higher the value the higher conductivity)	1	1	50	2	2	2	8	8
bff	Base flow factor, used to calculate return flow travel time	0.5	0.1	3	0.5	0.3	0.3	0.3	0.45
abf	Alpha factor for groundwater. This parameter characterizes the ground water recession	0.001	0.0005	0.95	0.04	0.001	0.001	0.001	0.001
delay	Groundwater delay (days). The time it takes for water leaving the bottom of the root zone until it reaches the shallow aquifer where it can become groundwater flow	2	1	200	50	50	50	50	50
revapc	Fraction of recharge that "re-evaporates" directly from the shallow groundwater aquifer	0	0	0.3	0.02	0.15	0.15	0.1	0.1
rchrgc	Deep aquifer percolation coefficient. The amount of water that is allowed to percolate from shallow into the deep aquifer	0	1	1	0.02	0.15	0.15	0.1	0.1
revapmn	Revap storage (mm). Shallow aquifer storage must exceed REVAPMN before groundwater flow can begin	0			0.02	0.15	0.15	0.1	0.1
tlrch	Transmission losses, riverbed	1.1	0	3 (0 = no losses)	1	1.1	1.1	1	1

The results presented in Table 26 and Figure 40 come from simulations carried out by SWIM after the parameterization, calibration and validation of the SWIM model on the Bafing watershed in Dakka Saidou at the Bafing Makana stations. The results of the calibration show that the SWIM model reproduces the observed flow very satisfactorily. For the Bafing Makana station, the NSE, R^2 and KGE values equal to 0.8 and a Pbias value of 15.4 (Table 26) are

obtained. For the station of Dakka Saidou, the NSE, R^2 and KGE equal to 0.8 and an acceptable Pbias value of 20.5 (Table) are obtained. The model tends to overestimate peak flows but simulates low flows satisfactorily (Figure 40).

The efficiency of the simulation decreases between the calibration and the validation in terms of the performance criteria. Nevertheless, the model's performance in validation respects the conditions of satisfaction (Table 26). In addition, the model overestimates the average flows between 15 and 20% in the calibration and up to 30% in the validation period. It is observed that improving the representation of peak flows leads to a deterioration in calibration performance and an overestimation of low flow. Similar conclusions were found for the Kayanga-Anambe watershed (Velingara/Senegal), where the results of SWAT model calibration showed that peak flows are overestimated, while flood and low-water flows are better represented. It has also been observed that attempts to improve the representation of peak flows lead to a deterioration in calibration performance, as well as an overestimation of low-water flows. This result may be due to the type of input data (soil data etc..) used for the modelling. According to visual examination and the performance criteria obtained during the calibration and validation process, the model satisfactorily simulates the hydrology of the Bafing watershed and can therefore be used to answer the questions of this study. The hydrographs of observed and simulated flows for calibration and validation are presented in Figure 40.

Table 26: Performance of the model during calibration and validation with LULC of 1986

Stations		**Period**	**Pbias**	**NSE**	**R^2**	**KGE**
Bafing Makana	Calibration	1979-1986	15.4	0.8	0.8	0.8
	Validation	1987-1993	27.7	0.8	0.8	0.7
Dakka Saidou	Calibration	1979-1986	20.5	0.8	0.8	0.8
	Validation	1987-1993	28.5	0.8	0.8	0.7

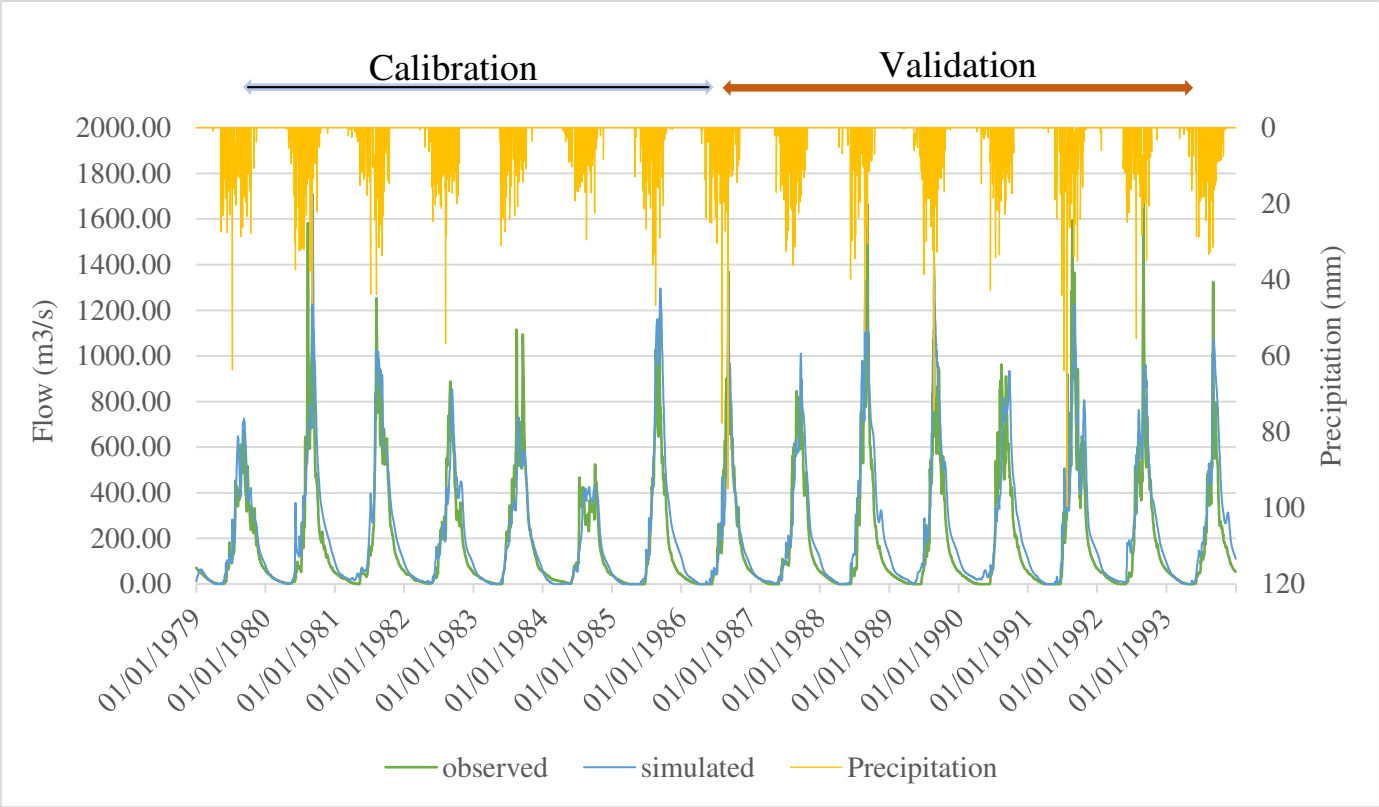

Figure 40: Simulated discharges during the calibration period (1979-1986) and validation periods (1987-1993).

6.1.3 SWIM reservoir module configuration

The results of the simulation of the Manantali dam are presented in Figure 41 and Table 27. Figure 41 shows the daily variations in simulated and observed inflows and outflows of the dam. The graphical comparison and the corresponding statistical indices show that the model satisfactorily reproduces the dynamics of inflows, outflows, and the water level of the Manantali dam (Table 27). Observed hydropower generation data were unavailable to validate the hydropower simulated by the SWIM model.

Table 27: Comparison between the observed and simulated inflow, outflow and water level of the Manantali dam

Period	**Dam**	**Pbias**	**NSE**	**R^2**	**KGE**
Calibration (2003-2006)	Inflow	-8.5	0.63	0.497	0.749
	Water level	-0.3	0.171	0.541	0.582
Validation (2007-2009)	Inflow	-5.9	0.729	0.657	0.85
	Water level	-0.4	0.6	0.672	0.822

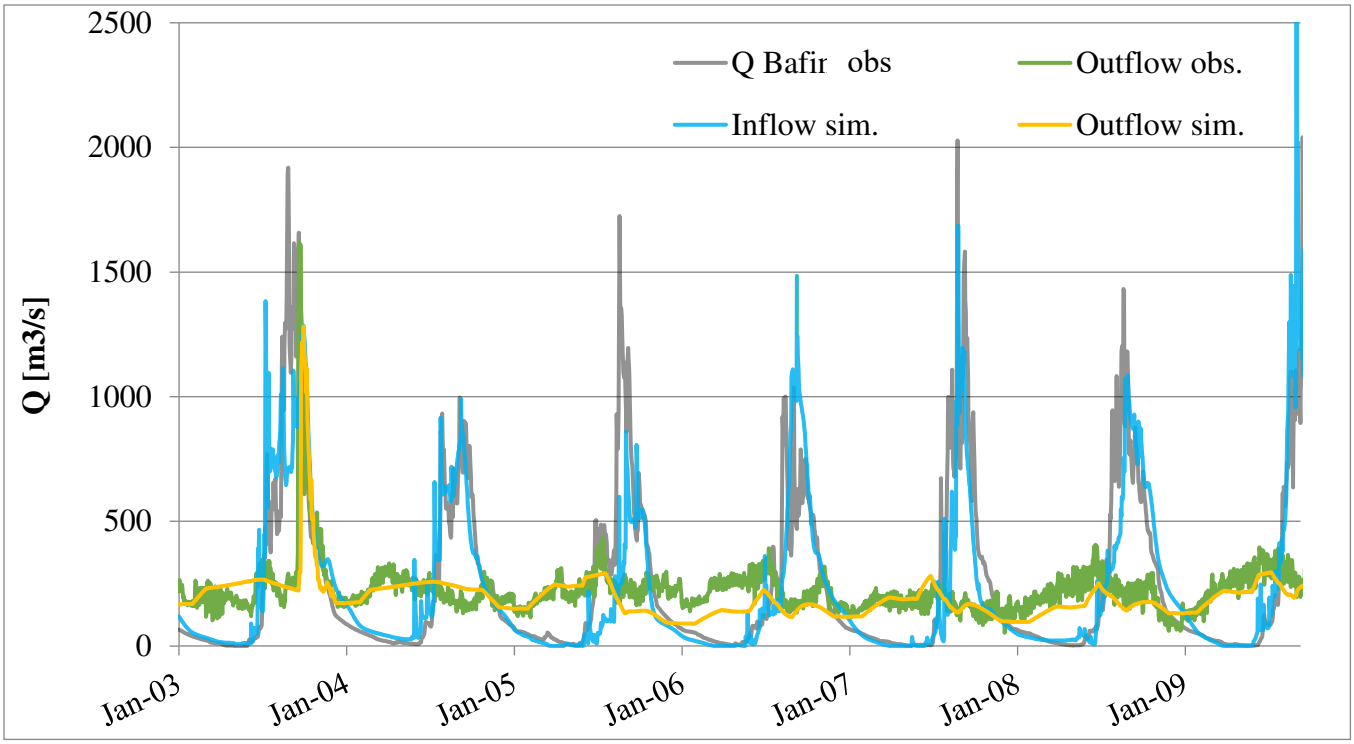

Figure 41:Comparison between the observed and simulated inflow/outflow of the Manantali dam

6.1.4 Hydrological water balance

The water balance shows that out of an annual average of 1140 mm of precipitation, about 126.3 mm returns to the atmosphere by evapotranspiration. The stream flow as simulated by SWIM totals 5516.4 m^3/s which is divided into direct runoff (190.1 m^3/s), lateral flow into the soil (331.2 m^3/s) and percolation from shallow aquifers (1184.5 m^3/s).

Table 28: Water Balance

Year	Precipitation (mm)	Percolation (mm)	PET (mm)	Groundwater	Runoff (m3/s)	Seepage
1979	1122.6	1092.1	120.8	1609.2	6206.7	313.9
1980	1194.5	1326.6	125.8	1874.4	5511.5	347.2
1981	1245.9	1358.0	124.6	2016.1	5935.0	367.5
1982	1136.7	1050.4	125.0	1567.8	5837.3	327.9
1983	971.3	778.7	128.1	1212.1	5335.3	269.6
1984	969.5	765.3	127.9	1036.5	4836.2	242.4
1985	1079.3	1176.6	128.2	1613.5	4498.2	292.8
1986	1125.7	1129.9	124.7	1576.4	5451.1	312.2
1987	1095.3	1099.9	127.8	1579.3	5354.1	302.6
1988	1230.6	1461.2	127.1	2052.6	5199.9	360.1
1989	1275.5	1577.9	127.1	2254.5	5985.4	396.5
1990	1132.0	1185.7	128.4	1922.5	5706.8	355.6
1991	1211.8	1431.7	128.2	2018.7	5592.6	380.4
1992	1098.8	1096.3	125.6	1788.3	5583.0	344.6
1993	1210.5	1237.4	125.1	1763.0	5712.9	354.3
Mean	1140.0	1184.5	126.3	1725.6	5516.4	331.2

6.2 Futures impacts on the hydrology of the Manantali dam

6.2.1 Impact of climate change on the hydrology of the Manantali dam

To analyze only the impact of climate change on the hydrology of the Manantali dam, the SWIM and dam module were simulated with the assumption that LULC of 1986 remains unchanged for future periods (P1, P2). The results are presented in Table 28 and Figure 42.

- **On an annual scale**

The inflows into the Manantali dam follow the general trends of precipitation projections. In the near future (P1), the inflows are projected to either increase by 6% under ssp126 or decrease by -1% under ssp370 (Table 28). The outflow of the Manantali dam is also projected to increase by 7% under ssp 126 or decrease by -1% under ssp 370 in the near future (P1). In the far future (P2), a decrease of inflows by 4% and 8% under ssp126 and ssp370, respectively is projected. The outflow of the Manantali dam is also expected to decrease by -7% and -15 % respectively under ssp 126 and ssp 370 (Table 28). Consistent with the temperature projections, evapotranspiration (Eta) over the Manantali dam is projected to increase by 3% under the ssp

126 and the ssp 370 in the near future and by 3% and 5% respectively under the ssp 126 and the ssp 370 in the far future (P2).

Table 29: Hydrology (water balance) at the Manantali dam under climate change (DS1) at an annual scale.

ssp 126					
Period	Pr (mm)	Inflow (m3/s)	Outflow (m3/s)	ET (mm)	Seep (mm)
P0 (1984-2014)	443	9213.2	7848.1	860	897.1
P1 (2035-2065)	445	9765.1	8364	889.2	909.5
P2 (2066-2095)	423.8	8633.5	7272.9	886.3	858.3
ssp 370					
Period	Pr (mm)	Inflow (m3/s)	Outflow (m3/s)	Et (mm)	Seep (mm)
P0 (1984-2014)	443	9213.2	7848.1	860	897.1
P1 (2035-2065)	440.1	9130.5	7735.5	885.7	894.9
P2 (2066-2095)	407.6	7988	6700.8	906.2	824.1

- **On a monthly scale**

Due to the concentration of precipitation during the rainy season, it is important to project seasonal changes in water resources in the basin associated with future climate change. The seasonal flow shows more clearly the impacts of future climate change on the monthly flow. In the near future, the results indicate an increase in inflow during the rainy season (*from May to October)* of 7% for ssp 126, while there is no change in inflow for ssp 370 (Table 28 and Figure 42). An increase in inflow of 1% for ssp 126 and a decrease of -7% ssp 370 are projected during the dry period.

In the far future, the general trend indicates a decrease in inflow for all seasons (Figure 42). However, the decrease is observed more during the dry season than during the rainy season. It should also be noted that large relative changes in dry periods are not significant relative to annual flows.

(a) Near future

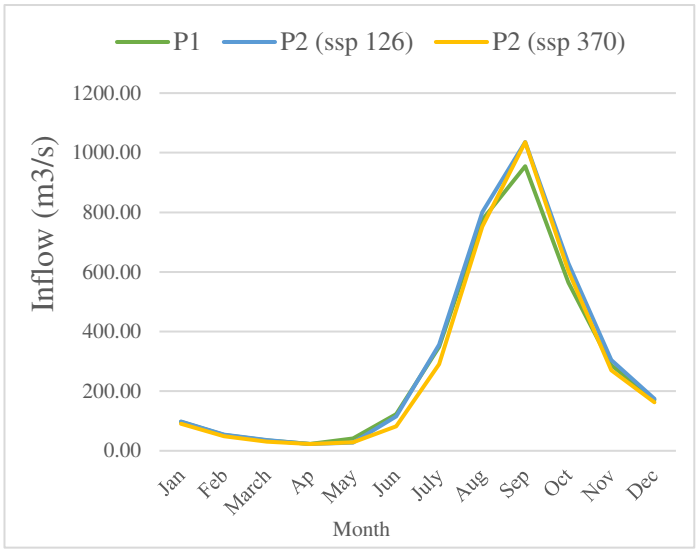

(b) Far future

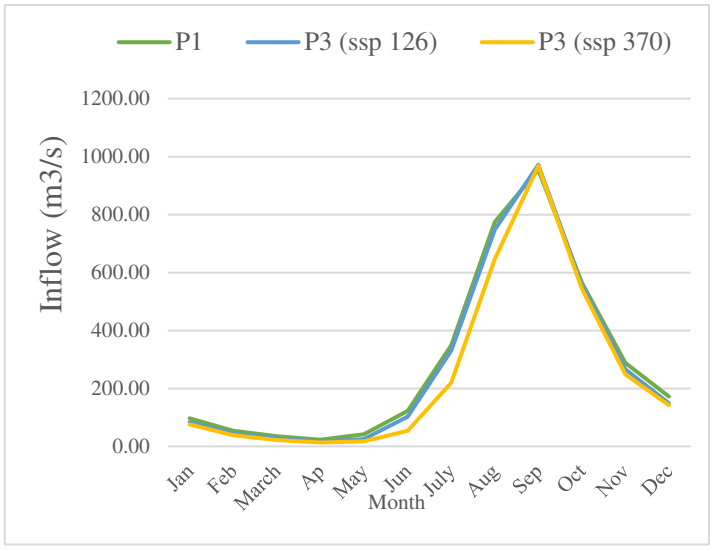

Figure 42: Variations in mean monthly inflow for (a) the near future (P1: 2035-2065) and (b) far future (P2: 2065-2095) compared to the reference period (P0: 1984-2014) under ssp 126 and ssp 370.

6.2.2 Impact of Land use/land cover change under reference period on the hydrology of the Manantali dam

The simulation of the SWIM and dam module was performed considering the LULC change from 1986 to 2020 and from 1986 to 2050 using the climate during the reference period (P0), to study only the impact of LULC change on the hydrology of the Manantali dam. The results show that changes in monthly, seasonal and annual flows are significantly affected by changes in LULC. Indeed, the results indicate a reduction in annual flows of – 5.7% (Table 29). During the rainy season, a decrease of -5% and during the dry season, a decrease of -12% is simulated (Figure 43). There is a reduction in the outflow of the Manantali dam, which is consistent with the decrease in inflow. Evapotranspiration (Eta) over the Manantali dam will not vary with the LULC change.

Table 30: Relative changes in the Manantali dam's hydrology based on LULC change from 1986 to 2020 and from 1986 to 2050 in the reference period (P0)

Water balance component	LULC (1986)	LULC (2020)	Relative change (%)	LULC (2050)	Relative change (%)
Pr (mm)	443	443	0%	443	0%
Inflow (Mm3)	9213.2	8638.5	-5.7%	8755.6	-5%
Tot_in (Mm3)	9663	9088.3	-6%	9205.5	-5%
Outflow (Mm3)	7848.1	7296.6	-7%	7408.3	-6%
Eta	860	875.9	2%	877	2%
Inflow (Rainy season m3/s)	2775.8	2638.8	-5%	2697.2	-3%
Inflow (dry season m3/s)	673.4	594.5	-12%	575.2	-15%

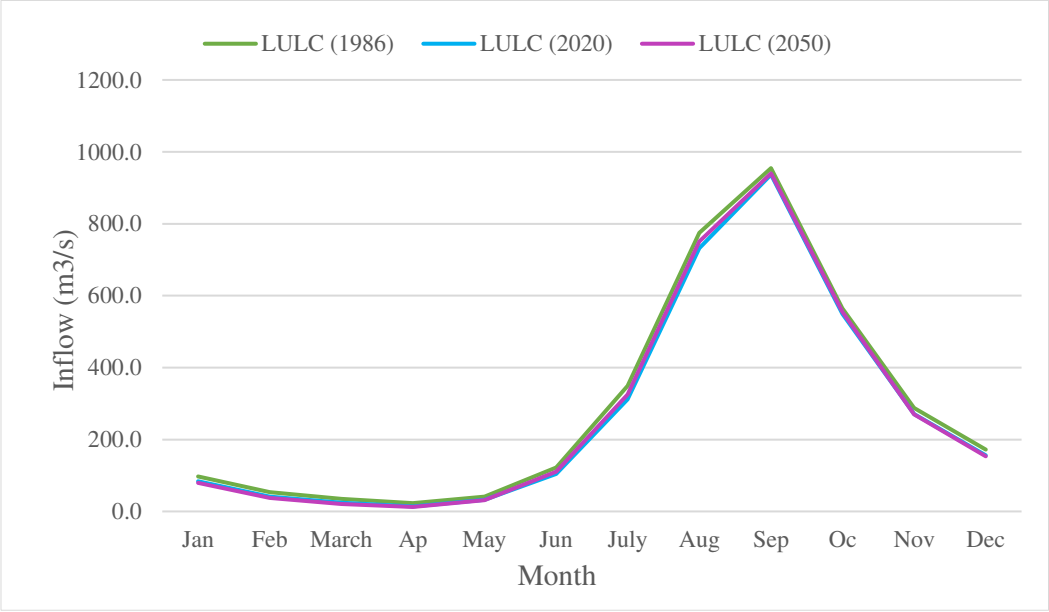

Figure 43: Variations in mean monthly inflow based on LULC change from 1986 to 2020 and from 1986 to 2050 under the reference period (P0)

6.2.3 Combined impact of climate change and LULC on the hydrology of the Manantali dam

The SWIM and dam module was simulated with LULC map from 1986 to 2050 and climate data under ssp 126 and ssp 370 as input data to analyze the combined impact of climate change and LULC change on the hydrology of the Manantali dam.

In the near future, the annual inflows are projected to increase by 1% under ssp126 or decrease by -6% under ssp370 (Table 30). The results indicate an increase by +3% change in inflow under ssp126 and a decrease by -3% during the rainy season under ssp370. A decrease in inflow of -12% for ssp126 and -19% for ssp370 is projected during the dry season (Figure 45). In the far future, the general trend indicates a decrease in the annual inflow for both scenarios (Table 30). In the near future, the annual outflows are projected to increase by 0.4% for ssp 126 and to decrease by -7% for ssp 370. In the far future, the annual outflows are projected to decrease by -12% for ssp 126 and -20% for ssp 370. Evapotranspiration (Eta) over the Manantali dam is projected to increase under the ssp 126 and the ssp 370 in both futures.

Tableau 31: Relative changes in the Manantali dam's hydrology based on LULC change from 1986 to 2050 and climate change during the near future (P1:2035-2065) and the far future (P2 :2065-2095) compared to the reference period (P0)

Water balance component	P0 (LULC 1986)	P1 (LULC 2050)				P2 (LULC 2050)			
		ssp126	Relative change (%)	ssp370	Relative change (%)	ssp126	Relative change (%)	ssp370	Relative change (%)
Pr (mm)	443	445	1%	440.1	-1%	423.8	-4%	407.6	-8%
Inflow (BCM)	9213.2	9260	1%	8661	-6%	8257.8	-10%	7550	-18%
Total_in (BCM)	9663	973	1%	9107.5	-6%	8692.5	-10%	7965.1	-18%
Outflow (BCM)	7848.1	7878	0.40%	7289.6	-7%	6918.1	-12%	6296.9	-20%
Eta	860	905.9	5%	903.3	5%	904.7	5%	920.6	7%
Inflow (Rainy season m3/s)	2776	286	3%	2684.524	-3%	2607.159	-6%	2342.398	-16%
Inflow (dry season m^3/s)	673	591	-12%	545.040	-19%	511.317	-24%	470.753	-30%

The separation of the effects of climate change and LULC change on the inflow shows that LULC change significantly affects annual flow. However, climate change has a more significant effect on the annual flow than LULC changes. In the near future (P1) under ssp 126, an increase of 1% in annual flow is projected. The analysis of climate and LULC's contribution to the annual flow reveals that the precipitation induces an increase in flow, while LULC induces a decrease in flow (Figure 44). In the near future (P1) under ssp 370, an annual decrease is projected in the flow induced by LULC and climate (Figure 44).

These results are consistent with the expected change in LULC and the climate projection in the Bafing watershed. Indeed, the period between 1986 and 2050 corresponds to a remarkable increase in vegetation and cultivated area, favoring processes such as infiltration at the expense of runoff. Precipitation is expected to increase by 1%. The results presented in Figure 45 indicate that the impact of climate change is more significant during the rainy season, while the effects of LULC are more important during the dry season.

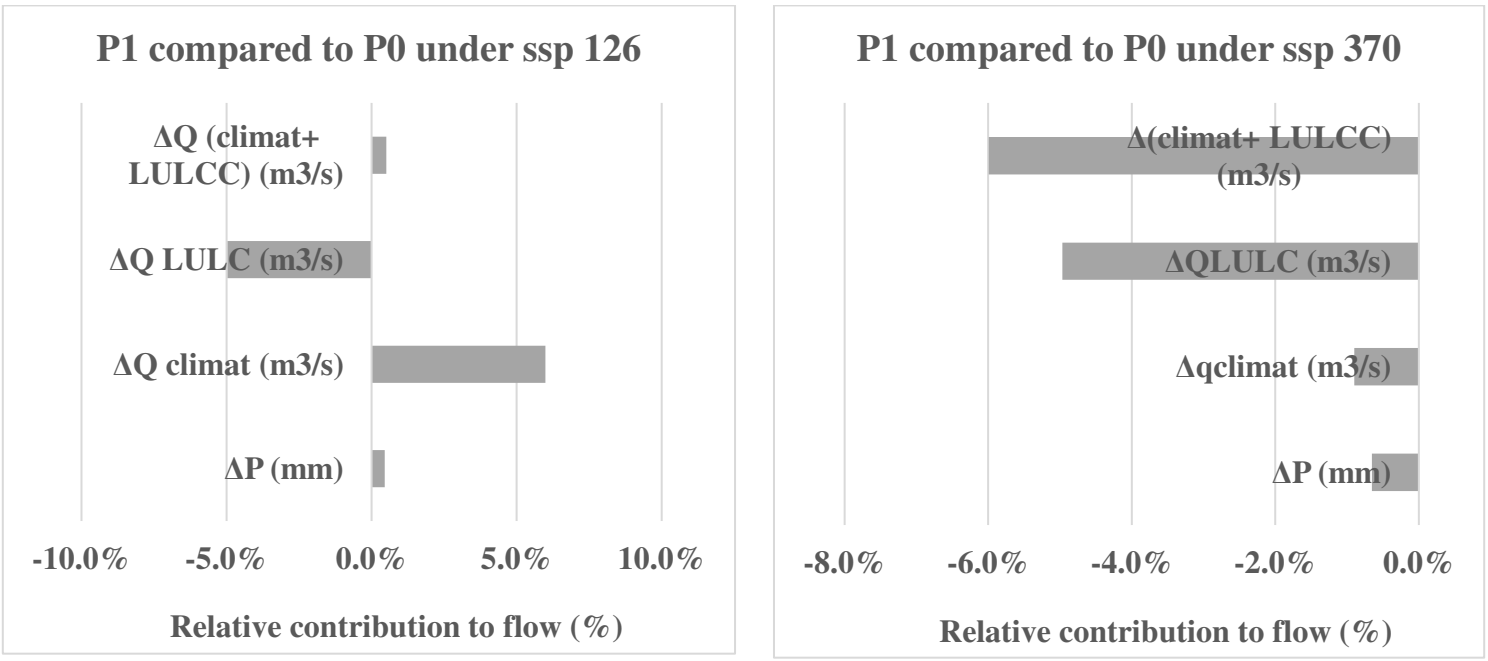

Figure 44: Relative contributions of climate (ssp 126, ssp 370) and LULC (LULC 1986, LULC 2050) on the inflow evolution at the Manantali dam in the near future (P1). The negative relative contributions indicate that the corresponding factor induces a decrease in inflow, while positive contributions indicate that the factor contributes to an increase in inflow.

a) P1

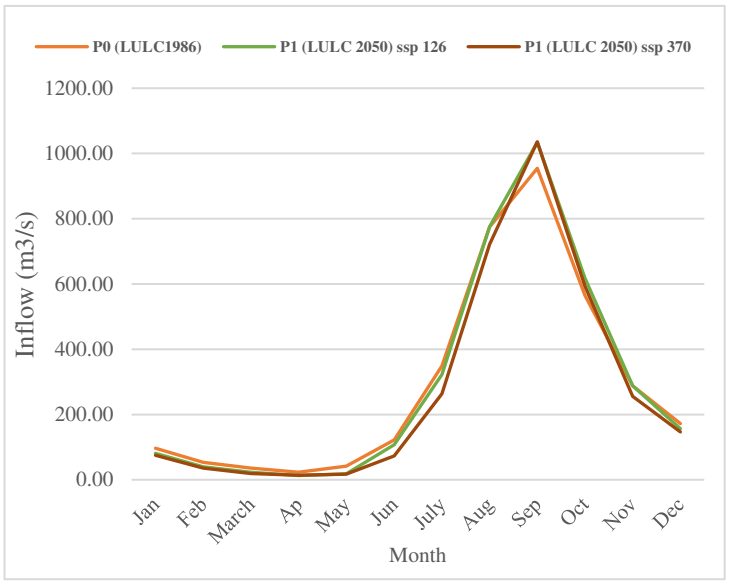

b) P2

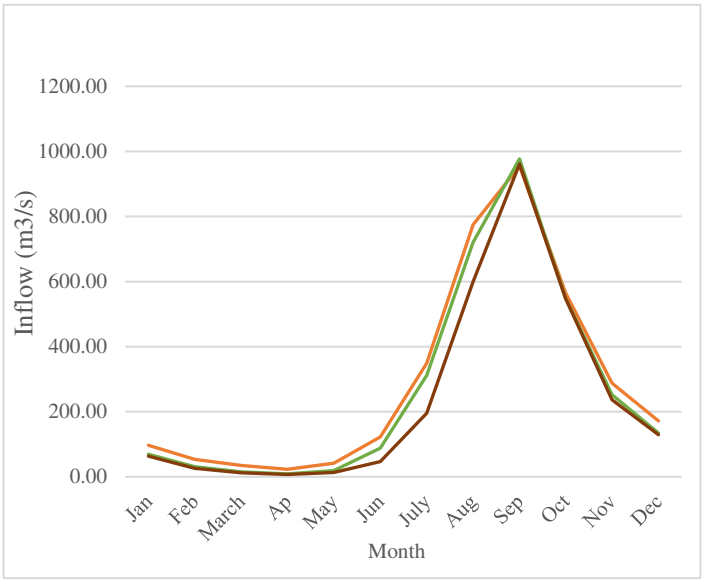

Figure 45: Monthly inflow variation in the Manantali dam according to LULC 2050 under ssp 126 and ssp 370
a) in the near future (P1: 2035-2065) compared to the reference period (P0:1984-2014) and LULC 1986;
b) in the far future (P1: 2065-2095) compared to the reference period (P0:1984-2014) and LULC 1986.

6.2.4 Impact of future dam developments on the hydrology of the Manantali

The simulation of the SWIM and dam module was carried out considering the LULC of 1986 and the climate data during the reference period (P0: 1984-2014) to assess only the impact of future development (DS2, DS3) on the hydrology of the Manantali dam. On an annual scale, the development of future dams will reduce the inflow of the Manantali dam by -6% for DS2 and -12% for DS3 (Table 31). Future dams will lead to a sharp increase in monthly flows from January to June, from 54% to 508% for DS2 and from 64% to 580% for DS3.

On a monthly scale, future dams will decrease in the inflow of the Manantali dam from July to December from -3 to -34% for DS2 and from -4% to -42% for DS3 (Figure 46). During the rainy season, September is more affected by the decrease of the inflow of the Manantali dam, with a reduction of -34% and -42%, respectively, for DS2 and DS3 compared to DS1 (Figure 46). the results show there is no change in evapotranspiration (Eta) of the Manantali dam with the Koukoutamba dam (DS2), but a decrease by -4% in evapotranspiration (Eta) with the

Koukoutamba and Boureya dam (DS3) (Table 31). The results are presented in Table 31, Figure 46.

Table 32: Relative changes (%) in the hydrology of the Manantali dam according to the construction of the Koukoutamba (DS2) and Koukoutamba and Boureya (DS3) dams during the reference period (P0: 1984-2014).

Water balance component	DS1	DS2	Relative change (%)	DS3	Relative change (%)
Pr	443	443	0%	443	0%
Inflow	9213.2	8692	-6%	8112.5	-12%
Tot_in	9663	9141.9	-5%	8555.7	-11%
Outflow	7848.1	7313.1	-7%	6838.4	-13%
Eta	860	862	0%	828	-4%

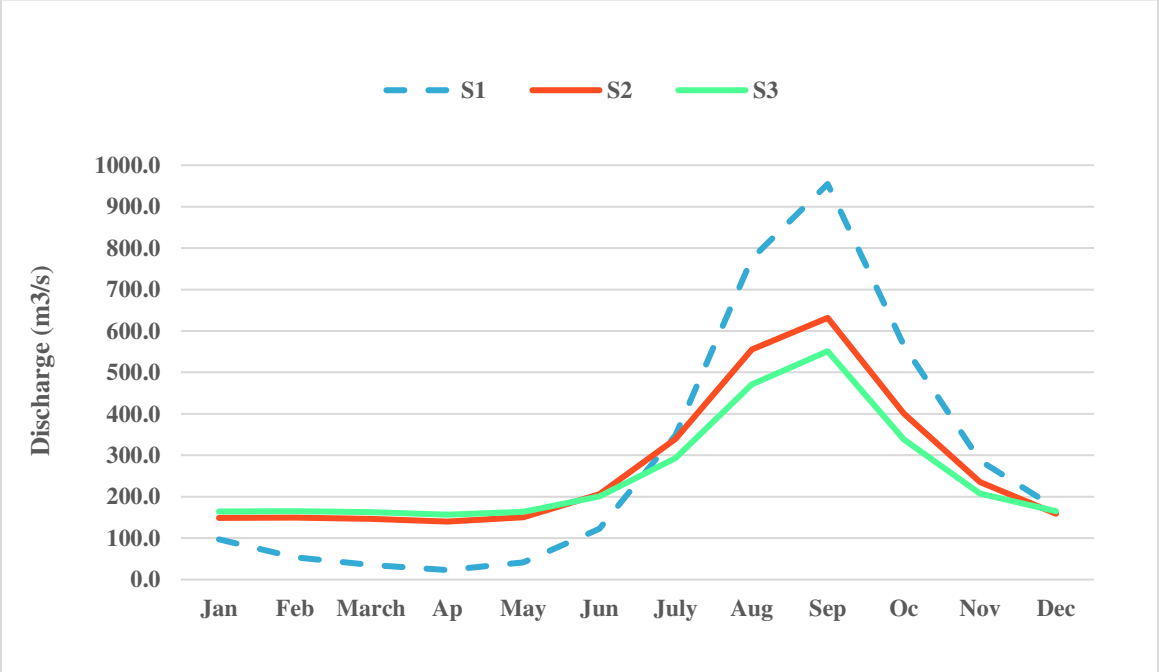

Figure 46: Monthly inflow variation of the Manantali dam with the Koukoutamba dam (S2) and Koukoutamba and Boureya (S2 and S3) during the reference period (P0: 1984-2014).

6.3 Conclusion

Since water is a fundamental component of the planet's life support system, establishing a sustainable water resources management system is essential. Including sustainability criteria in water resources management requires considering the changing and uncertain nature of our socio-economic and natural environments, such as climate, LULC, and water management infrastructure. The objective of this chapter is to assess the effects of future changes (climate, LULC, new dams) on the hydrology of the Manantali dam in the near future (P1:2035-2065) and the far future (P2: 2065-2095) compared to the reference period (1984-2014) under ssp126 and ssp 370, LULC change (1986, 2020, 2050) and the future development scenarios of planned dams.

The SWIM model was chosen because it was considered a suitable hydrological model in the Bafing watershed. It has a dam module capable of representing the changing conditions generated by climate change, LULC change and taking into account existing and future dams in the basin. The modelling results show that the SWIM model and the dam module adequately represented past flow dynamics and dam management. The Nash-Sutcliffe efficiency (NSE) and Kling-Gupta efficiency (KGE) between 0.8 and 0.7 demonstrate the model's ability to simulate river flow, although the model overestimates it.

Regarding the possible impacts of climate change, the median of MME shows differences in how the hydrology of the Manantali dam is projected to change, depending on the future projections, but also the different scenarios used (ssp 123 and ssp 370). The results of the analysis of the impact of climate change on the inflow of the Manantali dam indicate a variation of inflow of 6% for ssp 126 and -1% for ssp370 in the near future. A decrease in inflow is expected for both scenarios in the far future compared to the reference period. There are significant differences between our results and those of Bodian et al. (2018) and Mbaye et al. (2016) on the impacts of climate change on water resources in the Bafing watershed. Bodian et al. (2018) investigated the effect of climate change on the Bafing watershed by using six GCM and two scenarios (RCP4.5 and RCP8.5) in 2050 compared to the reference period (1971-2000). The results showed that the mean of MME predicted a decrease in annual flow of -8% (RCP4.5) and -16% (RCP8.5) in the Bafing watershed. Mbaye et al. (2016) assessed the potential impacts of climate change on water resources and the effect of correcting statistical biases on the projected climate change signal in hydrological variables over the Upper SRB at the end of the 21st century (2071-2100) compared to the historical period (1971-2000). Their results indicate

that no change in flow is expected in the highlands of Guinea corresponding to the study area. These differences could be caused by the selection of different sets of GCMs, scenario assumptions, future periods, and the reference period used to assess the impact (Liersch et al., 2020). These discrepancies in results highlight the significant uncertainties of the impact of climate change on water resources. This proves that considering climate change in impact assessments remains a challenge in the Bafing watershed. This has important implications for climate change considerations for decision-makers formulating long-term strategic development plans.

The change in LULC has a negative effect on the inflow of the Manantali dam. This situation can be explained by the increase of vegetation and cultivated area and the decrease of bareground. Indeed, the results of the detection of post-classification changes have shown that the area occupied by vegetation has steadily increased, from 36% to 44% between 1986-2020 and 49% between 1986-2050. In 1986, the area covered by bareground was the most dominant LULC class, covering 60% of the watershed. Over the past 34 years, this area has gradually decreased to almost half, from 60% to 30%. The projected increase in vegetation and cultivated area (at the expense of bareground), have a lower runoff potential. Indeed, according to Descroix (2020), Guinean and Sudanese areas covered with dense vegetation are less prone to runoff.

A comparison between the impact of climate change and LULC change on the inflow of the Manantali dam showed that although LULC change has a significant impact on the inflow of the Manantali dam, but it is lower than the climate change impact. Separating the effects of climate and LULC change on the inflow of the Manantali dam shows that the two factors do not affect the evolution of the inflow of the Manantali dam in the same way. For example, under ssp 126, in the near future, climate tends to increase the inflow; as opposed to LULC, which tends to decrease the inflow. Climate becomes dominant in the flow control, resulting in increased flow. These results confirm the hypothesis of Albergel (1987) and Bernadette Nnomo (2016) that for a Sudanian watershed such as the Bafing watershed, the decrease in flow is an effect of climate deterioration rather than LULC change.

The results of the study also show that the exploitation of future dams will lead to a reduction of inflow during the wet season and an increase of inflow during the dry season. On an annual scale, they will reduce the inflow of the Manantali dam. Notwithstanding some of the negative effects of the planned dams, they will increase water storage and improve water management

in the Bafing watershed. Considering these changes with uncertain effects, an adaptive and participatory strategy is needed for sustainable water management in the Bafing watershed.

Chapter 7: Assessment of the potential impacts on the hydropower potential in the Bafing watershed

This chapter analyzes the impacts of climate change and land use/land cover change (LULC change) on the hydropower potential (HPP) in the Bafing watershed. The Swim model was simulated by using ten GCMs data and the LULC maps 1986, 2020 and 2050 as input data. The analysis was done by considering existing dam (Manantali) and planned dams (Koukoutamba and Boureya). A separation method was used to distinguish the respective contributions of climate change and LULC change, which are considered independent. A separation method consists of changing one factor at a time (either climate or LULC) by keeping the other constant (Fenta Mekonnen et al. 2018) and combining the two factors (climate and LULC). Additionally, relevant performance indicators such as spill, and probabilities of exceedance (P99, P95, P90) were used to compare future scenarios (the near future (P1:2035-2065) and the far future (P2:2065-2095); LULC 2050) with the reference period (P0: 1984-2014; LULC 1986).

7.1 Impact of climate change on the hydropower potential at the Manantali dam

The SWIM model and dam module were simulated with the assumption that LULC from 1986 remains unchanged for the future period (P1, P2) to analyze only the impact of climate change on hydropower generation at the Manantali dam. The results are presented in Table 32 and Figure 47.

On an annual scale, the projected HPP is consistent with the inflow projections under ssp 126 and ssp 370 (Figure 47).

In the near future, a change in the annual HPP of the Manantali dam of +3% for ssp126 and -1 % for ssp370 is projected. However, there is an increase of P 95, P 90 and P 99 for ssp 126 and ssp 370, indicating an improvement in the reliability of the hydropower potential. There is also a 50% increase in the spilled volume for ssp126 and 7% for ssp370. This reflects an increase in peak inflows above the dam's storage capacity (Table 32).

In the far future, the annual HPP of the Manantali dam is expected to decrease by -8% for ssp 126 and -14% for ssp 370. There is also a decrease of P 95, P 90 and P 99 for ssp126 and ssp370, consistent with the reduction in annual inflow in the Manantali dam. Interestingly, there was an increase in the volume spilled of 12% for ssp 126 and a decrease of 54% for ssp 370. This

reflects the fact that there is an increase in peak flows under ssp 126, which will not lead to an increase in annual HPP (Table 32).

Table 33: annual HPP at the Manantali dam under climate change (DS1)

LULC 1986	P0	P1				P2			
		ssp 126	Relative change (%)	ssp 370	Relative change (%)	ssp 126	Relative change (%)	ssp 370	Relative change (%)
Pr (mm)	443	445	1%	440.1	-1%	423.8	-4%	407.6	-8%
Inflow (BCM)	9213.2	9765.1	6%	9130.5	-1%	8633.5	-6%	7988	-13%
Spill (%)	0.677	1.023	51%	0.726	7%	0.755	12%	0.313	-54%
HPP GWh/y)	820	846	3%	814	-1%	757	-8%	702	-14%
EP_90_(MW)	60.7	71.6	18%	60.5	-0.3%	54	-11%	43.7	-28%
EP_95_(MW)	48	61.7	29%	52.5	9%	45.2	-6%	36.1	-25%
EP_99_(MW)	35	48.1	37%	41.8	16%	34.5	-1%	25.8	-26%

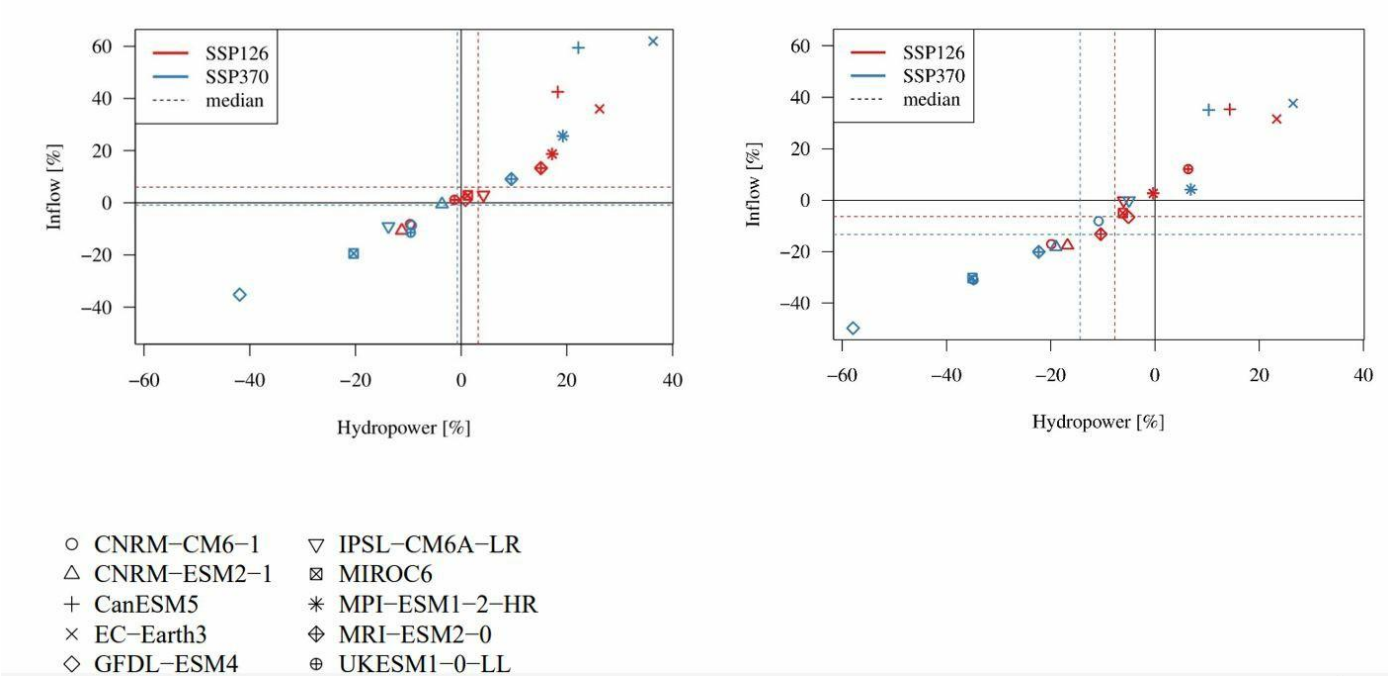

Figure 47: Projection of inflow and HPP of the Manantali dam in the near future (P1, left) and far future (P2, right) compared to the reference period under ssp 126 and ssp 370

On a monthly basis, in the near future, HPP of the Manantali dam will increase for all months for ssp126 and except August, September, November and December for ssp370. In the far

future, there is an overall decrease in HPP for all months for all scenarios (ssp 126, ssp 370) (Figure 48).

Near future (P1) compared to reference period (P0)

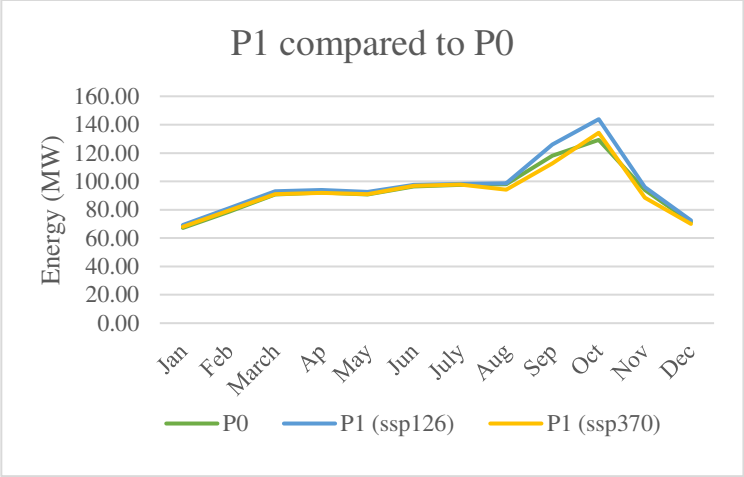

Far future (P2) compared to reference period (P1)

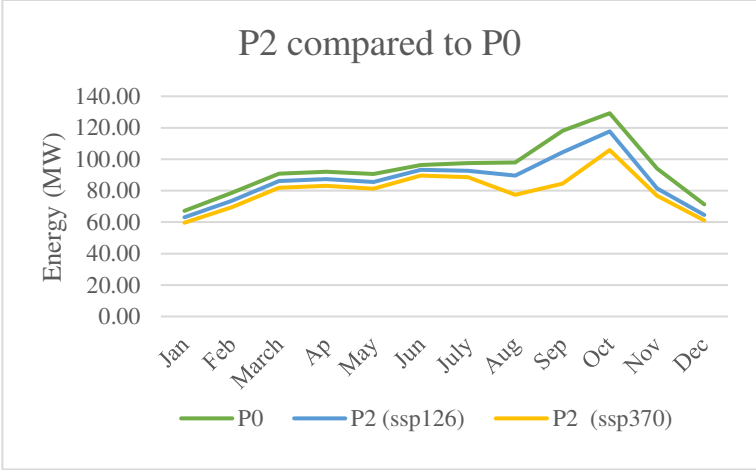

Figure 48:Monthly HPP variation of the Manantali dam in the near future (P1, left) and the far future (P2, right) compared to the reference period (P0) under ssp 126 and ssp 370

7.2 Impact of LULC change on the hydropower potential (HPP) at the Manantali dam

To study only the impact of LULC change on the HPP of the Manantali dam, the SWIM simulation was performed considering the LULC change from 1986 to 2020 and from 1986 to 2050 under the climate during the reference period (P0).

The results show that monthly and annual HPP of the Manantali dam will be negatively affected by LULC change (Table, Figure). Indeed, the results indicate a change in the annual HPP of the Manantali dam of -5.7%, respectively, between 1986 and 2050 (Table 33). These findings can be explained by the result obtained with the analysis of the post-classification change detection between 1986, 2020 and 2050. The analysis and detection of post classification change reveals that the main conversions were from bareground to vegetation, cultivated area and settlement during the study period. Hence, bareground with high runoff coefficients was converted to vegetation and cultivated area with lower runoff coefficients. There is also a decrease in EP 95, EP 90 and EP 99, indicating a decrease in the reliability of hydropower potential. There is a decrease in the volume spilled, which is consistent with the reduction in the projected inflow. The same situation is noted on a monthly scale (Figure 49).

Table 34: Relative change in annual HPP according to LULC change between 1986-2020 and between 1986-2050 based on the reference period (P0: 1984-2014)

Water balance component	LULC 1986	LULC 2020	Relative change (%)	LULC 2050	Relative change (%)
Pr (mm)	443	443	0%	443	0%
Inflow (BCM)	9213.2	8638.5	-6%	8755.6	-5%
Spill (BCM (%))	0.677	0.477	-30%	0.519	-30%
HPP (GWh_a)	813.5	760.9	-6.5%	769.6	-5.7%
EP_90_(MW)	60.7	54.6	-10%	56.9	-7%
EP_95_(MW)	48	43.2	-10%	45.6	-5%
EP_99_(MW)	35	30.6	-13%	32.9	-6%

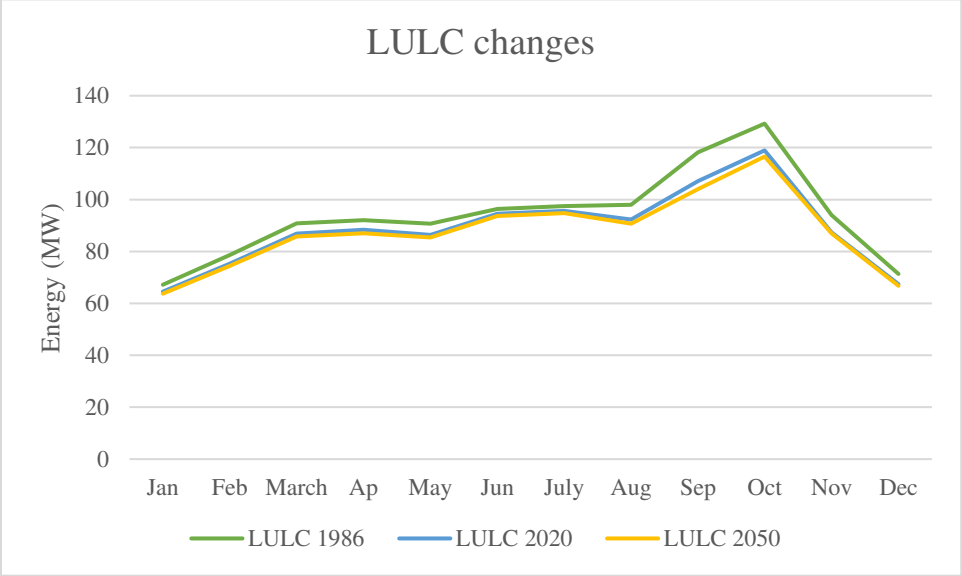

Figure 49: Projected change in monthly HPP according to LULC change between 1986-2020 and between 1986-2050 based on the reference period (P0: 1984-2014)

7.3 Combined impact of climate change and LULC change on the hydropower potential of the Manantali dam

To analyze the combined impact of climate change and LULC change on the HPP at Manantali dam, the SWIM model was simulated with LULC map from 1986 to 2050 and climate data for the near future (P1) and far future (P2) under ssp 126 and ssp 370.

In the near future (P1), the annual HPP of the Manantali dam is projected to either increase by 3% under ssp126 or decrease by -4% under ssp370 (Table 34). Although the LULC change (only) reduces the HPP of the Manantali dam by -5% in P1 under ssp126, but due to the increase in precipitation (1%) and flow (6%), the combined climate and LULC simulations still project an increase of 3.2% in the HPP of the Manantali dam (Figure 50). Under ssp 370, in the near future, both factors will affect the HPP of the Manantali dam in the same downward trend. These results suggest that the HPP of Manantali dam follows the general trends of climate change because the relative contribution of climate to the HPP of the Manantali dam is greater than that of LULC (Figure 50). The spilled volumes will either increase by 15% under ssp 126 or decrease by -18% under ssp370. P90, P95 and P99 values will either increase under ssp 126 or decrease under ssp370.

In the far future, the HPP of the Manantali dam is expected to decrease for ssp 126 and ssp 370 (Table 34). The spilled volumes and the P90, P95 and P99 values will also decrease under ssp 126 and under ssp370.

Table 35: Relative change in annual HPP according to LULC change between 1986 to 2050 and CC in the near future (P1) and the far future (P2) compared to reference period (P0) under ssp 126 and ssp 370.

Water balance component		P1 (LULC 2050)				P2 (LULC 2050)			
	P0 (LULC 1986)	ssp 126	Relative change (%)	ssp 370	Relative change (%)	ssp 126	Relative change (%)	ssp 370	Relative change (%)
Pr (mm)	443	445	1%	440.1	-1%	423.8	-4%	407.6	-8%
Inflow (BCM)	9213.2	9260.4	1%	8661	-6%	8257.8	-10%	7550	-18%
Spill (BCM (%))	0.677	0.778	15%	0.573	-18%	0.599	-12%	0.228	-66%
HPP (GWh_a)	820	849	4%	771	-6.40%	777	-5.20%	659	-20%
EP_90 (MW)	60.7	65.8	8%	54.1	-12.20%	50.7	-16%	40.6	-33%
EP_95 (MW)	48	57.3	19%	47.3	-1%	43.5	-9%	33.9	-29%
EP_99 (MW)	35	45.3	29%	38.1	8%	32.8	-6%	24.7	-29%

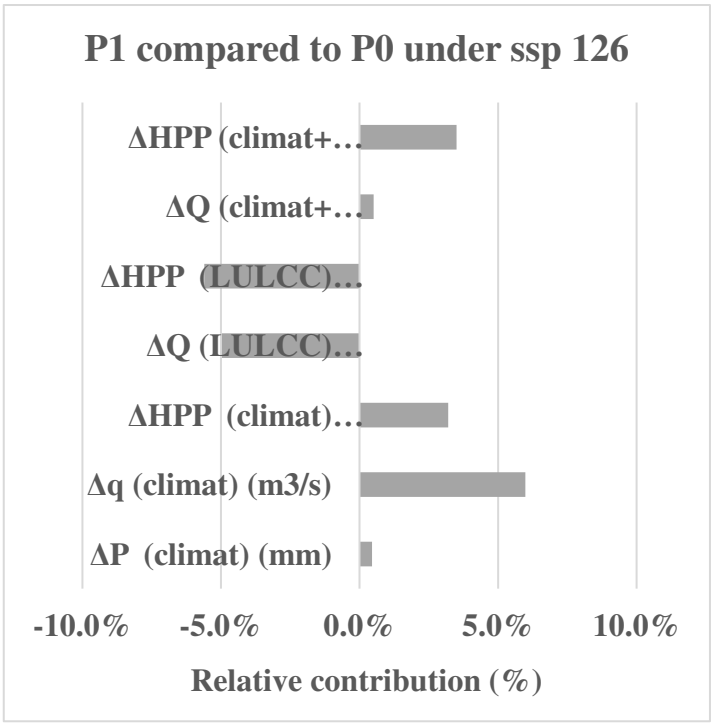

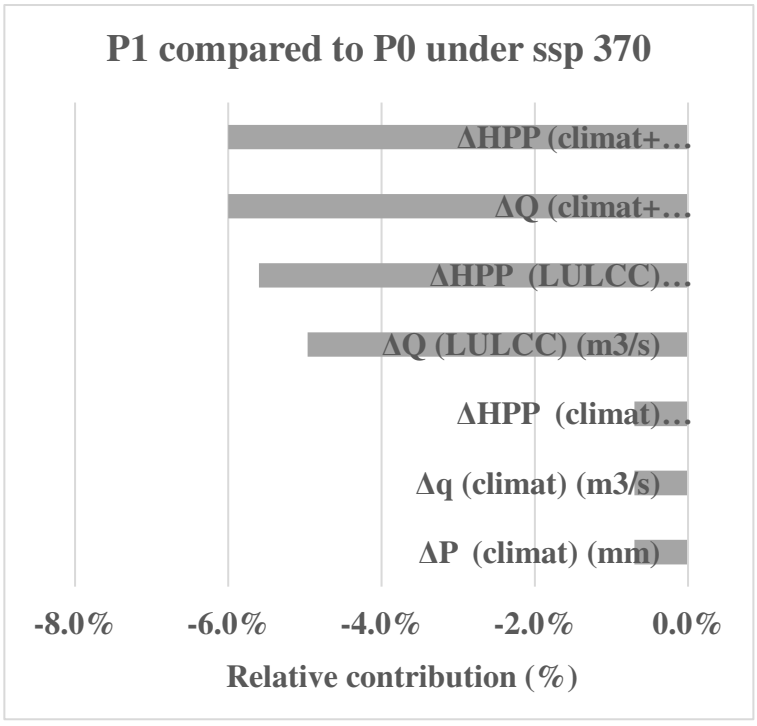

Figure 50: Relative contributions of climate (ssp 126, ssp 370) and LULC (LULC 1986, LULC 2050) on the HPP evolution at the Manantali dam in the near future (P1). The negative relative contributions indicate that the corresponding factor induces a decrease in flow, while positive contributions indicate that the factor contribute.

7.4 Impact of future dams on the hydropower of the Manantali dam

The simulation of the SWIM and dam module was carried out considering the LULC map of 1986 and the climate data during the reference period (P0: 1984-2014) to analyze only the effect of future dams (Koukoutamba and Boureya) on the HPP of the Manantali dam.

On an annual scale, the results show that the construction of dams will reduce the HPP of the Manantali dam (Figure 51, Table 35). Indeed, the DS2 will reduce the HPP at the Manantali dam by -3%. SD3 will result in an annual reduction of -10% of the HPP at the Manantali dam (Figure 51). These results are consistent with the performance indicators obtained. The EP 90 values decrease by -6% for DS2 and -12% for SD3, which shows a lower average production due to the decrease in the volumes of turbinated water in the long term.

The results also show that the future dams (DS2 and DS3) positively influence the HPP at the Manantali dam and flood peaks. For instance, there is a decrease in spilled volume of -31% and -64% in DS2 and DS3, thanks to a substantial decrease in extreme high inflows buffered by the upstream storage. There is also an increase of P95 of 2% and 3%, respectively, in DS2 and DS3, which means an improvement in the reliability of the hydropower potential because the risk of water levels in the Manantali dam reaching the lower turbine threshold is reduced.

Table 36: Relative changes in annual HPP according to future development scenario DS2 (Manantali and Koukoutamba dams) and DS3 (Manantali, Koukoutamba and Boureya dams) compared to DS1 (Manantali dam) under the reference period (P0:1984-2014).

Water balance component	DS1	DS2	Relative change (%)	DS3	Relative change (%)
Pr	443	443	0%	443	0%
Inflow	9213.2	8692	-6%	8112.5	-12%
Spill BCM (%)	0.677	0.468	-31%	0.241	-64%
GWh_a	820	793	-3%	727	-11%
EP_90_(MW)	60.7	57.3	-6%	53.3	-12%
EP_95_(MW)	48	48.9	2%	49.4	3%
EP_99_(MW)	35	38.7	11%	37.8	8%

On a monthly basis, there is a decrease in the HPP of the Manantali dam for all months except November, December, January, February, and August for DS2 and November, December and January for DS3 compared to DS1 (Figure 51).

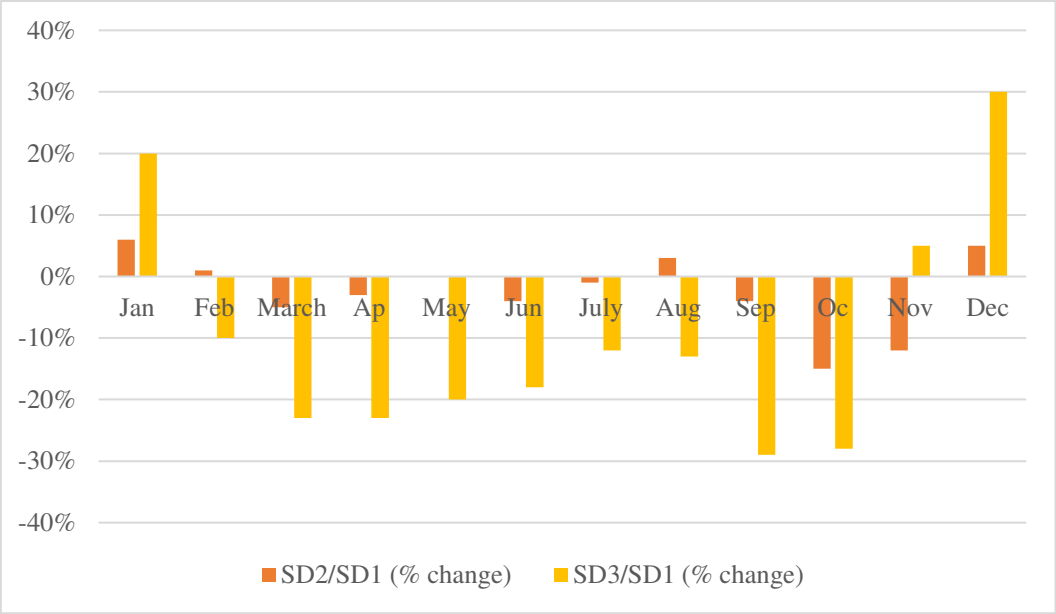

Figure 51: Monthly relative changes (%) on the HPP of the Manantali dam under DS2 and DS3 compared to DS1 based on the reference period (P0: 1984-2014)

7.5 Combined impact of climate change, LULC change and future dams developments on the HPP of the Manantali dam

The result of section 7.3, based on the combined impact of climate change and LULC change showed that the HPP of the Manantali dam follows the general trends of climate change, although LULC influences HPP. Therefore, in this section, the impact analysis is based on climate change and the development of future dams.

On an annual scale, the result shows that climate change and the future dams (DS2, DS3) will have a negative impact on the HPP of the Manantali dam (Table 36). In the near future (P1), in DS3 compared to DS1, the HPP of the Manantali dam is expected to decrease by -6.7% under ssp 126 and -11.8% under ssp 370, which is consistent with the decline in E90 values. Under climate change alone in P1 under ssp126, there would normally be a 6% increase in the inflow, but due to upstream dams, the positive trend will turn into a negative one (-6.7%). Under climate change alone, in the near future under ssp 370, there would normally be a decrease of -1% in HPP; but due to upstream developments, the decrease will be accentuated to -11.8% in the Manantali dam. Despite a decrease in HPP, there is an improvement of the reliability in HPP with an increase of 13% under ssp 126 and 8% under ssp 370 of the values of EP 95, which means that the risk that the water level in the Manantali dam reaches the lower turbine threshold decreases. The spilled volumes will decrease by -42% under ssp 126 and -60% under ssp370. This decrease in spilled volumes is caused by a substantial decrease in extreme high inflows due to upstream storage.

In the far future (P2), in DS3 compared to DS1, the HPP of the Manantali dam is expected to decrease by -17% and -30% under ssp126 and ssp370, respectively, with a decrease of EP 90 and EP 95. There is also a decrease in spilled volume of -62% and -91% under ssp126 and ssp370, respectively, led by the inflow decrease. The risk of the water levels in the Manantali dam reaching the lower turbine threshold is high, especially under scenario ssp370.

Table 37: Projected annual HPP according to future development scenario DS3 (Manantali dam, Koukoutamba, and Boureya) compared to DS1 (Manantali dam) and climate change in the near future (P1:2035-2065) and the far future (P2:2065-2095) compared to reference period (P0:1984-2014) under ssp 126 and ssp 370

Water balance component	P0		P1 (DS3)		P2 (DS3)	
	DS1	DS3	ssp 126	ssp 370	ssp 126	ssp 370
Pr (mm)	443	443	445	440.1	423.8	407.6
Inflow (BCM)	9213.2	8112.5	8597.7	7996.8	7522.2	6935.1
Spill (BCM (%))	0.677	0.241	0.393	0.272	0.254	0.061
HPP (GWh/y)	820	727	779	723	661	592
EP_90 (MW)	60.7	53.3	60.1	56.4	50.6	43.2
EP_95 MW)	48	49.4	54.4	51.9	47.1	37.8
EP_99 (MW)	35	37.8	48.6	40.5	42	29.7
Reliability (%)	86	64	82	72	63	31

7.6 Combined impact of climate change and LULC change on the hydropower potential of the Bafing Makana based on the existing (Manantali) and planned dams (Koukoutamba and Boureya)

The construction of future dams (DS2 and DS3) increases the annual HPP in the basin (Figure 52,53). However, while investment in future dams brings benefits, these benefits are very different from those achieved without climate and LULC changes.

Indeed, in the near future, the annual HPP of Koukoutamba, Boureya and Manantali dams will increase under ssp126 or decrease under ssp370 (Table 37). In the far future, the annual HPP of Koukoutamba, Boureya and Manantali dams will decreases in both scenarios, the loss will be more accentuated under ssp 370 (Table 37). LULC change from 1986 to 2050 will reduce the annual HPP of Koukoutamba, Boureya and Manantali dams (Table 37).

Table 38: The annual HPP (GWh/y) of the Bafing watershed under three development scenarios (DS1, DS2, DS3), based on CC for the near future (P1: 2035-2065) and the far future (P2: 2065-2095) under ssp 126 and ssp 370 and LULC change from 1986 to 2050.

Development scenarios	Dams	P0 (LULC 1986)	P0 (LULC 2050)	P1 (LULC 2050)		P2 (LULC 2050)	
				SSP1-2.6	SSP 370	SSP1-2.6	SSP 370
DS1	Manantali	820	774	849	771	777	659
DS2	Manantali	793	742	782	740	674	619
	Koukoutamba	879	911	934	890	851	783
DS3	Manantali	727	675	726	563	609	454
	Koukoutamba	879	911	934	890	851	783
	Boureya	601	617	631	604	580	538

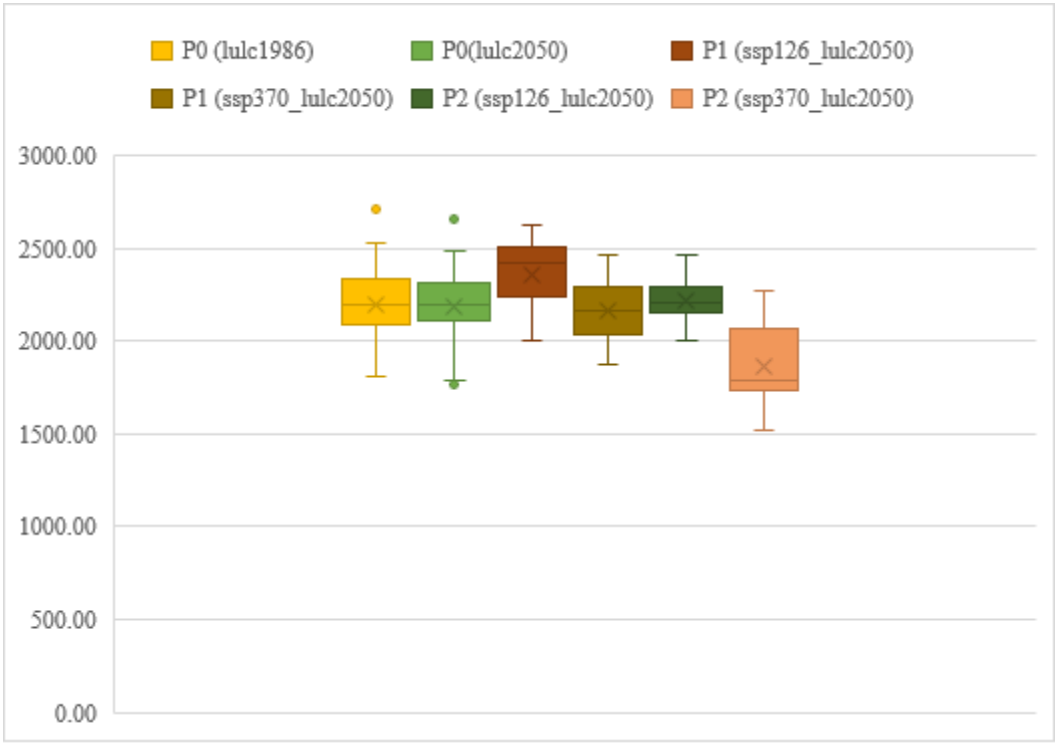

Figure 52: Simulated hydropower potential according to the development scenarios 3 (DS3) based on CC for the near future (P1: 2035-2065) and the far future (P2: 2065-2095) compared to reference period (P0: 1984-2014) under ssp 126 and ssp 370 and LULC.

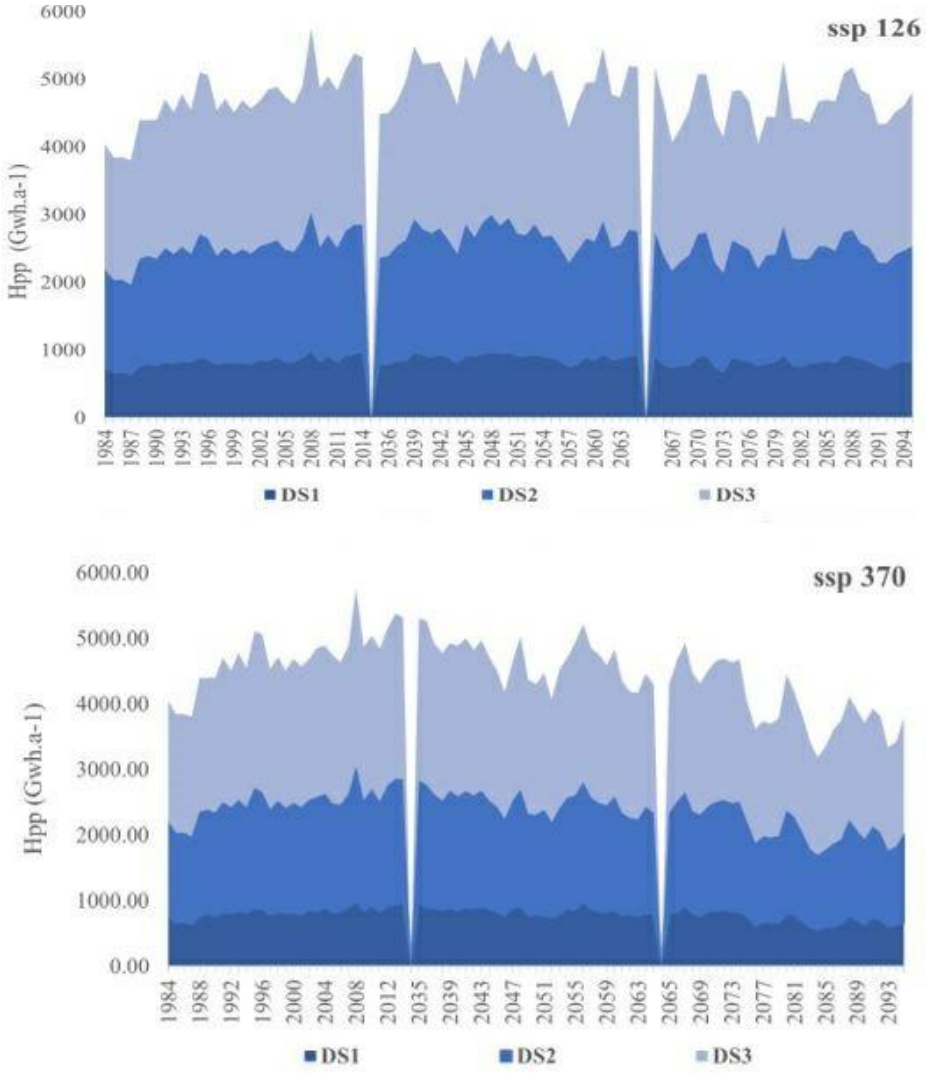

Figure 53: Simulated hydropower potential according to the development scenarios (DS1, DS2 and DS3) for the near future (P1: 2035-2065) and the far future (P2: 2065-2095) based on ssp 126 and ssp 370 compared to reference period (P0: 1984-2014).

7.7 Conclusion

Hydropower is a low-cost, well-established technology that may be an essential element of climate change adaptation in spite of its environmental and social implications (Berga, 2016). Climate and weather conditions significantly impact water resources and hydropower generation (Wasti et al., 2022). The analysis of the impacts of climate change and LULC change on the hydropower potential (HPP) and the management of the new dams in the face of future changes (climate, LULC) gives relevant information to decision-makers.

Regarding the possible impacts of climate change on the hydropower potential (HPP) of the Manantali dam, the median (MME) projects a reduction in future HPP except in the near future under ssp126 where an increase of 3% is projected despite the evaporative losses caused by the increase in temperature that are offset by the increase in precipitation during this period. The climate change projection over the Bafing watershed can explain these results. Indeed, the result of the projection of the GCMs from ISIMIP3b indicates that an increase of +1 % in precipitation would result in an increase of +1% in flow under ssp 126, and a decrease of -1% would lead to a decrease of -6% in flow under ssp 370, in the near future (P1). In the far future (P2), both scenarios project a decrease in precipitation that will lead to a decrease in flow. Temperature is expected to increase in the near and the far future under ssp 126 and ssp 370 compared to the reference period. Uncertainties about the projection are high in the near future. The future of the Bafing watershed depends heavily on global pathways. According to the moderate scenario (ssp 126), the world is moving progressively, but pervasively, towards a more sustainable path, with an emphasis on more inclusive development that respects perceived environmental limits. According to the ssp 370, the focus is on competitiveness and regional conflicts, instead of broder development leading to severe environmental degradation in some regions.

There is also a projected increase in spilled volume, except in ssp 370 in the far future, which may trigger an increase in flooding downstream that poses a severe threat in the Senegal River Valley. Indeed, the Senegal River valley experienced flooding in 1999 and 2003 due to heavy rainfall, leading to frequent releases of water from the Manantali dam and uncontrolled flows from the Bakoye and Faleme tributaries (OMVS, 2013). Emphasis should also be laid on the fact that retaining water in the dam for hydropower generation may conflict with maintaining a free volume for flood protection due to an elevated risk of flooding.

Regarding the possible impacts of LULC change on the HPP of the Manantali dam, the results show that LULC change will have a negative impact on the inflow, leading to a decrease of HPP of the Manantali dam. These findings can be explained by the conversion from bareground

(with high runoff coefficients) to vegetation and cultivated area (lower runoff coefficients) during the study period (1986, 2020, 2050). It is largely documented that surface water dynamics are highly dependent on soil and vegetation conditions. The vegetation is dense in the Sudanian and Guinean regions where the Bafing watershed is located; translating into runoff resistance.

Concerning the impacts of climate change and LULC change on the HPP of the Manantali dam, a comparison between the two factors showed that the HPP of the Manantali dam follows the general trend of climate change. The relative contribution of climate to the HPP of the Manantali dam is greater than that of LULC. Indeed, the combined CC and LULC simulations still predict an increase in the HPP of the Manantali dam of 3.2%, even if the LULC change only reduces the HPP of the Manantali dam by -5% in P1 under ssp126. This increase of the HPP of the Manantali dam is due to higher precipitation (1%) and flow (6%) in P1 under ssp126. These results confirm the hypothesis of Albergel (1987) and Bernadette Nnomo (2016) that for a Sudanian watershed such as the Bafing watershed, the decrease in flow is an effect of climate deterioration rather than LULC change.

The impacts of the future dams on the HPP of the Bafing watershed are mixed. On the one hand, the upstream dams will lead to a decrease in HPP although the operation of the Manantali dam has been adjusted after the incorporation of the two planned dams. On the other hand, the upstream dams will improve the reliability of the HPP of the Manantali dam by reducing the risk that the water level in the Manantali dam reaches the lower turbine threshold. They will also contribute to reducing the spilled volumes by controlling peak flow upstream of the dam, thus reducing the risk of flooding in Bakel. The joint operation of the three dams increases the mean annual HPP in the Bafing watershed from 820 GWh/y (Manantali) to 2207 GWh/y (Manantali, Koukoutamba and Boureya).

As for the possible impacts of climate change on the future dams, the results suggest that climate change will have a significant impact on the HPP. Indeed, the results show that although the planned dams will increase the HPP in the basin, climate change will negatively affect them except in the near future (P1) under ssp 126. These results are consistent with those of Obahoundje et al. (2021). According to Nassopoulos (2013), the increase in storage capacity related to the construction of planned dams is the first option for adaptation to climate change for water availability despite the negative social and environmental consequences. Thus, operational rules must be dynamically adjusted to adapt to climate change. Our results are consistent with the findings of Padiyedath Gopalan et al. (2021) which suggest that additional

coping strategies are needed. One adaptation technique is to improve the operation of these three dams through an optimization program. Optimizing the programming of a group of hydropower dams on a basin has various advantages. It allows the full use of water resources at all scales and the adjustment and compensation of the effects of interannual climate variables on each power plant (Shu et al., 2018). The other option is to study the complementarities between hydro, solar and wind energy at the local or regional scale. (Sterl et al., 2018,2020) highlight that the appropriate management of existing and future hydropower plants in West Africa and the adoption of a new common energy policy promoting an energy mix that prioritizes renewable energies, namely hydropower, solar and wind, are essential to exploit West Africa's renewable energy potential optimally.

Chapter 8: General conclusion and perspectives

Chapter 8 presents the main conclusions of our research, its contributions to knowledge, its limitations and expectation for future research.

8.1 Conclusion and contributions to knowledge

The main objective of the study was to analyze the impacts of climate change and land use/land cover on the water availability and the hydropower potential in the Bafing watershed considering the existing (Manantali) and future dams (Koukoutamba and Boureya). The proposed approach is based on the "Water-Energy" Nexus.

To this end, three specific objectives were established right at the onset.

The first specific objective was to evaluate the performance of ten (10) bias-adjusted and downscaled Global Climate Model (GCM) of CMIP 6 from ISIMIP 3b in reproducing the observed climate (1979-2014) and to analyze future temperature and precipitation trends for the near future (P1: 2035-2065) and the far future (P2: 2065-2095) compared to the reference period (P0: 1984-2014) under the two climate scenarios (ssp 126 (moderate) and ssp 370 (medium-high-end)).

To achieve this objective, the two-precipitation products W-era5 (reanalysis) and CHIRPS (satellite) were compared to observed precipitation at the Bafing Makana. This was done because observation data have a low spatial coverage in the Bafing watershed and are insufficient for modelling purposes in terms of time series length (1979-1986 and 2001-2003) and data gaps. The performance of the two products to represent observed patterns was analyzed based on statistical indicators, such as R^2, RMSE, Pbias, NSE, Taylor diagram at the monthly and annual time steps and seasonal analysis. The comparison result indicates that W-era5 represents the observed precipitation pattern more accurately than CHIRPS. Indeed, data from the W-era5 era are perfectly in line with data from available station. Thus, the performance of GCMs from ISIMIP 3b using the W-era5 dataset as reference data was also evaluated because the bias-adjustment and downscaling were conducted with W-era5. The statistical findings show that the GCMs can accurately reproduce the temperature and precipitation of W-era5. The results from the Taylor diagram (RMSE, correlation) agree with the statistical findings. The outcome also showed that GCMs can fairly reproduce the unimodal structure of the precipitation, the bimodal structure of the temperature, and the historical trend of the W-era precipitation and temperature.

However, underestimation or overestimation is observed due to enduring biases in some models. According to the statistical analysis results, the median of MME is more effective at reproducing the reference data than the mean of MME and the individual GCM. These findings suggest that median of MME can produce accurate estimates and can successfully simulate precipitation and temperature of W-era5. Therefore, the median of MME was used to analyze and describe the future trends in the near future (P1) and the far future (P2) compared to the reference period (P0). According to the median (MME), an increase in temperature is projected, in the near future and the far future under ssp 126 and ssp 370. On the other side, there are many uncertainties associated with the precipitation projection. In fact, precipitation is projected to increase under ssp126 or decrease under ssp 370 in the near future (P1). In the far future (P2), precipitation is expected to decrease under both climate scenarios (ssp126 and ssp 370).

The second specific objective was to analyze the past and future spatio-temporal changes in LULC from 1986 to 2050. To come up with this, LULC changes over a 34-year period (1986, 1986, 2020) and simulated future changes in LULC in 2050 with the status quo (BAU) assumption (1986-2020) were evaluated. Landsat images from 1986, 2006 and 2020, image processing (index calculation), supervised classification with Random Forest (RF), and classification accuracy were used in Google Earth Engine (GEE) to establish LULC maps for each corresponding year. Five LULC classes ((1) settlement, (2) water, (3) vegetation, (4) cultivated area, (5) bareground) were used in the classification. The results of the classified LULC maps indicate that RF results provide very satisfactory classification with good accuracy. The results of the post-classification change detection technique from 1986-2020 show that significant change in LULC happened between 1986 and 2020. Indeed, the study shows that bareground has decreased by almost half in favor of settlement, cultivated area, vegetation and water. In the context of socioeconomic growth, population expansion and deforestation, the increase in vegetation between 1986 and 2020 is an interesting finding. The area occupied by vegetation increased from 36% to 44%, becoming the most dominant LULC class in 2020. The increase in vegetation suggests that when population growth is accompanied by adopting sustainable land management practices, it can lead to better land and water conservation.
Indeed, in the south of the Bafing watershed in Guinea (Fouta Djallon), the ecological intensification of rural activities has long been established and vegetation is not threatened. In the north of the Bafing watershed in Mali, several projects, such as the Bafing Faunal Reserve (Mali), the status of biosphere reserve (Mali), have been adopted to fight biodiversity losses

after the construction of the Manantali Dam. The modelling of the future LULC changes was entirely realized in the Land Change Modeller (LCM) with the Multilayer Perceptron and Markov Chain (MLP-MC) model based on five steps: change detection and analysis, determination of the explanatory variables, creation of transition potential maps, prediction of changes, and model validation. LULC maps of the years 1986 and 2006 were employed to analyze the trend of change, to calculate transition potential maps and to predict the LULC map of 2020. For model validation, the LULC map 2020 was compared with the predicted LULC map 2020 with the validation indicators (ROC, kia, Klo, and kno). The results indicate that the LCM through the MLP-MC model has reasonably simulated the LULC map of 2020 and can be used to project future LULC (2050) in the Bafing watershed. In 2050, vegetation will cover 49% of the study area, an increase of 3% compared to 2020. Settlement will be the second dominant LULC (with an increase of 1% compared to 2020). Bareground will be the third most dominant LULC class with 22%, representing a loss of 6%. Water and cultivated area will increase to 4.8% of the area. The Bafing watershed has seen a trend towards "more people, more trees".

The third specific objective was to assess the impact of climate and LULC changes on the hydrology and the HPP of the existing Manantali dam (DS1), the Manantali, Koukoutamba dam system (DS2), and the Manantali, Koukoutamba and Boureya dam system (DS3). The assumption that climate change and LULC change are independent was taken into account in order to separate the respective contributions of these two factors. Their effects were calculated using a separation method that involves changing one factor at a time (either climate or LULC by keeping the other constant) (Fenta Mekonnen et al. 2018) and combining the two factors (climate and LULC). A set of pertinent performance indicators was used to compare future changes with the reference period. These metrics include reliability, spill, and probabilities of exceedance. The spill was considered in this instance as a failure related to the maximum capacity, which could negatively impact hydropower generation.

The SWIM hydrological model was used to simulate the hydrological processes in the Bafing watershed, the inflows and dams management of the three dams. The SWIM hydrological model proved to be satisfactory in reproducing the flows with a NSE and KGE value of 0.8 and 0.7, respectively, in the calibration (1979-1986) and the validation (1987-1993) period. Although the model tends to overestimate peak flows, it well replicates low flows. The SWIM

Dam module satisfactorily reproduces the dynamics of inflows, outflows, and the water level of the Manantali dam.

At first, the impact of climate change on the hydrology and the HPP of the Manantali dam was analyzed for the near future (P1) and the far future (P2) compared to the reference period (P0) under ssp 126 and ssp 370. The results show that the inflow and the HPP of the Manantali follow the general trend of the projected precipitation. For the near future, an increase in the inflow of 6% will lead to an increase in HPP of 3% under ssp 126 or a reduction in the inflow of -1% will cause a loss of HPP of -1% under ssp 370. For the far future, a decrease in inflow of -4% and -8% will cause a decrease in HPP of -8% and -14% respectively under ssp 126, ssp 370. Eta is expected to increase in the future over the Manantali dam, which is compatible with the predicted temperature.

Then, the impact of LULC change on hydrology and the HPP of the Manantali dam from 1986 to 2050 were evaluated. The results indicate that LULC change negatively impact the inflow and the HPP at the Manantali dam. Indeed, LULC change will lead to a decrease of -5% in the inflow and -5.7% in HPP between 1986 and 2050.

After, the analysis of the combined impact of climate change and LULC change showed that although LULC change has a significant effect on the Manantali dam hydrology and HPP, it is smaller than climate change. Even though the LULC change (only) reduces the HPP of the Manantali dam by -5% in P1 under ssp126, the combined climate and LULC simulations still project an increase of 3.2% in the HPP of the Manantali dam. These results confirm the hypothesis of Albergel (1987) and Bernadette Nnomo (2016) that for a Sudanian watershed such as the Bafing watershed, the decrease in flow is an effect of climate deterioration rather than LULC change. These findings support the hypothesis that the variation in flow in a Sudanian watershed such as the Bafing watershed is due to climate change rather than LULC change.

After, the effect of the future dams (DS2, DS3) on the HPP of the Bafing watershed also occupy a central place in the analysis. The findings show that joint operation of the three dams (DS3) increases average annual HPP in the Bafing watershed from 820 GWh/y (Manantali) to 2207 GWh/y (Manantali, Koukoutamba and Boureya) in P0. In addition, future dams (Koukoutamba and Boureya) will reduce the risk of the water level in the Manantali dam reaching the lower threshold of the turbine, which will improve the reliability of the HPP. Future dams will also contribute to the reduction of spilled volumes by regulating the peak flow upstream of the Manantali dam; thus reducing the risk of flooding in the Senegal River valley. However, though

future dams will increase the HPP in the Bafing, they will negatively be affected by climate change and LULC change except in the near future under ssp 126.

8.2 Limitations and expectations for future research

The first limitation of the study was the use of W-era5 reanalysis data as reference data because of the lack of observed data of quality. Even if W-era5 reproduces very accurately the observed data, high quality observed data will give more precise results for the performance evaluation of the GCMs and the calibration and validation of the SWIM model.

The second limitation of the study is the use of MLP-MC to simulate future changes in LULC in 2050 with the status quo assumption (BAU). LULC change prediction is based on two aspects: the amount of change, and the spatial distribution of change. The result of the simulation show that the MLP-MC model failed to represent accurately the spatial distribution of changes. Indeed, while the percentages of LULC between the reference map (2020) and the simulated map (2020)' have a very high degree of concordance; the spatial distribution appears to be quite different. Therefore, a hybrid model that integrates spatial distribution of change such as Multi-Layer Perceptron Markov Chain Cellular Automata (MLP-MC-CA) and Logistic Regression Markov Model Cellular Automata (LR-MC-CA) should be considered in future research. These models have shown improvements in prediction and enabled a more precise simulation of LULC (Gaur et al., 2020; Sankarrao et al., 2021; Girma et al., 2022)

The third limitation of the study is that it did not consider stakeholder participation in the LULC change modelling methods. Stakeholder knowledge of LULC change drivers, reconstruction of timelines of significant past events, and perspective on potential future trajectories of land-use change are crucial to achieve comprehensive results in a participatory manner and complement model results (Hewitt et al.,2014).

The fourth limitation of the study is the non-integration of other Manantali dam objectives into the simulation and analysis. Actually, the Manantali dam is a multi-purpose hydropower dam designed and operated to provide services such as generating approximately 876 GWh of electricity per year; mitigation of floods that are too large to prevent their devastating effects; low-flow support for navigation and irrigated agriculture in the valley and for the supply of drinking water; flood support ensuring sufficient annual flooding in the valley for traditional agriculture practices and ecosystem maintenance (Bader and Albergel., 2015). Some of these objectives are contradictory, making the sustainable management of the Manantali dam

problematic. According to the work of Bader et al. (2003), flood support dedicated to ecological flow can, for instance, lead to a loss of energy production of up to an average of 14% in a dry year. The two objectives are proving to be very competitive in the context of low water, in the Senegal River Basin (Bruckmann, 2016). These conflicts make sustainable management problematic. Therefore, further study could focus on the impact of LULC change and climate change on Manantali dam and the system “Manantali dam, koukoutama and Boureya (DS3)”, taking into account the other objectives of the Manantali dam.

The fourth limitation of the study is the used of the FAO soil database, which is not very precise for each watershed. it is essential for decision makers to build up soil type databases to improve the quality of hydrological modelling.

As a perspective, additional information on the loss of hydropower potential to other uses such as irrigation, flood support for flood recession agriculture and related ecosystem services will be of paramount importance to enable an integrated management strategy for hydropower schemes in line with the Sustainable Development Goals (SDGs), in particular zero hunger (2), clean water and sanitation (6), clean and affordable energy (7), aquatic life (14). The objective will be to propose a decision support system for the optimal management of the water resource to allow decision-makers to have a wide range of choices on the actions to take. The approach could eventually be based on the "Water-Energy-food" Nexus taking into account climate change and LULC change.

Considering these limitations and perspective, we hope that future research can fill the gaps.

Reference

Abdulkareem, J.H., Sulaiman, W.N.A., 2016. Trend analysis of precipitation data in flood source areas of kelantan river basin. J. Teknol. 78, 115–127. https://doi.org/10.11113/jt.v78.9705

Adigun, P.A., Ezekwe, L.C., Rhaji, I.A., Sciences, M., Doko, H.M., 2022. Added Value of Bias Adjusted and statistical downscaled ISIMIP Models in Simulating Extreme Precipitation Characteristics over West Africa 1–28.

Agarwal, C., Green, G.M., Grove, J.M., Evans, T.P., Schweik, C.M., 2002. A Review and Assessment of Land-Use Change Models: Dynamics of Space, Time, and Human Choice. Apollo Int. Mag. Art Antiq. 62.

Ahbari, A., 2013. Mémoire de fin d'études intitulé :le bassin versant de Rhéraya: Modélisation et prédiction du comportement hydrologique 101.

Akinsanola, A.A., Ogunjobi, K.O., 2017. Evaluation of present-day rainfall simulations over West Africa in CORDEX regional climate models. Environ. Earth Sci. 76, 1–20. https://doi.org/10.1007/s12665-017-6691-9

Akinsanola, A.A., Zhou, W., 2019. Projections of West African summer monsoon rainfall extremes from two CORDEX models. Clim. Dyn. 52, 2017–2028. https://doi.org/10.1007/s00382-018-4238-8

Albergel, J., 1987. PREDETERMINATION, GENESE ET CRUES, DES FASO, AU BURKINA.

Ali, M.H., Abustan, I., 2014. A new novel index for evaluating model performance. J. Nat. Resour. Dev. 1–9. https://doi.org/10.5027/jnrd.v4i0.01

Almazroui, M., Saeed, F., Saeed, S., Nazrul Islam, M., Ismail, M., Klutse, N.A.B., Siddiqui, M.H., 2020. Projected Change in Temperature and Precipitation Over Africa from CMIP6. Earth Syst. Environ. 4, 455–475. https://doi.org/10.1007/s41748-020-00161-x

Ambrizzi, T., Reboita, M.S., da Rocha, R.P., Llopart, M., 2019. The state of the art and fundamental aspects of regional climate modeling in South America. Ann. N. Y. Acad. Sci. 1436, 98–120. https://doi.org/10.1111/nyas.13932

Amini, S., Saber, M., Rabiei-Dastjerdi, H., Homayouni, S., 2022. Urban Land Use and Land Cover Change Analysis Using Random Forest Classification of Landsat Time Series. Remote Sens. 14, 1–23. https://doi.org/10.3390/rs14112654

Andrieu, J., 2018. Land cover changes on the West-African coastline from the Saloum Delta (Senegal) to Rio Geba (Guinea-Bissau) between 1979 and 2015 Land cover changes on the West-African coastline from the Saloum Delta. Eur. J. Remote Sens. 51, 314–325. https://doi.org/10.1080/22797254.2018.1432295

Anne, A., Laurent, B., Jonathan, L., 2017. Fleuve Sénégal Analyse des projets potentiels liés à l'énergie : Focus sur le Sénégal 2017.

Anwar, Z., Alam, A., Elahi, N., Shah, I., 2022. Assessing the trends and drivers of land use land cover change in district Abbottabad lower Himalayan Region Pakistan. Geocarto Int. https://doi.org/10.1080/10106049.2022.2040604

Ardoin-Bardin, S., 2004. Variabilité hydroclimatique et impacts sur les ressources en eau de grands bassins hydrographiques en zone soudano-sahélienne. Thèse l'Université Montpellier II Sci. Tech. du Languedoc, Montpellier, Fr. 608.

Asfaw, D., Workineh, G., 2019. Quantitative analysis of morphometry on Ribb and Gumara watersheds: Implications for soil and water conservation. Int. Soil Water Conserv. Res. 7, 150–157. https://doi.org/10.1016/j.iswcr.2019.02.003

Ashenafi, A.A., 2014. Modeling Hydrological Responses to Changes in Land Cover and Climate in Geba River Basin , Northern Ethiopia. PhD Thesis, Freie Univ. Berlin, Ger. 187.

Azari, M., Billa, L., Chan, A., 2022. Multi-temporal analysis of past and future land cover change in the highly urbanized state of Selangor, Malaysia. Ecol. Process. 11. https://doi.org/10.1186/s13717-021-00350-0

Bader J-C., 2014. Monographie hydrologique du fleuve Sénégal : de l'origines mesures jusqu'en 2011., IRd Edition.

Bader, J.-C., Belaud, G., Lamagat, J.-P., Ferret, T., Vauchel, P., 2016. Modélisation de propagation d'écoulement entre lits mineur et majeur sur les fleuves Sénégal et Niger. Hydrol. Sci. J. 62, 1–

20. https://doi.org/10.1080/02626667.2016.1148815
Bader, J., Rolland, D., Pouget, J., 2015. S i m u l s e n: Logiciel de simulation de gestion d'un barrage à objectifs multiples, au pas de temps journalier.
Bader, J., Rolland, D., Pouget, J., 2005. Logiciel de simulation de gestion d'un barrage à objectifs multiples, au pas de temps journalier.
Bader, J.C., 2001. Programme d'optimisation de la gestion des réservoirs : manuel de gestion du barrage de Diama : version finale.
Bahati, H.K., Ogenrwoth, A., Sempewo, J.I., 2021. Quantifying the potential impacts of land-use and climate change on hydropower reliability of muzizi hydropower plant, Uganda. J. Water Clim. Chang. 12, 2526–2554. https://doi.org/10.2166/wcc.2021.273
Bamweyana, I., Musinguzi, M., Kayondo, L.M., 2021. Evaluation of CHIRPS Satellite Gridded Dataset as an Alternative Rainfall Estimate for Localized Modelling over Uganda. Atmos. Clim. Sci. 11, 797–811. https://doi.org/10.4236/acs.2021.114046
Barnieh, B.A., Jia, L., Menenti, M., Zhou, J., 2020. Mapping Land Use Land Cover Transitions at Di ff erent Spatiotemporal Scales in West Africa. Sustain. 2020,. https://doi.org/doi:10.3390/su12208565
Bates, B.C., Z.W. Kundzewicz, S. Wu and J.P. Palutikof, E., 2008. Climate Change and Water. Technical Paper of the Intergovernmental Panel on Climate Change, Eos, Transactions American Geophysical Union. https://doi.org/10.1029/90EO00112
Berga, L., 2016. The Role of Hydropower in Climate Change Mitigation and Adaptation: A Review. Engineering 2, 313–318. https://doi.org/10.1016/J.ENG.2016.03.004
Berihun, M.L., Tsunekawa, A., Haregeweyn, N., Meshesha, D.T., Adgo, E., Tsubo, M., Masunaga, T., Fenta, A.A., Sultan, D., Yibeltal, M., 2019. Exploring land use/land cover changes, drivers and their implications in contrasting agro-ecological environments of Ethiopia. Land use policy 87, 104052. https://doi.org/10.1016/j.landusepol.2019.104052
Bernadette Nnomo, N., 2016. Contribution à l ' actualisation des normes hydrologiques en relation avec les changements climatiques et environnementaux en Afrique de l ' Ouest.
Biasutti, M., 2019. Rainfall trends in the African Sahel: Characteristics, processes, and causes. Wiley Interdiscip. Rev. Clim. Chang. 10, 1–22. https://doi.org/10.1002/wcc.591
Biau, G., Scornet, E., 2016. A random forest guided tour. Test 25, 197–227. https://doi.org/10.1007/s11749-016-0481-7
Bichet, A., Diedhiou, A., Hingray, B., Evin, G., Touré, N.E., Browne, K.N.A., Kouadio, K., 2020. Assessing uncertainties in the regional projections of precipitation in CORDEX-AFRICA. Clim. Change 162, 583–601. https://doi.org/10.1007/s10584-020-02833-z
Blöschl, G., Marc F.P. Bierkens, Antonio Chambel, C.C., 2019. Twenty-three unsolved problems in hydrology (UPH)–a community perspective. Hydrol. Sci. J. 64, 1141–1158. https://doi.org/10.1080/02626667.2019.1620507
Bodian, A., 2012. Apport de la modélisation pluie-débit pour la connaissance de la ressource en eau : application au haut Bassin du Fleuve Sénégal. Climatologie. https://doi.org/10.4267/climatologie.223
Bodian, A., Dezetter, A., Diop, L., Deme, A., Djaman, K., Diop, A., 2018. Future climate change impacts on streamflows of Two Main West Africa River Basins: Senegal and Gambia. Hydrology 5. https://doi.org/10.3390/hydrology5010021
Bodian, A., Diop, L., Panthou, G., Dacosta, H., Deme, A., Dezetter, A., Ndiaye, P.M., Diouf, I., Visch, T., 2020. Recent trend in hydroclimatic conditions in the Senegal River basin. Water (Switzerland) 12, 1–12. https://doi.org/10.3390/w12020436
Breiman, L., 2001. Random Forests, Lecture Notes in Computer Science (including subseries Lecture Notes in Artificial Intelligence and Lecture Notes in Bioinformatics). https://doi.org/10.1007/978-3-030-62008-0_35
Bruckmann, L., 2016. L'intégration des zones inondables dans la gestion de l'eau et le développement de l'irrigation d'une vallée fluviale sahélienne. Le cas des terres de décrue de la moyenne vallée du Sénégal 597.
Brundtland Harlem, 1987. Commission mondiale sur l ' environnement et le développementde l ' ONU , présidée par Madame Gro Harlem Brundtland Table des matières.

Cabral, A.I.R., Lagos, F., 2017. Land cover changes and landscape pattern dynamics in Senegal and Guinea Bissau borderland. Appl. Geogr. 82, 115–128. https://doi.org/10.1016/j.apgeog.2017.03.010
Cantoni, R., Musso, M., 2018. L'énergie en Afrique: Les faits et les chiffres Introduction. Afr. Contemp. 261–262, 9–23. https://doi.org/10.3917/afco.261.0009
CEDEAO, 2015. L'agriculture et l'alimentation en Afrique de l'Ouest 138, 138.
Chang, Y., Hou, K., Li, X., Zhang, Y., Chen, P., 2018. Review of Land Use and Land Cover Change research progress. IOP Conf. Ser. Earth Environ. Sci. 113. https://doi.org/10.1088/1755-1315/113/1/012087
Chinwendu, O.G., 2019. KWAME NKRUMAH UNIVERSITY OF SCIENCE AND MODELING THE HYDROLOGICAL RESPONSE OF THE DANO CATCHMENT , IN THE VOLTA BASIN TO LANDUSE LANDCOVER By (B . Sc . Water Resources Management and Agromeotrology , M . Sc . Climate Change and Adapted Land use) A thesi.
Chirag, H.., 2022. Environmental Law Research Paper Topic : Impact Of Dams On The Environment. SSRN. https://doi.org/http://dx.doi.org/10.2139/ssrn.4137886
Choudhari, P.P., Nigam, G.K., Singh, S.K., Thakur, S., 2018. Morphometric based prioritization of watershed for groundwater potential of Mula river basin, Maharashtra, India. Geol. Ecol. Landscapes 2, 256–267. https://doi.org/10.1080/24749508.2018.1452482
Cisse, M.T., Sambou, S., Dieme, Y., Diatta, C., Bop, M., 2014. Analysis of flow in the Senegal River basin from 1960 to 2008. Rev. des Sci. l'Eau 27, 167–187. https://doi.org/10.7202/1025566ar
Congalton, R.G., 1991. A review of assessing the accuracy of classifications of remotely sensed data. Remote Sens. Environ. 37, 35–46. https://doi.org/10.1016/0034-4257(91)90048-B
Conway, D., Dalin, C., Landman, W.A., Osborn, T.J., 2017. Hydropower plans in eastern and southern Africa increase risk of concurrent climate-related electricity supply disruption. Nat. Energy 2, 946–953. https://doi.org/10.1038/s41560-017-0037-4
Cucchi, M., P. Weedon, G., Amici, A., Bellouin, N., Lange, S., Müller Schmied, H., Hersbach, H., Buontempo, C., 2020. WFDE5: Bias-adjusted ERA5 reanalysis data for impact studies. Earth Syst. Sci. Data 12, 2097–2120. https://doi.org/10.5194/essd-12-2097-2020
Dang, A.N., Kawasaki, A., 2016. A review of methodological integration in land-use change models. Int. J. Agric. Environ. Inf. Syst. 7, 1–25. https://doi.org/10.4018/IJAEIS.2016040101
Descroix, L., 2020. Ruissellement et infiltration en Afrique de l'Ouest : zonalité et azonalité.
Descroix, L., Bouzou, I., Genthon, P., Sighomnou, D., Mahe, G., Mamadou, I., Vandervaere, J.-P., Gautier, E., Faran, O., Rajot, J.-L., Malam, M., Dessay, N., Ingatan, A., Noma, I., Souley, K., Karambiri, H., Fensholt, R., Albergel, J., Olivry, J.-C., 2013a. Impact of Drought and Land – Use Changes on Surface – Water Quality and Quantity: The Sahelian Paradox. Curr. Perspect. Contam. Hydrol. Water Resour. Sustain. https://doi.org/10.5772/54536
Descroix, L., Diongue Niang, A., Dacosta, H., Panthou, G., Quantin, G., Diedhiou, A., 2013b. Évolution des pluies de cumul élevé et recrudescence des crues depuis 1951 dans le bassin du Niger moyen (Sahel). Climatologie 10, 37–49. https://doi.org/10.4267/climatologie.78
Descroix, L., Faty, B., Manga, S.P., Diedhiou, A.B., Lambert, L.A., Soumaré, S., Andrieu, J., Ogilvie, A., Fall, A., Mahé, G., Diallo, F.B.S., Diallo, A., Diallo, Kadiatou, Albergel, J., Tanimoun, B.A., Amadou, I., Bader, J.C., Barry, A., Bodian, A., Boulvert, Y., Braquet, N., Couture, J.L., Dacosta, H., Dejacquelot, G., Diakité, M., Diallo, Kourahoye, Gallese, E., Ferry, L., Konaté, L., Nnomo, B.N., Olivry, J.C., Orange, D., Sakho, Y., Sambou, S., Vandervaere, J.P., 2020. Are the fouta djallon highlands still the water tower of west africa?, Water (Switzerland). https://doi.org/10.3390/w12112968
Diakhaté, M., Mbaye, M.L., Camara, I., Barry, M.B., 2022. Projected Changes in the Rainfall Annual Cycle over the Senegal River Basin Using CMIP5 bias-Corrected Simulations. Am. J. Environ. Prot. 10, 41–46. https://doi.org/10.12691/env-10-1-5
Diallo, B.A., Zhengyu, B.A.O., 2018. Land Cover Change Assessment Using Remote Sensing : Case Study of Bamako , Land Cover Change Assessment Using Remote Sensing : Case Study of Bamako , Mali.
Diallo, M.A., Badiane, A.S., Diongue, K., Sakandé, L., Ndiaye, M., Seck, M.C., Ndiaye, D., 2020. A twenty-eight-year laboratory-based retrospective trend analysis of malaria in Dakar, Senegal.

PLoS One 15, 1–12. https://doi.org/10.1371/journal.pone.0231587
Didovets, I., 2021. SWIM model setup.
Diedhiou, A., Bichet, A., Wartenburger, R., Seneviratne, S.I., Rowell, D.P., Sylla, M.B., Diallo, I., Todzo, S., Touré, N.E., Camara, M., Ngatchah, B.N., Kane, N.A., Tall, L., Affholder, F., 2018. Changes in climate extremes over West and Central Africa at 1.5 °c and 2 °c global warming. Environ. Res. Lett. 13. https://doi.org/10.1088/1748-9326/aac3e5
Diop, L., Bodian, A., Diallo, D., 2016. Spatiotemporal Trend Analysis of the Mean Annual Rainfall in Senegal. Eur. Sci. Journal, ESJ 12, 231. https://doi.org/10.19044/esj.2016.v12n12p231
Dosio, A., Jones, R.G., Jack, C., Lennard, C., Nikulin, G., Hewitson, B., 2019. What can we know about future precipitation in Africa? Robustness, significance and added value of projections from a large ensemble of regional climate models. Clim. Dyn. 53, 5833–5858. https://doi.org/10.1007/s00382-019-04900-3
Dosio, A., Turner, A.G., Tamoffo, A.T., Sylla, M.B., Lennard, C., Jones, R.G., Terray, L., Nikulin, G., Hewitson, B., 2020. A tale of two futures: Contrasting scenarios of future precipitation for West Africa from an ensemble of regional climate models. Environ. Res. Lett. 15. https://doi.org/10.1088/1748-9326/ab7fde
Dubertret, F., Tourneau, F. Le, Villarreal, M., Dubertret, F., Tourneau, F. Le, Villarreal, M., An-, L.N.M., Dubertret, F., Tourneau, F. Le, Villarreal, M.L., 2022. Monitoring Annual Land Use / Land Cover Change in the Tucson Metropolitan Area with Google Earth Engine (1986-2020) To cite this version : HAL Id : hal-03655087 Monitoring Annual Land Use / Land Cover Change in the Tucson Metropolitan Area with Google E.
Eastman, J.R., Toledano, J., 2018. A Short Presentation of the Land Change Modeler (LCM) 499–505. https://doi.org/10.1007/978-3-319-60801-3_36
Economique, M.D.E.D., Detaille, A.P., 1976. AMENAGEMENT HYDROELECTRIQUE DE KOUKOUTAMBA.
ECREEE, 2017. GIS Hydropower Resource Mapping and Climate Change Scenarios for the ECOWAS Region.
Eyring, V., Bony, S., Meehl, G.A., Senior, C.A., Stevens, B., Stouffer, R.J., Taylor, K.E., Dynamique, D.M., Pierre, I., Laplace, S., Ipsl, L.M.D., 2016. Overview of the Coupled Model Intercomparison Project Phase 6 (CMIP6) experimental design and organization 1937–1958. https://doi.org/10.5194/gmd-9-1937-2016
Fan, J., Hu, J., Zhang, X., Kong, L., Li, F., Mi, Z., 2020. ScienceDirect Impacts of climate change on hydropower generation in China. Math. Comput. Simul. 167, 4–18. https://doi.org/10.1016/j.matcom.2018.01.002
Fan, J.L., Hu, J.W., Zhang, X., Kong, L.S., Li, F., Mi, Z., 2020. Impacts of climate change on hydropower generation in China. Math. Comput. Simul. 167, 4–18. https://doi.org/10.1016/j.matcom.2018.01.002
Fathizad, H., Rostami, N., Faramarzi, M., 2015. Detection and prediction of land cover changes using Markov chain model in semi-arid rangeland in western Iran. Environ. Monit. Assess. 187. https://doi.org/10.1007/s10661-015-4805-y
Faty, A., 2017. Modelisation hydrologique du haut bassin versant du fleuve senegal dans un contexte de variabilite hydro-climatique : Apport de la télédétection et du modèle Mike SHE. Université Cheikh Anta Diop de Dakar.
Fawagreh, K., Gaber, M.M., Elyan, E., 2014. Random forests: From early developments to recent advancements. Syst. Sci. Control Eng. 2, 602–609. https://doi.org/10.1080/21642583.2014.956265
Faye, C., 2023. Water Resources Management and Hydraulic Infrastructures in the Senegal River Basin: The Case Study of Senegal, Mali and Mauritania. River Basin Manag. - Under a Chang. Clim. https://doi.org/10.5772/intechopen.105633
Faye, C., 2017. Variabilité et tendances observées sur les débits moyens mensuels, saisonniers et annuels dans le bassin de la Falémé (Sénégal). Hydrol. Sci. J. 62, 259–269. https://doi.org/10.1080/02626667.2014.990967
Faye, C., 2015. Impact Du Changement Climatique Et Du Barrage De Manantali Sur La Dynamique Du Régime Hydrologique Du Fleuve Sénégal À Bakel (1950-2014). BSGLg. 64, 69–82.

Faye, C., Diop, E.H.S., Mbaye, I., 2015. Impacts des changements de climat et des aménagements sur les ressources en eau du fleuve sénégal: Caractérisation et évolution des régimes hydrologiques de sous-bassins versants naturels et aménagés. Belgeo 0–25. https://doi.org/10.4000/belgeo.17626
Fenta Mekonnen, D., Duan, Z., Rientjes, T., Disse, M., 2018. Analysis of combined and isolated effects of land-use and land-cover changes and climate change on the upper Blue Nile River basin's streamflow. Hydrol. Earth Syst. Sci. 22, 6187–6207. https://doi.org/10.5194/hess-22-6187-2018
Foody, G.M., 2020. Explaining the unsuitability of the kappa coefficient in the assessment and comparison of the accuracy of thematic maps obtained by image classification. Remote Sens. Environ. 239, 111630. https://doi.org/10.1016/j.rse.2019.111630
Foody Giles M, 2022. Land Cover Classification Accuracy Assessment. Springer Geogr. 80, 105–118. https://doi.org/10.1007/978-981-16-5149-6_6
François, : Baptiste, 2013. Gestion optimale d ' un réservoir hydraulique multiusages et changement climatique . Modèles , projections et incertitudes.
François, B., 2014. Gestion optimale d ' un réservoir hydraulique multiusages et changement climatique . Modèles , projections et incertitudes : Application à la réserve de Serre-Ponçon Baptiste François To cite this version : HAL Id : tel-00997012 Gestion optimale d ' un ré.
Gao, F., Zhang, Y., Chen, Q., Wang, P., Yang, H., Yao, Y., Cai, W., 2018. Comparison of two long-term and high-resolution satellite precipitation datasets in Xinjiang, China. Atmos. Res. 212, 150–157. https://doi.org/10.1016/j.atmosres.2018.05.016
Gao, X., Zhu, Q., Yang, Z., Wang, H., 2018. Evaluation and hydrological application of CMADS against TRMM 3B42V7, PERSIANN-CDR, NCEP-CFSR, and gauge-based datasets in Xiang River basin of China. Water (Switzerland) 10, 1–24. https://doi.org/10.3390/w10091225
Gaur, S., Mittal, A., Bandyopadhyay, A., Holman, I., Singh, R., 2020. Spatio-temporal analysis of land use and land cover change: a systematic model inter-comparison driven by integrated modelling techniques. Int. J. Remote Sens. 41, 9229–9255. https://doi.org/10.1080/01431161.2020.1815890
Gibba, P., Sylla, M.B., Okogbue, E.C., Gaye, A.T., Nikiema, M., Kebe, I., 2019. State-of-the-art climate modeling of extreme precipitation over Africa: analysis of CORDEX added-value over CMIP5. Theor. Appl. Climatol. 137, 1041–1057. https://doi.org/10.1007/s00704-018-2650-y
Giorgi, F., Jones, C., Asrar, G., 2009. Addressing climate information needs at the regional level: the CORDEX framework. … Organ. Bull. 58, 175–183.
Girma, R., Fürst, C., Moges, A., 2022. Land use land cover change modeling by integrating artificial neural network with cellular Automata-Markov chain model in Gidabo river basin, main Ethiopian rift. Environ. Challenges 6, 100419. https://doi.org/10.1016/j.envc.2021.100419
Gislason, P.O., Benediktsson, J.A., Sveinsson, J.R., 2006. Random forests for land cover classification. Pattern Recognit. Lett. 27, 294–300. https://doi.org/10.1016/j.patrec.2005.08.011
Gnouma, R., 2006. Aide a la calibration d'un modèle hydrologique distribue au moyen d'une analyse des processus hydrologiques : application au bassin versant de l'Yzeron.
Golub, M., Thiery, W., Marcé, R., Pierson, D., Vanderkelen, I., Mercado-bettin, D., 2022. A framework for ensemble modelling of climate change impacts on lakes worldwide : the ISIMIP Lake Sector 4597–4623.
Gorelick, N., Hancher, M., Dixon, M., Ilyushchenko, S., Thau, D., Moore, R., 2017. Google Earth Engine: Planetary-scale geospatial analysis for everyone. Remote Sens. Environ. 202, 18–27. https://doi.org/10.1016/j.rse.2017.06.031
Gupta, H. V., Kling, H., Yilmaz, K.K., Martinez, G.F., 2009. Decomposition of the mean squared error and NSE performance criteria: Implications for improving hydrological modelling. J. Hydrol. 377, 80–91. https://doi.org/10.1016/j.jhydrol.2009.08.003
Hamududu, B., Killingtveit, A., 2012. Assessing climate change impacts on global hydropower. Energies 5, 305–322. https://doi.org/10.3390/en5020305
Harrison, G., Whittington, H., Gundry, S., 1998. Climate change impacts on hydroelectric power. Proc Univ Power Eng Conf 1, 391–394.
Hausfather, Z., Drake, H.F., Abbott, T., Schmidt, G.A., 2020. Evaluating the Performance of Past Climate Model Projections. Geophys. Res. Lett. 47, 1–10.

https://doi.org/10.1029/2019GL085378
Herrmann, S.M., Brandt, M., Rasmussen, K., Fensholt, R., 2020. Accelerating land cover change in West Africa over four decades as population pressure increased. Commun. Earth Environ. 1, 1–10. https://doi.org/10.1038/s43247-020-00053-y
Hewitt, R., van Delden, H., Escobar, F., 2014. Participatory land use modelling, pathways to an integrated approach. Environ. Model. Softw. 52, 149–165. https://doi.org/10.1016/j.envsoft.2013.10.019
Horning, N., 2004. Land cover classification methods.
ICWE, 1992. Conférence internationale sur reçu et l ' environnement : DECLARATION DE DUBLIN 67.
IHA, 2022. Hydropower status report.
IHA, 2019. Hydropower status report 2019: Sector trends and insights, Hydropower Status Report.
IPCC, 2021a. Climate Change 2021: The Physical Science Basis - Summary for the Policymakers (Working Group I), Climate Change 2021: The Physical Science Basis.
IPCC, 2021b. Framing, Context, and Methods. In Climate Change 2021. https://doi.org/doi:10.1017/9781009157896.003.
ISIMIP, 2018. The Inter-Sectoral Impact Model Intercomparison Project (ISIMIP) Mission & Implementation Document.
Ito, R., Shiogama, H., Nakaegawa, T., Takayabu, I., 2020. Uncertainties in climate change projections covered by the ISIMIP and CORDEX model subsets from CMIP5 859–872.
Jampani, M., Amerasinghe, P., Liedl, R., Locher-Krause, K., Hülsmann, S., 2020. Multi-functionality and land use dynamics in a peri-urban environment influenced by wastewater irrigation. Sustain. Cities Soc. 62. https://doi.org/10.1016/j.scs.2020.102305
Jean-claude, B., Albergel, J., 2015. Artificial flood support on Senegal river : a challenge to protect natural resources in the valley 13, 1576–1580.
Jensen, J.R., 2006. Remote Sensing of the Environment: An Earth Resource Perspective, 2nd edition 2006.
Kabanza, A., Dondeyne, S., Tenga, J., Kimaro, D., Poesen, J., Kafiriti, E., Deckers, J., 2013. More people, more trees in South Eastern Tanzania: local and global drivers of land-use/cover changes. African Geogr. Rev. 32, 44–58. https://doi.org/10.1080/19376812.2012.746093
Kabo-Bah, A. and D.C., 2018. Sustainable Hydropower in West Africa Planning, Operation, and Challenges.
Kanda, N., Negi, H.S., Rishi, M.S., Kumar, A., 2020. Performance of various gridded temperature and precipitation datasets over northwest himalayan region. Environ. Res. Commun. 2. https://doi.org/10.1088/2515-7620/ab9991
Kaptué, A.T., Prihodko, L., Hanan, N.P., Turner, B.L., 2015. On regreening and degradation in Sahelian watersheds. Proc. Natl. Acad. Sci. U. S. A. 112, 12133–12138. https://doi.org/10.1073/pnas.1509645112
Karambiri, H., Ribolzi, O., Delhoume, J.P., Ducloux, J., Coudrain-Ribstein, A., Casenave, A., 2003. Importance of soil surface characteristics on water erosion in a small grazed Sahelian catchment. Hydrol. Process. 17, 1495–1507. https://doi.org/10.1002/hyp.1195
Kattsov, V., Federation, R., Reason, C., Africa, S., Uk, A.A., Uk, T.A., Baehr, J., Uk, A.B., Catto, J., Canada, J.S., Uk, A.S., 2013. Evaluation of climate models. Clim. Chang. 2013 Phys. Sci. Basis Work. Gr. I Contrib. to Fifth Assess. Rep. Intergov. Panel Clim. Chang. 9781107057, 741–866. https://doi.org/10.1017/CBO9781107415324.020
Keeble, B.R., 1988. Report of the World Commission on Environment and Development: Our Common Future. Med. War 4, 17–25. https://doi.org/10.1080/07488008808408783
Kim, S.J., Asadzadeh, M., Stadnyk, T.A., 2022. Climate change impact on water supply and hydropower generation potential in Northern Manitoba. J. Hydrol. Reg. Stud. 41, 101077. https://doi.org/10.1016/j.ejrh.2022.101077
Kleemann, J., Baysal, G., Bulley, H.N.N., Fürst, C., 2017. Assessing driving forces of land use and land cover change by a mixed-method approach in north-eastern Ghana, West Africa. J. Environ. Manage. 196, 411–442. https://doi.org/10.1016/j.jenvman.2017.01.053
Kling, H., Fuchs, M., Paulin, M., 2012. Runoff conditions in the upper Danube basin under an

ensemble of climate change scenarios. J. Hydrol. 424–425, 264–277. https://doi.org/10.1016/j.jhydrol.2012.01.011
Koch, H., Liersch, S., 2021. Reservoir-module of the eco-hydrological model SWIM (Version 12-2021).
Koch, H., Liersch, S., Hattermann, F.F., 2013. Integrating water resources management in eco-hydrological modelling. Water Sci. Technol. 67, 1525–1533. https://doi.org/10.2166/wst.2013.022
Koch, H., Silva, A.L.C., Liersch, S., de Azevedo, J.R.G., Hattermann, F.F., 2020. Effects of model calibration on hydrological and water resources management simulations under climate change in a semi-arid watershed. Clim. Change 163, 1247–1266. https://doi.org/10.1007/s10584-020-02917-w
Krysanova, V., Hattermann, F., Huang, S., Hesse, C., Vetter, T., Liersch, S., Koch, H., Kundzewicz, Z.W., 2015a. Modelling climate and land-use change impacts with SWIM: lessons learnt from multiple applications. Hydrol. Sci. J. 60, 606–635. https://doi.org/10.1080/02626667.2014.925560
Krysanova, V., Hattermann, F., Huang, S., Hesse, C., Vetter, T., Liersch, S., Koch, H., Kundzewicz, Z.W., 2015b. Modélisation des impacts des changements climatiques et d'occupation des sols avec SWIM: enseignements tirés d'applications multiples. Hydrol. Sci. J. 60, 606–635. https://doi.org/10.1080/02626667.2014.925560
Krysanova, V., Hattermann, F., Wechsung, F., 2005. Development of the ecohydrological model SWIM for regional impact studies and vulnerability assessment. Hydrol. Process. 19, 763–783. https://doi.org/10.1002/hyp.5619
Krysanova, V., Wechsung, F., Arnold, J., Srinivasan, R., Williams, J., 2021. SWIM (Soil and Water Integrated Model) User Manual, PIK Report.
Kulkarni, A.D., Lowe, B., 2016. Random Forest Algorithm for Land Cover Classification. Int. J. Recent Innov. Trends Comput. Commun. 4, 58–63.
Kulkarni, K., Vijaya, P., 2021. NDBI Based Prediction of Land Use Land Cover Change. J. Indian Soc. Remote Sens. 49, 2523–2537. https://doi.org/10.1007/s12524-021-01411-9
Kumar et al, 2011, 2011. Hydropower: IPCC Special Report on Renewable Energy Sources and Climate Change Mitigation. pp. 437–496.
Lambin, E.F., Coomes, O.T., Turner, B.L., Geist, H.J., Agbola, S.B., Angelsen, A., Folke, C., Bruce, J.W., Coomes, O.T., Dirzo, R., George, P.S., Homewood, K., Imbernon, J., Leemans, R., Li, X., Moran, E.F., Mortimore, M., Ramakrishnan, P.S., Richards, J.F., Vogel, C., Xu, J., 2001. The causes of land-use and land-cover change : Moving beyond the myths. Glob. Environ. Chang. 11, 261–269.
Lambin, E.F., Geist, H.J., Lepers, E., 2003. Dynamics of land-use and land-cover change in tropical regions. Annu. Rev. Environ. Resour. 28, 205–241. https://doi.org/10.1146/annurev.energy.28.050302.105459
Lamontagne, J.R., Barber, C.A., Vogel, R.M., 2020. Improved Estimators of Model Performance Efficiency for Skewed Hydrologic Data. Water Resour. Res. 56, 1–25. https://doi.org/10.1029/2020WR027101
Lange, S., 2020. ISIMIP3b bias adjustment fact sheet Observational dataset Bias adjustment and statistical downscaling method.
Lange, S., 2019. Trend-preserving bias adjustment and statistical downscaling with ISIMIP3BASD (v1.0). Geosci. Model Dev. 12, 3055–3070. https://doi.org/10.5194/gmd-12-3055-2019
Lantman, J. van S., Verburg, P.H., Bregt, A., Geertman, S.G., 2011. Core Principles and Concepts in Land-Use Modelling: A Literature Review 35–57. https://doi.org/10.1007/978-94-007-1822-7
Lawin, A.E., Hounguè, R., M'Po, Y.N.T., Hounguè, N.R., Attogouinon, A., Afouda, A.A., 2019. Mid-century climate change impacts on Ouémé River discharge at Bonou Outlet (Benin). Hydrology 6. https://doi.org/10.3390/hydrology6030072
Lebel, T., Cappelaere, B., Galle, S., Hanan, N., Kergoat, L., Levis, S., Vieux, B., Descroix, L., Gosset, M., Mougin, E., Peugeot, C., Seguis, L., 2009. AMMA-CATCH studies in the Sahelian region of West-Africa: An overview. J. Hydrol. 375, 3–13. https://doi.org/10.1016/j.jhydrol.2009.03.020
Leta, M.K., Demissie, T.A., Tränckner, J., 2021. Modeling and prediction of land use land cover

change dynamics based on land change modeler (Lcm) in nashe watershed, upper blue nile basin, Ethiopia. Sustain. 13. https://doi.org/10.3390/su13073740
Leye, I., 2023. Contribution à la modélisation hydrologique et hydraulique des hydro systèmes en vue de l ' optimisation de la ressource en eau : Application au système Kayanga-Anambé (Vélingara / Sénégal).
Liersch, S., Drews, M., Pilz, T., Salack, S., Sietz, D., Aich, V., Larsen, M.A.D., Gädeke, A., Halsnæs, K., Thiery, W., Huang, S., Lobanova, A., Koch, H., Hattermann, F.F., 2020. One simulation, different conclusions—the baseline period makes the difference! Environ. Res. Lett. 15. https://doi.org/10.1088/1748-9326/aba3d7
Liersch, S., Koch, H., Abungba, J.A., Salack, S., Hattermann, F.F., 2023. Attributing synergies and trade-offs in water resources planning and management in the Volta River basin under climate change. Environ. Res. Lett. 18. https://doi.org/10.1088/1748-9326/acad14
Liersch, S., Koch, H., Hattermann, F.F., 2017. Management scenarios of the Grand Ethiopian Renaissance Dam and their impacts under recent and future climates. Water (Switzerland) 9, 1–24. https://doi.org/10.3390/w9100728
Liersch, S., Tecklenburg, J., Rust, H., Dobler, A., Fischer, M., Kruschke, T., Koch, H., Hattermann, F.F., 2018. Are we using the right fuel to drive hydrological models? A climate impact study in the Upper Blue Nile. Hydrol. Earth Syst. Sci. 22, 2163–2185. https://doi.org/10.5194/hess-22-2163-2018
Liping, C., Yujun, S., Saeed, S., 2018. Monitoring and predicting land use and land cover changes using remote sensing and GIS techniques—A case study of a hilly area, Jiangle, China. PLoS One 13, 1–23. https://doi.org/10.1371/journal.pone.0200493
Liu, J., Shangguan, D., Liu, S., Ding, Y., Wang, S., Wang, X., 2019. Evaluation and comparison of CHIRPS and MSWEP daily-precipitation products in the Qinghai-Tibet Plateau during the period of 1981–2015. Atmos. Res. 230, 104634. https://doi.org/10.1016/j.atmosres.2019.104634
Lobanova, A., Koch, H., Liersch, S., Hattermann, F.F., Krysanova, V., 2016. Impacts of changing climate on the hydrology and hydropower production of the Tagus River basin. Hydrol. Process. 30, 5039–5052. https://doi.org/10.1002/hyp.10966
López-Bermeo, C., Montoya, R.D., Caro-Lopera, F.J., Díaz-García, J.A., 2022. Validation of the accuracy of the CHIRPS precipitation dataset at representing climate variability in a tropical mountainous region of South America. Phys. Chem. Earth 127. https://doi.org/10.1016/j.pce.2022.103184
Loucks, Van, E., Beek, D.P., 2016. Water resource systems planning and analysis-An Introduction to Methods, Models, and Applications, Advances in Water Resources.
Lu, D., Mausel, P., Brondízio, E., Moran, E., 2004. Change detection techniques. Int. J. Remote Sens. 25, 2365–2401. https://doi.org/10.1080/0143116031000139863
Lu, D., Weng, Q., 2007. A survey of image classification methods and techniques for improving classification performance. Int. J. Remote Sens. 28, 823–870. https://doi.org/10.1080/01431160600746456
Ly, M., Segnon, A.C., D'haen, S., Totin, E., Noblet, M., Camara, I., Pfleiderer, P., 2019. COMPRENDRE ET INTERPRÉTER LES SORTIES DE MODÈLES CLIMATIQUES VULNÉRABILITÉ Guide à l ' attention des praticiens. Clim. Anal.
Ma, L., Liu, Y., Zhang, X., Ye, Y., Yin, G., Johnson, B.A., 2019. Deep learning in remote sensing applications: A meta-analysis and review. ISPRS J. Photogramm. Remote Sens. 152, 166–177. https://doi.org/10.1016/j.isprsjprs.2019.04.015
Macarringue, L.S., Bolfe, É.L., Pereira, P.R.M., 2022. Developments in Land Use and Land Cover Classification Techniques in Remote Sensing: A Review. J. Geogr. Inf. Syst. 14, 1–28. https://doi.org/10.4236/jgis.2022.141001
Mahe, G., Lienou, G., Bamba, F., Paturel, J.E., Adeaga, O., 2011. Le fleuve Niger et le changement climatique au cours des 100 dernières années (The Niger River and climate change over the past 100 years). Hydro-climatology Var. Chang. Symp. J-H02 held Dur. IUGG2011 Melbourne, Aust. 131–137.
Martignac, C., 2005. Guide critique d ' utilisation des informations produites dans le cadre du projet TEMOS à La Réunion 0–64.

Mas, J., Kolb, M., Paegelow, M., Camacho, M.T., Houet, T., Mas, J., Kolb, M., Paegelow, M., Teresa, M., Olmedo, C., Houet, T., 2014. Inductive pattern-based land use / cover change models : A comparison of four software packages. Elsevier, 2014, pp.94-111. 10.1016/j.envsoft.2013.09.010 . hal-01187569 HAL. Environ. Model. Softw.

Mas, J.F., Flores, J.J., 2008. The application of artificial neural networks to the analysis of remotely sensed data. Int. J. Remote Sens. 29, 617–663. https://doi.org/10.1080/01431160701352154

Masson-Delmotte, V., Zhai, A., Pirani, A., 2021. Climate Change 2021: The Physical Science Basis. Contribution of Working Group I to the Sixth Assessment Report of the Intergovernmental Panel on Climate Change 2021.

Mbaye, M.L., Diatta, S., Gaye, A.T., 2018. Climate Change Signals Over Senegal River Basin Using Regional Climate Models of the CORDEX Africa Simulations, Lecture Notes of the Institute for Computer Sciences, Social-Informatics and Telecommunications Engineering, LNICST. Springer International Publishing. https://doi.org/10.1007/978-3-319-98878-8_12

Mbaye, M.L., Haensler, A., Hagemann, S., Gaye, A.T., Moseley, C., Afouda, A., 2016. Impact of statistical bias correction on the projected climate change signals of the regional climate model REMO over the Senegal River Basin. Int. J. Climatol. 36, 2035–2049. https://doi.org/10.1002/joc.4478

Mbaye, M.L., Hagemann, S., Haensler, A., Stacke, T., Gaye, A.T., Afouda, A., 2015. Assessment of Climate Change Impact on Water Resources in the Upper Senegal Basin (West Africa). Am. J. Clim. Chang. 04, 77–93. https://doi.org/10.4236/ajcc.2015.41008

Meinshausen, M., Nicholls, Z.R.J., Lewis, J., Gidden, M.J., Vogel, E., Freund, M., Beyerle, U., Gessner, C., Nauels, A., Bauer, N., Canadell, J.G., Daniel, J.S., John, A., Krummel, P.B., Luderer, G., Meinshausen, N., Montzka, S.A., Rayner, P.J., Reimann, S., Smith, S.J., Van Den Berg, M., Velders, G.J.M., Vollmer, M.K., Wang, R.H.J., 2020. The shared socio-economic pathway (SSP) greenhouse gas concentrations and their extensions to 2500. Geosci. Model Dev. 13, 3571–3605. https://doi.org/10.5194/gmd-13-3571-2020

Mishra, N., Khare, D., Shukla, R., Kumar, K., 2014. Trend Analysis of Air Temperature Time Series by Mann Kendall Test - A Case Study of Upper Ganga Canal Command (1901-2002). Br. J. Appl. Sci. Technol. 4, 4066–4082. https://doi.org/10.9734/bjast/2014/8650

Mishra, V., Rai, P., Mohan, K., 2014. Prediction of land use changes based on land change modeler (LCM) using remote sensing: A case study of Muzaffarpur (Bihar), India. J. Geogr. Inst. Jovan Cvijic, SASA 64, 111–127. https://doi.org/10.2298/ijgi1401111m

Mishra, V.N., Rai, P.K., Prasad, R., Punia, M., Nistor, M.M., 2018. Prediction of spatio-temporal land use/land cover dynamics in rapidly developing Varanasi district of Uttar Pradesh, India, using geospatial approach: a comparison of hybrid models. Appl. Geomatics 10, 257–276. https://doi.org/10.1007/s12518-018-0223-5

Moges, D.M., Kmoch, A., Uuemaa, E., 2022. Application of satellite and reanalysis precipitation products for hydrological modeling in the data-scarce Porijõgi catchment, Estonia. J. Hydrol. Reg. Stud. 41. https://doi.org/10.1016/j.ejrh.2022.101070

Mondon, S., Imbard, O.M., 2013. Scénarios RCP et SSP. Ministère l'écologie, du Développement durable l'énergieéveloppement durable l'énergie.

Moriasi, D.N., Arnold, J.G., Liew, M.W. Van, Bingner, R.L., R. D. Harmel, T.L.V., 2007. MODEL EVALUATION GUIDELINES FOR SYSTEMATIC QUANTIFICATION OF ACCURACY IN WATERSHED SIMULATIONS. Colomb. Med. 39, 227–234.

Murgante, B., Misra, S., Rocha, A.M.A.., Torre, C., Rocha, J.G., Falcao, M.I., Taniar, D., Apduhan, B.O., Gervasi, O., 2014. Computational Science and Its Applications.

Nadoushan, M.A., Soffianian, A., Alebrahim, A., 2012. Predicting urban expansion in arak metropolitan area using two land change models. World Appl. Sci. J. 18, 1124–1132. https://doi.org/10.5829/idosi.wasj.2012.18.08.1217

Nash, J.E., Sutcliffe, J. V., 1970. River flow forecasting through conceptual models part I - A discussion of principles. J. Hydrol. 10, 282–290. https://doi.org/10.1016/0022-1694(70)90255-6

Nasiri, V., Deljouei, A., Moradi, F., Sadeghi, S.M.M., Borz, S.A., 2022. Land Use and Land Cover Mapping Using Sentinel-2, Landsat-8 Satellite Images, and Google Earth Engine: A Comparison of Two Composition Methods. Remote Sens. 14. https://doi.org/10.3390/rs14091977

Nassopoulos, H., 2013. Les impacts du changement climatique sur les ressources en eaux en Méditerranée.
Ndione, D.M., Sambou, S., Kane, S., Diatta, S., Sane, M.L., Leye, I., 2020. Ensemble forecasting system for the management of the Senegal River discharge: application upstream the Manantali dam. Appl. Water Sci. 10, 1–15. https://doi.org/10.1007/s13201-020-01199-y
Ndione, D.M., Sambou, S., Sane, M.L., Kane, S., Leye, I., Tamba, S., Diedhiou, R., Cisse, M.T., Ngom, I., 2018. Modeling ensemble streamflow: Application to the Senegal River upper the Manantali Dam. African J. Environ. Sci. Technol. 12, 469–479. https://doi.org/10.5897/ajest2018.2567
Nikulin, G., Jones, C., Giorgi, F., Asrar, G., Büchner, M., Cerezo-Mota, R., Christensen, O.B., Déqué, M., Fernandez, J., Hänsler, A., van Meijgaard, E., Samuelsson, P., Sylla, M.B., Sushama, L., 2012. Precipitation climatology in an ensemble of CORDEX-Africa regional climate simulations. J. Clim. 25, 6057–6078. https://doi.org/10.1175/JCLI-D-11-00375.1
Nikulin, G., Lennard, C., Dosio, A., Kjellström, E., Chen, Y., Hansler, A., Kupiainen, M., Laprise, R., Mariotti, L., Maule, C.F., Van Meijgaard, E., Panitz, H.J., Scinocca, J.F., Somot, S., 2018. The effects of 1.5 and 2 degrees of global warming on Africa in the CORDEX ensemble. Environ. Res. Lett. 13. https://doi.org/10.1088/1748-9326/aab1b1
Noi Phan, T., Kuch, V., Lehnert, L.W., 2020. Land cover classification using google earth engine and random forest classifier-the role of image composition. Remote Sens. 12. https://doi.org/10.3390/RS12152411
Noszczyk, T., 2019. A review of approaches to land use changes modeling. Hum. Ecol. Risk Assess. 25, 1377–1405. https://doi.org/10.1080/10807039.2018.1468994
Nouaceur, Z., Murarescu, O., 2020. Rainfall Variability and Trend Analysis of Multiannual. Water 17.
Obahoundje, S., Diedhiou, A., 2022. Potential impacts of climate, land use and land cover changes on hydropower generation in West Africa: A review. Environ. Res. Lett. 17. https://doi.org/10.1088/1748-9326/ac5b3b
Obahoundje, S., Youan Ta, M., Diedhiou, A., Amoussou, E., Kouadio, K., 2021. Sensitivity of Hydropower Generation to Changes in Climate and Land Use in the Mono Basin (West Africa) using CORDEX Dataset and WEAP Model. Environ. Process. 8, 1073–1097. https://doi.org/10.1007/s40710-021-00516-0
Olofsson, P., Foody, G.M., Herold, M., Stehman, S. V, Woodcock, C.E., Wulder, M.A., 2014. Remote Sensing of Environment Good practices for estimating area and assessing accuracy of land change. Remote Sens. Environ. 148, 42–57. https://doi.org/10.1016/j.rse.2014.02.015
Olsson, G., Lund, P.D., 2017. Water and Energy - Interconnections and Conflicts. Glob. Challenges 1, 1700056. https://doi.org/10.1002/gch2.201700056
OMVS, 2013. Étude d'évaluation des inondations dans le Bassin du fleuve Sénégal.
OMVS, 2012a. Schéma Directeur d'Aménagement et de Gestion des Eaux du Fleuve Sénégal.
OMVS, 2012b. Étude de faisabilité et d'avant-projet sommaire (APS) de l'aménagement hydroélectrique de Gourbassi.
OMVS, 2011. Aménagement hydroélectrique de Boureya en république de Guinée.
Oñate-Valdivieso, F., Bosque-Sendra, J., Sastre-Merlin, A., Ponce, V.M., 2016. Calibration, validation and evaluation of a lumped hydrologic model in a mountain area in Southern Ecuador. Agrociencia 50, 945–963.
Orange, D., 1990. Dynamique Actuelle D ' Un Vieux Paysage Lateritique.
Ougahi, J.H., Mahmood, S.A., 2022. Evaluation of satellite-based and reanalysis precipitation datasets by hydrologic simulation in the Chenab river basin. J. Water Clim. Chang. 13, 1563–1582. https://doi.org/10.2166/wcc.2022.410
Oyebande, L., Odunuga, S., 2013. Climate Change Impact on Water Resources at the Transboundary Level in West Africa: The Cases of the Senegal, Niger and Volta Basins. Open Hydrol. J. 4, 163–172. https://doi.org/10.2174/1874378101004010163
Padiyedath Gopalan, S., Hanasaki, N., Champathong, A., Tebakari, T., 2021. Impact assessment of reservoir operation in the context of climate change adaptation in the Chao Phraya River basin. Hydrol. Process. 35, 1–19. https://doi.org/10.1002/hyp.14005
Pandey, P.C., Koutsias, N., Petropoulos, G.P., Srivastava, P.K., Ben Dor, E., 2021. Land use/land

cover in view of earth observation: data sources, input dimensions, and classifiers—a review of the state of the art. Geocarto Int. 36, 957–988. https://doi.org/10.1080/10106049.2019.1629647
Pocewicz, A., Nielsen-Pincus, M., Goldberg, C.S., Johnson, M.H., Morgan, P., Force, J.E., Waits, L.P., Vierling, L., 2008. Predicting land use change: Comparison of models based on landowner surveys and historical land cover trends. Landsc. Ecol. 23, 195–210. https://doi.org/10.1007/s10980-007-9159-6
Poncelet, C., 2016. Du bassin au paramètre : jusqu ' où peut-on régionaliser un modèle hydrologique conceptuel ? Par Carine Poncelet Dirigée par Vazken Andréassian et Ludovic Oudin.
Pontius, R.G., Batchu, K., 2003. Using the Relative Operating Characteristic to Quantify Certainty in Prediction of Location of Land Cover Change in India 7, 467–484. https://doi.org/https://onlinelibrary.wiley.com/doi/10.1111/1467-9671.00159
Pulighe, G., Bonati, G., Colangeli, M., Traverso, L., Lupia, F., Altobelli, F., Marta, A.D., Napoli, M., 2020. Predicting streamflow and nutrient loadings in a semi-arid Mediterranean watershed with ephemeral streams using the SWAT model. Agronomy 10. https://doi.org/10.3390/agronomy10010002
Ranzani, A., Bonato, M., Patro, E.R., Gaudard, L., De Michele, C., 2018. Hydropower future: Between climate change, renewable deployment, carbon and fuel prices. Water (Switzerland) 10, 1–17. https://doi.org/10.3390/w10091197
Riahi, K., Van Vuuren, D., Kriegler, E., 2017. The Shared Socioeconomic Pathways and their energy, land use, and greenhouse gas emissions implications: An overview 2017.
Richards, J.A., 2006. Remote Sensing Digital Image Analysis, Remote Sensing Digital Image Analysis. https://doi.org/10.1007/3-540-29711-1
Richaud, B., Huber, D.H.I.S., Gras, D.H.I., 2019. projection des impacts du changement climatique OMVS, DHI, UNITAR/UN.
Roland, Y.O., 2021. Dynamique spatio-temporelle des états de surface et influence sur le ruissellement sur un bassin de type sahélien : cas du bassin de Tougou (Nord Burkina Faso). https://doi.org/10.13140/RG.2.2.11834.82883
Rowell, D.P., Senior, C.A., Vellinga, M., Graham, R.J., 2016. Can climate projection uncertainty be constrained over Africa using metrics of contemporary performance ? 621–633. https://doi.org/10.1007/s10584-015-1554-4
Roy, H.G., Fox, D.M., Emsellem, K., 2015. Spatial dynamics of land cover change in a Euro-Mediterranean catchment (1950–2008). J. Land Use Sci. 10, 277–297. https://doi.org/10.1080/1747423X.2014.898105
Rwanga, S.S., Ndambuki, J.M., 2017. Accuracy Assessment of Land Use/Land Cover Classification Using Remote Sensing and GIS. Int. J. Geosci. 08, 611–622. https://doi.org/10.4236/ijg.2017.84033
Sadar Shahraki, A., Shahraki, J., Hashemi Monfared, S.A., 2016. An Application of WEAP Model in Water Resources Management Considering the Environmental Scenarios and Economic Assessment Case Study: Hirmand Catchment. Mod. Appl. Sci. 10, 49. https://doi.org/10.5539/mas.v10n5p49
Sadio, P.M., Mbaye, M.L., Diatta, S., Sylla, M.B., 2020. Hydro-climate variability and change in the Casamance river basin (Senegal). Houille Blanche 2021-March, 89–96. https://doi.org/10.1051/lhb/2021002
Sahlu, D., Moges, S.A., Nikolopoulos, E.I., Anagnostou, E.N., Hailu, D., 2017. Evaluation of High-Resolution Multisatellite and Reanalysis Rainfall Products over East Africa. Adv. Meteorol. 2017. https://doi.org/10.1155/2017/4957960
Sambou, S., Boye, M., Malang, B.A., Malanda-nimy, E.N., Bodian, A., Mussa, K., Adama, M., Fatogoma, B., Raymond, M., Alpha, B., Alioune, K., Fall, M.M.E., Niang, A.W.A., Soumare, H., 2003. Calage et validation des modèles hydrologiques GR4J et GR2M sur le bassin du Bafing en amont de Bafing-Makana : vers l ' étude de l ' impact du climat sur les ressources en eau de la retenue de Manantali 2–7.
Sambou, S., Deme, A., Diouf, I., Oceanic, N., 2018. Contribution of TRMM 3B42 Data to Improve Knowledge on Rainfall in the Kayanga / Geba River Basin (Republic of Guinea , Senegal and Guinea- Bissau) Abdoulaye Deme. https://doi.org/10.19044/esj.2018.v14n9p260

Sambou, S., Diémé, Y., Touré, A.K., Badji, A.M., Malanda-Nimy, E.N., 2019. Effet du barrage de Manantali sur les modifications du régime hydrologique du fleuve Sénégal dans le bassin amont : une approche statistique. Sécheresse 20, 104–111. https://doi.org/10.1684/sec.2009.0176
Sane, M.L., Sambou, S., Diatta, S., Leye, I., Ndione, D.M., Sauvage, S., Sanchez-Perez, J.M., Kane, S., 2019. Trends and shifts in time series of climate data generated by GCM from 2006 to 2090. Int. J. Sci. Eng. Res. 10, 212–229. https://doi.org/10.14299/ijser.2019.05.01
Sane, M.L., Sambou, S., Leye, I., Ndione, D.M., Diatta, S., Ndiaye, I., Badji, M.L., Kane, S., 2020. Calibration and Validation of the SWAT Model on the Watershed of Bafing River, Main Upstream Tributary of Senegal River: Checking for the Influence of the Period of Study. Open J. Mod. Hydrol. 10, 81–104. https://doi.org/10.4236/ojmh.2020.104006
Sane, M.L., Sambou, S., Ndione, D.M., Leye, I., 2017. Moussé Landing SANE et al . ANALYSE ET TRAITEMENT DES SÉRIES DE DÉBITS ANNUELS ET MENSUELS SUR LE FLEUVE SÉNÉGAL EN.
Sankarrao, L., Ghose, D.K., Rathinsamy, M., 2021. Predicting land-use change: Intercomparison of different hybrid machine learning models. Environ. Model. Softw. 145, 105207. https://doi.org/10.1016/j.envsoft.2021.105207
Schaeffer, R., Szklo, A.S., Pereira de Lucena, A.F., Moreira Cesar Borba, B.S., Pupo Nogueira, L.P., Fleming, F.P., Troccoli, A., Harrison, M., Boulahya, M.S., 2012. Energy sector vulnerability to climate change: A review. Energy 38, 1–12. https://doi.org/10.1016/j.energy.2011.11.056
Schaefli, B., Hingray, B., Musy, A., 2007. Climate change and hydropower production in the Swiss Alps: Quantification of potential impacts and related modelling uncertainties. Hydrol. Earth Syst. Sci. 11, 1191–1205. https://doi.org/10.5194/hess-11-1191-2007
Shelestov, A., Lavreniuk, M., Kussul, N., Novikov, A., Skakun, S., 2017. Exploring Google earth engine platform for big data processing: Classification of multi-temporal satellite imagery for crop mapping. Front. Earth Sci. 5, 1–10. https://doi.org/10.3389/feart.2017.00017
Shu, J., Qu, J.J., Motha, R., Xu, J.C., Dong, D.F., 2018. Impacts of climate change on hydropower development and sustainability: A review. IOP Conf. Ser. Earth Environ. Sci. 163. https://doi.org/10.1088/1755-1315/163/1/012126
Silva, L.P. e., Xavier, A.P.C., da Silva, R.M., Santos, C.A.G., 2020. Modeling land cover change based on an artificial neural network for a semiarid river basin in northeastern Brazil. Glob. Ecol. Conserv. 21. https://doi.org/10.1016/j.gecco.2019.e00811
Singh, S.K., Mustak, S., Srivastava, P.K., Szabó, S., Islam, T., 2015. Predicting Spatial and Decadal LULC Changes Through Cellular Automata Markov Chain Models Using Earth Observation Datasets and Geo-information. Environ. Process. 2, 61–78. https://doi.org/10.1007/s40710-015-0062-x
Singh, V.G., Singh, S.K., Kumar, N., Singh, R.P., 2022. Simulation of land use/land cover change at a basin scale using satellite data and markov chain model. Geocarto Int. 37, 11339–11364. https://doi.org/10.1080/10106049.2022.2052976
Singh, V.P., 1995. Computer models of watershed Hydrology, in: Water Resources Publications. p. Chapter 25: 909-1000.
Solly, B., Dieye, E.H.B., Oumar, S.Y., Jarju, A.M., Sane, T., 2021. Detection des zones de degradation et de regeneration de la couverture vegetale dans le sud du Senegal a travers l'analyse des tendances de series temporelles modis ndvi et des changements d'occupation des sols a partir d'images landsat. Rev. Fr. Photogramm. Teledetect. 223, 1–15. https://doi.org/10.52638/rfpt.2021.580
Soro, T.D., Soro, N., Oga, Y.M., Lasm, T., Soro, G., Ahoussi, K.E., Bieme, J., 2011. LA VARIABILITÉ CLIMATIQUE ET SON IMPACT SUR CARRÉ DE GRAND-LAHOU (SUD-OUEST DE LA CÔTE D ' IVOIRE) V, 55–73.
Spalding-Fecher, R., Joyce, B., Winkler, H., 2017. Climate change and hydropower in the Southern African Power Pool and Zambezi River Basin: System-wide impacts and policy implications. Energy Policy 103, 84–97. https://doi.org/10.1016/j.enpol.2016.12.009
Stehman, S. V., 2014. Estimating area and map accuracy for stratified random sampling when the strata are different from the map classes. Int. J. Remote Sens. 35, 4923–4939. https://doi.org/10.1080/01431161.2014.930207

Sterl, S., Liersch, S., Koch, H., Lipzig, N.P.M.V., Thiery, W., 2018. A new approach for assessing synergies of solar and wind power: Implications for West Africa. Environ. Res. Lett. 13. https://doi.org/10.1088/1748-9326/aad8f6
Sterl, S., Vanderkelen, I., Chawanda, C.J., Russo, D., Brecha, R.J., van Griensven, A., van Lipzig, N.P.M., Thiery, W., 2020. Smart renewable electricity portfolios in West Africa. Nat. Sustain. 3, 710–719. https://doi.org/10.1038/s41893-020-0539-0
Subedi, P., Subedi, K., Thapa, B., 2013. Application of a Hybrid Cellular Automaton – Markov (CA-Markov) Model in Land-Use Change Prediction: A Case Study of Saddle Creek Drainage Basin, Florida. Appl. Ecol. Environ. Sci. 1, 126–132. https://doi.org/10.12691/aees-1-6-5
Sun, J., Yan, H., Bao, Z., Wang, G., 2022. Investigating Impacts of Climate Change on Runoff from the Qinhuai River by Using the SWAT Model and CMIP6 Scenarios. Water (Switzerland) 14. https://doi.org/10.3390/w14111778
Sun, L., Zhou, X., Gu, A., 2022. Effects of Climate Change on Hydropower Generation in China Based on a WEAP Model. Sustain. 14. https://doi.org/10.3390/su14095467
Sylla, M.B., Pal, J.S., Faye, A., Dimobe, K., Kunstmann, H., 2018. Climate change to severely impact West African basin scale irrigation in 2 °C and 1.5 °C global warming scenarios. Sci. Rep. 8, 1–9. https://doi.org/10.1038/s41598-018-32736-0
Szantoi, Z., Jaffrain, G., Gallaun, H., Bielski, C., Ruf, K., Lupi, A., Miletich, P., 2021. Quality assurance and assessment framework for land cover maps validation in the Copernicus Hot Spot Monitoring activity. Eur. J. Remote Sens. 54, 537–556. https://doi.org/10.1080/22797254.2021.1978001
Tabutin, D., Schoumaker, B., 2020. La démographie de l'Afrique subsaharienne au XXIe siècle, Population. https://doi.org/10.3917/popu.2002.0169
Talukdar, S., Singha, P., Mahato, S., Pal, S., 2020. Land-Use Land-Cover Classification by Machine Learning Classifiers for Satellite Observations — A Review. https://doi.org/https://doi.org/10.3390/rs12071135
Tarroja, B., Forrest, K., Chiang, F., AghaKouchak, A., Samuelsen, S., 2019a. Implications of hydropower variability from climate change for a future, highly-renewable electric grid in California. Appl. Energy 237, 353–366. https://doi.org/10.1016/j.apenergy.2018.12.079
Tarroja, B., Forrest, K., Chiang, F., AghaKouchak, A., Samuelsen, S., 2019b. Implications of hydropower variability from climate change for a future, highly-renewable electric grid in California. Appl. Energy 237, 353–366. https://doi.org/10.1016/j.apenergy.2018.12.079
Tarroja, B., Forrest, K., Chiang, F., AghaKouchak, A., Samuelsen, S., 2019c. Implications of hydropower variability from climate change for a future, highly-renewable electric grid in California. Appl. Energy 237, 353–366. https://doi.org/10.1016/j.apenergy.2018.12.079
Taylor, K.E., 2001. Summarizing multiple aspects of model performance in a single diagram 106, 7183–7192.
Teotónio, C., Fortes, P., Roebeling, P., Rodriguez, M., Robaina-Alves, M., 2017. Assessing the impacts of climate change on hydropower generation and the power sector in Portugal: A partial equilibrium approach. Renew. Sustain. Energy Rev. 74, 788–799. https://doi.org/10.1016/j.rser.2017.03.002
Tewkesbury, A.P., Comber, A.J., Tate, N.J., Lamb, A., Fisher, P.F., 2015. A critical synthesis of remotely sensed optical image change detection techniques. Remote Sens. Environ. 160, 1–14. https://doi.org/10.1016/j.rse.2015.01.006
Thiam, N.A., 2016. Allocation optimale de l'eau dans le bassin versant du fleuve Sénégal.
Thiam, S., Salas, E.A.L., Rholan, N., Delos, A., Almoradie, S., Verleysdonk, S., Adounkpe, J.G., Komi, K., 2022. Modelling Land Use and Land Cover in the Transboundary Mono River Catchment of Togo and Benin Using Markov Chain and Stakeholder ' s Perspectives.
Thiam, S., Villamor, G.B., Faye, L.C., Sène, J.H.B., Diwediga, B., Kyei-Baffour, N., 2021. Monitoring land use and soil salinity changes in coastal landscape: a case study from Senegal. Environ. Monit. Assess. 193. https://doi.org/10.1007/s10661-021-08958-7
Tiné, M., Perez, L., Molowny-Horas, R., 2019. Hybrid spatiotemporal simulation of future changes in open wetlands: A study of the Abitibi-Témiscamingue region, Québec, Canada. Int. J. Appl. Earth Obs. Geoinf. 74, 302–313. https://doi.org/10.1016/j.jag.2018.10.001

Traore, A., 2018. Land-Cover Change Analysis and Simulation in Conakry (Guinea), Using Hybrid Cellular-Automata and Markov Model 1–16. https://doi.org/10.3390/urbansci2020039
Traore, S.S., Dembele, S., Dembele, D., Diakite, N., Diakite, C.H., 2022. Dynamique de l'occupation du sol et trajectoire du couvert végétal autour de trois sites miniers du Sud Mali entre 1988 et 2019. Physio-Géo 17, 151–166. https://doi.org/10.4000/physio-geo.14565
Treut, L., Somerville, R., Cubasch, U., Ding, Y., Mauritzen, C., Mokssit, a, Peterson, T., Prather, M., Qin, D., Manning, M., Chen, Z., Marquis, M., Averyt, K.B., Tignor, M., 2007. Historical Overview of Climate Change Science. Earth Chapter 1, 93–127. https://doi.org/10.1016/j.soilbio.2010.04.001
Tsai, Y.H., Stow, D., Chen, H.L., Lewison, R., An, L., Shi, L., 2018. Mapping vegetation and land use types in Fanjingshan National Nature Reserve using google earth engine. Remote Sens. 10. https://doi.org/10.3390/rs10060927
UCAD, 2019. Final Report Climate Vulnerability and Water Resources Variability in West Africa Senegal and Gambia River Basin Cases 1–131.
van Griensven, a., 2009. Sensitivity , auto-calibration , uncertainty and model evaluation in SWAT2005 Ann van Griensven Sensitivity , auto-calibration , uncertainty and model evaluation in SWAT2005 I Theory 1–48.
Verburg, P., Neuman, K., Nolz, L., 2011. Challenges in using land use and land cover data for global change studies. Glob. Chang. Biol. 974–989. https://doi.org/10.1111/j.1365-2486.2010.02307.x
Victora, C.G., Adair, L., Fall, C., Hallal, P.C., Martorell, R., Richter, L., Sachdev, H.S., 2008. Maternal and child undernutrition: consequences for adult health and human capital. Lancet 371, 340–357. https://doi.org/10.1016/S0140-6736(07)61692-4
Vicuña, S., Dracup, J.A., Dale, L., 2011. Climate change impacts on two high-elevation hydropower systems in California. Clim. Change 109, 151–169. https://doi.org/10.1007/s10584-011-0301-8
Vissin, E.W., 2007. Impact de la variabilité climatique et de la dynamique des états de surfacesur les écoulements du bassin béninois du fleuve Niger. Cent. Rech. en Climatol. (CNRS-UMR 5210) Thèse de d, 310p.
Wahap, N.A., Shafri, H.Z.M., 2020. Utilization of Google Earth Engine (GEE) for land cover monitoring over Klang Valley, Malaysia. IOP Conf. Ser. Earth Environ. Sci. 540. https://doi.org/10.1088/1755-1315/540/1/012003
Wang, J., Bretz, M., Dewan, M.A.A., Delavar, M.A., 2022. Machine learning in modelling land-use and land cover-change (LULCC): Current status, challenges and prospects. Sci. Total Environ. 822, 153559. https://doi.org/10.1016/j.scitotenv.2022.153559
Wang, P., 2012. A framework for social impact analysis of large dams: A case study of cascading dams on the Upper-Mekong River, China. MSc Thesis, Faculty of the Graduate School of Cornell University. A Framew. Soc. impact Anal. large dams 159.
Wang, S.W., Munkhnasan, L., Lee, W.K., 2021. Land use and land cover change detection and prediction in Bhutan's high altitude city of Thimphu, using cellular automata and Markov chain. Environ. Challenges 2. https://doi.org/10.1016/j.envc.2020.100017
Wasti, A., Ray, P., Wi, S., Folch, C., Ubierna, M., Karki, P., 2022. Climate change and the hydropower sector: A global review. Wiley Interdiscip. Rev. Clim. Chang. 13, 1–29. https://doi.org/10.1002/wcc.757
Winkler, K., Fuchs, R., Rounsevell, M., Herold, M., 2019. Global land use changes are four times greater than previously estimated. Nat. Commun. 1–10. https://doi.org/10.1038/s41467-021-22702-2
Woodcock, C.E., Allen, R., Anderson, M., Belward, A., Bindschadler, R., Cohen, W., Gao, F., Goward, S.N., Helder, D., Helmer, E., Nemani, R., Oreopoulos, L., Schott, J., Thenkabail, P.S., Vermote, E.F., Vogelmann, J., Wulder, M.A., Wynne, R., 2008. Free access to landsat imagery. Science (80-.). 320, 1011. https://doi.org/10.1126/science.320.5879.1011a
Wortmann, M., Krysanova, V., Kundzewicz, Z.W., Su, B., Li, X., 2014. Assessing the influence of the Merzbacher Lake outburst floods on discharge using the hydrological model SWIM in the Aksu headwaters, Kyrgyzstan/NW China. Hydrol. Process. 28, 6337–6350. https://doi.org/10.1002/hyp.10118
Wulder, M.A., Loveland, T.R., Roy, D.P., Crawford, C.J., Masek, J.G., Woodcock, C.E., Allen, R.G.,

Anderson, M.C., Belward, A.S., Cohen, W.B., Dwyer, J., Erb, A., Gao, F., Griffiths, P., Helder, D., Hermosilla, T., Hipple, J.D., Hostert, P., Hughes, M.J., Huntington, J., Johnson, D.M., Kennedy, R., Kilic, A., Li, Z., Lymburner, L., McCorkel, J., Pahlevan, N., Scambos, T.A., Schaaf, C., Schott, J.R., Sheng, Y., Storey, J., Vermote, E., Vogelmann, J., White, J.C., Wynne, R.H., Zhu, Z., 2019. Current status of Landsat program, science, and applications. Remote Sens. Environ. 225, 127–147. https://doi.org/10.1016/j.rse.2019.02.015

Yamazaki, D., Ikeshima, D., Tawatari, R., Yamaguchi, T., O'Loughlin, F., Neal, J.C., Sampson, C.C., Kanae, S., Bates, P.D., 2017. A high-accuracy map of global terrain elevations. Geophys. Res. Lett. 44, 5844–5853. https://doi.org/10.1002/2017GL072874

Yang, Y., Yang, D., Wang, X., Zhang, Z., Nawaz, Z., 2021. Testing accuracy of land cover classification algorithms in the qilian mountains based on gee cloud platform. Remote Sens. 13. https://doi.org/10.3390/rs13245064

Zadbagher, E., Becek, K., Berberoglu, S., 2018. Modeling land use/land cover change using remote sensing and geographic information systems: case study of the Seyhan Basin, Turkey. Environ. Monit. Assess. 190. https://doi.org/10.1007/s10661-018-6877-y

Zakara, M., 2007. Pour l ' accès à l ' énergie en Afrique Constats Enjeux 1–6.

Zhu, L., Suomalainen, J., Liu, J., Hyyppä, J., Kaartinen, H., Haggren, H., 2018. A Review: Remote Sensing Sensors. Multi-purposeful Appl. Geospatial Data. https://doi.org/10.5772/intechopen.71049

Zurqani, H.A., Post, C.J., Mikhailova, E.A., Schlautman, M.A., Sharp, J.L., 2018. Geospatial analysis of land use change in the Savannah River Basin using Google Earth Engine. Int. J. Appl. Earth Obs. Geoinf. 69, 175–185. https://doi.org/10.1016/j.jag.2017.12.006

Annexes

List of published papers

- Mame Henriette Astou Sambou, Jean Albergel, Expédit Wilfrid Vissin, Stefan Liersch, Hagen Koch, Zoltan Szantoi, Wassim Baba, Moussé Landing Sane & Ibrahima Toure (2023) Prediction of land use and land cover change in two watersheds in the Senegal Riverbasin (West Africa) using the Multilayer Perceptron and Markov chain model, European Journal of Remote Sensing, 56:1, 2231137, DOI: 10.1080/22797254.2023.

- Sambou, M.H.A.; Liersch, S.; Koch, H.; Vissin, E.W.; Albergel, J.;Sane, M.L. Synergies and Trade-Offsin Water Resources Management in the Bafing Watershed under Climate Change. Water 2023, 15, 2067.https://doi.org/10.3390/w15112067

List of co-authors published papers

- Ibrahima TOURE, Didier Maria NDIONE, Issa Leye, Mame Henriette Astou SAMBOU et Moussé Landing SANE (2022), Analyse des tendances dans les séries pluviométriques au Sénégal, Afrique SCIENCE 21(1) (2022) 122 - 135 122ISSN 1813-548X, http://www.afriquescience.net.

Mame Henriette Astou SAMBOU is born on July 16, 1992, at Guediawaye/Dakar, Senegal. She got her baccalaureat in 2010. She holds a bachelor in Math-Info at the University of Cheikh Anta Diop of Dakar in 2013. She has a bachelor and master's in water and Sanitation at the Institut International d'Ingénierie de l'Eau et de l'Environnement of Burkina Faso (2ie) in 2015 and 2017. She is now completing a PhD in climate change and water resources.

Abstract :

Located between Mali, Senegal, Mauritania and Guinea, the Senegal River Basin (SRB) is a strategic region for the socio-economic development of these countries. The Senegal River Basin is divided into three main parts: The upper basin, the valley and the delta. The Bafing watershed is the main tributary of the Senegal River and is located in the upper Senegal River Basin. The management of the Bafing watershed in time and space is possible thanks to the Manantali hydropower dam. The Manantali dam aims to meet the growing water, energy and agriculture need of the member states (Senegal, Mali, Guinea, Mauritania). The organization for the development of the Senegal River (OMVS) plans to build new hydropower dams (Koukoutamba, Boureya) upstream of the Manantali dam to increase hydropower potential in the Bafing watershed.

In the future, water availability and hydropower generation are expected to be profoundly impacted, mainly due to the change in river flow caused by population growth, climate change, and Land use/land cover change. In the coming decades, climate change and changes in land use and land cover will further increase the constraints on the already scarce water resources in West Africa. Despite the amount of documentation and numerous projects on the Bafing watershed, there are not yet studies that have addressed the hydrological and hydropower potential (HPP) response considering the combined impact of future climate change, the land use/land cover (LULC) change and the future development of planned dams in the Bafing watershed. Therefore, this study aims to fill this gap by investigating the future impacts of climate change, land use, land cover change, and altered water resource management on the water availability and hydropower potential (HPP) in the Bafing watershed.

Firstly, two precipitation products (reanalysis (W-era5) and satellite (CHIRPS)) were compared to the observed precipitation of Bafing Makana station due to insufficient data caused by numerous gaps in the historical time series. This exercise was done to select the best precipitation product to reproduce the observed precipitation. The results showed that W-era5 represents the observed data more accurately than CHIRPS. After, ten downscaled and bias-adjusted Global Climate Models from ISIMIP 3b were investigated to determine whether the models satisfactorily replicate the reference climate (temperature and precipitation of W-era5) of the Bafing watershed. The results indicated that the tens GCMs could successfully replicate the reference climate. Hence, the median of the 10 GCMs (MME) was used to analyze the future trend in the near future (P1:2035-2065) and the far future (P2:2065-205) compared to the reference period (P0:1984-2014) under ssp 126 and ssp 370. The results indicated that, according to the median (MME), a rise in temperature by 1.4°C and 2.0°C under ssp126 and ssp370 is predicted in the near future. In the far future, the difference between both climate scenarios is much larger and spans from 1.6°C to 3.7°C. Projected precipitation is uncertain in the future. Indeed, precipitation is predicted to increase under ssp126 or decrease below ssp 370 in the near future. In the far future, precipitation is expected to decrease under both scenarios.

Secondly, the past and future LULC change was analyzed between 1986 to 2020 and 2020 to 2050. Landsat images and the random forest classification method were used to map LULC of 1986, 2006 and 2020. Future LULC map in 2050 were simulated under business-as-usual assumptions with the Multi-Layer Perceptron and Markov Chain method embedded in the Land Change Modeller software. The LULC change was analyzing using the post classification change detection technique, a pixel-based method. The results showed that between 1986 to 2020, vegetation, settlement, cultivated area and water increased, while the bareground decreased. Between 2020-2050, the results indicated that vegetation, settlement, cultivated area, and water are projected to increase in Bafing. The Bafing watershed has seen a trend towards "more people, more trees".

Thirdly, an eco-hydrological water management model, the Soil and Water Integrated Model (SWIM), was set up and used to generate river discharge and simulate existing and future dams. SWIM model was driven by ten downscaled and bias adjusted GCMs under ssp 126 and ssp 370 and land use/land cover maps (1986, 2020, 2050). The analysis was carried out using a separation method that includes combining the two components (climate and LULC) and adjusting one factor at a time while holding the other constant. The result indicated that SWIM satisfactorily reproduces the observed flow with statistical performance measures (NSE, KGE) between 0.7 and 0.8. Reservoir module also satisfactory reproduce the inflow, outflow, and water level of the Manantali dam. Under the impact of climate change, the result of the SWIM simulation indicated that the inflow and hydropower potential of the Manantali dam will decrease except in the near future under ssp 126, following the general trend of precipitation in the future. Under the impact of LULC change, the inflow and hydropower potential (HPP) of the Manantali dam will decrease by -5% and -5.7 respectively due to the conversion of bareground (with high runoff coefficients) to vegetation and cultivated area (low runoff coefficients) during the period 1986-2050. Under the effects of climate change and LULC change, the result of the SWIM simulation pointed out that LULC change has less impact on the inflow and hydropower potential of the Manantali dam than climate change.

Investment in future dams has advantages, such as increased water storage, greater hydropower potential and improved flood protection. However, future dams will be negatively affected by climate change in the future (except in the near future under ssp 126), and their operation will lead to a loss in the hydropower potential of the Manantali dam. Therefore, the implementation of adaptation techniques to mitigate the effects of the environmental and social impacts of these dams, as well as the impact of climate change and LULC change. Adaptation techniques can be an optimization program or adopting a new common energy policy promoting an energy mix that prioritizes renewable energies, namely solar and wind. The results of this study provide relevant information to the OMVS for the management of the Bafing watershed.

keyword: Climate change, Land use land cover change, Hydropower generation, water resource management, Bafing watershed, Senegal River Basin

PhD

Mame Henriette Astou SAMBOU

CLIMATE CHANGE AND LAND USE LAND COVER CHANGE IMPACTS ON THE HYDROPOWER POTENTIAL IN THE BAFING WATERSHED (SENEGAL RIVER BASIN)

GRP/CCWR/WASCAL – UAC April, 2024